

Near Surface Seismoelectrics in Comparative Field Studies

Dissertation
zur Erlangung des Doktorgrades
der Mathematisch-Naturwissenschaftlichen Fakultät
der Christian-Albrechts-Universität
zu Kiel

vorgelegt von

Matthias Hans Per Strahser

Kiel

2006

| | |
|----------------------------|---------------------------|
| Referent | Prof. Dr. Wolfgang Rabbel |
| Korreferent | Prof. Dr. Thomas Bohlen |
| Tag der mündlichen Prüfung | 02. Februar 2007 |
| Zum Druck genehmigt | 07. Februar 2007 |

gez. Dekan J. Grotemeyer

Abstract

In porous saturated media, seismic compressional waves can cause electric and electromagnetic signals via electrokinetic coupling. These seismoelectric signals are created by fluid flow in pore space and could provide valuable hydrogeophysical information. They can be measured in the form of a potential difference between two electrodes. Usually several of these dipoles are deployed in a profile line and connected to a seismograph.

There are two main seismoelectric wave types, the coseismic and the converted seismoelectric signals. The coseismic waves accompany seismic compressional waves in saturated porous media, whereas the converted seismoelectric signals have their origin in the subsurface at interfaces separating layers of different elastic, electrical or hydrological properties. In most seismoelectric applications, these converted waves are the signal of interest because they are expected to contain information about subsurface boundaries.

Despite increasing interest in the seismoelectric method, little material has been published on actual field measurements. This means that more seismoelectric field studies are needed if the potential of the method is to be realized. So far it is relatively unknown if and how changing ground conditions influence seismoelectric data. In order to address this deficiency, several sites in Northern Germany were visited at different times to investigate the repeatability and variability of seismoelectric signals. Some locations yield high-quality data with converted seismoelectric signals at almost every shotpoint. Other sites, especially urban ones, show a very bad signal-to-noise ratio.

In general, there is a strong correlation between the overall quality of seismoelectric data and the quality of the associated seismic data. Factors like the electrical resistivity or electrode coupling are less significant. It is important that measurements are made in areas free from strong anthropogenic noise. There is a moderate correlation between data quality and the hardness of the ground. In general, favorable conditions for seismoelectric measurements seem to be: sandy ground (preferably dry rather than wet), low electromagnetic noise level, and clear subsurface boundaries. Data obtained in open fields seem to be better than those obtained in forested areas.

In order to study the dependence of seismoelectric signals on electrical resistivity, I compare VSP (vertical seismic profiling) and VSEP (vertical seismoelectric profiling) measurements to borehole geoelectric measurements. The seismoelectric amplitude (normalized with respect to the seismic amplitudes) is strongly dependent on the pH value, but is not or is only very weakly dependent on dipole length and electrical resistivity.

A hodogram analysis of three-component seismoelectric data reveals that the polarization mainly follows theoretical predictions. The converted signals are clearest on the vertical and radial components where they also have their maximum amplitudes. However, their amplitudes relative to one another can be explained by taking into account destructive interference of the converted signals that originate from layer boundaries at 4 m and 5 m depth. The converted signals also appear on the transverse component, probably due to the dip of the layers.

In spite of the progress in seismoelectric field techniques in recent years, numerous problems remain. The measurements, interpretations and comparisons with other methods presented in this work will help to assess the chances of successful application of seismoelectric measurements in near surface geophysical studies.

Zusammenfassung

Seismische Kompressionswellen können in porösen gesättigten Medien durch elektrokinetische Kopplung seismoelektrische Signale verursachen. Diese werden durch Fluidfluss im Porenraum erzeugt und könnten daher für die Hydrogeophysik wertvolle Informationen liefern. Sie sind messbar in Form einer Potenzialdifferenz zwischen zwei Elektroden. Üblicherweise werden mehrere solcher Dipole profilweise angeordnet und an einen Seismographen angeschlossen. Die beiden Haupttypen seismoelektrischer Wellen werden als koseismische bzw. konvertierte seismoelektrische Signale bezeichnet. Die koseismischen Wellen werden von seismischen Kompressionswellen mitgeführt, während die konvertierten seismoelektrischen Signale ihren Ursprung an Grenzen zwischen Schichten mit unterschiedlichen elastischen, elektrischen oder hydrologischen Eigenschaften haben. Für die meisten Anwendungen sind diese letzteren konvertierten Signale die Nutzsignale, da man sich von ihnen Informationen über die konvertierenden Grenzschichten erhofft.

Trotz zunehmenden Interesses an der Seismoelektrik wurden bisher nur wenige Ergebnisse seismoelektrischer Feldmessungen veröffentlicht. Weitere Feldstudien sind vonnöten, um das Potenzial dieser Methode beurteilen zu können. Es ist bisher unbekannt, ob und wie seismoelektrische Daten durch sich verändernde Boden- und Messbedingungen beeinflusst werden. An mehreren Orten hauptsächlich in Norddeutschland wurden zu verschiedenen Zeitpunkten Messungen durchgeführt, um die Wiederholbarkeit und Variabilität seismoelektrischer Signale zu untersuchen. An einigen Lokationen konnten Daten mit hoher Signalqualität und mit Konvertierten an beinahe jedem Schusspunkt gewonnen werden. Andere Lokationen, vor allem stadtnahe, zeichnen sich durch ein sehr schlechtes Signal-Rausch-Verhältnis aus. Im Allgemeinen besteht eine starke Korrelation zwischen seismoelektrischer und seismischer Datenqualität. Faktoren wie der spezifische elektrische Widerstand oder Ankopplung der Elektroden sind weniger entscheidend. Da elektromagnetische Störsignale eine große Beeinträchtigung darstellen, sollten Messungen an elektromagnetisch ruhigen Orten stattfinden. Eine mäßige Korrelation zwischen Datenqualität und Härte des Bodens konnte festgestellt werden. Generell bedeuten Messungen auf offenem Feld statt in bewaldetem Gebiet günstige Bedingungen für die Seismoelektrik, ebenso wie sandige Böden (vorzugsweise trocken), ein niedriges elektromagnetisches Störsignalniveau und klare Grenzschichten im Untergrund.

Um die Abhängigkeit seismoelektrischer Signale vom spezifischen elektrischen Widerstand zu untersuchen, werden VSP-Messungen (vertikales seismisches Profil) und VSEP-Messungen (vertikales seismoelektrisches Profil) mit Bohrlochgeoelektrikmessungen verglichen. Die seismoelektrischen Amplituden (normiert relativ zu den seismischen Amplituden) hängen stark vom pH-Wert ab, jedoch nicht bzw. nur schwach von der Dipollänge oder vom spezifischen elektrischen Widerstand.

Hodogrammanalysen von Dreikomponenten-Seismoelektrikdaten machen deutlich, dass die Polarisation der Signale hauptsächlich den theoretischen Vorhersagen folgt. Die konvertierten Signale sind auf den Vertikal- und Radialkomponenten am klarsten zu erkennen. Ihre Amplitudenverhältnisse relativ zueinander können durch die Annahme einer destruktiven Interferenz zwischen konvertierten Signalen von Schichtgrenzen in 4 m und 5 m Tiefe erklärt werden. Die konvertierten Signale erscheinen auch auf der Transversalkomponente, vermutlich verursacht durch ein Einfallen der Schichten.

Trotz des Fortschritts in seismoelektrischer Feldtechnik in den letzten Jahren besteht weiterhin eine Vielzahl von Problemen. Diese Arbeit liefert einen Beitrag zur Einschätzung der seismoelektrischen Methode in oberflächennahen geophysikalischen Untersuchungen.

Contents

| | | |
|----------|--|-----------|
| 1 | Introduction | 4 |
| 1.1 | Theoretical background | 5 |
| 1.1.1 | Seismoelectric wave types | 6 |
| 1.1.1.1 | Coseismic waves | 6 |
| 1.1.1.2 | Converted signals | 8 |
| 1.1.1.3 | Experimental evidence | 9 |
| 1.1.2 | The constitutive equations | 9 |
| 1.2 | History of seismoelectric field measurements | 12 |
| 1.3 | Hopes and expectations on the seismoelectric method | 12 |
| 1.3.1 | Sensitivity analysis | 13 |
| 1.3.2 | Possible areas of application of the seismoelectric method | 14 |
| 1.3.2.1 | Low-velocity layers | 14 |
| 1.3.2.2 | Thin layers | 14 |
| 1.3.2.3 | Detection of layers invisible to seismics | 15 |
| 1.3.2.4 | Salinity contrasts | 15 |
| 1.3.2.5 | Other possible applications | 15 |
| 1.4 | Conclusions | 16 |
| 2 | Seismoelectric field measurement technique | 17 |
| 2.1 | Introduction | 17 |
| 2.2 | Measurement components | 17 |
| 2.2.1 | Seismic sources | 18 |
| 2.2.1.1 | Sledgehammer | 19 |
| 2.2.1.2 | Sissy | 20 |
| 2.2.1.3 | Accelerated weight drop | 22 |
| 2.2.2 | Trigger mechanism and ground plate | 24 |
| 2.2.2.1 | Short-circuit trigger | 24 |
| 2.2.2.2 | Accelerator trigger | 24 |
| 2.2.2.3 | Comparison of the different trigger mechanisms | 26 |
| 2.2.2.4 | Aspects of measurement convenience | 31 |
| 2.2.2.5 | Comparison with manual trigger | 31 |
| 2.2.3 | Dipoles | 33 |
| 2.2.3.1 | Dipole length | 33 |
| 2.2.3.2 | Electrode types | 35 |
| 2.2.3.3 | How to place the dipoles | 35 |
| 2.2.4 | Preamplifiers | 35 |
| 2.3 | Problems with anthropogenic noise | 36 |

| | | |
|----------|--|-----------|
| 2.4 | The role of seismics | 36 |
| 2.4.1 | Identification of the seismoelectric events | 37 |
| 2.4.2 | Interpretation of the ground structure | 37 |
| 2.4.3 | Possible importance in filtering the coseismic waves | 37 |
| 2.4.4 | Contamination of seismoelectric records with geophone signals | 38 |
| 2.4.5 | Three-component seismics | 38 |
| 2.5 | Special configurations | 39 |
| 2.5.1 | Three-component seismoelectrics | 39 |
| 2.5.2 | Moving source technique | 41 |
| 2.5.3 | Vertical seismic and seismoelectric profiling | 43 |
| 2.6 | Future improvements in field technique | 43 |
| 2.7 | Conclusions | 45 |
| 3 | Identification and check of assumed converted seismoelectric events | 46 |
| 3.1 | Field setup | 46 |
| 3.2 | Acquired data | 47 |
| 3.3 | Processing | 49 |
| 3.4 | The seismoelectric checklist | 52 |
| 3.4.1 | Comparison with seismics | 52 |
| 3.4.2 | Confirmation of the filter results by other methods | 53 |
| 3.4.3 | Amplitude distribution | 54 |
| 3.4.4 | Repeatability | 57 |
| 3.4.5 | Converted signals on the transverse component | 59 |
| 3.5 | Conclusions | 59 |
| 4 | Seismoelectric measurements in different environments | 60 |
| 4.1 | Overview | 60 |
| 4.2 | Measurement sites | 61 |
| 4.3 | Fuhrberg | 65 |
| 4.3.1 | Geological setting - clearing site | 67 |
| 4.3.2 | Data and interpretation - clearing site | 67 |
| 4.3.2.1 | Geoelectrics | 67 |
| 4.3.2.2 | Seismoelectrics and seismics | 68 |
| 4.3.3 | Geological setting - waterworks site | 70 |
| 4.3.4 | Data and interpretation - waterworks site | 71 |
| 4.3.5 | Unified interpretation | 71 |
| 4.4 | Menzlin | 73 |
| 4.4.1 | Geometrical, geographical and geological setting | 73 |
| 4.4.2 | Determination of the ground structure - GPR | 73 |
| 4.4.3 | Determination of the ground structure - refraction seismics | 76 |
| 4.4.4 | Seismoelectric profiles | 77 |
| 4.4.5 | Extracting converted seismoelectric signals | 77 |
| 4.4.5.1 | Polarity flip | 78 |
| 4.4.5.2 | Velocity | 78 |
| 4.4.5.3 | Amplitude distribution | 78 |
| 4.4.5.4 | Arrival times / check with other methods | 81 |
| 4.4.6 | Conclusions | 82 |
| 4.5 | Selinunte/Sicily | 84 |

| | | |
|----------|--|------------|
| 4.6 | Segeberg Forest | 87 |
| 4.6.1 | Description of the site | 87 |
| 4.6.2 | Data | 92 |
| 4.6.2.1 | Borehole | 92 |
| 4.6.2.2 | Surface | 95 |
| 4.6.3 | Unified interpretation (borehole and surface) | 102 |
| 4.7 | GeoModel | 103 |
| 4.7.1 | Description | 103 |
| 4.7.2 | In front of the GeoModel | 107 |
| 4.7.3 | Unified interpretation | 112 |
| 4.8 | Comparison of the results from the different locations | 112 |
| 5 | Towards quantitative seismoelectrics | 118 |
| 5.1 | Introduction | 118 |
| 5.2 | Combined VSP, VSEP, and geoelectrics | 118 |
| 5.3 | Conclusions | 125 |
| 6 | Three-component seismoelectrics and polarisation | 127 |
| 6.1 | Polarization analysis | 127 |
| 6.1.1 | Introduction | 127 |
| 6.1.2 | Analysis | 127 |
| 6.1.3 | Hodogram analysis | 128 |
| 6.1.4 | Thin layer approach | 132 |
| 6.1.5 | Anisotropy | 134 |
| 6.1.6 | Conclusions | 135 |
| 6.2 | Calculation of seismoelectric potentials | 135 |
| 7 | Conclusions and outlook | 139 |
| 7.1 | Conclusions | 139 |
| 7.2 | Outlook | 144 |

Chapter 1

Introduction

“Because of overpopulation in many regions of the world, mass consumption and water pollution, the availability of drinking water per capita is inadequate and shrinking as of the year 2006. [...] UNESCO’s World Water Development Report (WWDR, 2003) from its World Water Assessment Program indicates that, in the next 20 years, the quantity of water available to everyone is predicted to decrease by 30%. 40% of the world’s inhabitants currently have insufficient fresh water for minimal hygiene. More than 2.2 million people died in 2000 from diseases related to the consumption of contaminated water or drought. In 2004, the UK charity WaterAid reported that a child dies every 15 seconds due to easily preventable water-related diseases.”

The need of water for humankind is evident from the preceding lines taken from Wikipedia, the free internet-based encyclopedia (20. September 2006)¹.

While the main problem can only be solved by a just distribution of water and a decrease of water wasting, it is also clear that geophysical techniques for groundwater exploration will receive more attention in the future. One of the main problems in this context is the determination of porosity and permeability. These quantities are needed to quantify flow rate and amount of groundwater in aquifers but they are hard to obtain with traditional geophysical techniques. It has been observed that seismic compressional waves cause weak electric signals (so-called seismoelectric signals) and that these signals depend on pore space and geometry which in turn are described by the quantities porosity and permeability. The seismoelectric method has therefore been proposed as a means to determine these quantities.

Although more and more working groups worldwide carry out research into the seismoelectric effect, the method is anything but widely used. Thus it is natural that quite some questions remain unanswered in seismoelectrics, especially seismoelectric field measurements:

- Is the seismoelectric method suitable for hydrogeophysics measurements?
- Can the signal of interest (converted seismoelectric signals) always be detected?

¹<http://en.wikipedia.org>

- Which conditions are most favorable? Which are not?
- Why are some conditions less favorable than others?
- What is the potential area of application of this method?

The focus of this thesis is not on theoretical developments or data processing perfection but on measurements to provide an oversight of the possible usage of the seismoelectric method in the real world. I will not try to determine actual quantities from seismoelectric data but try to render possible reliable seismoelectric measurements. All examples are from the shallow subsurface. The focus is more on groundwater and not on petroleum exploration in the domain of which seismoelectrics also has been proposed.

One of the main parameters controlling seismoelectric signals is the electrokinetic coupling coefficient which does not influence seismic waves at all. Thus, extra information could be gained with the help of seismoelectric measurements. The electrokinetic coupling coefficient in turn depends on parameters associated with fluid movement as porosity, pore fluid viscosity, and pore fluid resistivity amongst others. Hence the seismoelectric method could possibly be used in hydrogeophysics. Garambois & Dietrich (2002) showed that the converted seismoelectric field indeed is strongly sensitive on permeability contrasts.

A surge in seismoelectric publications is noticeable in the past few years. However, there have been very few publications on seismoelectric field data (Garambois & Dietrich, 2001; Kepic & Rosid, 2004, e.g.). It seems that although the seismoelectric method becomes more and more elucidated in terms of theoretical and numerical aspects, the difficulties that are connected with seismoelectric field measurements still prevent this method from being used in a larger scale. The scope of this thesis is therefore to shed some light on the possibilities and difficulties as well as on the advantages and disadvantages that come with seismoelectric field measurements. I survey the circumstances under which seismoelectric field measurements could be successful or problematic and suggest possible remedies.

This thesis is organized as follows: In this **first chapter** the method is presented and a theoretical and historical introduction is given, as well as possible areas of application for seismoelectric measurements. The **second chapter** contains a detailed description of seismoelectric field measurement techniques which in the **third chapter** is followed by a guideline how to identify and verify assumed converted seismoelectric signals in a data set. The **fourth chapter** comprises the main part of this thesis: A comparison of seismoelectric data on several different soils and measurement sites. Temporal and spacial variations of seismoelectric data quality will be shown and interpreted. Then I will depart on the way towards quantitative seismoelectrics in the **fifth chapter** which will be followed by an analysis of three-component seismoelectric data in terms of relative amplitude and polarization in the **sixth chapter**. Conclusions and an outlook complete the thesis in the **seventh chapter**.

1.1 Theoretical background

Seismoelectric effects emerge when seismic and electromagnetic energies are coupled. I will analyze only one of several possible couplings, in which seismic energy is partly converted to electro(magnetic) energy. The name of this effect varies in literature: Haartsen & Pride (1997) use the

term electroseismic while Haines (2004) uses the term seismoelectric, whereas others again (Beamish, 1999) refer to this effect as electrokinetic coupling. I chose the term seismoelectrics as it describes that seismic energy is converted to electric and electromagnetic energy. Garambois & Dietrich (2002) use the term seismoelectromagnetic which from a physics point of view is the most correct one. I prefer the term seismoelectrics since we only measure the electric component of the signal.

The other possible direction of coupling (what I call electroseismic) is the generation of seismic signals by injection of electromagnetic energy into the ground. Both theoretical and numerical studies appeared recently (Thompson et al., 2005; White, 2005). The name of the effect causing this conversion is electroosmosis. There are many more possible couplings of mechanical-electrical and electrical-mechanical energy (see, e.g., Santamarina & Fratta, 2003).

The seismoelectric effect is connected with Biot theory describing the propagation of seismic waves in saturated porous material (Biot, 1956). As Pride & Haartsen (1996) point out, there is (yet) no way to explain seismoelectric phenomena without using Biot theory which means that seismoelectric measurements are one of the most important proofs of the Biot theory.

1.1.1 Seismoelectric wave types

An electrokinetic origin of seismoelectric signals is generally assumed (e.g. Pride, 1994; Haartsen & Pride, 1997). Two types of seismoelectric waves, named coseismic and converted in the following, are predicted by theory and can also be detected in the field (see figure 1.1).

1.1.1.1 Coseismic waves

Most minerals have a net surface charge. As a consequence, in porous media saturated by an electrolyte, an *electric double layer* develops at the boundary between rock matrix and pore fluid, consisting of a layer of immobile charges at the grain surface and a diffuse counter charge layer in the pore fluid. Part of the diffuse counter layer is free to move with the pore fluid when a relative motion between rock matrix and pore space occurs, generating the so-called streaming current. The electrical potential at the shear plane of this diffuse counter layer is called the ζ (zeta) potential (see figure 1.2). When a seismic compressional wave passes such a medium, local compression and extension of the pore space causes excess of ions in the dilated parts of the medium and deficiency of ions in the compressed parts and thus an electric field. This field in turn provokes a conduction current which cancels out the streaming current in homogeneous media, i.e. no net current occurs and no independently propagating electromagnetic waves are generated. The amount of charge separation is fixed by the resistivity which means that high resistive media can be expected to yield higher seismoelectric amplitudes. The electric field is confined to the seismic wave (e.g. Haartsen & Pride, 1997). Garambois & Dietrich (2001) showed that the amplitude of this electric field is proportional to the particle acceleration caused by the P-wave (first time derivative of the appropriate part of the seismic traces). Hence these coseismic waves should be polarized perpendicular to the front of the P-wave time derivative. As will be seen later, the similarities between the seismoelectric section and the time derivative of the seismic section are obvious.

Since surface waves (e.g. Rayleigh waves) contain a compressional part, also these waves should

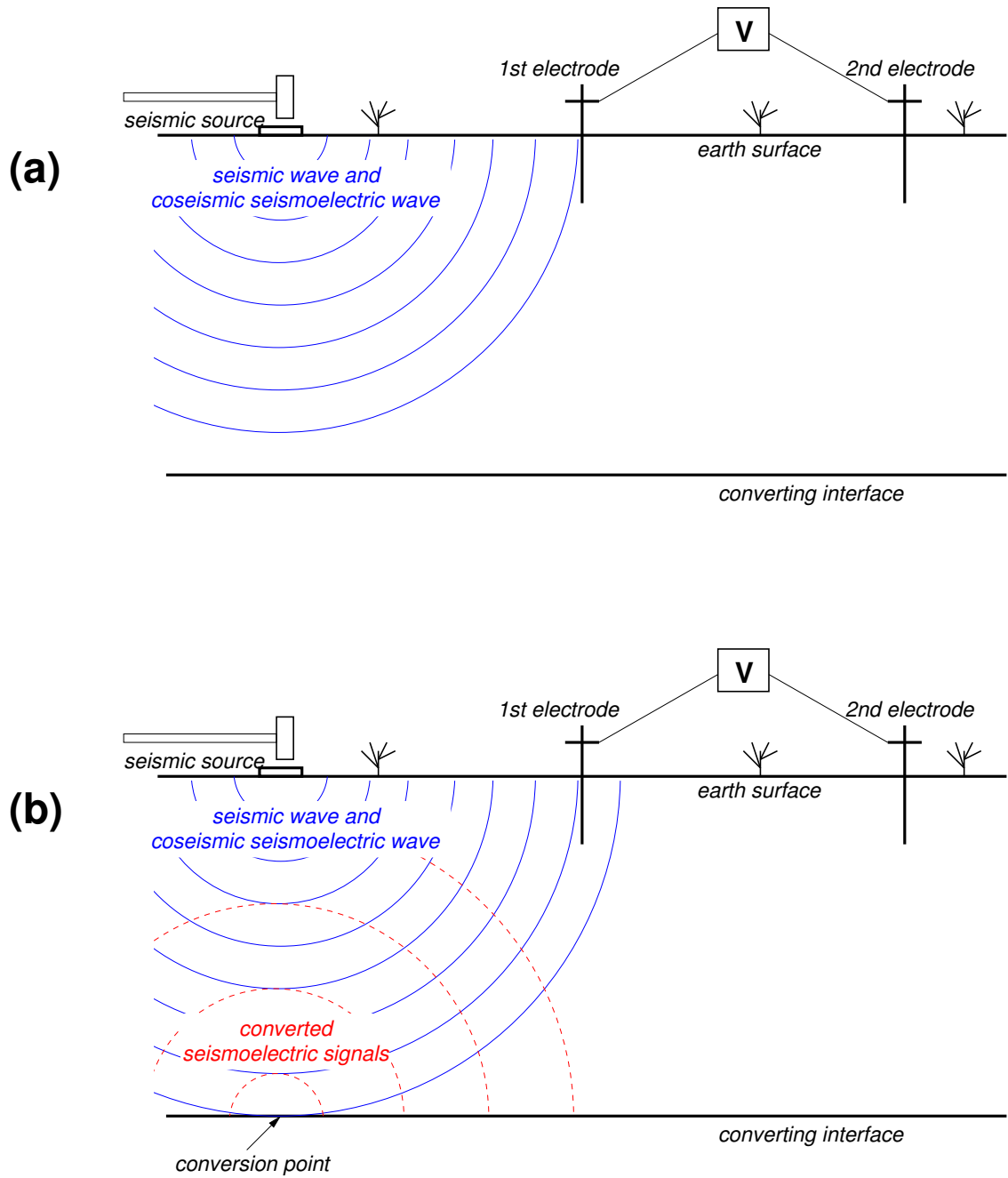


Figure 1.1: The two seismoelectric wave types. (a) Before the seismic wave traverses the interface, the only seismoelectric signals are those accompanying the seismic P-wave in saturated porous media. (b) After the seismic wave traverses the interface, converted seismoelectric signals are created which travel with electromagnetic velocity. The measurement technique is described in chapter 2.

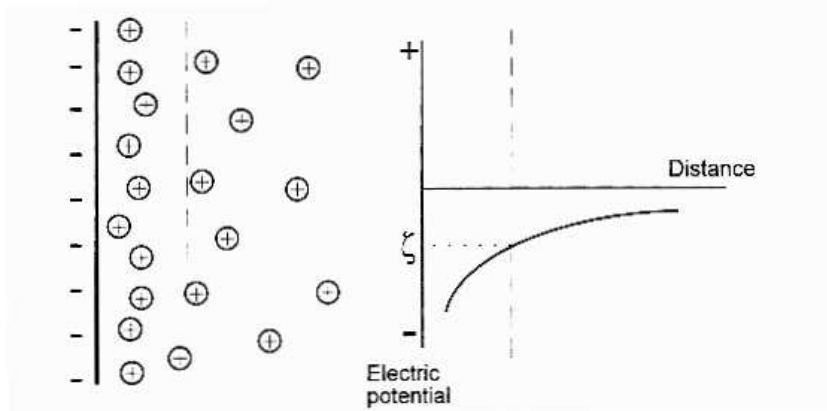


Figure 1.2: The electric double layer (left) with the rock matrix to the left and the pore fluid to the right. The dashed line represent the plane of shear. Right: The potential distribution across the electric double layer and the ζ -potential. Taken from Friborg (1996).

cause seismoelectric waves. While ground roll often dominates the later parts of the seismogram or its small offset areas, I discovered that it is usually much weaker on the seismoelectrogram. The same was detected by others before (e.g. Beamish, 1999) and probably reflects the fact that the compressive part of the Rayleigh wave is rather weak compared to its shear component.

1.1.1.2 Converted signals

These waves with an approximately infinite apparent velocity have their origin in the subsurface at boundaries separating layers of different elastic, electric or hydrological properties (e.g. Haartsen & Pride, 1997). Such interfaces may be represented by the groundwater table or within an aquifer by boundaries separating zones of different porosity, permeability or even salinity.

Due to the different hydraulic properties of the media on both sides of the boundary, the streaming currents are disrupted at the interface and the streaming current and the conduction current do not cancel out (Haartsen & Pride, 1997). Incident seismic waves can thus cause an unbalanced charge separation acting as a source of an electromagnetic wave. In analogy to PS-wave conversion at seismic interfaces, these “type-II” seismoelectric waves can be regarded as being “converted” from the incident P-wave. They travel independently from the seismic wave with electromagnetic wave velocity. They have the same frequency content as the incident seismic wave at the boundary causing the conversion, so the wavelength of the converted seismoelectric signals is much longer than the distance to the receivers, at least for near surface applications. It might therefore be more suitable to talk about a converted field rather than about a converted wave. At these low frequencies, electric and magnetic fields are decoupled to a large extent and thus have to be treated separately (Mikhailov et al., 2000). As we solely measure the electric field, the magnetic field will be ignored in the following.

Traveling downward from the source to the interface with seismic velocity and upward to the receivers with electromagnetic velocity, these converted signals appear at close to seismic one-way travel time in seismoelectrograms and usually have much lower amplitudes than coseismic signals. Haartsen & Pride (1997) have shown that the source of the converted signals is a multipole field with

a strong vertical dipole component centered below the seismic shot point in case of plane horizontal layering. Therefore to first order, the polarization of the converted seismoelectric waves observed at the earth surface can be expected to follow the field lines of an electric dipole source. However, it may be deformed by heterogeneities of the electrical conductivity and by interfering multipole components if the converting horizon is rather shallow.

1.1.1.3 Experimental evidence

Convincing experimental evidence for these types of waves has been presented, for example, by Mikhailov et al. (2000) and Garambois & Dietrich (2001). Most of the published seismoelectric field measurements could be explained, at least qualitatively, with the Biot type theory published by Pride (1994), Pride & Haartsen (1996), and Haartsen & Pride (1997) defining a dependence of seismoelectric fields on hydrological parameters among others. As the coseismic signals depend mainly on local properties close to the electrodes, seismoelectric prospecting will usually be based on converted seismoelectric signals or on borehole measurements (see Mikhailov et al., 2000) although special applications for the upper decimeters of the soil are imaginable. Therefore the feasibility of applying surface seismoelectrics for hydrological exploration depends critically on recording converted seismoelectric signals. Unfortunately, these are typically much weaker in amplitude than coseismic waves and thus more difficult to observe.

In addition to the seismoelectric fields, also seismomagnetic fields are created. Recent outcomes prove that the detection of those fields, albeit intricate, is possible (Zhu & Toksöz, 2005; Bordes et al., 2006). However, I will limit myself to the seismoelectric fields in this thesis.

1.1.2 The constitutive equations

Assuming an $e^{-i\omega t}$ time dependence and using volume-averaging, Pride (1994) obtained the following governing equations for seismoelectric signals

$$\nabla \cdot \boldsymbol{\tau} = -\omega^2 [\rho \mathbf{u} + \rho_f \mathbf{w}] + \mathbf{F} \quad (1.1)$$

$$\boldsymbol{\tau} = [K_G \nabla \cdot \mathbf{u} + C \nabla \cdot \mathbf{w}] \mathbf{I} + G \left[\nabla \mathbf{u} + \nabla \mathbf{u}^T - \frac{2}{3} \nabla \cdot \mathbf{u} \mathbf{I} \right] \quad (1.2)$$

$$-P = C \nabla \cdot \mathbf{u} + M \nabla \cdot \mathbf{w} \quad (1.3)$$

$$-i\omega \mathbf{w} = \frac{k}{\eta} [-\nabla P + \omega^2 \rho_f \mathbf{u} + \mathbf{f}] + L \mathbf{E} \quad (1.4)$$

$$\mathbf{J} = L [-\nabla P + \omega^2 \rho_f \mathbf{u} + \mathbf{f}] + \sigma \mathbf{E} \quad (1.5)$$

$$\nabla \times \mathbf{E} = i\omega \mathbf{B} - \mathbf{M} \quad (1.6)$$

$$\nabla \times \mathbf{H} = -i\omega \mathbf{D} + \mathbf{J} + \mathbf{C} \quad (1.7)$$

$$\mathbf{D} = \epsilon \mathbf{E} \quad (1.8)$$

$$\mathbf{B} = \mu \mathbf{H} \quad (1.9)$$

With

| | |
|----------------|--|
| τ | bulk-stress tensor |
| ω | radial frequency |
| ρ | bulk density |
| \mathbf{u} | average displacement of the solid grains |
| ρ_f | pore fluid density |
| \mathbf{w} | average relative fluid-solid displacement multiplied by porosity |
| \mathbf{F} | an applied body-force acting on the bulk material |
| K_G | Gassmann's bulk modulus |
| C | a coefficient |
| \mathbf{I} | identity matrix |
| G | stiffness |
| \mathbf{u}^T | \mathbf{u} transposed |
| P | pore fluid pressure |
| M | a coefficient |
| k | dynamic permeability |
| η | pore fluid viscosity |
| \mathbf{f} | an applied body-force acting on the fluid-phases |
| L | electrokinetic coupling coefficient |
| \mathbf{E} | electric field |
| \mathbf{J} | electric current density |
| σ | electrical conductivity |
| \mathbf{B} | magnetic flux density |
| \mathbf{M} | an applied magnetic-current source |
| \mathbf{H} | magnetic field |
| \mathbf{D} | dielectric displacement |
| \mathbf{C} | an applied current-density source |
| ϵ | electrical permittivity |
| μ | magnetic permeability. |

The coefficients K_G , C and M are defined in e.g. Pride (1994). $\sigma(\omega)$, $k(\omega)$, and $L(\omega)$ are complex and frequency-dependent.

Equations 1.1-1.4 describe the seismic wavefield and equations 1.5-1.9 the electromagnetic one. Equations 1.1-1.3 are the Biot equations (e.g. Biot, 1962) for a saturated porous medium, and equations 1.6-1.9 are the well-known Maxwell equations. The transport equations 1.4 and 1.5 specify the coupling between the seismic and the electromagnetic fields. The first term on the right hand side in equation 1.5 represents the share of the streaming current, while the second term represents the one of the conduction current. Equation 1.4 is a combination of Darcy's law (first term on the right hand side) and the part of the fluid flow caused by the electric field (electroosmosis, second term) (Haartsen & Pride, 1997).

Pride (1994) defines $k(\omega)$, $\sigma(\omega)$, and $L(\omega)$ as a product of a static coefficient and a frequency-dependent function:

$$\frac{k(\omega)}{k_0} = \left(\sqrt{1 - i \frac{\omega}{\omega_t} \frac{4}{m}} - i \frac{\omega}{\omega_t} \right)^{-1} \quad (1.10)$$

$$\frac{L(\omega)}{L_0} = \left[1 - i \frac{\omega}{\omega_t} \frac{4}{m} \left(1 - 2 \frac{\tilde{d}}{\Lambda} \right)^2 \left(1 - i^{(3/2)} \tilde{d} \sqrt{\frac{\omega \rho_f}{\eta}} \right)^2 \right]^{-\frac{1}{2}} \quad (1.11)$$

$$\sigma(\omega) = \frac{\phi \sigma_f}{\alpha_\infty} \left[1 + \frac{2[C_{em} + C_{os}(\omega)]}{\sigma_f \Lambda} \right] \quad (1.12)$$

where

$$L_0 = -\frac{\phi}{\alpha_\infty} \frac{\epsilon_0 \epsilon_f \zeta}{\eta} \left(1 - 2 \frac{\tilde{d}}{\Lambda} \right) \quad (1.13)$$

and $\tilde{d} \leq d$ with d being the Debye length (a measure of the thickness of the diffuse double layer which was explained in section 1.1.1.1), the parameter Λ is a weighted volume-to-surface ratio of the pore space (e.g. Garambois & Dietrich, 2001), ϕ : porosity, α_∞ : tortuosity, C_{em} is the excess conductance associated with the electromigration of double layer ions, and C_{os} the conductance due to electrically induced streaming (convection) of the excess double-layer ions, ϵ_0 the vacuum permittivity, ϵ_f the dielectric permittivity of the pore fluid, and ζ the zeta potential. The parameter m is defined as

$$m = \frac{\phi \Lambda^2}{\alpha_\infty k_0} \quad (1.14)$$

An important parameter in $k(\omega)$, $\sigma(\omega)$, and $L(\omega)$ is the transition frequency

$$\omega_t = \frac{\phi \eta}{\alpha_\infty k_0 \rho_f}, \quad (1.15)$$

separating the lower frequency domain, in which viscous flow dominates, from the higher frequency domain, in which inertial flow dominates. While there is (yet) no way to describe seismoelectrics without Biot theory, it should be noted that the equations of seismoelectricity based on Biot's equations are

- not totally correct, because Biot's equations are not totally correct in all aspects. Dvorkin et al. (1994), e.g., state that the Biot mechanism alone cannot explain observed velocity dispersions and attenuation.
- not complete as the Biot theory only describes a two-phase medium (Biot, 1962; Pride, 1994). Biot theory assumes full saturation of the pores with a pore liquid. However, Beamish (1999), Santamarina & Fratta (2003), Haines (2004) as well as my own results point out that even a partial saturation of the pores is sufficient to produce the described seismoelectric effects.

No alternative seismoelectric theory has been formulated so far and it therefore remains to see if all experimentally derived findings support the current theory.

1.2 History of seismoelectric field measurements

Experimental evidence of the seismoelectric effect has come up as early as in the 1930's (Thompson, 1936; Ivanov, 1939). Martner & Sparks (1959) detected converted seismoelectric signals for the first time. Since then a limited number of publications on seismoelectrics have appeared dealing with its theoretical and practical aspects and with its possible application to hydrogeological and other problems. The state of the art of seismoelectric prospecting was reviewed by Beamish & Peart (1998). A comprehensive overview of the most important seismoelectric publications can be found in Fourie (2003). In the 1990's the (small) surge of seismoelectrics started, in the beginning also considering other mechanisms than electrokinetic coupling, e.g. strongly non-linear conversions from sulphide ore bodies (Maxwell et al., 1992). Works on how to cope with the strong noise (e.g. Butler & Russel, 1993) and finally a theory for the observed phenomena (starting with Pride, 1994) triggered more and more field measurements. During the last 10 - 15 years improved instrumentation and computing facilities provided a lot of progress in gathering reliable field data and modeling:

- Thompson & Gist (1993) record converted seismoelectric signals from depths of up to than 300 m by using explosives as source.
- Butler et al. (1996) map a shallow boundary with sledgehammer-seismoelectrics.
- Beamish (1999) published studies of how electrode placement and dipole length influence seismoelectric data.
- Mikhailov et al. (2000) prove that seismoelectrics in boreholes have a great potential to characterize permeable zones and determine porosity by normalizing seismoelectric with seismic amplitudes.
- Garambois & Dietrich (2001) show some data examples and prove that the coseismic field is proportional to the grain acceleration.

Nevertheless, many fundamental questions concerning the origin and structure of seismoelectric signals are still unsolved.

1.3 Hopes and expectations on the seismoelectric method

The expectations often exceed the possibilities that hydrogeophysics provide. This is even more the case in methods that are far from being fully explored and investigated into such as the seismoelectric method. Unfortunately there is often a significant mismatch between field reality and theoretical results. Interestingly, Santamarina & Fratta (2003) report that amplitudes in field are up to a factor of 1000 stronger than predicted by theory and high frequency laboratory measurements. So it seems that there are still numerous open questions to be answered.

1.3.1 Sensitivity analysis

From a theoretical and numerical point of view, the potential importance of seismoelectrics in hydrogeological context is already proved by sensitivity analyses of the seismoelectric signals to some of the parameters relevant in hydrogeophysics. Garambois & Dietrich (2002) calculated some very encouraging results which are presented in figure 1.3. They varied the parameters porosity, permeability, salinity, and viscosity in the lower of two layers (one at a time with the other parameters being held constant and equal in both layers) and determined the root-mean-square electric and magnetic field amplitudes of the seismoelectric signals converted at the interface between the two layers. A confirmation of these investigations in field has not been done yet. My own research revealed that this task is not straight forward. This will be developed more in section 5.

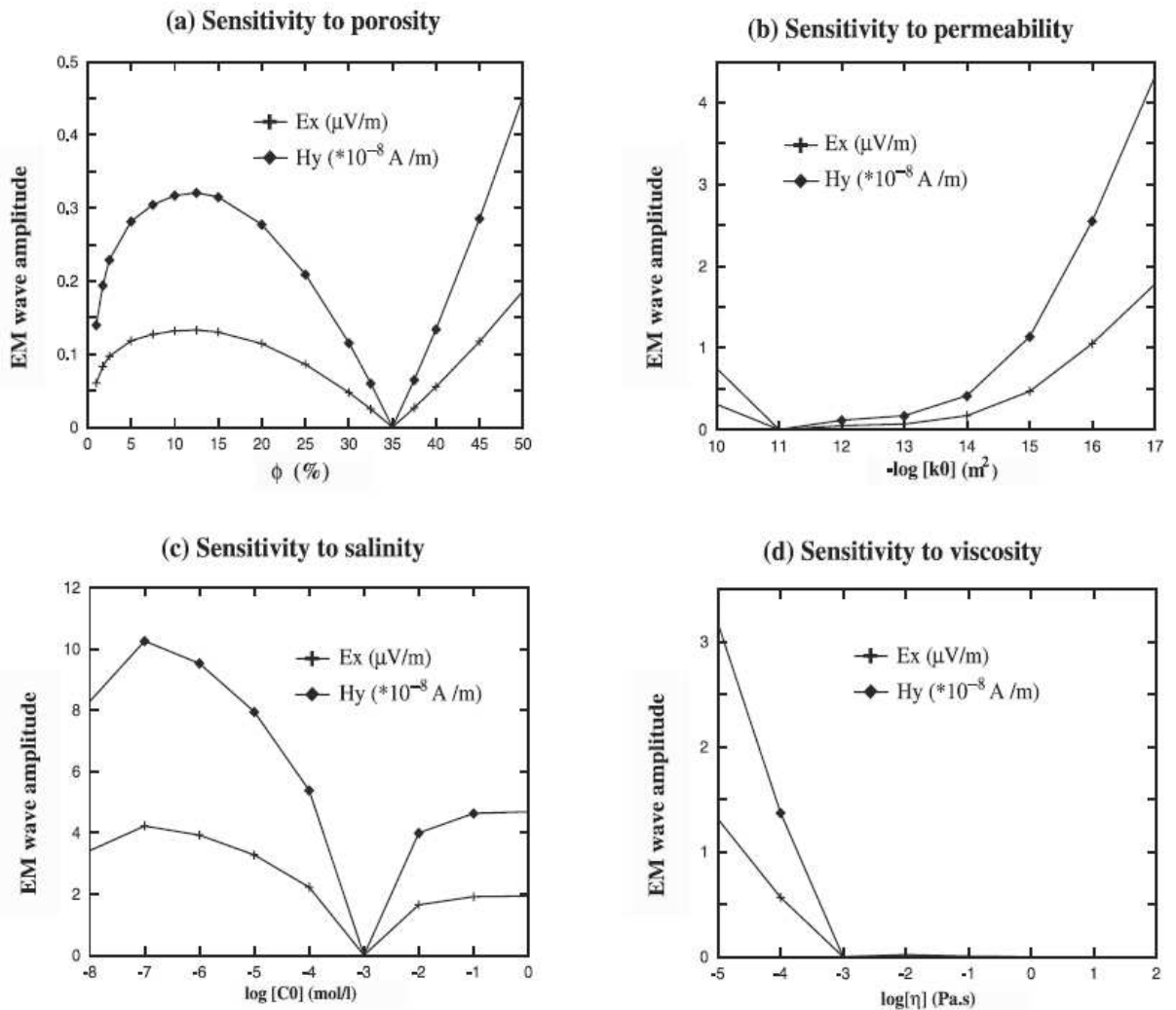


Figure 1.3: Results of a sensitivity analysis of seismoelectric and seismomagnetic signal amplitudes to contrasts in the parameters porosity, permeability, salinity, and viscosity. The respective other parameters are kept constant at porosity: 35%, permeability: 10^{-11}m^2 , salinity: 10^{-3} mol/L, and viscosity: 10^{-3}Pa s (figure taken from Garambois & Dietrich, 2002).

1.3.2 Possible areas of application of the seismoelectric method

The main motivation for seismoelectric studies is the hope of being able to determine properties important for hydrogeology that are not or not easily accessible by other methods, or only with insufficient resolution. This is definitely true for the hydraulic permeability. The scope of this work is not to provide a direct path from raw data to completely determined permeability of the investigated ground. At the present state of the art, it is rather difficult to set off to determine quantitative values with seismoelectrics, because there is a definite lack of field work experience. A necessary prerequisite is the free-from-doubt extraction of the converted seismoelectric field from a seismoelectrogram. One has to know under which conditions successful measurements can be expected. This is the focus of the thesis. The goal of approaching the quantitative determination of subsurface properties with seismoelectrics can only be reached with simultaneous research in the domain of theory, numerics, field technique, and data processing and a subsequent merging. Due to the complexity (also in a mathematical sense) of the seismoelectric theory, rule-of-thumb approximations for a quick and easy parameter determination still wait to see the day. Ideally, a seismoelectric inversion program would emerge. The first steps in this direction have been undertaken (Rañada Shaw, 2005). Without such an inversion program or at least a fast and easy-to-use modeling software, seismoelectric field measurements will probably remain in the qualitative area.

Besides these future goals, there are also other applications of the seismoelectric method already usable today which provide extra information that cannot be achieved with conventional seismic measurements. These are listed below.

1.3.2.1 Low-velocity layers

In refraction seismics, it is not possible to determine low-velocity layers (i.e. a layer that has a lower seismic velocity than the layer lying above it). This is possible with reflection seismics but usually at much higher costs. Low-velocity layers should be mappable with seismoelectrics, provided that the interface in question generates seismoelectric conversions.

1.3.2.2 Thin layers

It has been proposed that the seismoelectric method could be used in order to detect thin (relative to the seismic wavelength) layers. Haartsen & Pride (1997) mention a modeling result where a 1 m thin sand layer gave a stronger converted seismoelectric signal than its single-boundary equivalent. The layer was not visible at all in the (modeled) seismic data. However, calculations undertaken by Fourie (2003) show that such a constructive interference only occurs if the thin layer has a thickness of at least $\lambda/3$ (with λ being the seismic wavelength). With layers thinner than $\lambda/3$, the interference should rather be destructive, thus limiting the possibilities of detecting thin layers with the seismoelectric method to not so thin cases. My measurement analysis in section 6.1 indicates that it is possible to map a 1 m thin layer in 4 m depth with seismoelectrics. This layer is much thinner than $\lambda/3$.

1.3.2.3 Detection of layers invisible to seismics

Seismic reflections and refractions only occur at contrasts in seismic impedance (the product of seismic velocity and density). In the case of vertical incidence, the reflection coefficient of the reflected wave depends on the seismic impedance contrast as follows:

$$R = \frac{\rho_2 V_2 - \rho_1 V_1}{\rho_2 V_2 + \rho_1 V_1} \quad (1.16)$$

with ρ being the density, V the seismic velocity and indices 1 and 2 referring to the upper and lower layers, respectively. So one can easily think of layer boundaries that do not cause strong reflections. As has been stated before, seismoelectric conversions depend on a lot more parameters. A boundary might be seen in the seismoelectrogram although it does not leave a trace on the seismic traces. I came across such a situation at the site Menzlin, where boundaries could be mapped with GPR and seismoelectrics but not with refraction seismics (see section 4.4).

1.3.2.4 Salinity contrasts

Changes in salinity do not cause detectable changes in seismic velocity. The situation is strongly different in seismoelectrics. Numerical results by Haartsen & Pride (1997) predict large amplitudes for the converted seismoelectric field in case of a salinity contrast. The ζ -potential is very sensitive to resistivity and controls seismoelectric amplitudes via the coupling coefficient (equation 1.13).

1.3.2.5 Other possible applications

Other possible areas of application for the seismoelectric method stated in literature are

- petroleum exploration, e.g. to determine gas-water contact (Thompson & Gist, 1993)
- determining the position of cracks between boreholes (Zhu & Toksöz, 2003). Calculations indicate that this should be easier with seismoelectrics than with seismic tomography.
- exploration while drilling: vertical seismoelectric profiling for the detection of rock parameters and interfaces in advance (Haartsen & Pride, 1997)
- earthquake investigation (e.g. Khatiashvili & Perel'man, 1989; Pride et al., 2004)
- mineral exploration, especially quartz veins, sphalerite, and kimberlites (Maxwell et al., 1992)

For the near surface area, seismoelectrics is usually seen to be potentially applicable for mapping of changes in hydraulic permeability, porosity or fluid chemical properties (Wolfe et al., 1996; Haartsen & Pride, 1997; Beamish & Peart, 1998; Beamish, 1999; Mikhailov et al., 2000; Garambois & Dietrich, 2001;

Rosid & Kepic, 2004). Seismoelectrics could also be used to detect fracture zones or isolated fractures which could be important for groundwater exploration (Zhu & Toksöz, 2003). Provided that an appropriate downscaling is possible, one could even imagine possible uses of seismoelectrics in the medicinal domain.

1.4 Conclusions

There is a need for more seismoelectric field measurements to determine if the method can live up to its expectations in bringing information about aquifer characteristics, especially porosity and permeability. Despite increasing attention on the seismoelectric method, only little material on actual field measurements has been published so far. Pride (1994) derived the governing equations from first principles and thus provided a theoretical base for seismoelectrics. However, the current Biot-type theory is not valid in partly saturated or unsaturated media where nevertheless seismoelectric signals have been observed. Two main seismoelectric wave types exist, the coseismic and the converted seismoelectric signals. Coseismic waves accompany the seismic compressional waves and are restricted to these whereas converted seismoelectric signals are generated at subsurface interfaces and have the potential to provide information about these interfaces. Since the generation of seismoelectric signals is connected with pore space and pore geometry, there is hope for the method to be used in hydrogeophysics. The focus of this work is on establishing a solid ground for the measurements and not on actually deriving quantitative values from seismoelectric data. A number of possible applications such as the detection of layers invisible for seismics is thinkable already now and will partly be dealt with in the following chapters. Yet, all these conceivable applications critically depend on whether and under which circumstances seismoelectric signals can be measured.

Chapter 2

Seismoelectric field measurement technique

2.1 Introduction

As the name seismoelectric indicates, the field technique comprises elements from seismic as well as from geoelectric measurements. This means that hardly any new equipment needs to be purchased if seismic and geoelectric equipment is available. One needs to be aware though, that greater care has to be taken to prevent noise during seismoelectric measurements than is usually required in seismics or geoelectrics. The role and choice of the components used in a typical seismoelectric survey are explained in the following section 2.2, after which the main problems in seismoelectric measurements are dealt with in section 2.3. The role of seismics is explained in the next section (2.4). Very often, seismoelectric field measurements are not restricted to a simple standard surface profile. Section 2.5 presents the special configurations used most often in this thesis: Three-component seismoelectrics, the moving source technique and vertical seismoelectric profiling. In the final section 2.6 of this chapter, ideas for possible improvements are developed. In addition to seismoelectrics measurements, also refraction seismic, geoelectric and ground penetrating radar (GPR) measurements were carried out. The application of these methods in hydrogeophysics is described in Kirsch (2006) among others.

2.2 Measurement components

A typical seismoelectric field setup is shown in figure 2.1: The hammer hits the ground plate and creates seismic waves. A part of the seismic waves is transformed into seismoelectric signals as explained in section 1.1.1 which are then picked up by the dipoles. Preamplifiers amplify the signals which are finally lead to the seismograph via a seismic acquisition cable.

In seismoelectric field measurements the electromagnetic noise level can be quite high relative to the signal of interest. It is recommend to be very careful so that the equipment involved in the measurements does not cause additional electromagnetic noise itself. A cable e.g. lying on wet ground and used in a 220 V circuit caused strong electromagnetic noise in one of our measurements. It is

clear that the choice of the seismic source, the trigger mechanism, the dipoles, and the preamplifiers should be made with care. This will be analyzed in the following sections.

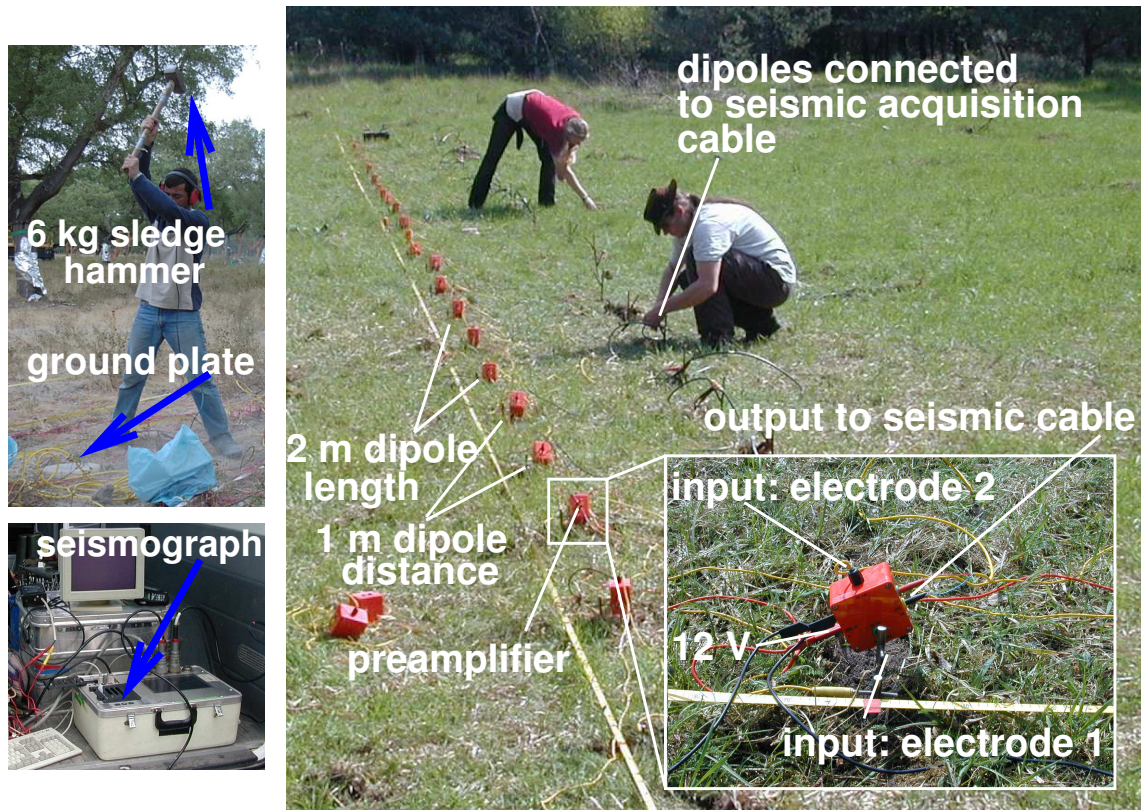


Figure 2.1: Field setup for seismoelectric measurements: The hammer hits the ground plate and the seismoelectric signals are picked up by a profile of dipoles with a length of 2 m (distance between the two electrodes of one dipole) and a dipole distance of 1 m. A preamplifier is placed at each dipole. One of the preamplifiers is shown in detail. The cables are connected to a 48 channel seismograph. Variations occur depending on the target of the measurements and the environment of the location.

2.2.1 Seismic sources

Since we aim to generate seismic waves, the source is the same as used in standard seismic measurements, i.e. the source type depends on the desired depth of interest. The investigations presented in this work are all near surface applications which is why we used the three following seismic sources: sledgehammer, Sissy, and accelerated weight drop. Although the last one is most often also used for deeper targets. For seismoelectric applications, one has to ensure that the source only generates seismic waves and not strong electromagnetic noise. Furthermore one should be aware that the signal-to-noise ratio is typically much weaker for seismoelectric than for seismic data so stronger sources could be helpful.

2.2.1.1 Sledgehammer

The most often used type of source in our experiments was a 6 kg sledgehammer hitting a metal ground plate as shown in figure 2.1. The hammer has the advantage of being easy to use and very reliable, since there is no electronic black box involved. It is easy to transport and can therefore also be used in dense forest or places hard to access. Under favorable conditions and with a desired depth of investigation of not more than some meters, a hammer is a fully suitable seismic source. Unless indicated otherwise, the data in this thesis were collected with a sledgehammer as seismic source.

It has the disadvantage though that operating the hammer the whole day is quite tiring, and the source is also limited in its strength. For seismoelectrics it seems that in some cases, a hammer is not strong enough if one restricts oneself to a sensible number of stacks (see section 4.7). Some authors report seismoelectric measurements with more than 100 stacks (Garambois & Dietrich, 2001).

A possible source of noise is the seismic source itself. When using a sledgehammer as seismic source, no electricity is involved in the source mechanism which is advantageous for seismoelectrics. In figure 2.2, I display a manually triggered seismoelectrogram with the time axis extending to negative times, corresponding to the time before hammer impact at 0 ms. I filtered all data in this thesis with a broad zero-phase bandpass filter (5 Hz - 500 Hz) with generous tapers (sine squared) at the ends. For visualization purposes I scaled the data with *automatic gain control* (agc): Each sample of each trace is divided by the rms value of the time window surrounding the sample. In some other data I normalize the traces, i.e. divide each trace with its rms (root mean square) value. As can be seen, there are no arrivals directly or very close to 0 ms, i.e. the sledgehammer does not influence the seismoelectric data.

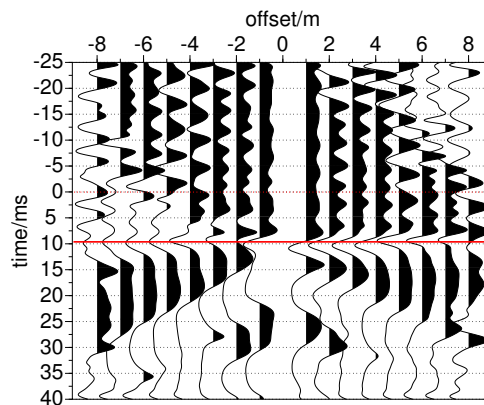


Figure 2.2: Seismoelectric data with agc from Fuhrberg Forest, September 2002, manually triggered. The hammer impact is at 0 ms (marked with a dotted line). The converted seismoelectric arrival (see section 1.1.1.2) is marked with a solid line.

2.2.1.2 Sissy

In April 2004 we conducted test measurements with the seismic source *Sissy*¹ from the *Amt für Geowissenschaftliche Gemeinschaftsaufgaben* (GGA) at the town of Neuwarmbüchen in Lower Saxony near Hanover. We express our thanks to Mr. Druivenga for providing and operating the Sissy. In spite of its name, the Sissy is a quite powerful seismic source which works with detonating compressed air cartridges. The only strenuous aspect involved with this source is that a shallow hole has to be drilled in which to place the Sissy.



Figure 2.3: Mr. Druivenga from the GGA operating the Sissy (Seismic Impulse Source System) at Neuwarmbüchen.

Stacking is in principle possible, but the source signal changes with every shot because as with every explosion, a void is created at the shot point changing the conditions for the next shot. The shot point can of course be laterally displaced instead but this also leads to slightly changed source signals. This, however, is less of a problem, as the Sissy signal is significantly stronger as a single hammer shot. Our tests even indicate that it is clearly stronger than twenty stacked hammer blows. The source is of course not directly comparable to hammer blows because the latter one is a vertical blow while the Sissy, being an explosive source, sends compression waves in all directions. Direct comparisons between hammer blow and Sissy seismoelectrics with otherwise identical measurement parameters at the site Neuwarmbüchen revealed a much better signal-to-noise ratio for the Sissy at almost every shot. One such example can be found in figure 2.4.

¹*Seismic Impulse Source System* (Wiederhold et al., 1998)

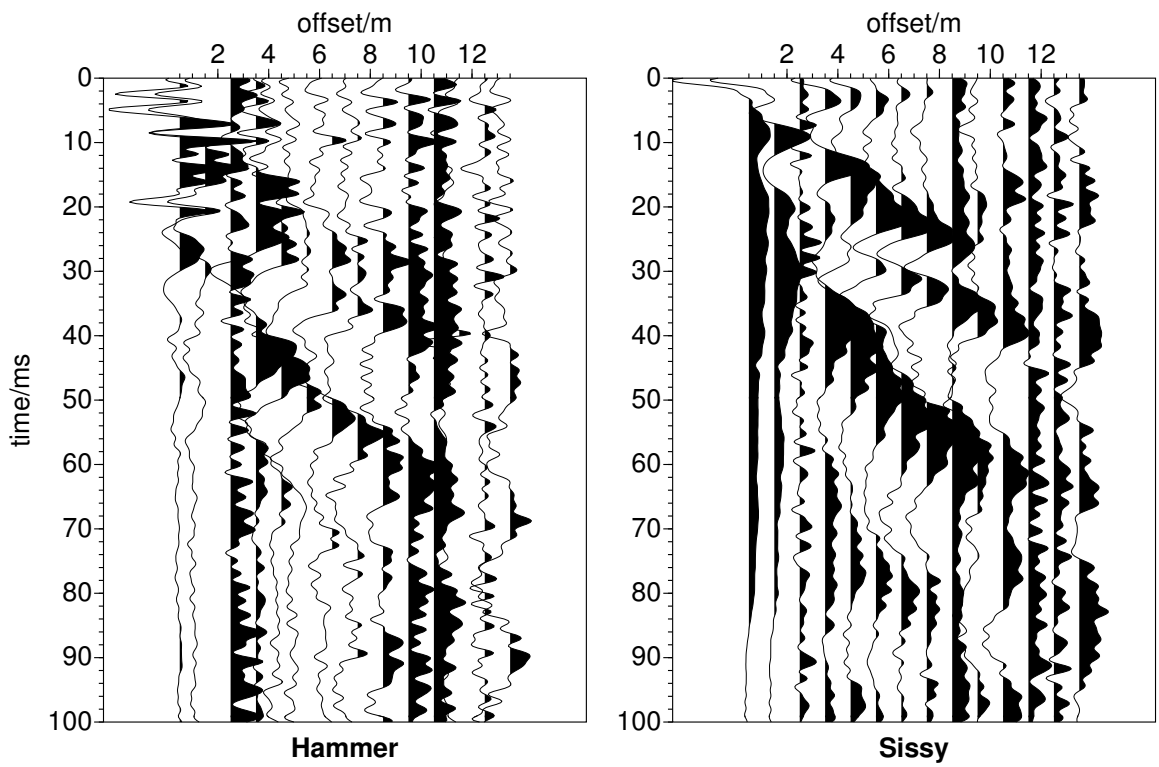


Figure 2.4: Comparison between seismoelectric traces with different sources: hammer (left) and Sissy (right). The data are trace normalized. Clearly, the Sissy traces have a much higher signal-to-noise ratio.

It can be expected that using a stronger source leads to improved signal-to-noise ratio also at other locations. This will be explored more in section 4.7. It might be possible to register the converted seismoelectric wave where it is not possible with a weak source signal such as a sledgehammer. When using a stronger source, one has to be aware that the source must not create strong trigger or other currents. The Sissy e.g. requires a trigger signal of several Amperes. Surprisingly, this did not influence the seismic traces. As we only tested the Sissy at one location, I cannot draw any conclusions if this is site-specific. Another advantage using the Sissy is the fast measurement progress and the low wear and tear of the field crew. Sissy seismoelectrics can be carried out on several consecutive days with a field crew of only two persons which is hardly possible with hammer seismoelectrics. More than 800 hammer blows per day do occur which means that this is only possible either with a numerous or a very motivated field crew (which luckily was available in my case). For longer field campaigns, the Sissy can amount to some costs which have to be taken into consideration, as every cartridge costs several Euros.

2.2.1.3 Accelerated weight drop

As I had to cope with low signal-to-noise ratio in some places, we hired an accelerated weight drop source from the company Geo-Center Nord in Quickborn for some days to evaluate its possible use for seismoelectric field measurements. The source consists of a heavy hollow metal bolt, which we filled with sand to further increase the weight. It is hydraulically drawn up against strong rubber bands (see figure 2.5) and released mechanically. The metal bolt then hits a ground plate as in hammer seismics. The source is very robust and stable which is also necessary with the high forces involved. It is operated with two 12 V batteries. These only provide the current necessary for the hydraulic system. There is no electricity involved from the moment on where the bolt is released which makes the source highly suitable for seismoelectrics because no electromagnetic noise will be generated. The source is quite strong (see section 4.7 for direct comparisons with the hammer source), easy to operate and physically not at all tiring as the only work involved with the source is the mounting and demounting which can be done in some minutes. This facilitates long measurement campaigns without growing dissatisfaction of the field crew.

Disadvantages are that only a manual trigger is possible with this source. There is no simple way to tie an accelerator trigger to the metal bolt. The use of a short-circuit trigger is thinkable but with the forces involved, the cables would have to be renewed quite often (see section 2.2.2 for a more in-depth investigation of the trigger question). This results in quite slow progress with the measurements as well as big data volumes because the data can only be stacked afterwards and not directly in field. Furthermore, the source consumes some battery power which can be a limiting factor in remote areas without access to electricity. In addition, the source needs a car to be fastened to. This turned out to be a disadvantage at the two sites where we measured: In the Segeberg Forest, access was limited to places near the forest path and even then included some interesting car maneuvers. At the GeoModel, it was not possible to drive right into the model itself to place the source where the hammer measurements produced the best results.

The usage of this source enabled sensible results at the GeoModel where a sledgehammer as seismic sources often just was not enough. This will be shown in section 4.7 while the results from the Segeberg Forest in comparison to hammer seismoelectrics will be shown in section 4.6.

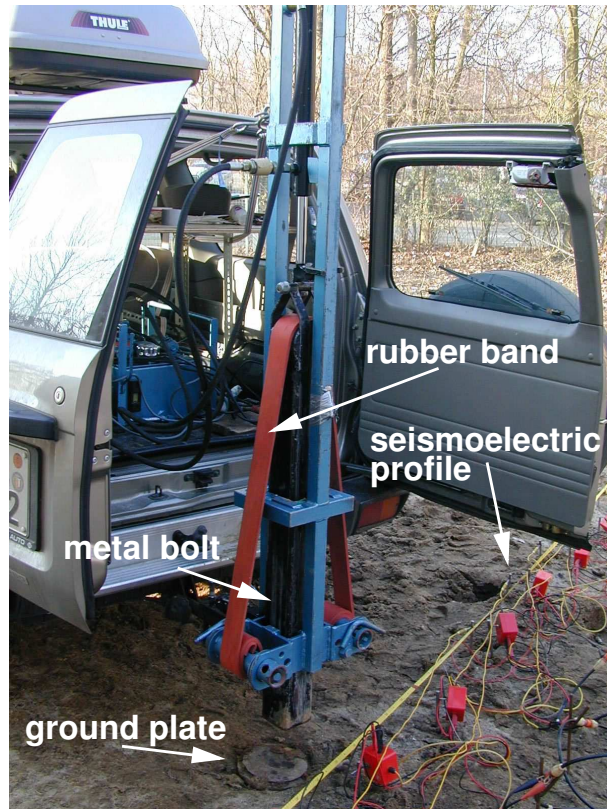


Figure 2.5: The accelerated weight drop source hired from Geo-Center Nord. The ground plate is a metal plate as routinely used in hammer seismics.

2.2.2 Trigger mechanism and ground plate

The trigger mechanism in seismic as well as in seismoelectric measurements ensures that the recording of the time series starts at a precisely defined time, usually equal to the time of the hammer impact or the explosion detonation. Especially if single shots are to be stacked, it is crucial that the trigger works accurately or else the stacking routine will not work correctly and the result will be smeared. In addition to this requirement, in seismoelectric measurements the trigger must not be a source of additional electromagnetic noise. In near surface applications, it is often the first ms of a time series that are important because the converted seismoelectric signals arrive quite early. If electromagnetic noise from the trigger mechanism covers the first ms of the time series, it can make the data useless. In the following subsections I elucidate the pros and cons of the two most common trigger mechanisms used in hammer seismics (accelerator trigger and short-circuit trigger) when applied to seismoelectrics (sections 2.2.2.1 and 2.2.2.2). I then show direct comparisons between the different trigger mechanisms (section 2.2.2.3) followed by a short investigation into the nature of measurement convenience of the different mechanisms (section 2.2.2.4) and a verification of the correctness of the accelerator trigger (section 2.2.2.5). Parts of the following subsections (acquiring the wooden plate and investigating the trigger experiments at the Segeberg Forest site) were done in cooperation with H. Petersen (Petersen et al., 2004, internal report).

2.2.2.1 Short-circuit trigger

The short-circuit trigger consists of two cables, of which one is screwed to the conducting ground plate and the other one to the conducting hammer head. When the hammer hits the plate, the circuit is closed and the registration triggered. Several ground plates were used. Most often, a standard metal plate as used in hammer seismics proved to be unproblematic (see figure 2.5). In some instances, especially if the ground was wet, this caused problems because the trigger current was picked up by the electrodes, and we had to provide for an insulation between the plate and the ground. For this we used a smaller metal ground plate of 1 cm thickness and 15 cm diameter screwed onto a wooden oak block of 25 x 25 x 25 cm³. The wooden block does not insulate perfectly if the wood is soaked. But we never measured in pouring rain because of the preamps, anyway, so this is not much of a problem. This plate will in the following be called *wooden plate*. Due to the high amounts of energy associated with the hammer hitting the plate, the wooden block has to be very stable. The first prototypes did not last very long as can be seen in figure 2.6. Another weak point are the screws fastening the metal disk to the wood. Even when using long and thick screws, they usually have to be replaced after a few hundred hammer blows. Recent tests with an equally insulating plate of fabric-base laminate fibers imbued in synthetic resin proved to work well with the accelerated weight drop source. Ironically, the plate broke when using a hammer although the accelerated weight drops are a stronger type of source than the man driven sledgehammer. When using a hammer, however, it can happen that the ground plate is hit with only a single edge and not with the whole front area. The force is concentrated on a smaller area and can thus break the plate.

2.2.2.2 Accelerator trigger

The acceleration sensor is fastened with cable binders to the hammer shaft shortly under the hammer head and connected to the seismograph via a cable (see figure 2.7).



Figure 2.6: Metal disc screwed onto a wooden block. Left: Backside of the prototype which turned out to be too thin (10 cm) for the strong mechanic strains. Right: Successor model after some hundred hammer blows. Two out of six screws have already loosened. The red trigger cable used for the short-circuit trigger is screwed to the metal plate.

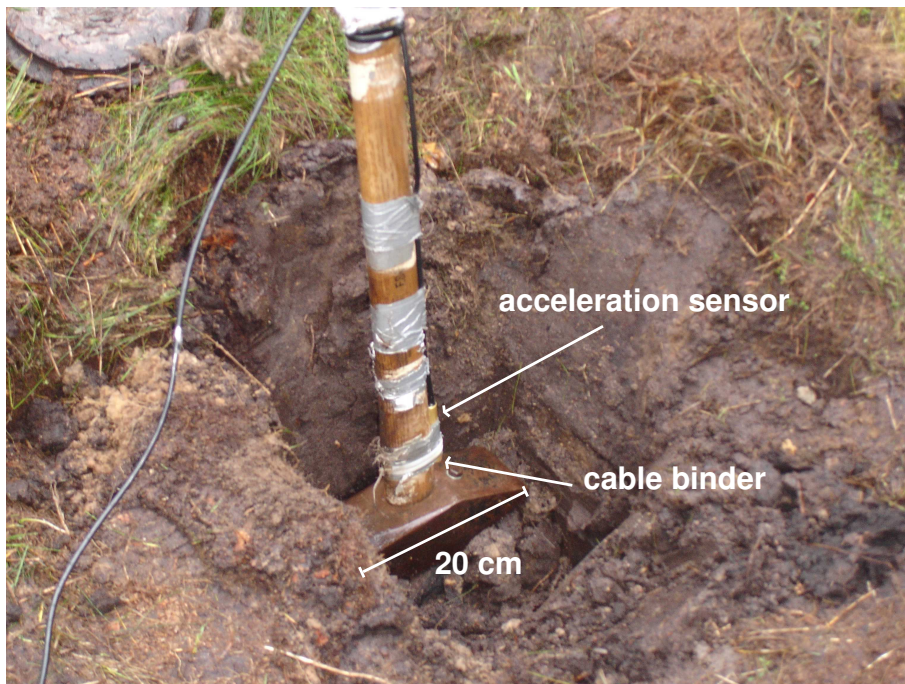


Figure 2.7: The accelerator trigger. The effect of brute force and repeated shot stacking on soft wet ground can also be seen.

It turned out that the trigger cable can cause problems when lying on wet ground. In one instance, we had to hang the cable into trees to prevent it from being too near to the ground. The accelerator trigger itself proved to be very stable and reliable. It did not cause problems once in four years. It was suspected that the timing of the accelerator trigger was less accurate than the short-circuit trigger which would have led to minor time shifts between shots to be stacked but tests showed that this was not the case in our measurements.

2.2.2.3 Comparison of the different trigger mechanisms

In figures 2.8 to 2.11 I examine the consequences of different trigger mechanisms and ground plates on the seismoelectric signals. The seismoelectrograms presented exhibit both coseismic and converted seismoelectric signals.

Figure 2.8 comprises comparisons between seismoelectric data from the location Fuhrberg Forest (April 2004) with different ground plates (wood and metal) and trigger mechanisms (short-circuit and accelerator). Seismic traces are also shown for comparison. The data are scaled with automatic gain control to enhance the weak events in the beginning. Some arrivals without moveout at around 3 ms and 10 ms can be seen clearly. They appear in all four registrations so it is quite unlikely that they are trigger noise, especially if one compares these signals with clear trigger noise as recorded in the Segeberg Forest (figure 2.9).

There is no conducting connection between the trigger cable and the ground via the plate, as the wooden block essentially acts as an insulator. These possibly converted seismoelectric signals do not manifest themselves on the seismic traces. There are hardly any differences between the four combinations of different trigger mechanisms and ground plates. In particular, no time difference can be observed between the accelerator and the short-circuit trigger which is important as already 1 ms erroneous time determination can result in a large spatial shift when analyzing converted seismoelectric signals, depending on the seismic velocity of the earth layers.

Figures 2.10 and 2.11 show the same combinations of trigger mechanisms and ground plates, this time from the site Menzlin (see section 4.4), again with the corresponding seismic traces added for comparison. However, this time a clear difference between the sections recorded with accelerator trigger and those recorded with short-circuit trigger is discernible. There seems to be trigger noise in the first ms on the bottom left figure of figure 2.10 (short-circuit trigger + wooden plate) and on both registrations with short-circuit trigger in figure 2.11. Here, the ground plate sunk down due to repeated vertical stacking and soft wet ground so that eventually a conductive connection between the ground plate and the wet ground was established. Thus the trigger signal travels through the earth and is picked up by the dipoles. Again, there no temporal shift between the two different trigger mechanisms.

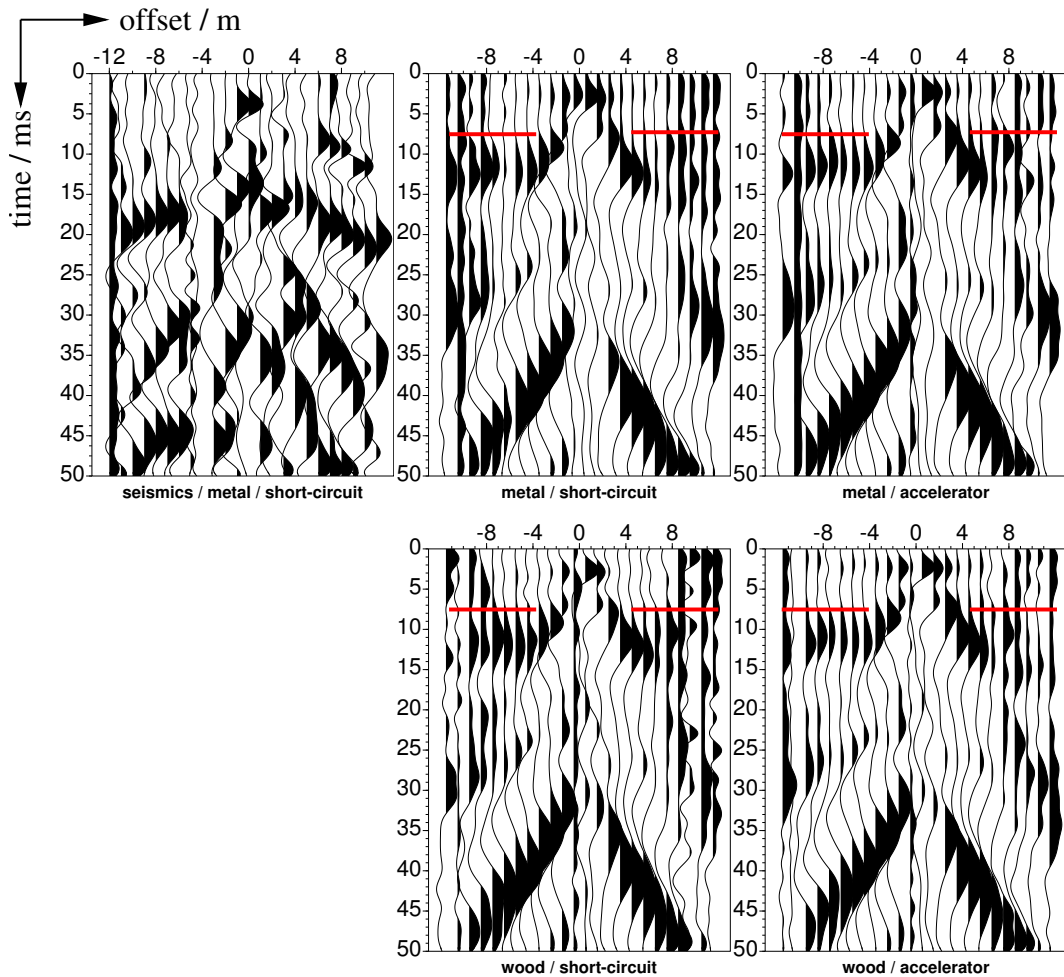


Figure 2.8: Comparison between seismoelectric data from the location Fuhrberg Forest (April 2004) with different ground plates (wood and metal) and trigger mechanisms (short-circuit and accelerator). The corresponding seismic data are added for comparison. The data are scaled with automatic gain control. An assumed converted seismoelectric arrival is marked with lines. There is no time difference between the different ground plate - trigger combinations.

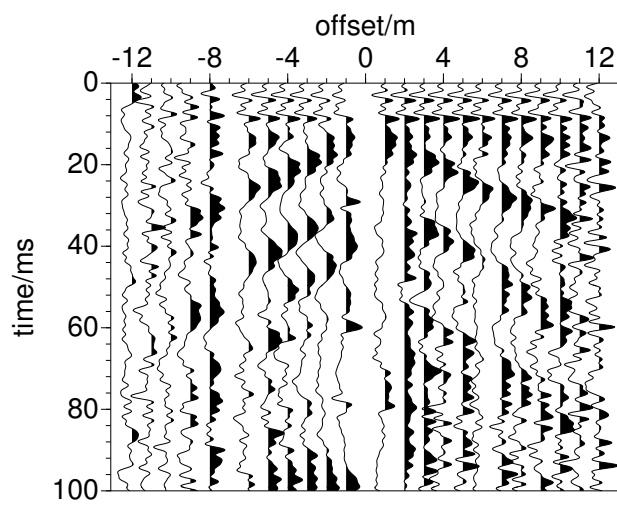


Figure 2.9: Example of a seismoelectric record with agc and strong trigger noise picked up by the dipoles. The example is from the site Segeberg Forest (December 2003). A short-circuit trigger in combination with a metal ground plate on moist soil was used.

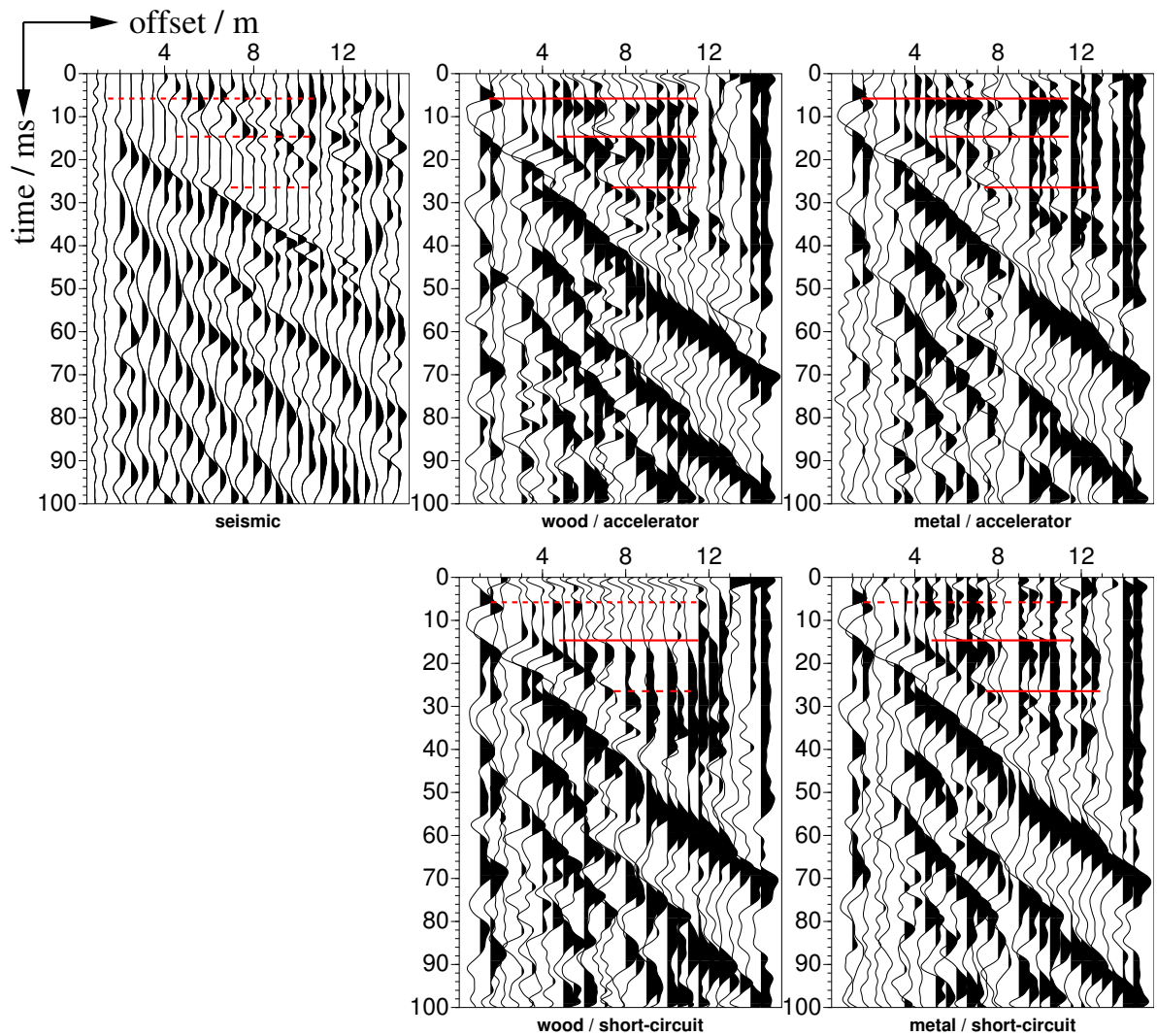


Figure 2.10: Comparison between seismoelectric data from Menzlin with agc and two different trigger mechanisms (acceleration: top row, short-circuit: bottom row) and two different ground plates (metal: right column, metal disk screwed onto a wooden block: middle column). The presented data were recorded at the shot point at 5 m. Data with the same configuration but from the shot point at 20 m are shown in figure 2.11. The corresponding seismic traces have been added for comparison (left column). Assumed converted seismoelectric arrivals are marked with lines.

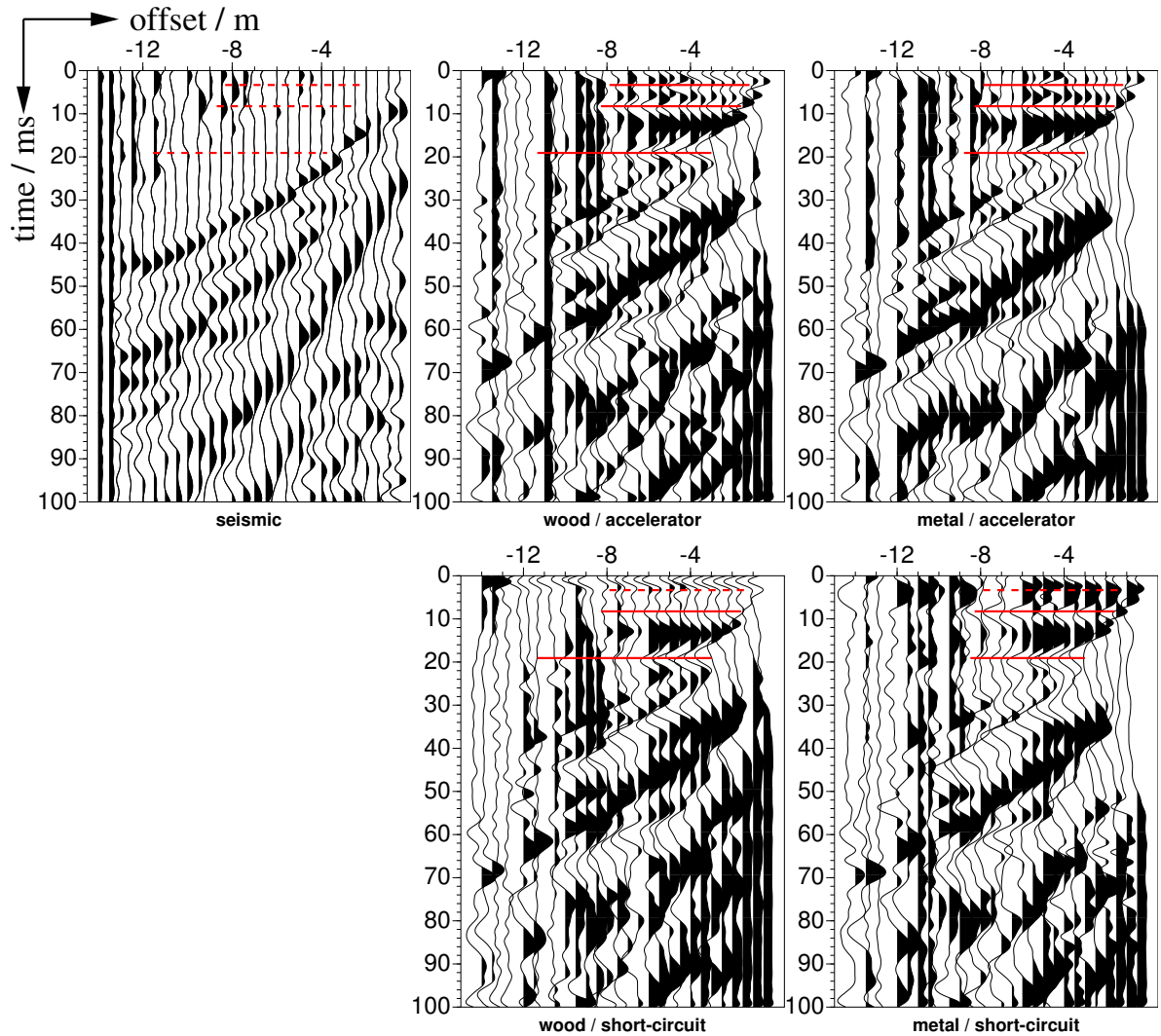


Figure 2.11: Comparison between seismoelectric data from Menzlin with *agc* and two different trigger mechanisms (acceleration: top row, short-circuit: bottom row) and two different ground plates (metal: right column, metal disk screwed onto a wooden block: middle column). The presented data were recorded at the shot point at 20 m. Data with the same configuration but from the shot point at 5 m are shown in figure 2.10. The corresponding seismic traces have been added for comparison (left column). Assumed converted seismoelectric arrivals are marked with lines.

2.2.2.4 Aspects of measurement convenience

If one looks to field suitability, the acceleration trigger is clearly preferable to the short-circuit trigger. As stated before, it did not cause problems at all during the last four years. The short-circuit trigger on the other hand, causes a lot of trouble because the trigger cable tends to loosen from the ground plate, especially if the ground is soft or wet and the plate sinks down one or two dm into the ground which delays the progress of the measurements. When the open cable lies directly on the ground, very often the trigger signal is picked up by electrodes (which should pick up seismoelectric signals, not triggerelectric signals). Possibly, a solution could be found by optimizing the connection of the cable to the plate. However, this is not motivated because the acceleration trigger has proved to be the preferable alternative.

2.2.2.5 Comparison with manual trigger

In order to verify that the acceleration trigger itself does not cause unwanted artifacts on the seismo-electric traces, we performed measurements with a manual trigger. This means that the registration time was increased and the person operating the seismograph triggered the measurements manually shortly before the impact of the hammer on the ground plate. Twenty single shots were collected and then later stacked after time correction using a cross correlation to determine the time shifts between the single shots. We frequently used this technique when we suspected the trigger mechanisms to cause spurious events. The time correction proved to work well. When the signal noise ratio is very weak so that no seismoelectric events can be distinguished, we use an extra geophone trace to be able to perform the time correction with cross correlation. It is quite often the case that only 50 Hz can be seen on the raw seismoelectric traces.

A clear drawback is that the measurement progress is hampered because it takes significantly more time to record twenty manually recorded single shots than to stack them directly in the field, mainly because the seismograph is busy storing the data. The data volume is increased at least fifty fold for twenty stacks because each shot has to be stored separately and because of the longer registration length. This can obviously cause data storage problems on longer campaigns.

The comparison between seismoelectric traces recorded with manual trigger and with acceleration trigger is demonstrated in figure 2.12. As there are practically no differences between the two different data sets and in particular also the events with almost infinite apparent velocity also are to be seen on the manually triggered traces, I judge the acceleration trigger as mostly harmless for seismoelectric measurements. This is also a consequence of the three preceding subsections.

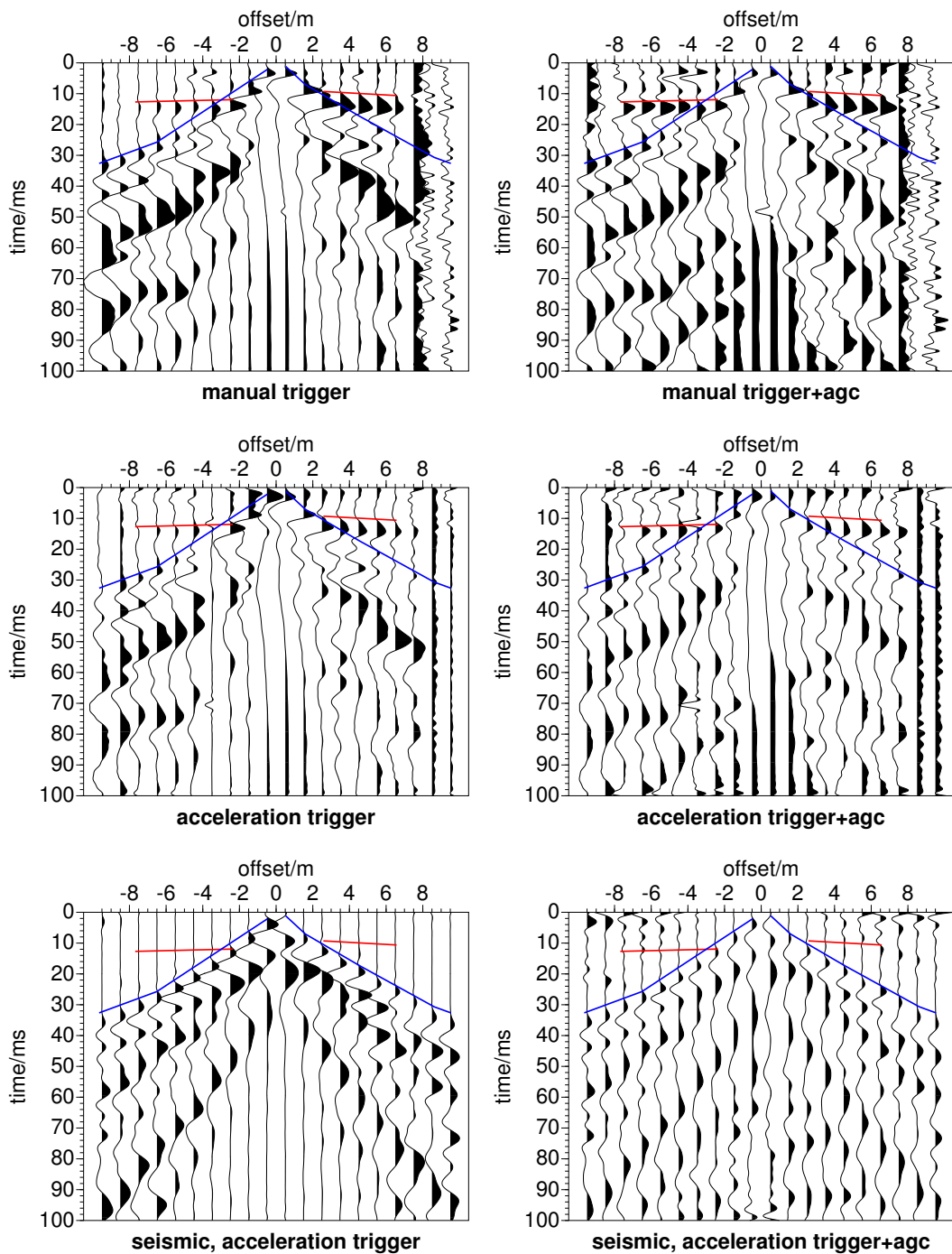


Figure 2.12: Comparison between seismoelectric recordings from Menzlin manually triggered (top row) and using an acceleration trigger (middle row). The data are trace normalized in the left column and scaled with *agc* in the right column. The corresponding seismic sections have been added for comparison in the bottom row. Converted seismoelectric arrivals are marked in red and the direct P-wave in blue. There are neither big differences between the seismoelectric sections with different trigger mechanisms nor temporal shifts to be seen.

2.2.3 Dipoles

While geophones are used to record ground velocity in seismics, we have to use two electrodes between which we measure the electric potential difference in seismoelectrics. We cannot measure the electric field at a point. The way the two electrodes are placed has consequences on the measured signal. Just as in seismics, the receivers can be organized in profiles to pick up the signals of interest at several points (usually with equal distances in between).

2.2.3.1 Dipole length

Beamish (1999) as well as my own results point out that it is mainly the inner electrode of the dipole (i.e. the one closer to the source) that controls amplitude and form of the signal. This is true for the coseismic waves. For coherent noise longer dipole lengths lead to a linear scaling of coherent background noise such as anthropogenic 50 Hz noise. This is because

$$\Delta V = E\Delta x \quad (2.1)$$

with ΔV being the measured potential difference, E the electric field, and Δx the distance between the two points at which ΔV is measured. E was assumed to be constant across Δx which is approximately valid, given the long wavelengths of the low-frequency field. Actually, it is not an electric field but an electromagnetic one. But with the described technique, we can only determine the electrical component.

For the wanted converted seismoelectric signals, the dependence of the signal amplitudes on dipole length is more complicated. It depends on both horizontal and vertical distance to the conversion point. Generally, longer dipole lengths lead to higher amplitudes (as can also be seen in the data of Mikhailov et al., 2000), but this is strongly non-linear. The influence of dipole lengths and positions of converted seismoelectric signals is analyzed in section 6.2. However, very long dipole lengths are not desirable because they average the field which implies a loss of information about the converting interface and its depth. Furthermore, the coherent electromagnetic noise will usually increase stronger than the wanted seismoelectric signals.

For the coseismic waves, also the wavelength of the “carrying” seismic wave is of importance. If the dipole length is equal to the wavelength, destructive interference weakens the coseismic waves. Analogously, with a dipole length of half the wavelength, destructive interference will enhance the coseismic signals. If the velocity of the uppermost layer is known, dipole length could be chosen to weaken the amplitudes of the coseismic waves. This has been explained in detail by Haines (2004). An example of the influence of dipole length on seismoelectric data quality is presented in figure 2.13 where converted and coseismic arrivals are marked with lines. The amplitude of the coseismic waves is almost the same for both dipole lengths. However, the diffuse noise is stronger for the shorter dipole lengths. Thompson & Gist (1993) suggest electrochemical electrode noise as limiting factor for short dipole lengths. As a consequence, when anthropogenic noise (see section 2.3) was strong, we used shorter dipole lengths. When electromagnetic noise was weak, 4 m dipole length proved to yield slightly better signal to noise ratios.

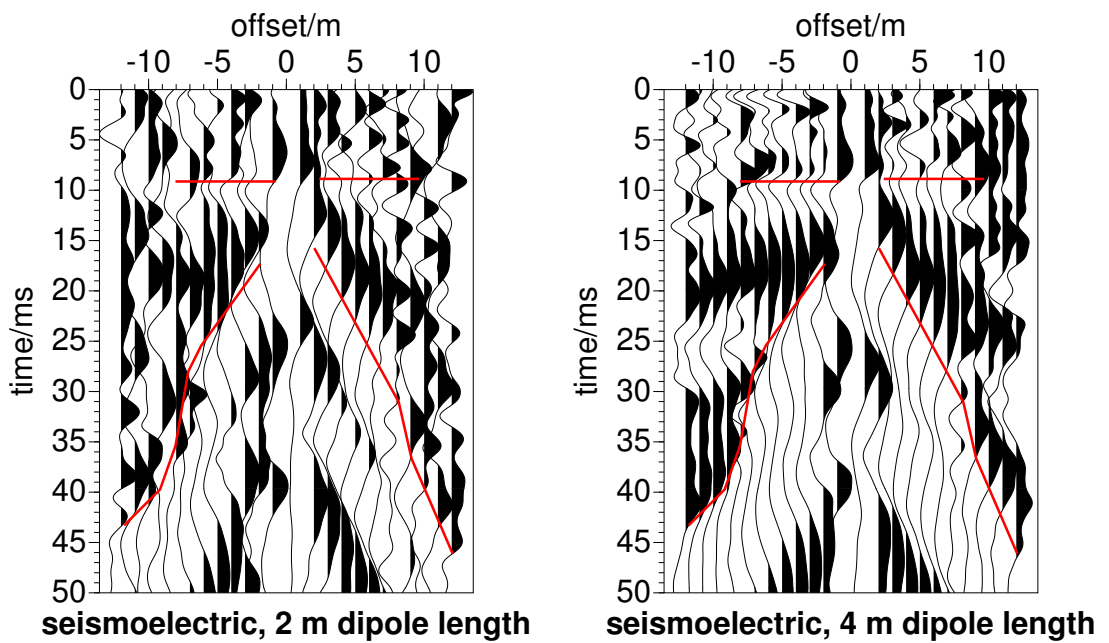


Figure 2.13: Comparison of the influence of different dipole lengths on seismoelectric data quality. Left: 2 m dipole length, right: 4 m dipole length. The data are scaled with agc . The 4 m dipole data are less noisy, however, all arrivals can also be detected in 2 m dipole data. The arrivals of converted and coseismic signals are marked with lines in the figure.

2.2.3.2 Electrode types

Basically we have the choice between simple stainless steel electrodes and unpolarizable electrodes like copper-copper-sulfate electrodes or silver-silver-chloride electrodes. Unpolarizable electrodes are often used in self-potential measurements in order to prevent polarization potentials which would degrade the results. This could also be useful in seismoelectrics. Unfortunately unpolarizable electrodes are usually less stable than plain stainless steel electrodes, because they are required to have a porous surface to enable small amounts of the sulphate solution to ooze out into the ground. Stainless steel electrodes are much more robust which means one can use a hammer to drive them into the earth which speeds up the planting enormously. Some of my early tests (Strahser, 2002) showed that the difference in signal quality are minimal between stainless steel electrodes and unpolarizable electrodes. We therefore exclusively made use of stainless steel electrodes.

2.2.3.3 How to place the dipoles

As pointed out in section 1.1.1.2, the electric field of the converted seismoelectric signals closely resembles the field of an electric dipole centered below the shot point (Garambois & Dietrich, 2002) and should cause a polarity reversal of the detected signals at the shot point. All data presented here were acquired with the dipoles set up symmetrically to the shot point, i.e. the first electrode of each dipole is the one closer to the shot point. We either set up the electrodes accordingly in field or corrected the polarity later in the data. A polarity reversal should therefore not occur in the seismoelectric data (see figure 1.1 on page 7). This holds true for coseismic as well as for converted seismoelectric signals. Only coherent background noise should have a polarity flip at the shot point with this configuration.

Usually I chose a dipole distance of 1 m or 0.5 m. It is important to have such short receiver distances if one aims to separate the converted from the coseismic signals. With too large distances between the receivers, the apparent velocities of the different waves and wave types cannot be accurately determined which complicates or even precludes a correct interpretation. Furthermore, seismoelectric signals become attenuated quite fast which is why short profiles with dense receiver spacing are preferable to long profiles with longer dipole distances.

2.2.4 Preamplifiers

Another important part one needs before being able to measure seismoelectric signals are the preamplifiers (shown in figure 2.1). The preamps we used are galvanically insulated impedance converters with tenfold amplification. Besides the amplification of the signal their task is to increase the input impedance so that a maximum part of the seismoelectric signal is recorded and only a minimal potential drop occurs in the ground. The preamps were manufactured by the company GeoServe, Kiel.

Garambois & Dietrich (2001) present good quality data which were acquired without preamps. At exceptionally good locations, we could also record high S/N ratio data without preamplifiers (*Fuhrberg Forest, Februar 2002*) but this does not seem to be the rule (see Strahser, 2002).

2.3 Problems with anthropogenic noise

Ironically, one of the biggest problems with applied seismoelectrics is human civilization. Even in areas where no human generated noise can be heard or contamination by civilization can be seen, the electromagnetic noise may be strong. 50 Hz (60 Hz in most North and South American countries) and its higher harmonics penetrate the Earth and air and are picked up by electrodes (see e.g. figure 4.35 on page 105). As explained in section 2.2.3.1, the electromagnetic noise is proportional to the dipole length.

This is particularly annoying because 50 Hz or 60 Hz are in the middle of the seismic (and seismo-electric) frequency band if one uses a sledgehammer as seismic source. A simple bandpass filter will not only strip the time series of electromagnetic noise but also of the seismoelectric signals. Even a very narrow bandpass filter (notch filter) will not work. If it is too wide, significant parts of the signal will be destroyed and if it is too narrow, artifacts due to the Gibbs' phenomenon will be created. The solution is not to perform the filter in the frequency-wavenumber domain but in the space-time domain. It is in the course of the Fourier transformation where the Gibbs' phenomenon causes problems. A technique called the sinusoid subtraction method (Butler & Russel, 1993, 2003) has become a kind of standard in seismoelectric processing and works fairly well and fast. I mostly used a similar technique described by Adam & Langlois (1995) which is slower but often worked better with my data. Both these approaches require the fundamental noise frequency to be set. This frequency is then adapted and amplitude and phase are determined to best fit the data.

Some authors record the coherent noise during the measurements with two dipoles set up perpendicular to one another and subtract the least squares linear combination of these two traces from the seismoelectric data. If the two extra dipoles are away far enough from the source, only background noise and no wanted signal is recorded. I tested this far-field subtraction technique but without good results. The sinusoid subtraction technique turned out to work better without preceding subtraction of the far field. Another way to reduce electromagnetic noise might be to perform the measurements at night, although this might be problematic in inhabited areas due to acoustic noise created by the source. The borehole data we collected were hardly ever contaminated by 50 Hz. It seems that the coherent electromagnetic noise does not penetrate very deep into the ground.

In spite of all these apparent difficulties, there are areas even in densely populated Germany (231 inhabitants/km²) that are almost completely free from anthropogenic electromagnetic noise. This, however, does not automatically guarantee first-quality seismoelectric data (see chapter 4.6).

2.4 The role of seismics

It is important for a variety of reasons to complement the seismoelectric measurements with seismic measurements:

1. Identification of the seismoelectric events
2. Help of interpretation of the ground structure
3. Possible importance in filtering the coseismic waves

2.4.1 Identification of the seismoelectric events

As the coseismic waves are confined to the seismic compressional waves, they can easily be identified by comparing the seismoelectrogram with the seismogram. As stated in section 1.1.1.1 the coseismic signals are proportional to the time derivative of the seismic signals of the same component. This can be particularly important in the case of seismoelectric signals being carried along the path of the seismic reflected wave. Seismic reflections show an apex near 0 m offset, i.e. their apparent velocity is very high at low offsets which could lead to an erroneous interpretation of these events as converted seismoelectric signals. Therefore assumed converted seismoelectric signals should be checked against possible seismic reflections. As stated before, a seismoelectric converted wave travels downward from the source to the converting interface as a seismic wave and then upward as an electromagnetic wave with much higher velocity. For that reason, they should arrive at close to seismic one-way travel time, opposed to the seismic reflections which arrive at seismic two-way travel time.

2.4.2 Interpretation of the ground structure

The seismoelectric method is still far from the point where it could be considered a stand-alone method. It will probably always be necessary to perform parallel seismic measurements. In order to correctly assign depths to the seismoelectric conversion times, a velocity-depth model is used which in the absence of boreholes could be determined by seismics, either refraction or reflection, depending on depth of interest, resolution, velocities etc. The processor must be aware of the fact that seismic reflections or refractions do not necessarily result in clear seismoelectric conversions. On the other hand, it is quite possible that seismoelectric conversions occur at interfaces that do not leave any traces in the seismogram, be it reflections or refractions. This is because a lot more properties are involved in the equations controlling the generation and propagation of seismoelectric signals than is the case in seismics (see chapter 1.1.2).

2.4.3 Possible importance in filtering the coseismic waves

The main filter technique used in this work to get rid of the coseismic waves (usually classified as noise in seismoelectrics) is a velocity filter performed in the frequency-wavenumber domain. For this filter there is no need for seismic traces, although the filter should be applied to the seismic traces with the same parameters as well as a test if possible artifacts were generated. This will be investigated more into in section 3. This filter however, albeit quick and simple, is surely not the optimum. It would be far more elegant and useful to somehow make use of the information one can get from the seismic records in order to eliminate the coseismic waves.

Simple experiments with adapting phase and amplitude of the time derivative of the radial component seismic direct compressional waves to fit and subtract the corresponding seismoelectric signals did not lead to usable results because there still are significant differences between the seismic and the seismoelectric data, among others in terms of data quality. Haines (2004) describes the promising technique of using prediction error filters (PEF) for extracting the signal of interest from seismoelectric records. These PEFs exploit the known amplitude pattern and dip of the signal of interest and need an input model of both signal and noise. Radial component geophone data could be used for an

input model of the coseismic noise. In the work of Haines (2004), the geophone data turned out to have too bad quality and were not used so a field test for this noise removal technique is still missing.

2.4.4 Contamination of seismoelectric records with geophone signals

Some authors warn not to perform seismic and seismoelectric measurements at the same time because the geophones could induce electric signals into the earth and be picked up by the electrodes. This would harm the seismoelectric data. Haines (2004) reports of no difficulties when combining seismic and seismoelectric sensors but this could be site-specific. Tests in my own research (Strahser, 2002) had shown that the geophones could induce seismic signals into the dipoles if both sorts of measurements were performed synchronously, so I generally chose not to run the risk. When true amplitudes are claimed, e.g. if quantitative values are to be extracted from the seismoelectric records, it might be necessary to perform seismic and seismoelectric measurements at the same time. One should then choose to place the geophones and dipoles a certain distance apart to keep the influence of the geophones as small as possible.

2.4.5 Three-component seismics

Ideally, the same components should be recorded in seismics and seismoelectrics to enable a direct comparison. The most meaningful component in seismoelectrics which is also easiest to collect is the radial one as opposed to the vertical component which is usually measured in seismic measurements, as the refracted and reflected waves are clearest on this component for geometrical reasons. Refracted and reflected waves usually travel upward from the deep and are quite weak on the horizontal components. So with both the radial and the vertical component being needed, one might as well collect all three components when three-component geophones are available. We used triphones which consist of three identical geophones with an angle of 54.7° towards the vertical and 120° azimuth between two components. This type of orientation guarantees identical transfer functions of all three geophone components (Gal'perin, 1984). These three components, called U, V, and W, can be transformed to the three Cartesian coordinates X, Y, and Z via the following relations (e.g. Meyer, 1989):

$$X = \frac{2U - V - W}{\sqrt{6}} \quad (2.2)$$

$$Y = \frac{V - W}{\sqrt{2}} \quad (2.3)$$

$$Z = \frac{U + V + W}{\sqrt{3}} \quad (2.4)$$

2.5 Special configurations

2.5.1 Three-component seismoelectrics

For geometrical reasons, it is usually the radial component which is recorded in seismoelectric surface measurements and the vertical component in seismoelectric borehole measurements. In order to study the complete three-component seismoelectric wavefield, one has to record all three seismoelectric components at one single point which in the case of seismics does not pose much of a problem if three-component geophones are available. The two horizontal seismoelectric components are also easy to measure by placing the dipole in line or cross line to the profile. We solved the problem of the vertical component by connecting a short electrode and a long electrode to a dipole. The long electrode was insulated with a shrinkable tube except of the deepest 30 cm (see figure 2.14).

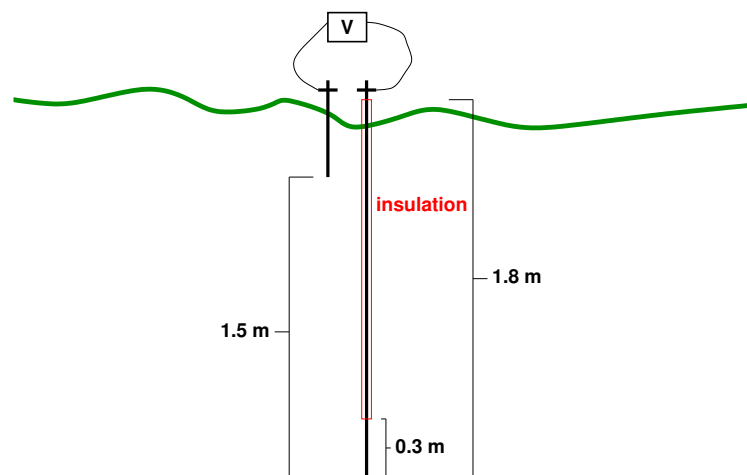


Figure 2.14: Configuration for the recording of the vertical seismoelectric component. The 1.8 m electrode is insulated with a shrinkable tube leaving only the lowest 30 cm conducting. This electrode is connected with a standard short electrode (30 cm length) thus resulting in a dipole length of 1.5 m.

Unfortunately, this insulation is easily damaged if the electrode is hammered into the ground directly. It became necessary to first make a small pilot hole with a drill rod and then place the long vertical electrode into the drilled hole. The last 30 cm or so, the long electrode was hammered to provide the necessary good coupling to the ground. In my case, the choice of dipole length was fixed by the long vertical dipoles. Their length of 1.8 m and the length of the short electrodes of around 0.3 m set the length of the vertical dipole to 1.5 m.

The first test of seismoelectric vertical component measurements (see section 6.1) was rather successful so it was decided to carry out these experiments in a routine manner. Depending on the local ground conditions, however, this turned out to be a rather cumbersome task. The main problem is to place the 1.8 m long and 20 mm thick electrodes into the ground. Dry and therefore most often hard ground made it if not impossible then very costly in both time and manpower to insert the drill rod with only using a man driven hammer. Figure 2.15 shows both the geometry of three-component seismoelectric measurements and also the insertion of the long electrodes.

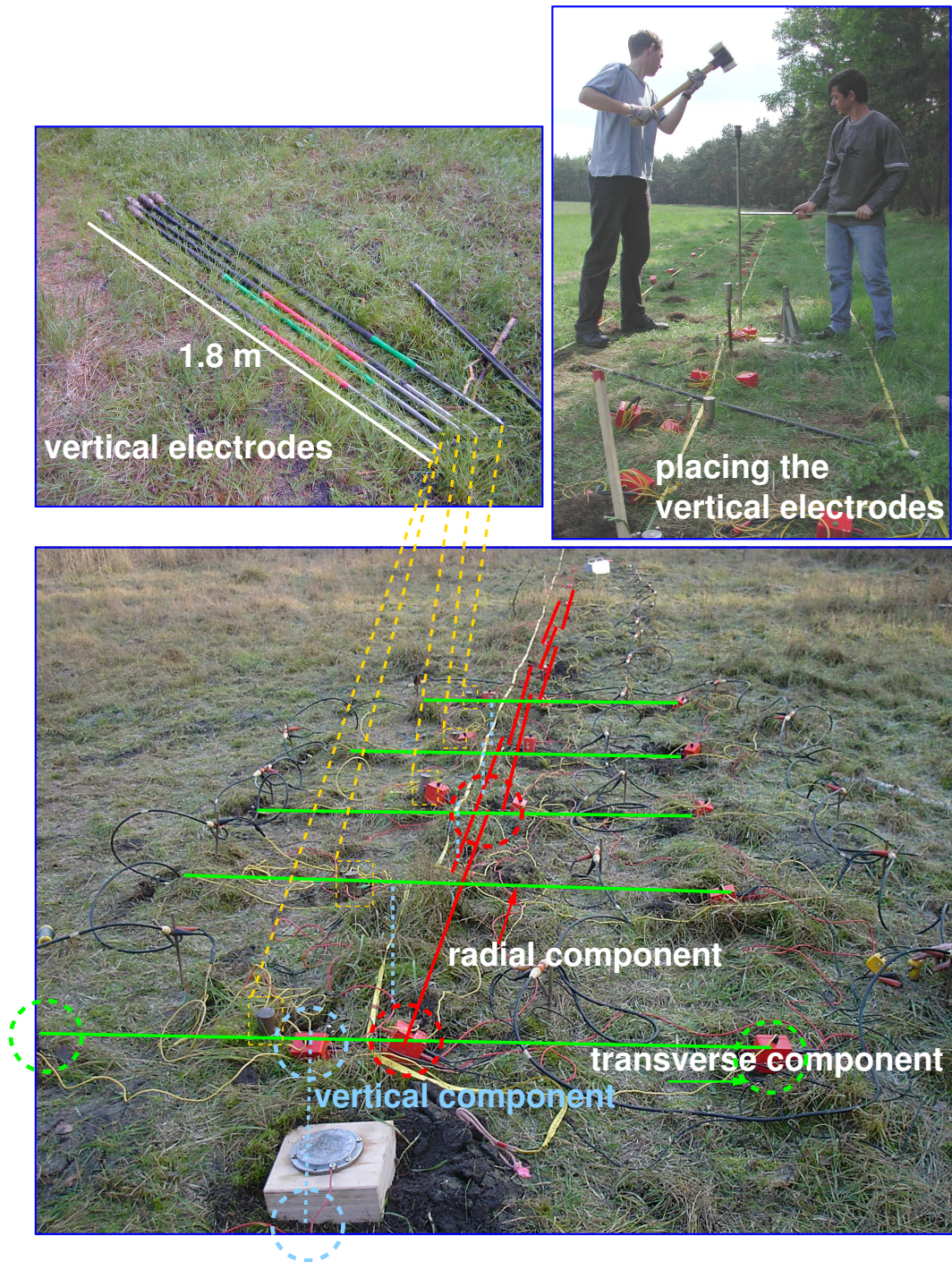


Figure 2.15: Bottom: Spatial orientation of the radial, transverse and vertical dipoles. The ground plate shown is a metal disk screwed onto a wooden block. Top left: The long vertical electrodes in detail. Top right: Placing of the long vertical electrodes.

It was decided to seek for a motorized solution of the problem. After several tests, a “Wacker” percussion drill proved to be a good remedy (thanks to Dr. W. Dörfler from the Institute of Pre- and Protohistory for lending us the percussion drill and to H. Petersen for the cooperation with the tests and for getting hold of this tool), a 25 kg, 80 cm³ device with a two-stroke engine (see figure 2.16). The only problem remaining when using the Wacker is to get the drill rod out of the ground again. Unfortunately, the Wacker operates one-way only. An electrode which is hard to get in is usually also hard to get out. Therefore three-component seismoelectric measurements still take a lot of time. Three-component seismoelectric data are analyzed in section 6.1.



Figure 2.16: Percussion drill “Wacker” in use in the Segeberg Forest. Left: While starting, right: while drilling.

2.5.2 Moving source technique

By combining several shot gathers, the number of traces used in one seismoelectrogram can be significantly augmented. This is especially handy in three-component seismoelectric measurements. The dipole positions are kept constant but the shot point is moved to several positions, each time giving more traces with different offsets as shown in figure 2.17. For three-component seismoelectric measurements I usually added traces from shots with 5 m shot point distance in between. Kepic & Rosid (2004) call a somewhat similar technique *virtual shot gather*.

It is even possible to double the amount of this augmented number of traces by shifting the shot point 0.5 m at every 5 m distance shot point. With this simple trick, the trace distance can be diminished to 0.5 m. In the case of horizontal layers, it is possible to get a lot of traces with quite little amount of work. If the layers are dipping, this technique is of limited use of course, because the conversion from seismic to electromagnetic energy takes place where the seismic wave first reaches the converting interface. So with dipping layers, the contributions from each single shot point to the combined

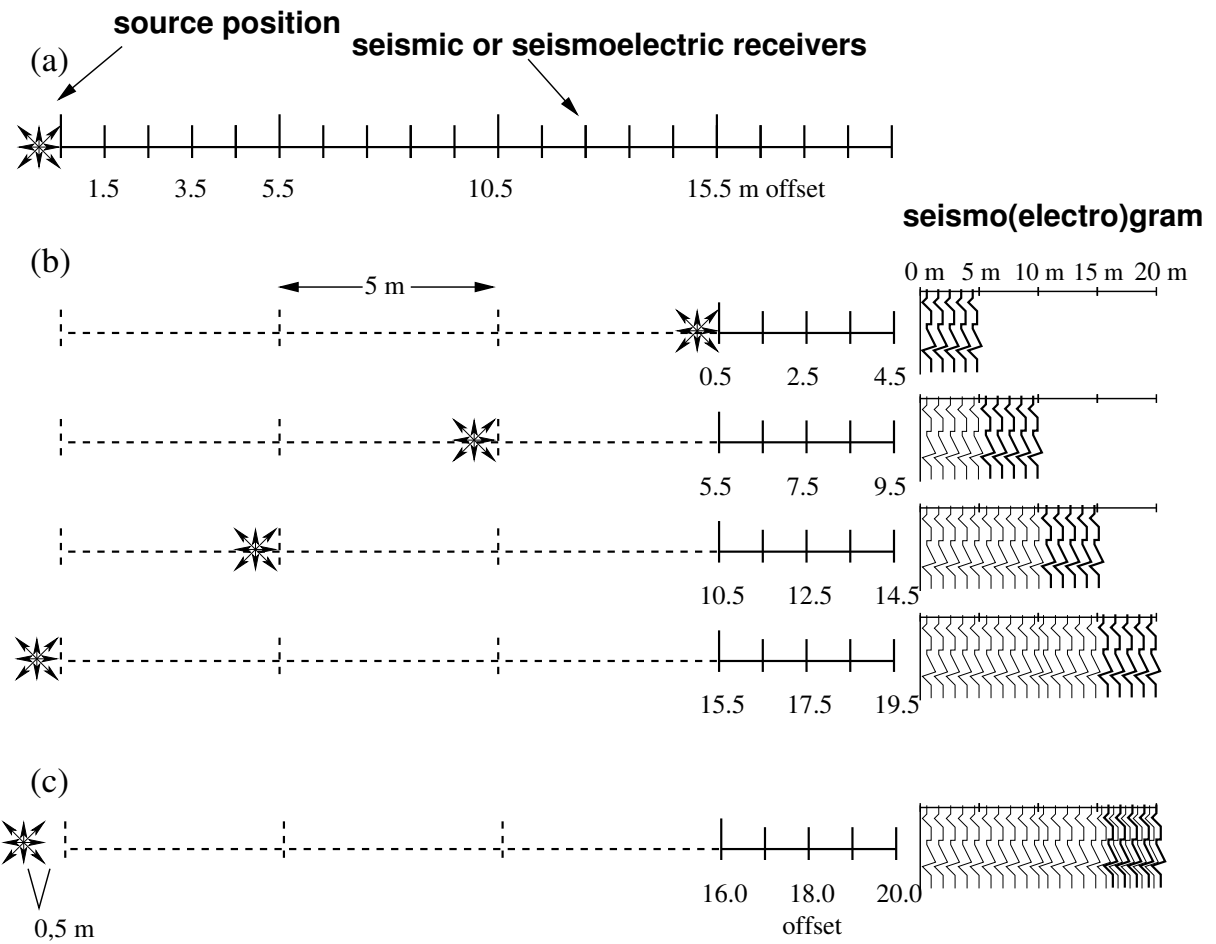


Figure 2.17: Schematic representation of the technique of the moving source for augmenting the number of traces in a seismoelectrogram. (a) Traditional, time-consuming method, (b) simplified, accelerated technique of the moving source. The shot point is shifted 5 m in this example between two subsequent shots. (c) It is even possible to double the amount of this augmented number of traces by shifting the shot point 0.5 m at every 5 m distance shot point. The seismoelectrogram at the right side shows how the traces are combined. This method was used for especially collecting three-component seismoelectric data.

seismoelectrogram will originate from different depth points on the converting interface. If the ground is very heterogeneous, even the combination of traces with the shot point shifted 0.5 m becomes problematic. This technique has the advantage that it is automatically a check of repeatability. If an event only can be detected at every second trace, it is probably no real seismoelectric event but some artifact or noise. We used this technique routinely. All seismoelectric data presented in this thesis with more than 24 traces (5 traces for the seismoelectric vertical component, respectively) or with trace distances of 0.5 m were combined from several single recordings.

2.5.3 Vertical seismic and seismoelectric profiling

Vertical seismic profiling is realized with a hydrophone or a geophone or a chain with several hydro- or geophones in a borehole instead of a geophone profile at the surface. These measurements have the advantage of the receivers being closer to the target than is the case in surface measurements. The same is true for borehole seismoelectrics. In that case, a borehole electrode chain is used from which two electrodes are connected to a dipole each. As with geoelectric borehole measurements, VSEP (vertical seismoelectric profiling) only works if the borehole is water filled and does not have metal casing. In a dry borehole, the electrodes do not have any coupling to the ground, and a metal borehole acts as a short circuit for the electric signals. In the case of a PVC cased borehole, the pipe has to be sliced (examples are shown in section 4.6), else it acts electrically insulating.

On an example of VSEP data from the Fuhrberg Forest location (see also section 4.3) in figure 2.18, an event can be spotted manifesting itself as a break (marked with A and B in the zoom figures to the right) in the otherwise very smooth downgoing P-wave (i.e. its coseismic field). In the case of the 8 m long dipoles (bottom), this break seems to consist of an event with almost infinite apparent velocity. In the case of the 4 m long dipoles (top), the break is rather undefinable and less smooth. The shown seismoelectrograms with 4 m and 8 m dipole length are combined from several single measurements as described in section 2.5.2 which means that the break in the seismoelectric event is highly repeatable. In the VSP (vertical seismic profiling) data of the same borehole there is no sign of this break. The tube waves (slower arrivals, also seen in VSEP data in figure 2.18 and marked with C) indicate clearly that there actually is a boundary at this depth. The impedance contrast is obviously too weak to produce detectable P wave reflections. This means that we have an event on the VSEP traces which arrives at some traces before the downgoing P-wave can reach them. There is no realistic way to explain this observation without converted seismoelectric signals.

2.6 Future improvements in field technique

As of now, seismoelectric field measurements involve lots of cable connecting. The question arises if in the age of wireless electronics all these hundreds of cable meters really are necessary. The problem is not to generate lots of disturbing electromagnetic noise. Improvements in this direction are on the way.

Another time consuming procedure is the planting of the electrodes, especially in areas with hard or rocky ground. Sometimes it is even harder to pull out the electrodes again after the profile is finished. It would be a great advantage to use some kind of an electrode land streamer or a system which is

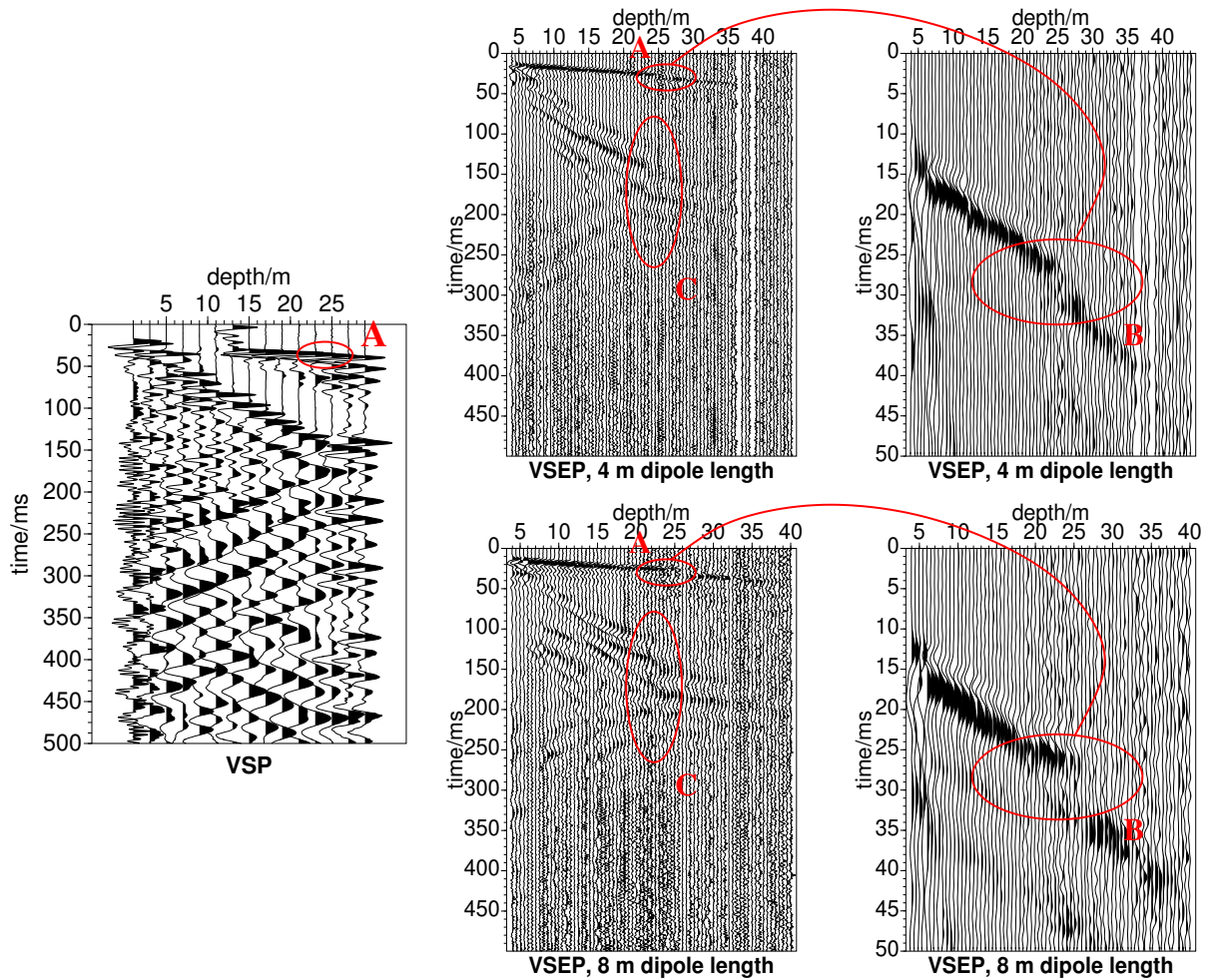


Figure 2.18: Assumed converted seisoelectric events in VSEP data (marked with A and B) which manifest themselves as break in the downgoing compressional wave (Fuhrberg clearing, September 2002). VSEP data are shown for 4 m (top) and 8 m (bottom) dipole lengths. The middle column depicts the first 500 ms of the record, the right column the first 50 ms. The corresponding VSP data are presented in the left column where there is no break in the downgoing compressional wave. Arrival C shows a reflection in the tube wave arrival. The data are scaled with agc .

increasingly used in agro-geophysics where a tractor pulls electrodes mounted on a wheel. Given the low amplitudes of seismoelectric signals, it is doubtful that such systems which usually imply a weaker electrode coupling lead to meaningful seismoelectric data. If electrode coupling really is a decisive factor in seismoelectric field measurements will be explored later.

As will be investigated in the data section (chapter 4), the use of a stronger source sometimes seems to be the only solution when having to cope with low amplitudes. However, a source which is as quick, easy, and reliable in use but much stronger as the man-driven sledgehammer and without generating electromagnetic noise still needs to be developed. There are examples of explosive sources in literature but there seem to be difficulties with the trigger signal (Butler et al., 1996). Up to now, nobody has tried vibro-seismoelectrics but in principle it should be possible.

2.7 Conclusions

Due to the generally low signal-to-noise ratio in seismoelectric field measurements, great care has to be taken with the selection and use of the field equipment. A strong seismic source is desirable but it must not create strong electromagnetic noise, just as all the other measurement components. Although rather weak, a standard sledgehammer proved to be usable. The Sissy source or accelerated weight drops are much stronger sources and give better results but are also slower and more awkward to use. The trigger mechanism is of equally high importance with the requirements of accurately determining the starting time of the measurements and not harming the seismoelectric recordings. I mostly used an acceleration sensor and proved that the trigger mechanisms in most cases give the same results. There are, however, examples of contamination of the seismoelectric traces with the trigger signal especially when using the short-circuit trigger. The converted seismoelectric signals and the coseismic signals behave differently concerning dipole length. A length of 4 m usually is a good option for our type of measurements.

We make use of preamplifiers in seismoelectric field measurements that also convert the input impedance to enhance the signal-to-noise ratio in the field. The main problem in seismoelectrics is anthropogenic noise. Suitable filter techniques do exist but residual noise causes problems, especially at urban sites. Accompanying seismic measurements are needed in order to correctly identify the seismoelectric signals and also for ground structure interpretation. Seismic data may also play a role in future filter techniques to separate the seismoelectric wavefields.

We often record all three components in seismics as well as in seismoelectrics. For the seismoelectric vertical component this involves inserting long electrodes into the ground which we speeded up where necessary by using a type of percussion drill ("Wacker"). To enlarge the number of recorded traces with minimal effort we frequently move the source instead of the dipoles and sort the traces by keyword. This technique leads to good results at locations with approximately horizontal boundaries.

To increase the depth of resolution one can either use a stronger source or record the seismoelectric signals in a borehole which can be realized by using a standard electrode chain. This only works in boreholes that also allow geoelectric measurements and not in metal cased holes. Possible future improvements of the field measurement technique should involve the use of a stronger source and faster electrode inserting or avoid the inserting all together. A common requirement for any new technique is that it does not create strong electromagnetic noise.

Chapter 3

Identification and check of assumed converted seismoelectric events

In this chapter, I will show the main seismoelectric processing steps in the form of a case study with data from the Fuhrberg Forest. It is in essence the content of the paper Strahser et al. (2006). I will begin with a description of the field setup and the recorded data in sections 3.1 and 3.2, respectively, followed by an overview of the main processing steps in seismoelectrics (section 3.3). Special attention will be given to the velocity filter which I use to separate the coseismic signals from the more interesting seismoelectric converted signals. To evaluate if an assumed converted arrival indeed is seismoelectric in nature, I developed a seismoelectric checklist which is presented and applied in section 3.4.

3.1 Field setup

This section merely lists the employed field setup components. For detailed descriptions and explanations see chapter 2. We recorded seismic and seismoelectric data with a 48-channel Bison seismograph and 10 Hz vertical component geophones with 1 m spacing. The seismic waves were created with a man driven 6 kg sledgehammer hitting a ground plate situated in the middle of the profile. Ten shots were stacked. The field layout for the seismoelectric measurements differs only slightly from the seismic one: Instead of geophones, dipoles consisting of two stainless steel electrodes were used. Each dipole was connected to a galvanically insulated amplifier in order to keep the relative noise level as low as possible. Sensor spacing was 1 m (in some cases 0.5 m), and the electrodes were coupled to dipoles of variable electrode distance, usually 2 m or 4 m. Apart from that, the seismic layout was left unchanged. With only 24 amplifiers being available, I combined several measurements with different offsets to acquire more traces (see section 2.5.2).

3.2 Acquired data

The location of the seismoelectric profile and the results from the refraction seismic survey are shown in figure 3.1. A more detailed description of the measurement location Fuhrberg Forest will follow together with the other locations in chapter 4. The seismoelectric spread extends from -12 m to +12 m distance with the shotpoint at 0 m.

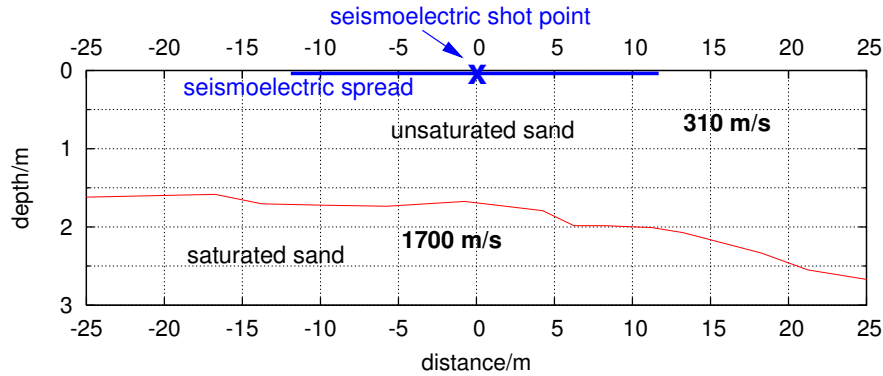


Figure 3.1: Results from seismic refraction analysis. Distance 0 m corresponds to the shot point of the seismoelectric data in this study. The seismoelectric spread extends from -12 m to +12 m.

Figure 3.2 shows a comparison between seismoelectric, seismic, and seismic time derivative data in two different time intervals. To facilitate the interpretation, some events in the seismic section have been highlighted with lines and can be grouped into three categories, depending on their apparent velocities:

1. 1670 m/s -1780 m/s (red): refracted waves
2. 280 m/s - 430 m/s (blue): direct wave interfering with reflected waves at larger offsets
3. < 250 m/s (green): ground roll

The lines marking the events in the seismic section were copied to the seismoelectric and seismic time derivative traces as well. In general, there is quite good agreement between the seismic and the seismoelectric data. Especially the seismoelectric signals confined to the direct wave are very clear. They seem to have a longer duration than the seismic direct wave itself. Furthermore they cover at least partially the arrivals of the Rayleigh wave resulting in a strong mixed arrival at around 40 ms - 60 ms. While ground roll dominates the later parts of the seismogram, it is much weaker on the seismoelectrogram. The same was detected by others before (e.g. Beamish, 1999) and probably reflects the fact that the compressive part of the Rayleigh wave is rather weak compared to its shear component.

In addition to the seismic arrivals, there are also events almost without moveout in the seismoelectric data (best seen in the bottom left image of figure 3.2, marked with dotted lines) preceding the coseismic arrivals.

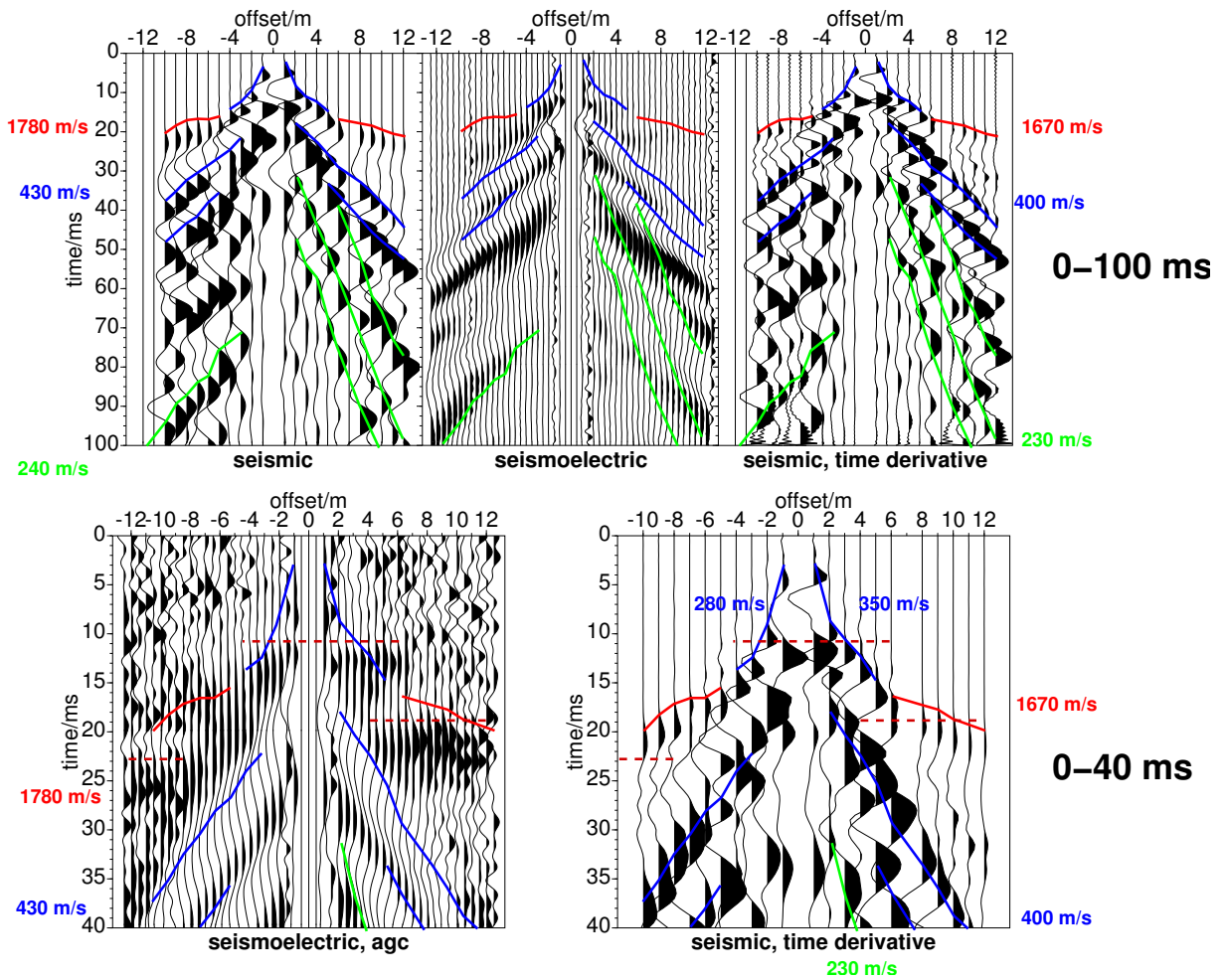


Figure 3.2: Comparison between seismic vertical component and seismoelectric radial component data (Fuhrberg clearing site, September 2002) in two different time intervals. Some events are picked in the seismic section and copied to the other sections as well as marked with their linear best-fit velocity. Top row: Seismic, seismoelectric, and seismic time derivative data, 0-100 ms time interval. Bottom row: Seismoelectric and seismic time derivative data, 0-40 ms time interval. Events without moveout in the seismoelectric data are marked with dotted lines. Red lines mark refracted waves, blue ones direct waves and green ones ground roll. The data are trace normalized except the bottom left data which are scaled with agc.

In addition to surface measurements we performed vertical seismic and seismoelectric profiling (“VSP” and “VSEP”, respectively) in a 30 m deep borehole located in the center of the profile. Downhole seismoelectric data were acquired with a GeoServe borehole electrode chain consisting of 16 electrodes which were combined to form eight vertical dipoles with lengths between 2 m and 8 m and a spacing of 2 m between adjacent dipoles. Seismic data were recorded with a 10 Hz three-component borehole geophone of which I here only show the vertical component. A comparison of the respective sections (figure 3.3) shows that the only clear seismoelectric signals are coseismic waves confined to downward traveling compressional and to some extent also to tube waves. The P-wave velocity of the aquifer is approx. 1700 m/s. These results are in agreement with the refraction seismic outcome (figure 3.1).

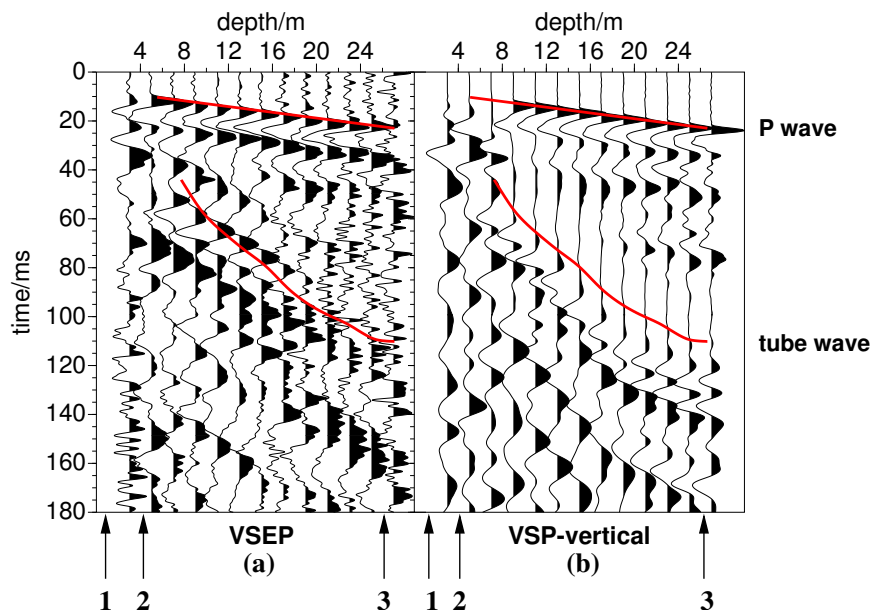


Figure 3.3: Vertical seismoelectric and seismic profiles (VSEP and VSP, respectively) with agc at the Fuhrberg site (September 2002). a) Vertical-dipole seismoelectrics (4 m dipole length), b) vertical component of seismic wavefields. The fast arrival is the compressional wave and is almost identical in seismic and seismoelectric traces. The slow arrival is a tube wave. Arrows at the bottom of the figure indicate the depths and seismoelectric responses at subsurface interfaces based on geological and logging data. 1) groundwater table ($z=1.6$ m), 2) sand-silt interface (4 m), and 3) sand-clay interface (27 m).

3.3 Processing

As mentioned in the introduction, the main obstacle in analyzing converted seismoelectric signals is that the converted signals are often concealed by the much stronger coseismic signals arriving simultaneously with the seismic waves. In addition, even these stronger seismoelectric waves may be covered with man-made 50 Hz noise and its lower and higher harmonics.

Following the literature, it seems to be a rather exceptional case that converted seismoelectric signals

can be discovered in raw data. This might be one of the reasons why seismoelectric measurements still persist in the experimental stage. To get rid of the above mentioned twofold concealment, a double filtering technique has to be applied.

Step 1 is to remove anthropogenic monofrequent noise. Usually I applied an efficient adaptive filtering procedure described in detail by Adam & Langlois (1995) or Butler & Russel (2003). However, because of the low electromagnetic noise level, none of the data from the Fuhrberg Forest had to be filtered from monofrequent noise.

Step 2 is to further enhance converted signals by suppressing coseismic signals with appropriate filter techniques. To my surprise I found that corresponding efforts have only seldom been reported in the literature. To my knowledge only Thompson & Gist (1993) and Haines (2004) used velocity filters. Other authors mostly preferred single trace bandpass filters. As multi-channel data are available, I take advantage of the different apparent propagation velocities of the different types of seismoelectric waves.

Haines (2004) compares three different means of separating the coseismic waves from the converted seismoelectric signals: velocity filters in the frequency-wavenumber (fk) domain, radon filters in the τ - p domain with Cauchy regularization and prediction error filters (PEF). The best performing filter, PEF, needs good pattern models that closely approximate signal and noise and can be quite costly. For a good performance of the radon filter, at least 48 seismoelectric traces should be available and the data quality has to be good enough. I concentrate here on the fk filter. Of the three filters mentioned above, it is the most universally and easily applicable one.

Since converted seismoelectric signals arrive with almost zero slowness (compared to the moveout of seismic waves), that is “infinite” apparent velocity, they can be separated from the much slower coseismic waves in the frequency-wavenumber domain (fk domain) after 2D Fourier transform. In the fk domain waves plot along lines the slope of which is determined by their phase velocity $v = df/dk$. So, zero-slowness waves plot along the frequency axis whereas waves of finite phase velocity are imaged along lines of respective dip. The effect of the fk -velocity filter on seismoelectric data can be seen in figure 3.4.

The low-velocity events were almost completely removed. Nevertheless, there are three aspects which may limit the success of fk filtering especially in separating converted seismoelectric arrivals from the rest of the seismoelectric wave field:

1. Converted arrivals show a strong amplitude decrease transversely to their propagation direction giving them the appearance of a diffusive wave. If this transverse diffusion is too strong, its energy will not be concentrated strictly along the f -axis after fk transformation but it will spread over a significantly larger part of fk space and, possibly, mix with the energy of other arrivals.
2. Vice versa: Due to the limitation of spread length and sensor spacing, spectral remnants of slow arrivals may smear across the f -axis thus mixing with the converted seismoelectric signals after filtering.
3. Travel-time curves of seismic reflections show an apex near the shot point so these waves as well as their seismoelectric equivalents (coseismic waves) have spectral components at zero slowness. The arrivals of the seismic reflected wave appear at two-way travel time while seismoelectric signals arrive almost at one-way travel time due to the large velocity of electromag-

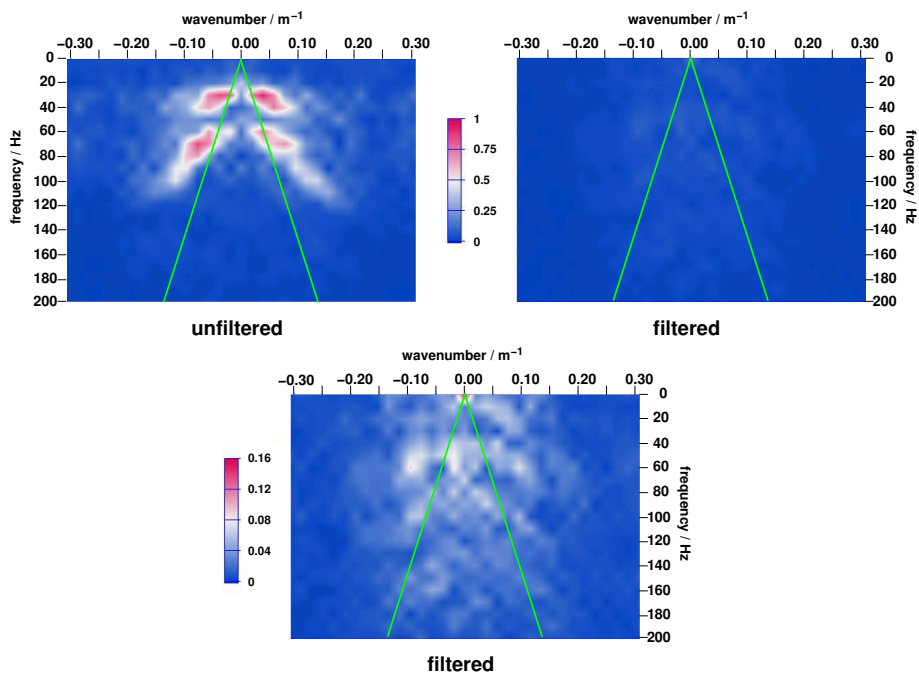


Figure 3.4: Seismoelectric data before (top left) and after (top right) velocity filter in the frequency-wavenumber domain with the same color scale (normalized values). The bottom figure is the same as the top right but with a different color scale. The lines denote the velocity threshold of 1500 m/s below which the data are removed. A generous taper has been used in order to avoid artifacts due to the Gibbs effect. The same seismoelectric data are shown in figure 3.5 in the time-distance domain.

netic waves. Apart from different arrival times the converted seismoelectric wave should also have an amplitude distribution different from the seismic one as pointed out in the description of the converted seismoelectric waves, i.e. the maximum should not occur at zero offset.

3.4 The seismoelectric checklist

There are five circumstances making it plausible that the arrivals observed after and partly also before filtering indeed represent the converted seismoelectric response of the subsurface: a) comparison with seismics, b) confirmation of the results by other methods, c) amplitude distribution, d) identical arrivals at several recordings, and e) converted signals also on the transverse component.

3.4.1 Comparison with seismics

Figure 3.5 shows a comparison between the velocity-filtered seismoelectric radial section and the time derivative of the corresponding seismic traces (vertical 10 Hz geophones) from the same profile, velocity-filtered with the same parameters. Obviously, the strong near horizontal arrivals observed in the seismoelectric section do not have significant counterparts in the filtered seismic section. At around 25 ms, the seismic refracted and the seismoelectric converted wave seem to coincide but can be distinguished from one another by their different apparent velocities. Since the unfiltered seismic and seismoelectric sections are very similar to one another, filter artifacts should have roughly the same effect on both sorts of sections. As there is always a certain risk of gaining artifacts in narrow band pass filtering I recommend to compare filtered seismoelectric and seismic sections to avoid misinterpretation.

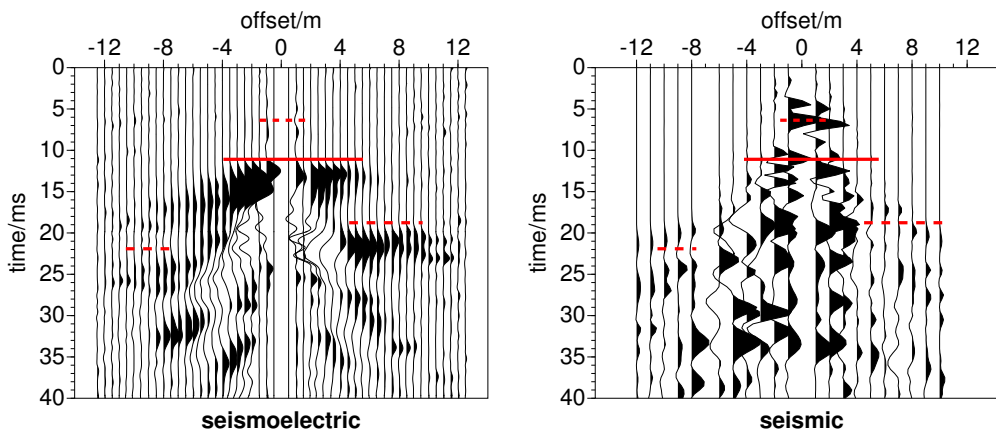


Figure 3.5: Comparison between seismoelectric (left) and seismic time derivative data (right). The data (from September 2002) are velocity-filtered with *agc* removed after filtering. The assumed converted seismoelectric signals have been marked with lines (doubtful events with dotted lines). Obviously, they only appear in the seismoelectric data. The seismoelectric data are shown in figure 3.4 in the frequency-wavenumber domain.

3.4.2 Confirmation of the filter results by other methods

The shallow converted arrivals around 10 ms and around 20 ms can be observed in both filtered and unfiltered sections. Their travel times are confirmed with VSP and VSEP by the arrival times of the seismic waves in the borehole at the layer boundaries. The relation between depth and travel times can be deduced directly from combining the depth of the known layer boundaries¹ and figure 3.3a (VSEP) which yield the expected arrival times of the converted seismoelectric signals. This has been done in figure 3.6 where the expected arrival times are marked with lines. The arrival times of the converted seismoelectric signals should be very close to the seismic one-way travel time as pointed out in the introduction. At the time when the down-going compressional wave (marked in figure 3.6e) hits the indicated interface, the conversion to the seismoelectric signals should occur. At these expected arrival times, there are events without moveout in the surface seismoelectric data (marked in figure 3.6a-d). In the following, I will mostly refer to the arrival of the positive peak in the surface data at around 11 ms, since this arrival is more pronounced than the first break at around 9 ms.

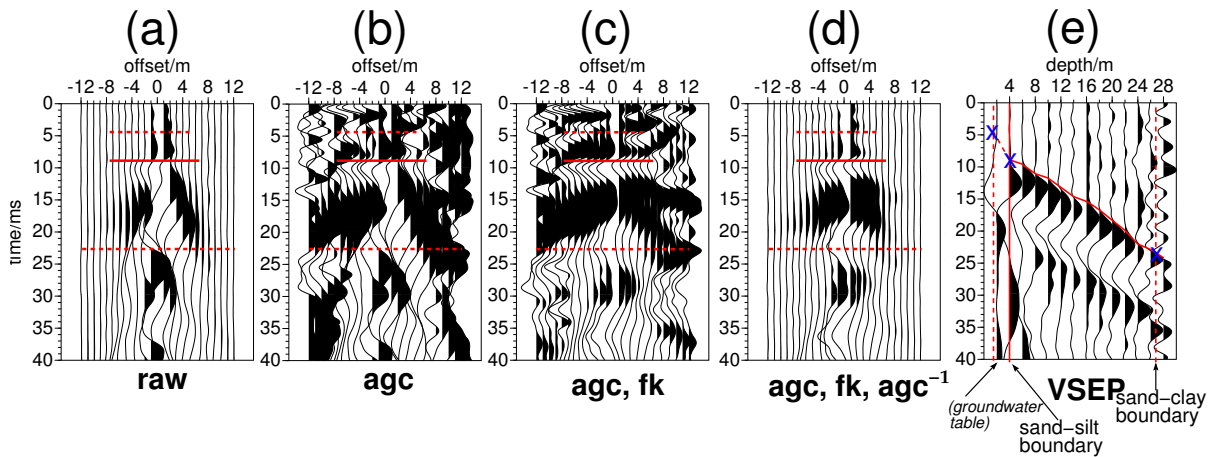


Figure 3.6: Simplified seismoelectric processing flow: (a) raw data, (b) with agc, (c) velocity filtered in the frequency-wavenumber domain, (d) agc removed, (e) VSEP data with layer boundaries from borehole logs (figure 4.3). The expected arrival times of the converted seismoelectric signals are marked with lines. The data are from February 2002.

So it turns out that these earliest converted arrivals correspond to the groundwater table and the shallow sand-silt layering which is connected with changes in porosity. However, the arrivals from the groundwater table are very faint and thus not too reliable (see section 3.4.4 and figure 3.9 for further investigations into this matter). The arrival at 22 ms could possibly be attributed to the sand-clay boundary at 27 m. But as can be seen in figure 3.5 this arrival is not symmetric, the arrival times are different on both sides of the shot point which should not be the case for converted seismoelectric signals, even if the interface is dipping.

One might ask why the assumed converted seismoelectric signals obviously do not occur on the VSEP traces. One reason could be that the electrode type and the coupling conditions were different in surface and in borehole measurements. In addition, the VSEP dipole distance of 2 m was probably too large to record weak and fast decaying converted signals on sufficiently many traces.

¹More information about the location Fuhrberg Forest will be presented in section 4.3.

3.4.3 Amplitude distribution

The amplitude distribution of the converted seismoelectric signals should be close to the one of a vertical electric dipole at the depth of the converting interface (Haartsen & Pride, 1997). Figure 3.7 explains the technique I applied to extract the amplitudes: The data with *agc* are velocity-filtered which leads to the enhancement of waves with very high velocities. The arrival times of the assumed seismoelectric converted signals are picked in the velocity-filtered data. By applying *agc*, however, the amplitude information is lost which is why I only use the time information from the velocity-filtered data while the amplitudes are taken from the raw data. These picked amplitudes are compared with the calculated amplitudes. Alternatively, one could also remove scaling with *agc* after the velocity filter procedure and analyze those amplitudes.

Note that it would not be correct to just use the plain electric field of a vertical electric dipole for comparisons with the measured amplitudes. As we measure the potential difference between two electrodes with a non-infinitesimal difference in between, the potential difference must be calculated between these two points, which leads to the maximum of the potential difference not occurring at an offset of half the depth as would be expected for the electric field of a vertical electric dipole but at smaller offsets. Furthermore, it has to be taken into account that the electric field experiences a distortion close to interfaces between layers of different resistivities, notably at the free surface. This is a consequence of the boundary conditions of electric fields which point out that the component normal to an interface has to be continuous across the interface. As there is no electric field beyond the free surface, no vertical component of the electric field is to be expected directly at the boundary to the free surface. The necessary calculations are explained in section 6.2.

This distortion must not be omitted as it can alter the amplitudes significantly. Note that only relative amplitudes can be compared because details of the hydraulic subsurface parameters are unknown and I made no attempt to calibrate the source signal.

A comparison of calculated and observed converted signals of the data set of figure 3.5 is shown in figure 3.8. As can be seen, the agreement between measured and calculated data is quite good. The response of the groundwater table is shown in figure 3.8a. Because of its shallow depth (1.6 m), it can be detected only at very small offsets. As pointed out by Garambois & Dietrich (2002), the approximation by the field of a vertical electric dipole is strictly valid only for converting horizons at a depth of more than one seismic wavelength. In the present case (70 Hz, 310 m/s) one seismic wavelength corresponds to about 4 m which is slightly more than the double distance to the groundwater table. However, the well fitting curve in figure 12 a seems to indicate that the dipole approximation may be not too bad even below the one-wavelength limit.

The differences between measured and calculated data are very small for the conversion from the sand-silt interface (figure 3.8b). The data would fit even better if either the measured or the calculated data were laterally shifted 2 m. This could be an indication of a dipping converting interface. The signals of the sand-clay-interface at 27 m depth could not be fitted comparably well probably because amplitudes are generally weaker and contain remnants of coseismic waves (cf. figure 3.7).

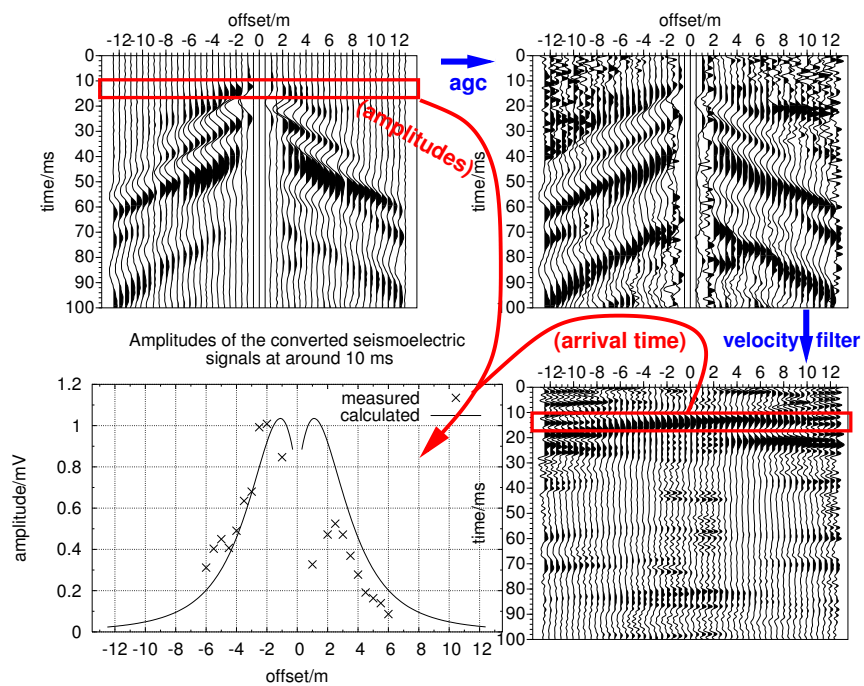


Figure 3.7: Extraction and amplitude analysis of converted seismoelectric signals (September 2002). The raw data (top left) are scaled with agc (top right) and velocity-filtered (bottom right). This latter section is used to identify possible converted signals enhanced by the filtering procedure. The amplitudes are taken from the raw data and compared with theoretical predictions (bottom left).

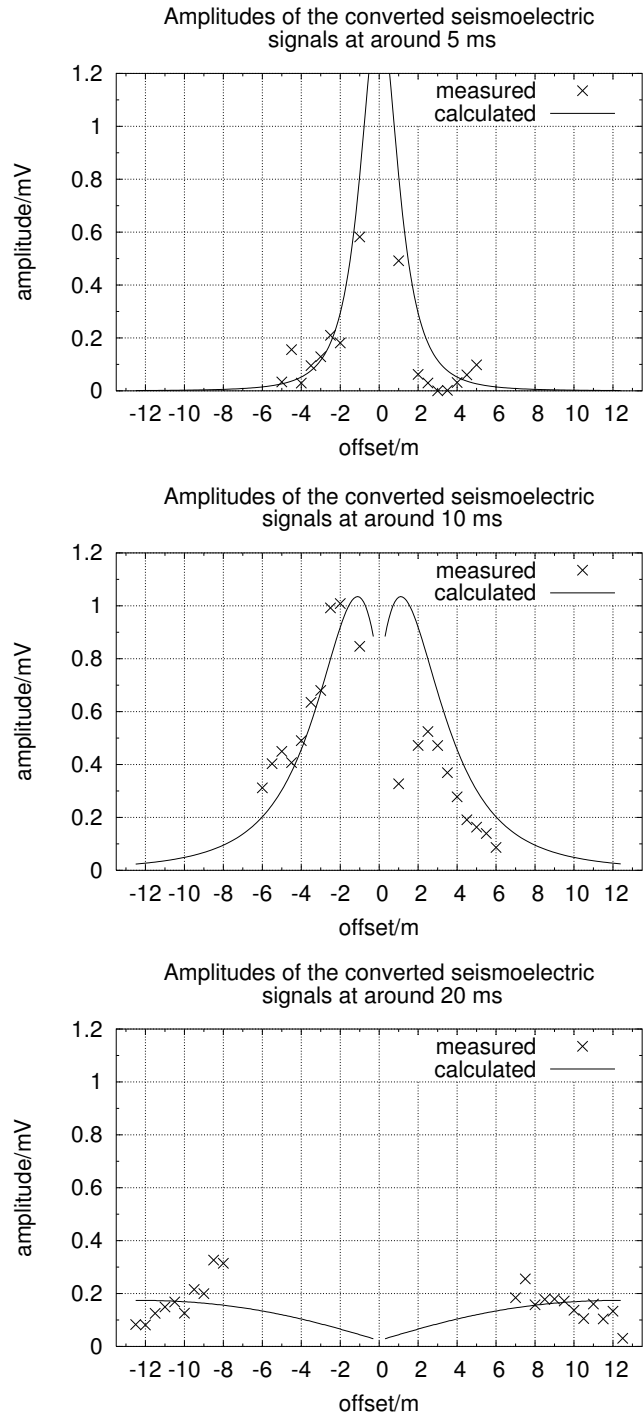


Figure 3.8: Comparison of measured amplitudes of converted seismoelectric signals and their calculated correspondences (relative amplitudes). Assumed origins of the converted seismoelectric signals are the groundwater table (a) at 1.6 m, the sand-silt interface at 4 m depth (b) and the sand-clay interface at 27 m (c).

3.4.4 Repeatability

Figure 3.9 proves that the same arrivals of the assumed converted seismoelectric wave can be seen in data measured with different trigger mechanisms, different dipole lengths, and at different times: manual trigger, 2 m dipole length, September 2002 (a), acceleration trigger, 4 m dipole length, February 2002 (b) and manual trigger, 4 m dipole length, February 2002 (c). Figures 3.9 d-f show the same data velocity filtered with agc removed. The filter procedure has clearly accentuated the assumed converted signals and the resemblance between the three data sets. Furthermore, each of the recordings shown in figure 3.9 is already a combination of several single recordings, proving the high repeatability of these results. On the other hand, there is a difference between the traces gathered in September 2002 (a and d) and in February 2002 (b,c,e,f). The arrival at around 22 ms (assumed to originate from the sand-clay-boundary in 27 m depth) can be spotted only in the September data whereas the arrival at around 5 ms (assumed to originate from the groundwater table) is discernible in the February data only. Possibly the conditions of the uppermost parts of the ground were more favorable in September for achieving a greater maximum depth. Since the amplitude distribution for the assumed converted field arriving at around 22 ms does not follow the expected pattern, it has to be doubted though that this arrival is a converted seismoelectric field (see section 3.4.3 and figure 3.8c).

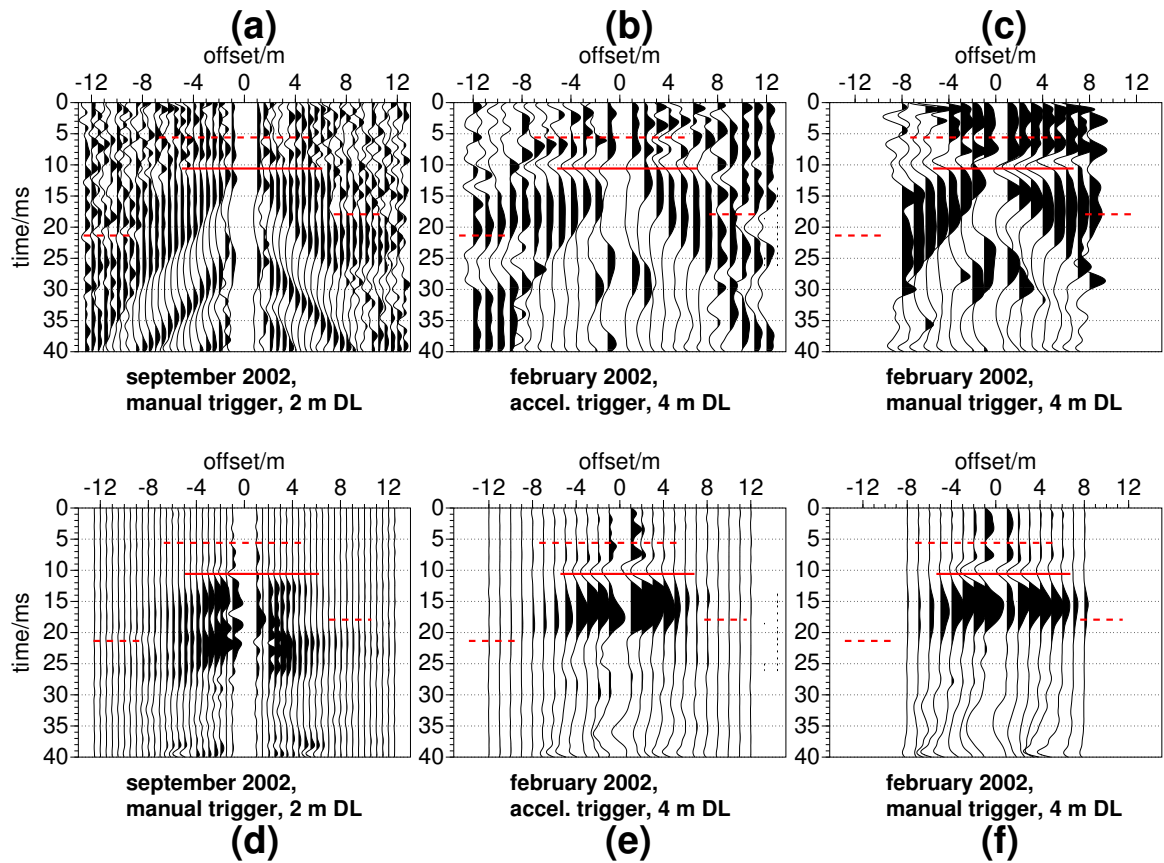


Figure 3.9: Comparison between different seismoelectric data sets with agc showing that the assumed converted seismoelectric signals (highlighted with lines) are repeatable and not caused by trigger artifacts. (a) manual trigger, 2 m dipole length, September 2002, (b) acceleration trigger, 4 m dipole length, February 2002, (c) manual trigger, 4 m dipole length, February 2002. The same data are shown in d-f after velocity filtering.

3.4.5 Converted signals on the transverse component

The fifth argument in favor of interpreting the filtered seismoelectric response as converted signals is the surprising observation that arrivals recorded on the transverse dipole component without any filtering show high similarity to the radial component records after filtering. This will be discussed in section 6.1 in more detail (cf. figure 6.5 left and right, respectively).

The strongest argument in favor of interpreting the fk filter output as converted seismoelectric signal is clearly that expected and measured arrival times as well as the amplitude distribution fit well. Filter artifacts such as noted above do not seem to play a significant role. However, in order to rule out doubts in interpretation, it is important to base an identification of assumed converted signals on a combination of the criteria noted above. For future development, one could think of a seismoelectric processing software that semi-automatically checks assumed converted seismoelectric events or identifies them from a seismoelectrogram. But as of now we still have to do these checks by hand and will apply them to data from other measurement locations in the following chapter.

3.5 Conclusions

The assumed converted seismoelectric signals measured in the Fuhrberg Forest were enhanced with velocity filters in the frequency-wavenumber domain. This filter effectively weakened the unwanted coseismic waves and the result was controlled in order to verify that no filter artifacts destroyed the seismoelectric traces:

1. Since the seismic traces are very close to their seismoelectric equivalents, the velocity filter should produce roughly the same artifacts if applied to the seismic and seismoelectric traces with the same filter parameters. However, the assumed converted seismoelectric signals only appear on the seismoelectric traces and are therefore probably not filter artifacts.
2. From vertical seismoelectric profiling, I determined the arrival times of the down-going compressional seismic wave at the known boundary layers. These arrival times coincide well with the arrival times of the assumed converted seismoelectric waves.
3. The amplitude distribution of these seismoelectric signals was compared with the calculated amplitude distribution generated by a vertical electric dipole directly under the shot point at the converting interface, which is a good approximation to the real amplitudes of the converted seismoelectric field. Two of the three assumed converted seismoelectric events match the calculated amplitude distributions well.
4. Furthermore, I compared several repeated recordings at the same location, with some months in between and with different dipole lengths and trigger mechanisms as well as with manual triggers. The mentioned events proved to be highly repeatable. It could also be shown that the trigger mechanism itself does not harm the seismoelectric traces which is an important prerequisite.

Chapter 4

Seismoelectric measurements in different environments

4.1 Overview

As already stated in chapter 1 there are very few examples of seismoelectric measurements in literature and consequently also only very few examples of different environments in which seismoelectric measurements were conducted. In the following table 4.1, the environments are listed in which meaningful seismoelectric signals were acquired and presented in literature (only field measurements). Parts of this list were done by Dr. T. Beilecke (now GGA) and Dr. S. Wölz.

The list is indeed very short. Apparently, most seismoelectric publications either deal with numerical, theoretical or laboratory measurement aspects. The need for further research in seismoelectric field measurements to elucidate its possibilities and suitabilities is evident. The listed seismoelectric data were recorded in different environments (sand, gravel, clay, crystalline rocks), but cross-checks from one publication to another are difficult because different authors use different sources, receivers, amplifiers, etc.

A broad overview is needed if one aims to evaluate a possible role of seismoelectrics in hydrogeophysics: How is the variability of seismoelectric data from one location to the next one? Can meaningful seismoelectric data only be collected on some isolated spots with optimum conditions? Or does seismoelectric acquisition prove to be equally successful at any location? There is no doubt that the ground conditions will influence seismoelectric data in one way or another but this has not been investigated up to now. Some authors do present approaches in this direction:

The data presented by Mikhailov et al. (2000) clearly show different seismoelectric amplitudes in granite and diorite because of the different ζ -potentials in both rock types. Soviet experiments showed higher amplitudes in limestone than in clay (Parkhomenko & Gaskarov, 1971).

Also the variability at one and the same location is of interest. So far, no real repeated measurements at one site were published. Thus it is unknown how changing ground conditions, e.g. due to seasons or water saturation, influence the seismoelectric data. We visited some sites over and over again

| Author(s) | Environment | Groundwater table | Converted signals detected? |
|-----------------------------|--|---|-----------------------------|
| Martner & Sparks (1959) | target: base of the weathered layer | coincident with base of the weathered layer | yes |
| Butler et al. (1996) | road fill above glacial till above bedrock | around the first boundary | yes |
| Mikhailov et al. (1997) | top soil above unsat. and saturated glacial till above bedrock | 10.5 ft in glacial till | if so, then weak |
| Beamish (1999) | a) boulder clay above sandstone | ? | no |
| | b) river sand channel in crystalline rocks (mostly granite) | 0.5 m in sand | no |
| Mikhailov et al. (2000) | granite and diorite | (water well) | yes |
| Garambois & Dietrich (2001) | a) alluvial sediments (alternating layers of gravel, sand, and clay) | 1.5 m | probably yes |
| | b) 1 m vegetal soil over gravel and sand | 7 m | no |
| Haines (2004) | a) trench with wet sand in clayey soil | / | yes |
| | b) clayey soil above bedrock | | no |

Table 4.1: Overview of seismoelectric field measurements in literature.

(Fuhrberg Forest, Segeberg Forest, GeoModel) to investigate into the repeatability of seismoelectric signals. If the results changed completely with no significantly changed ground conditions, one would be forced to be very doubtful about the relevance of this method.

4.2 Measurement sites

In the course of the seismoelectric project at Kiel University, numerous field sites were visited and seismoelectric field measurements were conducted, usually in combination with additional seismic and/or geoelectric or GPR measurements. The sites are presented in figure 4.1.

This collection is probably the most comprehensive in seismoelectrics so far. In the following sections, I will compare data from the locations Fuhrberg (section 4.3), Menzlin (section 4.4), Selinunte/Sicily (section 4.5), Segeberger Forest (section 4.6), and the GeoModel on the university campus (section 4.7). The unified interpretation at the end of this chapter (section 4.8) combines the findings of the preceding sections. The aim of this thesis is not to list all obtained results but to present the broad variability of the data and to give reasons for this variability. As can be seen in table 4.2,

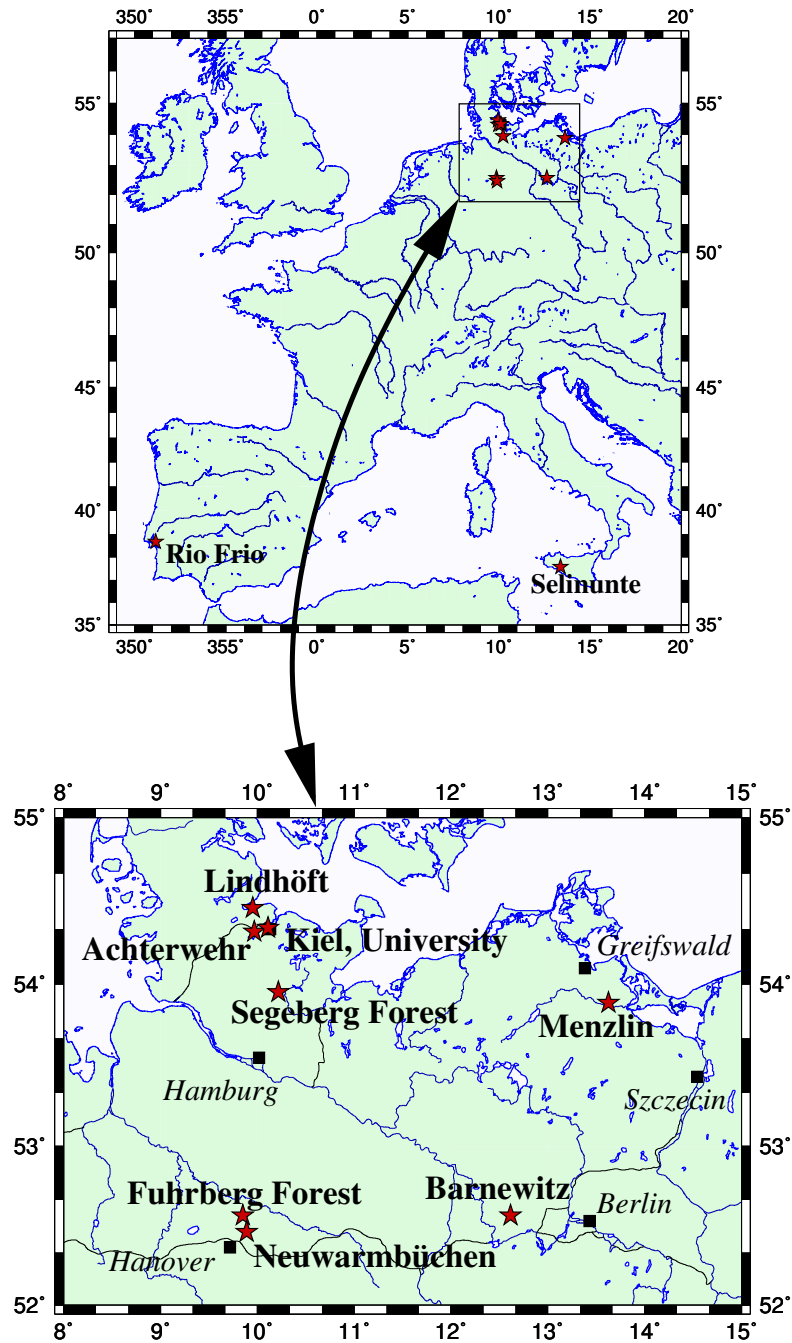


Figure 4.1: Locations where seismoelectric measurements were conducted in the course of the seismoelectric project at Kiel University. Most sites are concentrated in Northern Germany (zoomed area). The more detailed locations of some of the sites will be shown in the respective sections.

| measurement site | date of measurements | |
|---|-------------------------|---|
| Sports ground of Kiel University | July 19, 2001 | clayey soil |
| Segeberg Forest (Schleswig-Holstein) | September 5, 2001 | sandy forest ground |
| Segeberg Forest | September 17, 2001 | sandy forest ground |
| sports ground | September 28, 2001 | clayey soil |
| sports ground | November 14, 2001 | clayey soil |
| sports ground | December 5, 2001 | clayey soil |
| Fuhrberg Forest (Lower Saxony) | February 7-8, 2002 | sand aquifer above clay aquiclude |
| sports ground | February 27, 2002 | clayey soil |
| sports ground | May 28, 2002 | clayey soil |
| Frauendamm near Achterwehr (Schleswig-Holstein) | June 6, 2002 | unknown |
| Fuhrberg Forest | September 10-12, 2002 | sand aquifer above clay aquiclude |
| Selinunte/Sicily | October 16-17, 2002 | alluvial soil and sand dune |
| Barnewitz near Berlin (Brandenburg) | May 8-10, 2003 | sand and silt layers |
| Rio Frio/Portugal | Juni 29 - July 9, 2003 | dry sand and clay |
| Lindhof (Schleswig-Holstein) | November 5 and 19, 2003 | very heterogeneous layers of clay, clayey sand and sand |
| Segeberg Forest | December 2, 2003 | glacial sand on ground moraine |
| Fuhrberg Forest | January 8, 2004 | sand aquifer above clay aquiclude |
| Fuhrberg Forest | April 25-26, 2004 | sand aquifer above clay aquiclude |
| Neuwarmbüchen (Lower Saxony) | April 26, 2004 | unknown |
| Segeberg Forest | May 27, 2004 | glacial sand on ground moraine |
| Segeberg Forest | June 3, 2004 | glacial sand on ground moraine |
| Segeberg Forest | June 16, 2004 | glacial sand on ground moraine |
| Menzlin (Mecklenburg-Western Pomerania) | August 22, 2004 | ground moraine overlain by sand dunes |
| GeoModel/University Campus | March 22, 2005 | artificial sand basin |
| GeoModel | June 1, 2005 | artificial sand basin |
| GeoModel | July 5, 2005 | artificial sand basin |
| Bornhöved (Schleswig-Holstein) | July 14, 2005 | sandy cultivated field |
| GeoModel | July 28, 2005 | artificial sand basin |
| Segeberg Forest | October 14, 2005 | glacial sand on ground moraine |
| Segeberg Forest | November 1, 2005 | glacial sand on ground moraine |
| Segeberg Forest | December 6-7, 2005 | glacial sand on ground moraine |
| Segeberg Forest | January 24-25, 2006 | glacial sand on ground moraine |
| GeoModel | February 13-16, 2006 | artificial sand basin |
| Segeberg Forest | February 20-21, 2006 | glacial sand on ground moraine |

Table 4.2: Overview of the measurement locations visited in the course of the seismoelectric project at Kiel University.

we visited the sites GeoModel and Segeberg Forest quite often which permits to compare different data from the same location at different points in time. The data analyzed in the following sections are from very different sites, ranging from rather remote areas with very high signal to noise ratio (Fuhrberg, section 4.3, and Menzlin, section 4.4) to urban sites with strong coherent electromagnetic noise (GeoModel, section 4.7), very dry sites where seismoelectric signals were not expected (Selinunte, section 4.5) and sites with very broad variability (Segeberg Forest, section 4.6) in order to get the most general picture possible. It is clear that one has to concentrate on some locations and that I cannot list all results from the selected sites, either.

4.3 Fuhrberg

The key findings of the data from this location in terms of the converted signals have already been presented in section 3. Here, I concentrate on data not yet shown as well as on repeated measurements.

Seismic and seismoelectric field data were acquired in the Holocene sedimentary environment of the Fuhrberg Forest near the city of Hanover (N Germany, State of Lower Saxony in February and September 2002 and in April 2004. The site was chosen because of its low level of anthropogenic seismic and electromagnetic noise, its simple geological structure and the availability of boreholes and geophysical borehole logs for ground truthing. There are two boreholes at the Fuhrberg site in the near of which we conducted the measurements, named *clearing* and *waterworks* locations in the following. The locations of the two boreholes are shown in figure 4.2. Most Fuhrberg data shown in this thesis are from the clearing location as the data quality tends to be higher there. This location will be analyzed first (sections 4.3.1 and 4.3.2) followed by the waterworks location in sections 4.3.3 and 4.3.4.

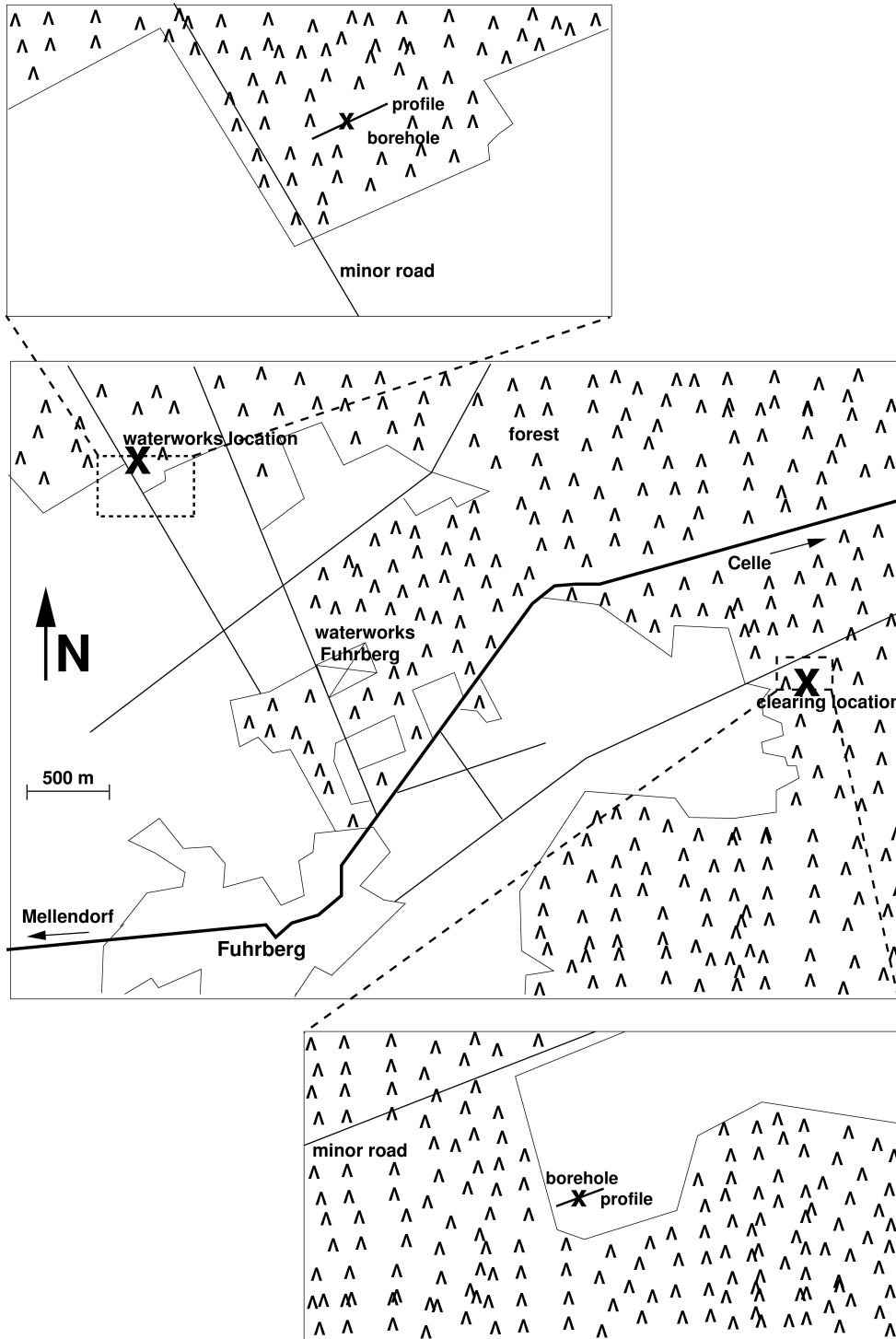


Figure 4.2: Location of the two measurement sites in the Fuhrberg Forest. The general location of the town of Fuhrberg can be seen in figure 4.1.

4.3.1 Geological setting - clearing site

The geological setting of this site (a clearing in a forest) can be characterized by a shallow groundwater table at between 1.5 m and 2.5 m depth, depending on the time of measurement, found within a 27 m thick aquifer consisting of sand and a thin silt layer between 4 m and 5 m depth. The sand layer is followed by a clay aquiclude (see figure 4.3). Converted seismoelectric signals were expected to be generated at these interfaces. A seismic refraction interpretation as well as the existence of seismoelectric converted signals were presented in section 3.

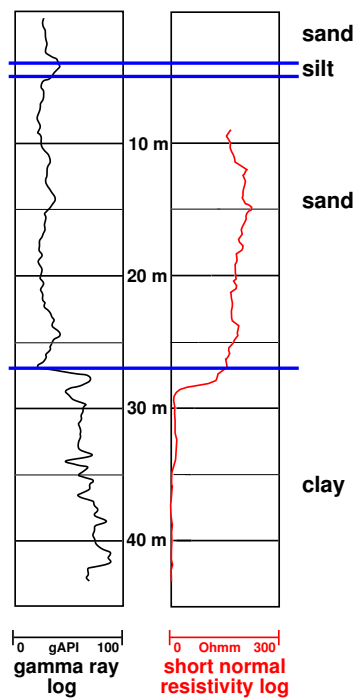


Figure 4.3: Geological profile and borehole logs from the clearing site at the measurement area Fuhrberg Forest. The borehole was drilled and the logs were measured by the Federal Institute for Geosciences and Natural Resources.

4.3.2 Data and interpretation - clearing site

4.3.2.1 Geoelectrics

We performed Wenner- α profiling across the Fuhrberg Forest clearing location, the result of which is presented in figure 4.4. The middle of the profile is close to the borehole (with some meters crossline distance). All resistivity data in this thesis were interpreted using 2D smoothness constrained inversion, employing a quasi-Newton technique to reduce calculations (Loke & Barker, 1996). The resistivity decreases strongly below 2 m depth, roughly corresponding to the groundwater table which at

the time of measurement (January 2004) was at 1.5 m. No influence of the borehole on the resistivity can be seen which is expected because the borehole wall is made of PVC.

In contrast to the seismic refraction result from this profile (figure 3.1 on page 47), the groundwater table shows only a weak decrease towards greater positive offsets could have to do with the times of measurements: While the seismic refraction profile was collected in April, when the trees consume a lot of water, the geoelectric profile was recorded in January, i.e. not in the growth phase so the groundwater table should be less influenced from water consumption by the trees.

The comparison between the Wenner profile and the borehole log is a bit difficult because the resistivity log starts at a depth of 10 m whereas the Wenner profile extends to a depth of 16 m only, so the overlapping area is not very large. In this area, however, the resistivities range between 200 Ω M and 300 Ω M in both the surface and the borehole data. For the depth covered with this surface geoelectrics survey, I do not expect any significant lateral variability and assume plain layers.

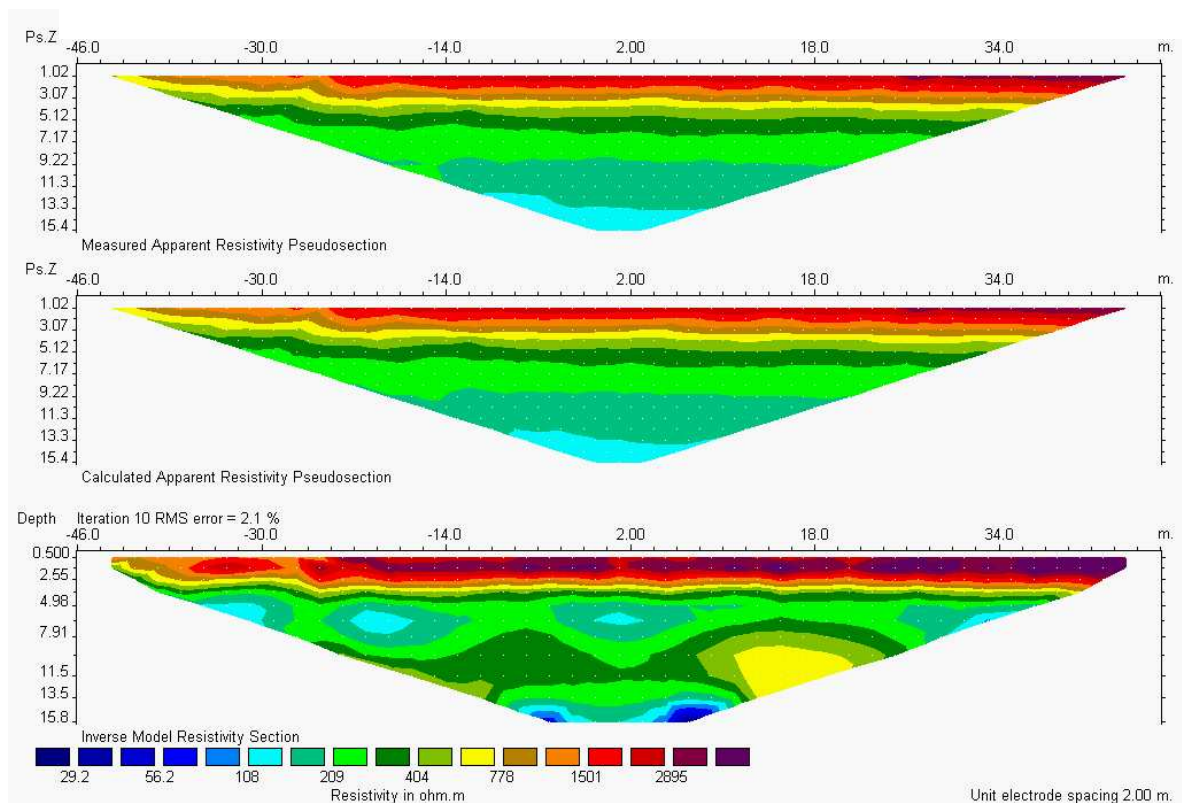


Figure 4.4: Surface geoelectric profile from the Fuhrberg clearing site. The middle of the profile is close to the borehole and the positive offsets point towards west. Top: measured pseudosection, middle: calculated pseudosection, bottom: resistivity model.

4.3.2.2 Seismoelectrics and seismics

As already shown in chapter 3 and especially in figure 3.9 on page 58, the seismoelectric data from the clearing site at the Fuhrberg Forest location is generally good. But there are also examples of

much worse data from this site (figure 4.5). These data were collected in April 2004. We acquired the best data in February 2002 (where we stacked only 10 times instead of 20 as we normally did thereafter). The shot point in the April 2004 data was not the same as shown in the other Fuhrberg clearing site data presented in this thesis, but the distance was only some 20 m and neither the seismic data nor the geoelectric data from the site suggest strong lateral differences which could account for this strong discrepancy in data quality. Also the equipment used is more or less the same. There are no signs of 50 Hz electromagnetic noise in the bad quality data, so the changes are either in the ground conditions or in the cabling. However, the cabling remained essentially the same in all measurements, which leaves the changed ground conditions as the sole remaining parameter.

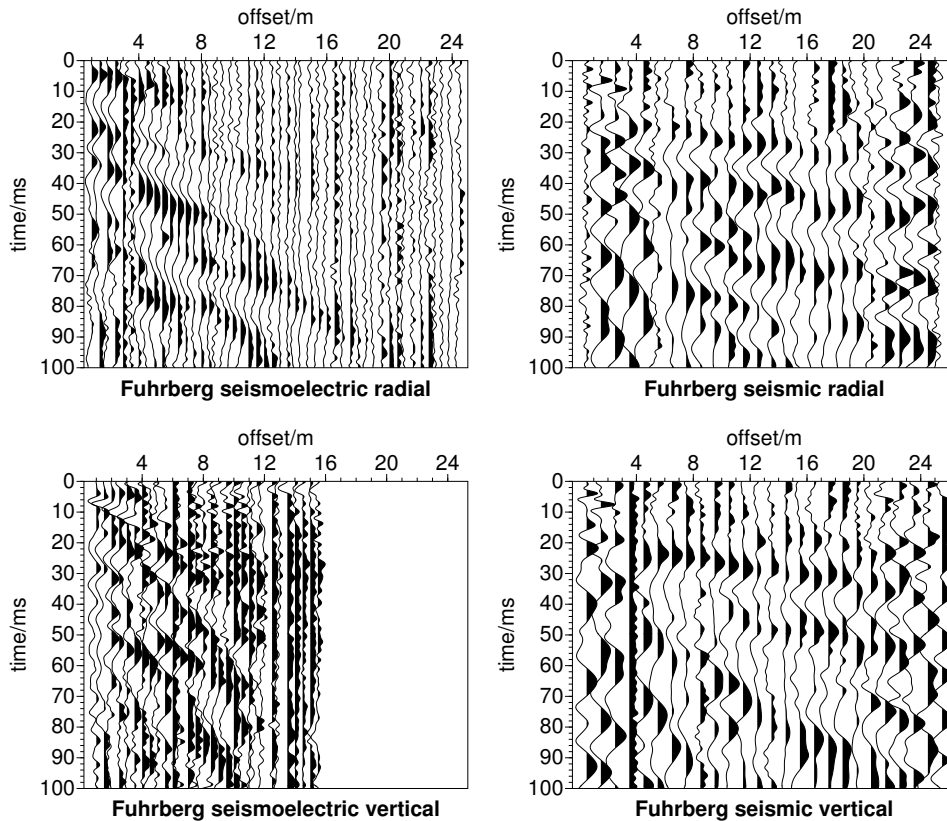


Figure 4.5: Examples of quite bad data with *agc* from the Fuhrberg Forest site (April 2004). Left: seismo-electric, right: corresponding seismic data. Top: radial component, bottom: vertical component. These data can be compared with data from the same location but with much better data quality (see figure 3.9).

4.3.3 Geological setting - waterworks site

The geological setting of this site can be characterized by a shallow groundwater table at between 2.5 m and 3.6 m depth, depending on the time of measurement, found within a 24 m thick aquifer consisting of sand. In contrast to the situation found at the clearing location (section 4.3.1), there is no silt layer at shallow depth. The sand layer is followed by a clay aquiclude (figure 4.6). We were not able to collect surface geoelectric data because a metal fence runs parallel close to the profile and would have harmed the electric data. I will not investigate into this any further because I will not study any converted seismoelectric signals at this site but only compare the general data quality in comparison with the seismoelectric data from the other Fuhrberg location in section 4.3.2. While the clearing site at Fuhrberg was an open field with forest on all sides except to the north, this profile at the waterworks site was in the forest.

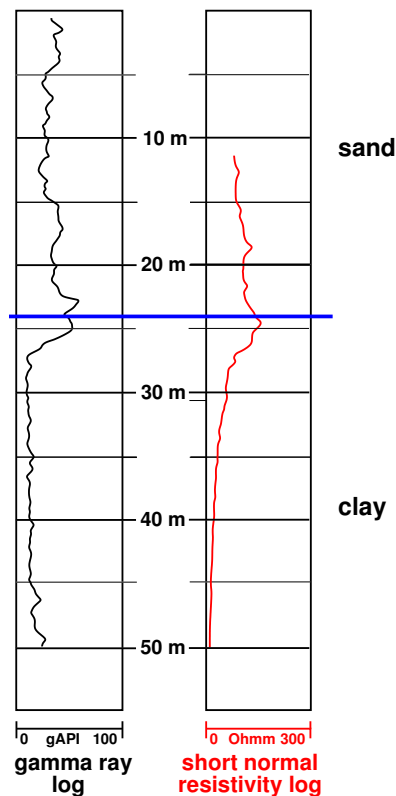


Figure 4.6: Geological profile and borehole logs from the waterworks site in the measurement area Fuhrberg Forest. The borehole was drilled and the logs were measured by the Federal Institute for Geosciences and Natural Resources.

4.3.4 Data and interpretation - waterworks site

Figure 4.7 consists of a comparison between seismoelectric and seismic radial and vertical components from the waterworks site at the Fuhrberg Forest location. The data quality is by far best on the radial seismoelectric component and on the vertical seismic component. It is significantly poorer on the radial seismic component and especially on the vertical seismoelectric component but that later fact is most likely attributed to the shorter dipole length of this component. Due to the hard ground which was full of massive tree roots, it was impossible to drive the long vertical electrodes into the ground in a reasonable amount of time so we limited the vertical dipole length to 1 m instead of 1.5 m like at other locations. Close to the surface, the electric amplitudes diminish very fast because of the boundary conditions of electric fields (see chapter 3.4.3 on page 54) so that this seemingly small difference in dipole length can have a strong effect.

Although the data quality of the radial seismoelectric component is perfectly comparable with the examples from the clearing site, no converted seismoelectric signals can be detected. One of the reasons could be an presumable strong seismic attenuation at depth because of the thick tree roots. Thus, the seismic waves would be too weak to generate detectable converted seismoelectric signals at the interface at 24 m depth (see figure 4.6). It could also be that the contrast at this boundary simply is not strong enough. As is apparent in figure 4.6, neither the normal logs nor the γ -logs show strong changes as the boundary.

4.3.5 Unified interpretation

In general, the data quality tends to be higher at the clearing site. The reason for this could be that there are no big tree roots at the clearing site that could attenuate the seismic energy as much as it seems to be the case at the waterworks site. The two sites seem to be roughly equally remote without or with only very weak signs of anthropogenic electromagnetic noise in the seismoelectric data. Although generally high, the signal-to-noise ratio nevertheless shows quite remarkable variability, obviously depending on the time of measurement and probably on the ground conditions.

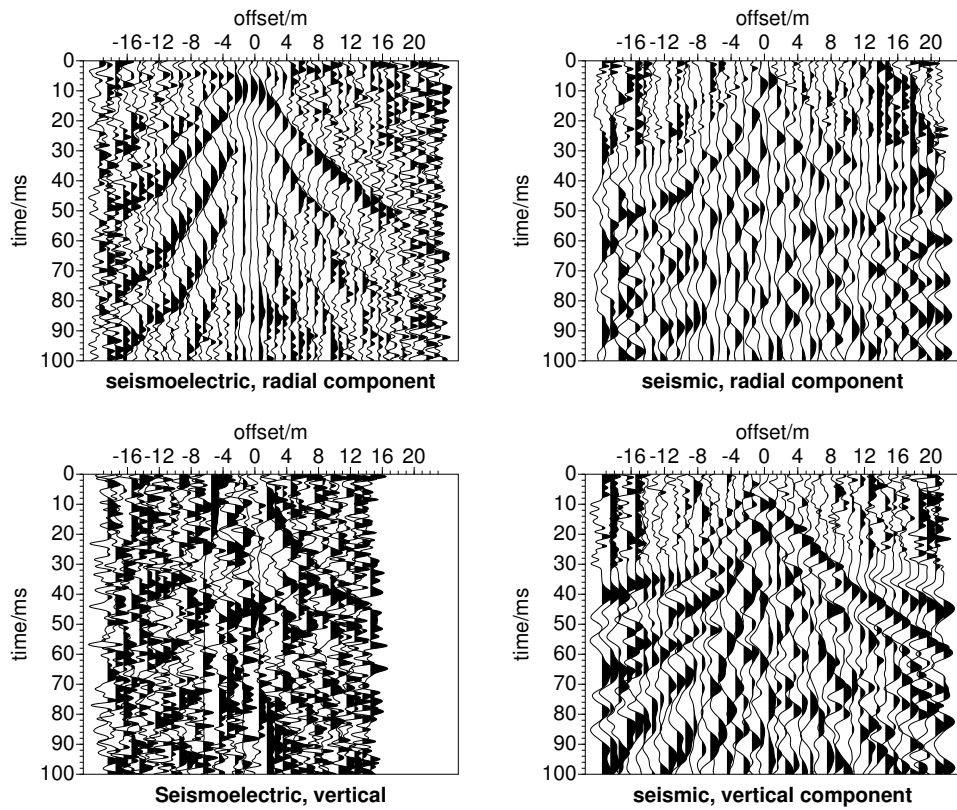


Figure 4.7: Examples from the Fuhrberg waterworks site measured in January 2004 with agc. Left: seismoelectric sections, right: corresponding seismic sections. Top: radial component, bottom: vertical component. The dipole length of the vertical component is only 1 m and the data quality quite poor.

4.4 Menzlin

The data in this section are from a rather remote area in Western Pomerania without any trace of 50 Hz in the seismoelectric recordings. In contrast to other examples presented in this thesis (e.g. Fuhrberg Forest, Segeberg Forest, and the GeoModel), we visited the Menzlin site only once and can therefore not present any long-term repeatability measurements. Because the data presented in this section turned out to have the highest quality, I extend this section and show an example of seismoelectric mapping of a 3D structure. After the presentation of the location in section 4.4.1 I will determine the underground structure with GPR (section 4.4.2) and refraction seismics (section 4.4.3) before analyzing the two perpendicular seismoelectric profiles in section 4.4.4. I will then apply the seismoelectric checklist from section 3.4 on my data (section 4.4.5) and summarize the results in section 4.4.6.

4.4.1 Geometrical, geographical and geological setting

In order to check the repeatability of seismoelectric measurements and to investigate the possibility of seismoelectric mapping, we conducted measurements along two profiles perpendicular to another across a glacial dune structure near the village of Menzlin in Western Pomerania, close to the town of Anklam at the river Peene (see figure 4.8). One profile followed the strike of the dune and the other one the fall (see figure 4.9). In the following, these two profiles will be called fall and strike profile, respectively. The seismoelectric measurements were accompanied by a seismic refraction profile with the same shot points and receiver positions. On some positions, seismic as well as seismoelectric data were recorded in three dimensions. Parallel to the fall profile, also a ground penetrating radar (GPR) profile with a 200 MHz antenna was acquired. In addition, we also determined the topography and the coordinates with differential GPS (see figure 4.10) which made it possible to apply a topography correction in the following section 4.4.2.

The location Menzlin turned out to be almost free from electromagnetic noise and gave rise to seismoelectric data with an exceptionally high signal-to-noise ratio. Anthropogenic 50 Hz noise cannot be spotted on the traces. Before I turn to the extraction and verification of the seismoelectric signals, I will first determine the subsurface structure.

4.4.2 Determination of the ground structure - GPR

The GPR data are topography corrected, Kirchhoff migrated, and converted from time to depth with a velocity of 9 cm/ns. This velocity was determined from diffraction hyperbola analysis and is quite typical for partially saturated sand. For the GPR data processing I owe thanks to Dr. Ulrike Werban (now Umweltforschungszentrum (Centre for Environmental Research) Leipzig) and Christina Klein.

The profile (see figure 4.11) revealed a clear boundary which lies in approximately 3.5 m depth and some finer layering at shallower depth. After topography correction, migration, and depth conversion, the arrivals appear to be subhorizontal.

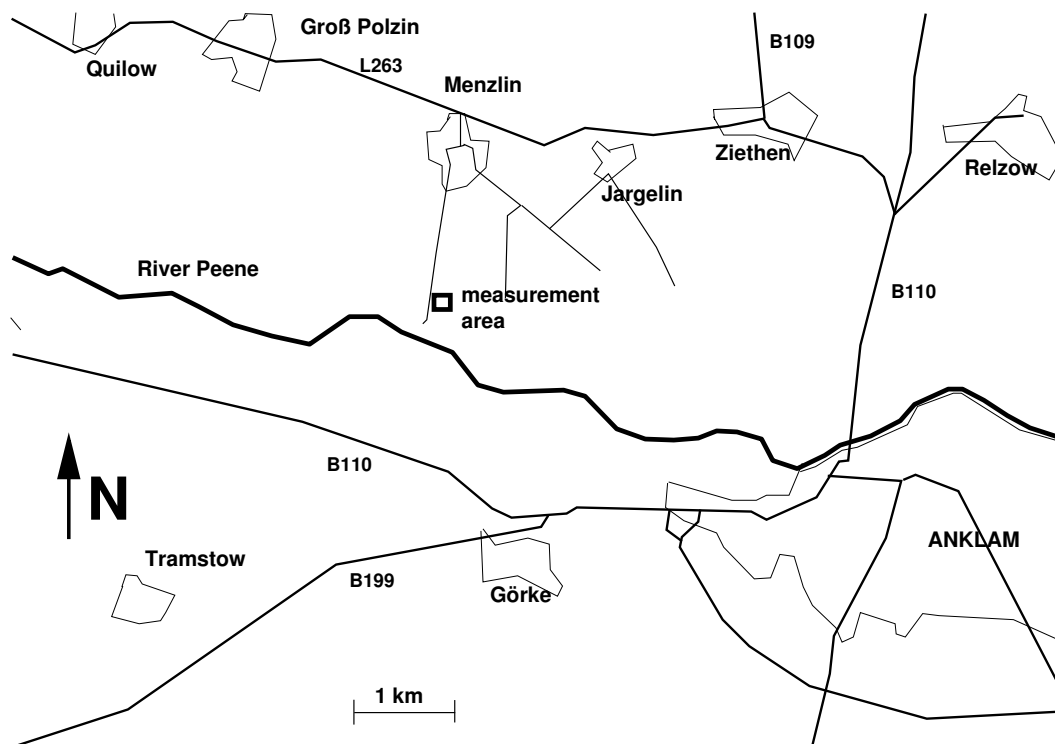


Figure 4.8: The measurement area Menzlin.

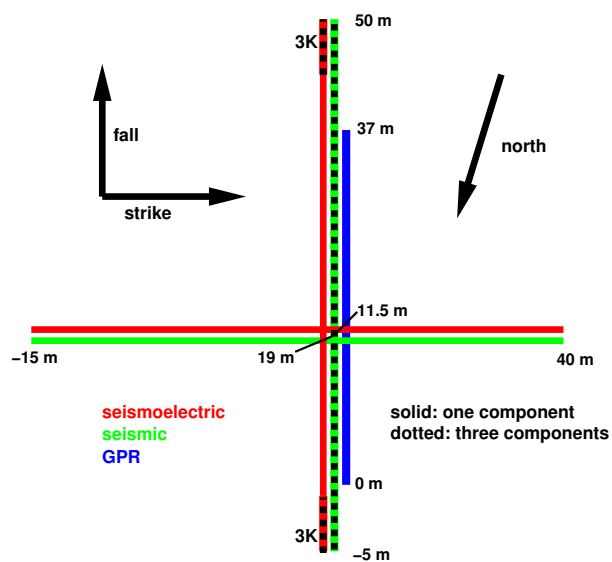


Figure 4.9: Overview of the different methods and their positions used at the Menzlin site. The two profiles are shown in 3D view in figure 4.10.

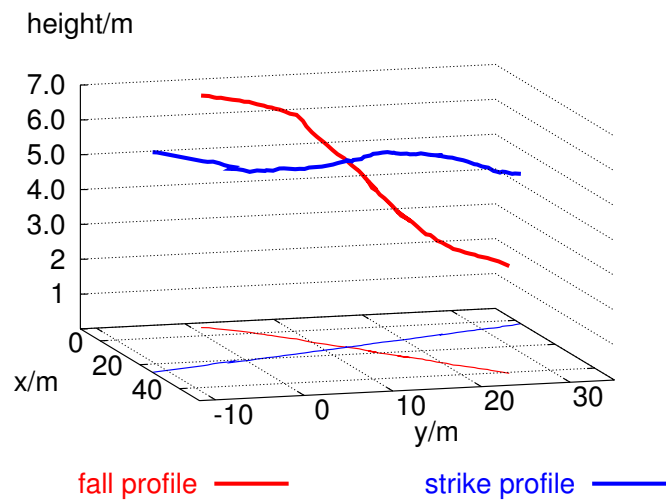


Figure 4.10: Position of the two perpendicular profiles in a 3D view. The two profiles are shown in 2D view in figure 4.9.

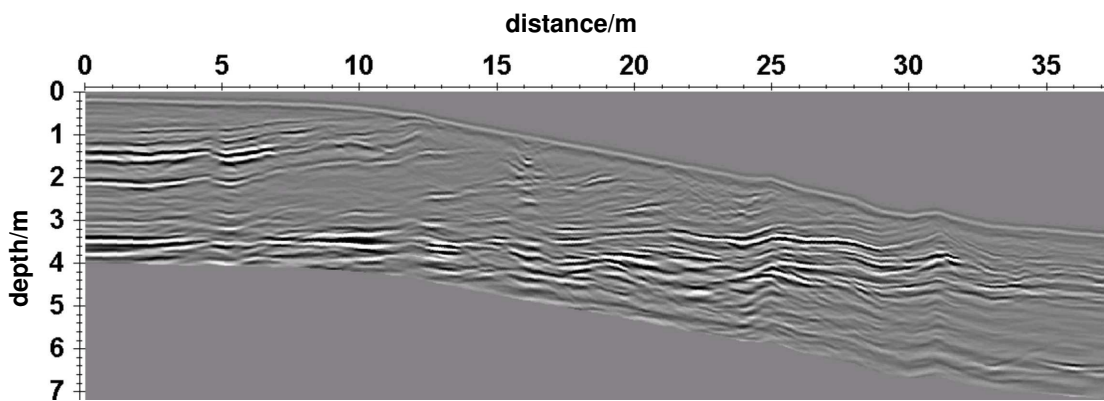


Figure 4.11: GPR data collected along the fall profile in Menzlin. A 200 MHz antenna was used and a topography correction applied. The data are Kirchhoff migrated and depth-converted with a velocity of 9 cm/ns.

4.4.3 Determination of the ground structure - refraction seismics

With the seismic data collected on the two profiles, a refraction seismic analysis could be carried out with the vertical component seismic data. I picked the first breaks and refined the seismic velocity model with trial-and-error aided by least-squares inversion until the calculated arrivals matched the picked breaks well. The calculations were done with a ray-tracing approximation algorithm as implemented in the software package Claritas. The technique is described by (Woodward, 1991). The results from both profiles are presented in figure 4.12. The velocity of 250 m/s for the first layer is typical for unsaturated, unconsolidated sand and the significantly higher velocity of the refractor (1650 m/s) is common for saturated sand. The analysis yielded the same depth for the refractor at the intersection of the two perpendicular profiles (indicated in figure 4.12). The main GPR reflector seems to be identical to this seismic refractor. This will be analyzed in more detail later in figure 4.19. The seismic velocity suggests that the groundwater table is responsible for the refraction. The fine layering visible in GPR data could not be delineated with refraction seismics, probably because of the marginal extent of the fine layers or because of too weak impedance contrasts.

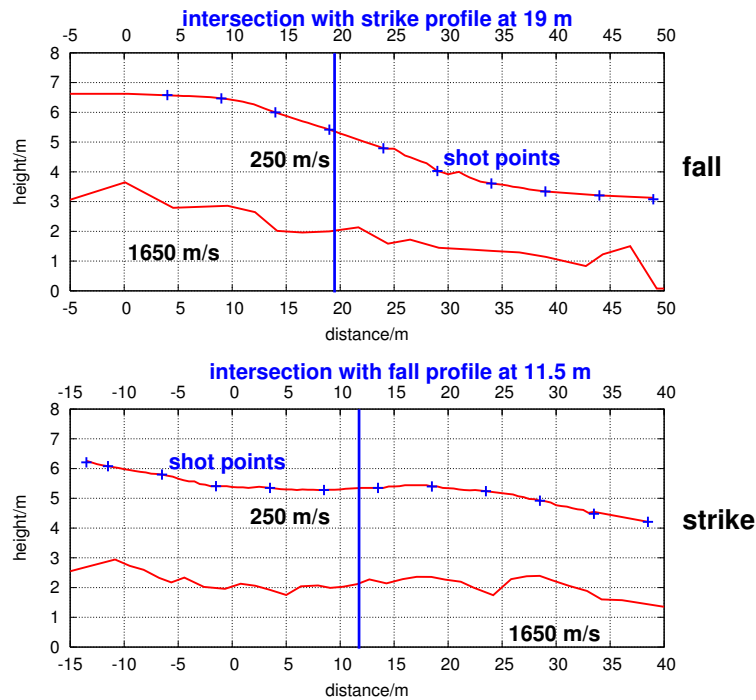


Figure 4.12: Results of the refraction seismic analysis from the fall and the strike profile (top and bottom, respectively).

In order to make a direct comparison between the seismic and the seismoelectric data, we used tri-phones (three-component geophones, section 2.4.5) to record all three components of the seismic wavefield, which was significantly easier than recording the three components of the seismoelectric wavefield (see sections 2.4.5 och 2.5.1). Normally the vertical component is collected in seismics and

the radial one in seismoelectrics (see figure 4.7 on page 72).

4.4.4 Seismoelectric profiles

The seismoelectric profiles were collected at exactly the same locations as the seismic refraction profile. As explained in section 2.4, I generally chose not to perform seismic and seismoelectric measurements at the same time. We first collected the seismoelectric data at all shot points at the fall profile, followed by the seismic measurements at the same profile. This procedure was kept at the strike profile, too.

Examples of the high data quality from this section were already shown in figure 2.10 on page 29.

4.4.5 Extracting converted seismoelectric signals

Section 4.3 provides a clear checklist how to differentiate between possible artifacts and real converted seismoelectric waves. I will apply this checklist also to the Menzlin data. A look at figure 4.13 already makes clear that the check will be much easier than described in section 4.3 because of the higher signal-to-noise ratio. Already in the unfiltered data, signals almost without moveout clearly looking like converted seismoelectric signals (marked with red) can be detected. A comparison with the corresponding seismic data from the same shot point clarifies that these cannot be coseismic waves, because they do not show any seismic equivalent events.

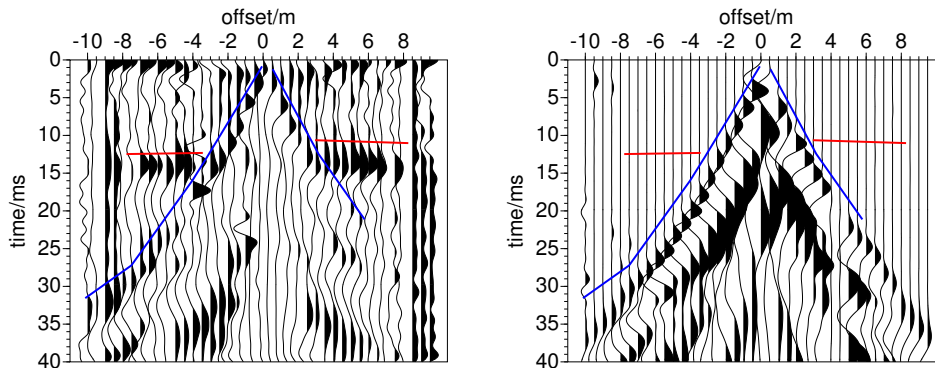


Figure 4.13: Example of seismoelectric (left) and seismic (right) data at the Menzlin site. Both the coseismic waves (marked with blue) and the converted seismoelectric signals (marked with red) can clearly be distinguished on the seismoelectric traces. The latter ones do not occur in the seismogram. The presented data are trace normalized but unfiltered except of a broad band-pass filter.

4.4.5.1 Polarity flip

As described in the field measurement technique section (section 2.2.3.3), converted seismoelectric signals should not have any polarity flip at the shot point because I already corrected for the offsets and polarities.

4.4.5.2 Velocity

It is required that the velocity of the converted seismoelectric waves is equal to the velocity of electromagnetic waves, i.e. much higher than any seismic wave. It can directly be seen in figure 4.13 that this is the case here.

4.4.5.3 Amplitude distribution

With the technique described in section 3.4.3, I determined the amplitudes of the assumed converted seismoelectric signals. For these calculations, the depth of the conversion is required. I calculate the depth of the converting interface by multiplying the seismoelectric arrival time with the seismic velocity of the first layer determined in the course of the refraction seismic analysis (section 4.4.3). The seismoelectric shot gathers (combined from several single shots as described in section 2.5.2) are listed together with an amplitude analysis for the assumed converted seismoelectric arrival in figure 4.14 (fall profile) and figure 4.15 (strike profile). The assumed converted seismoelectric events are marked in red in the seismoelectrograms. The picked measured amplitudes are drawn as red crosses while the calculated amplitudes are drawn as blue lines. Obviously, the correspondences are very good. The amplitudes were calculated as usually and as explained in section 4.3 which means that the amplitudes are merely relative and were adjusted with an arbitrary factor to best fit the picked measured amplitudes. So it is only the form of the amplitude curves that is analyzed, not the absolute values.

Most of the assumed “real” events as marked in figure 4.14 and 4.15 follow the expected amplitude distribution, i.e. as a vertical electric dipole at the converting interface. On some of the shown seismoelectrograms, there are strange events already at 0 ms (e.g. in figure 4.13). As can be seen, they change phase from one trace to the next one or are confined to some parts of the seismoelectrogram while they cannot be spotted at all in other parts. The distribution follows the composition of the shot record from single shots with less traces (see section 2.5.2). So they have to be classified as noise. The coseismic waves hinder the analysis of the arrivals with almost infinite apparent velocity. But these are so strong that there are still sufficient traces at somewhat greater offsets for an interpretation. It should again be stressed that the data quality is extraordinarily good in these seismoelectrograms. It is plain that the assumed converted seismoelectric events are repeatable because (a) they appear on traces of several shots at one shot point and (b) at almost every shot point.

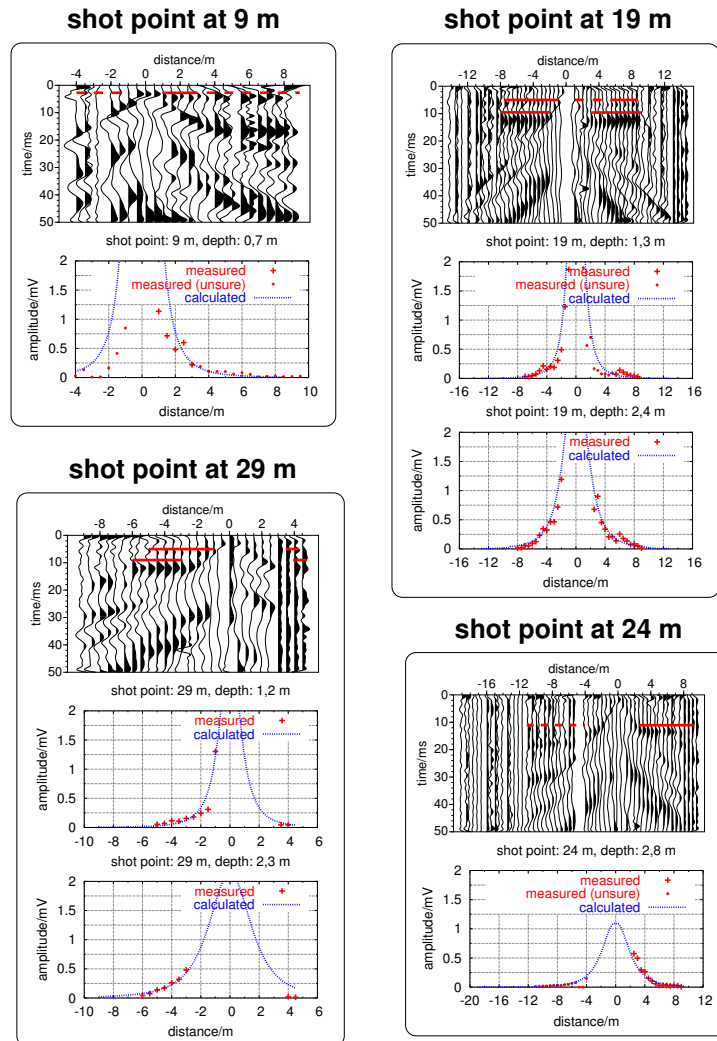


Figure 4.14: Seismoelectrograms with agc from the Menzlin fall profile together with the amplitudes of the assumed converted seismoelectric signals (marked in red in the seismoelectrograms). The picked measured amplitudes are drawn as red crosses while the calculated amplitudes are drawn as blue lines. Big symbols represent reliable values, smaller ones less reliable values. Obviously, the correspondences between observed and calculated amplitudes are very good. The corresponding figure for the strike profile is shown in figure 4.15.

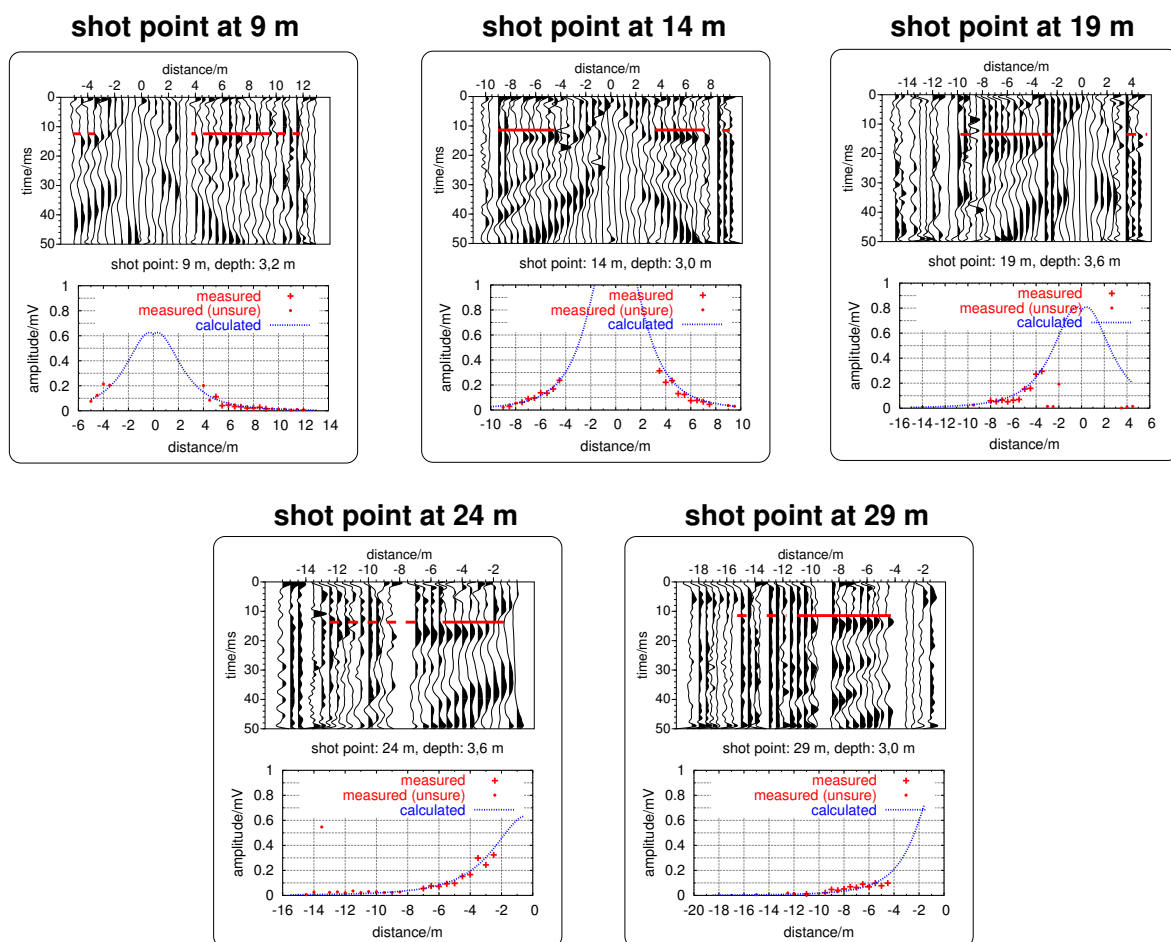


Figure 4.15: Seismoelectrograms with *agc* from the Menzlin strike profile together with the amplitudes of the assumed converted seismoelectric signals (marked in red in the seismoelectrograms). The picked measured amplitudes are drawn as red crosses while the calculated amplitudes are drawn as blue lines. Big symbols represent reliable values, smaller ones less reliable values. Obviously, the correspondences between observed and calculated amplitudes are very good. The corresponding figure for the strike profile is shown in figure 4.14.

4.4.5.4 Arrival times / check with other methods

Those events which passed the three precedent checks are combined with the results from the seismic refraction survey into one figure (strike profile data: see figure 4.16, fall profile data: see figure 4.17). The shot points of the seismoelectric measurements are directly above the conversion points at the surface.

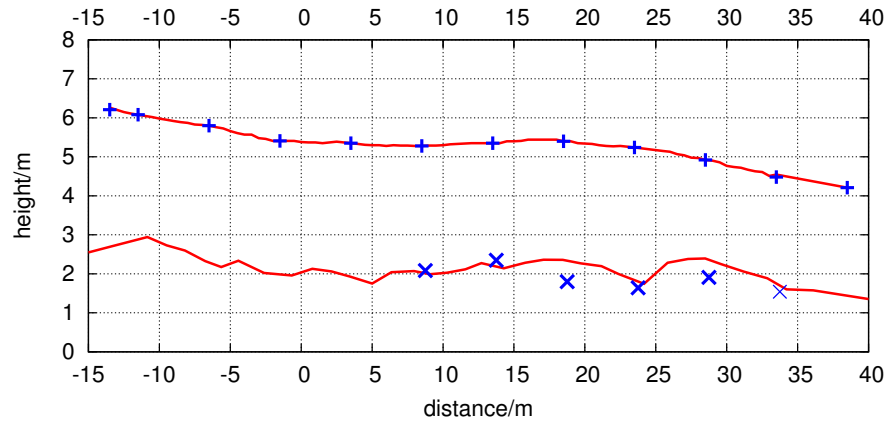


Figure 4.16: The Menzlin strike profile with topography and the boundary layer determined with refraction seismics. Shot points are marked with crosses at the surface. The arrival times of the assumed converted seismoelectric arrivals were transformed to depth with the velocities encountered in the seismic and seismoelectric data. Apparently, the seismoelectric converting interface and the seismic refractor are the same. The figure has vertical exaggeration. The fall profile is shown in figure 4.17.

It should be noted that it is not self-evident that seismic refractions and seismoelectric conversions occur at the same interfaces. The seismoelectric method is sensitive to a lot more parameters (see equations 1.1 - 1.9 on page 9). On the strike profile, however, the refractions and conversions do indeed seem to originate from the same horizon which is, as mentioned in section 4.4.3, probably identical with the groundwater table.

At a first glance, the situation seems to be completely different on the fall profile (figure 4.17), where there are many more seismoelectric conversions than seismic refractions. The assumed conversions all passed the seismoelectric checklist, though, so they seem to be real seismoelectric conversions.

In figure 4.18 I inserted the seismoelectric conversion results to the radargram and marked some GPR events. I also copied the combined GPR-seismoelectric results to the refraction seismic results from figure 4.17. The resulting combined GPR-seismoelectric-seismic result can be seen in figure 4.19. Obviously the seismic refractor, interpreted to be the groundwater table, and the lowest of the GPR reflectors are identical. The seismoelectric conversions fit quite well to the horizons only visible on the GPR profile, though a denser shot point coverage would have brought more insight into this question. It seems that the seismoelectric method here has a higher resolution than the seismic refraction method. The reader is again referred to the fact that the seismoelectric method is sensitive to a lot more parameters than the seismic method so it is quite possible that there simply are no seismic refractions or reflections generated at these interfaces. Irrespective of the reasons I can

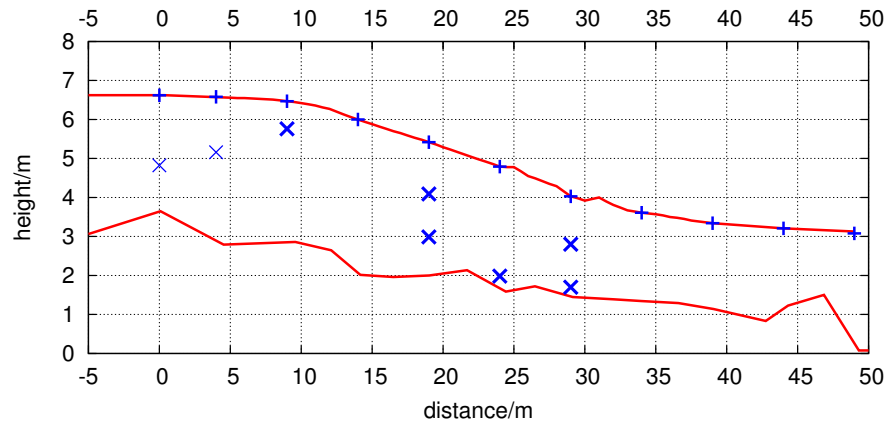


Figure 4.17: The Menzlin fall profile with topography and the boundary layer determined with refraction seismics. Shot points are marked with crosses at the surface. The arrival times of the assumed converted seismoelectric arrivals were transformed to depth with the velocities encountered in the seismic and seismoelectric data. The figure has vertical exaggeration. Large crosses refer to seismoelectric conversion events determined with good quality data and small crosses refer to events determined with data more unsure. The strike profile is shown in figure 4.16.

conclude that it was possible to delineate the fine layering with GPR and seismoelectric but not with seismic refraction.

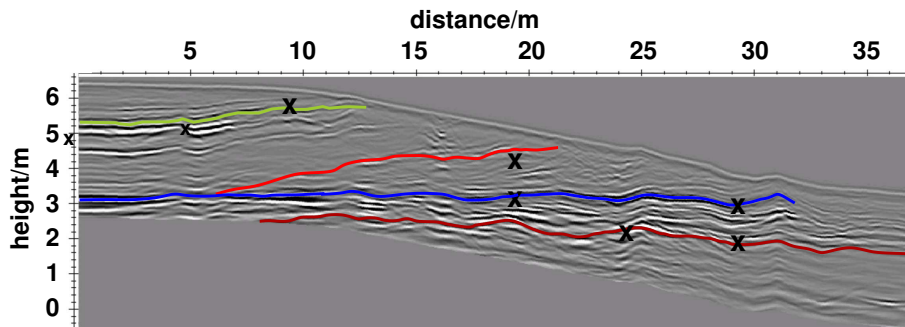


Figure 4.18: GPR data from the fall profile at the Menzlin site (see figure 4.11). Some events are marked with lines. The seismoelectric conversion points from figure 4.17 are added as crosses. The figure has vertical exaggeration.

4.4.6 Conclusions

The seismoelectric data collected at the Menzlin location exhibits extraordinarily good signal quality without any traces of anthropogenic 50 Hz noise. This enabled the mapping of an interface previously determined with GPR and refraction seismics. Direct comparisons prove that it is the same interface that causes the GPR reflections, seismic refractions, and seismoelectric conversions. The seismic velocities indicate that this boundary probably is the groundwater table. The repeatability of the

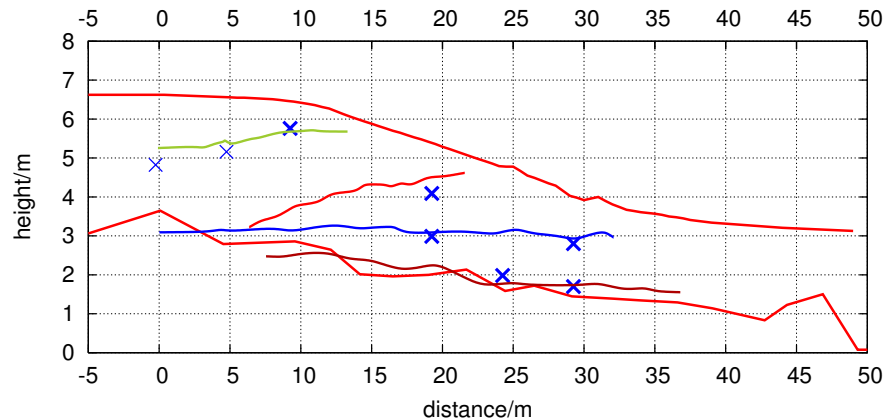


Figure 4.19: The results as shown in the above figure 4.18 are copied to the refraction seismic results already presented in figure 4.17. As can be seen, the seismic refractor and the lowest of the GPR reflectors seem to be identical. The figure has vertical exaggeration.

converted seismoelectric signals is evident: Each seismoelectric section is combined from several measurements and the converted events can be seen on all traces. Furthermore, at almost every shot point at least one arrival of converted seismoelectric signals could be registered. So they are surely not spurious events only appearing at isolated shots.

Comparable results were obtained on the two perpendicular profiles with the results at the intersection of the two profiles matching well. These measurements show that there are cases in realistic field work where subsurface boundaries can be detected with GPR and seismoelectrics, but not with refraction seismics. This proves that seismoelectrics could possibly be used for mapping such boundaries that do not possess a strong impedance contrast. The assumed converted events were checked with the checklist described in section 3.4 and most of them were confirmed and shown in this chapter. When looking at figures 4.16 and 4.17, it is striking that most converted signals were encountered in the mid parts of the profile. This coincides with the sandier parts of the dune. Towards the ends of the profiles, clayey/earthy soil dominates. It should be emphasized that seismoelectric converted arrivals are generated above the groundwater table in the vadoze zone showing that the Biot-based theory is only half part of the story.

A denser shot point coverage would have provided an even more certain interpretation. When the objective of the measurements is real mapping, a higher shot point density (depending on the extent of the desired target) is even more important.

Reasons for the extraordinarily good data quality are the low electromagnetic noise level at this rather remote site. Furthermore, the ground consists mainly of sand in which seismoelectric amplitudes generally seem to be higher than in clay. In addition, the sand dune on which the measurements were

done does not contain as many or as massive plant roots as a site like Segeberg Forest which seems to have a strong influence on attenuation.

4.5 Selinunte/Sicily

The data were recorded in the course of an archaeometry survey at the antique Greek town of Selinus (the modern Selinunte) on the island of Sicily in October 2002 by the archaeometry working group of our institute. Two profiles were measured: one on electrically very conducting alluvial soil and one on a dry sand dune. The dune sand was almost completely dry, yet seismoelectric coseismic waves could be measured (see figure 4.20). This is interesting because in the scope of Biot theories, saturated media are assumed (as already stated in section 1.1.2). Also other researchers came across similar observations (e.g. Haines, 2004). Possibly, the ground was not completely dry but some interstitial water remained which seems to have been enough to cause seismoelectric signals of observable amplitudes. It is also interesting that the dry ground could cause trigger noise signals which are clearly discernible on the seismoelectric records (figure 4.20, shotpoint at 12.5 m). It is quite unlikely that a conductive connection could have caused these signals.

In figure 4.21, the results of a geoelectric survey on top of the sand dune is shown. The sand dune has a vertical thickness of 3 m - 4 m and rests on dry marly sandstone. As indicated by the slightly lower resistivities above 3 m, the sand was a bit less dry at these depths compared to the surface. This could be the reason why seismoelectric signals could be measured at all at this location.

The profile on the alluvial soil turned out to not yield any sensible seismoelectric signals at all. The highly conductive soil might have caused short-circuits. It was even impossible to collect geoelectrical data because of the low resistivities.

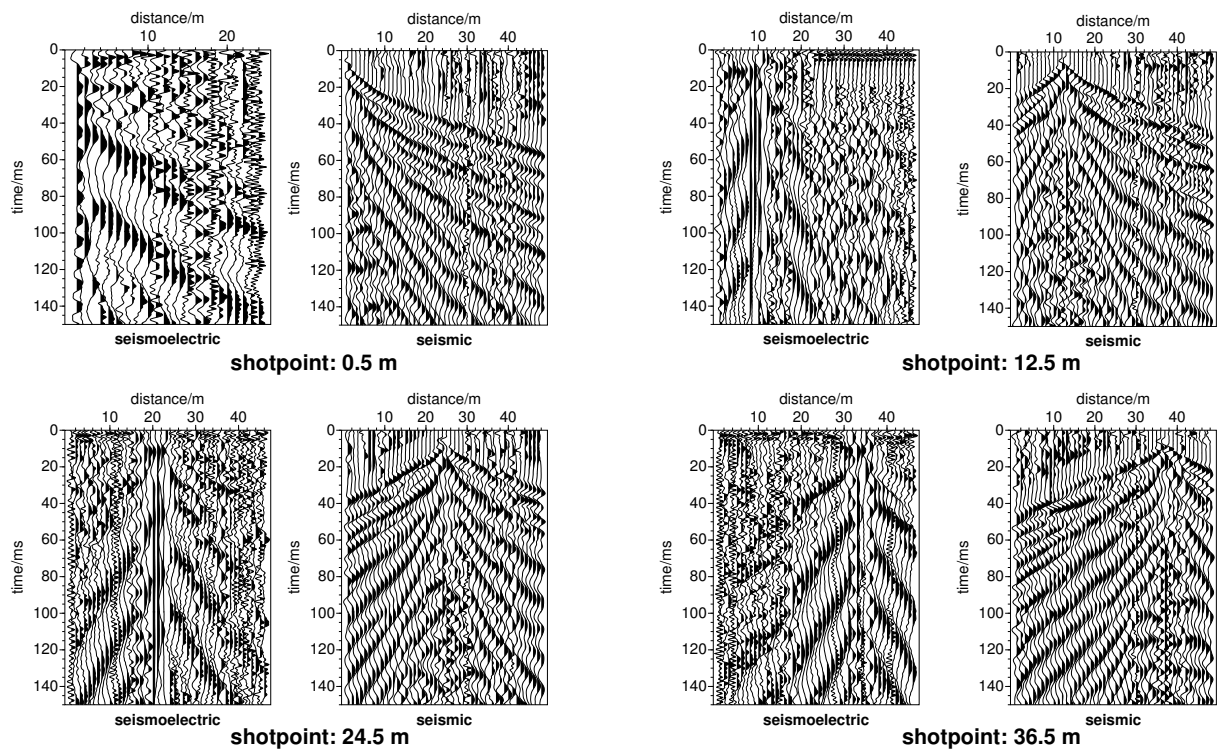


Figure 4.20: Seismoelectric and seismic data with agc from Selinunte/Sicily (sand dune profile). The left of every double image are seismoelectric and the right one seismic data. Shot points are from 0.5 m, 12.5 m, 24.5 m, and 36.5 m.

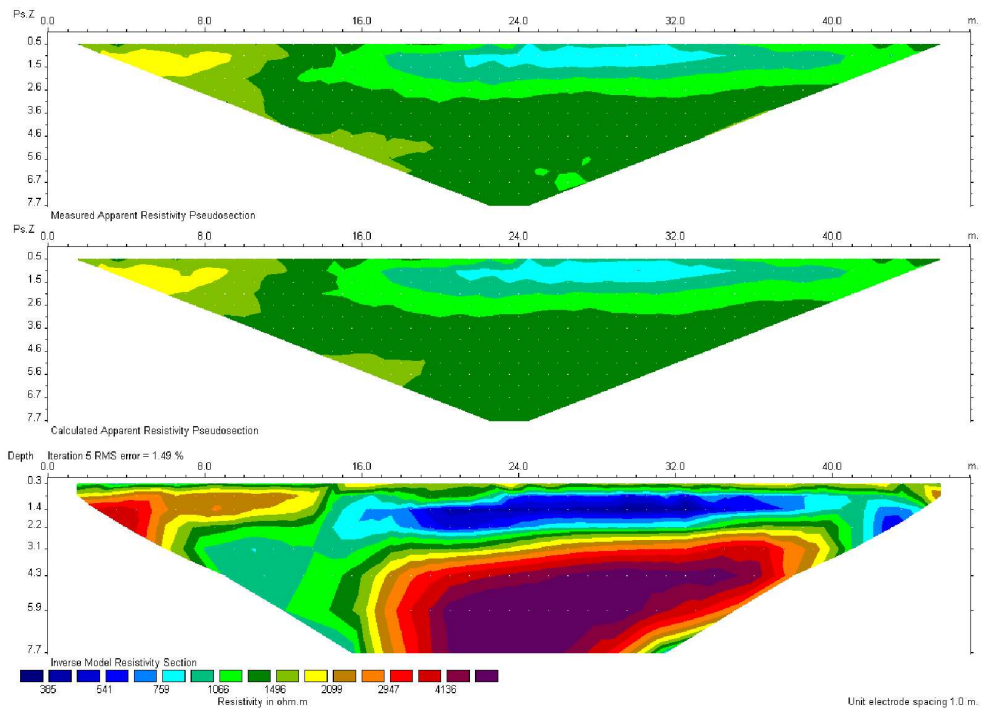


Figure 4.21: Surface geoelectric pseudosection and model from the dune profile at Selinunte/Sicily. Top: measured apparent resistivity, middle: calculated apparent resistivity, bottom: resistivity model. The structures explained in the text (dry sand dune on top of dry marly limestone) can be distinguished.

4.6 Segeberg Forest

The main scope of this section is to present how changing ground conditions can influence the quality of seismoelectric data. We visited the Segeberg Forest site several times at different seasons and under different weather conditions and encountered a broad variety of seismoelectric signal quality. We also applied a variety of measurement parameters, including different seismic sources, measurements in the borehole and at the surface and comparison with seismic and geoelectric data. In the following sections, I will describe the location (section 4.6.1), followed by the presentation of the data from the Segeberg Forest site (section 4.6.2) and a unified interpretation of the presented data (section 4.6.3).

4.6.1 Description of the site

In 1980 a borehole field was constructed in the Segeberg Forest about 40 km north of Hamburg, roughly between the cities of Bad Bramstedt and Bad Segeberg (see figure 4.22). Several tracer experiments were conducted in the early 1980's (e.g. Schröter, 1983) as well as geophysical measurements (Salem, 1990). The upper 30 m consist mainly of sand with some clay and stone layers (see figure 4.23).

The boreholes reach a maximal depth of 14 m to 32 m (for more information see Schröter, 1983). Their positions are shown in figure 4.24. In November 2005, we measured a surface geoelectric profile with borehole 12 being situated in the middle of the profile. The influence of the metal casing can clearly be seen in the anomaly in the central part of the resistivity model (figure 4.25). For the inversion shown in figure 4.25 I did not use the traditional least-squares optimization but so-called robust constrained inversion (Claerbout & Muir, 1973). The robust constraints option implies that rather the absolute value is minimized. It results in sharper boundaries than obtainable with the least-squares technique but has the drawback of almost constant resistivity values within regions of the model.

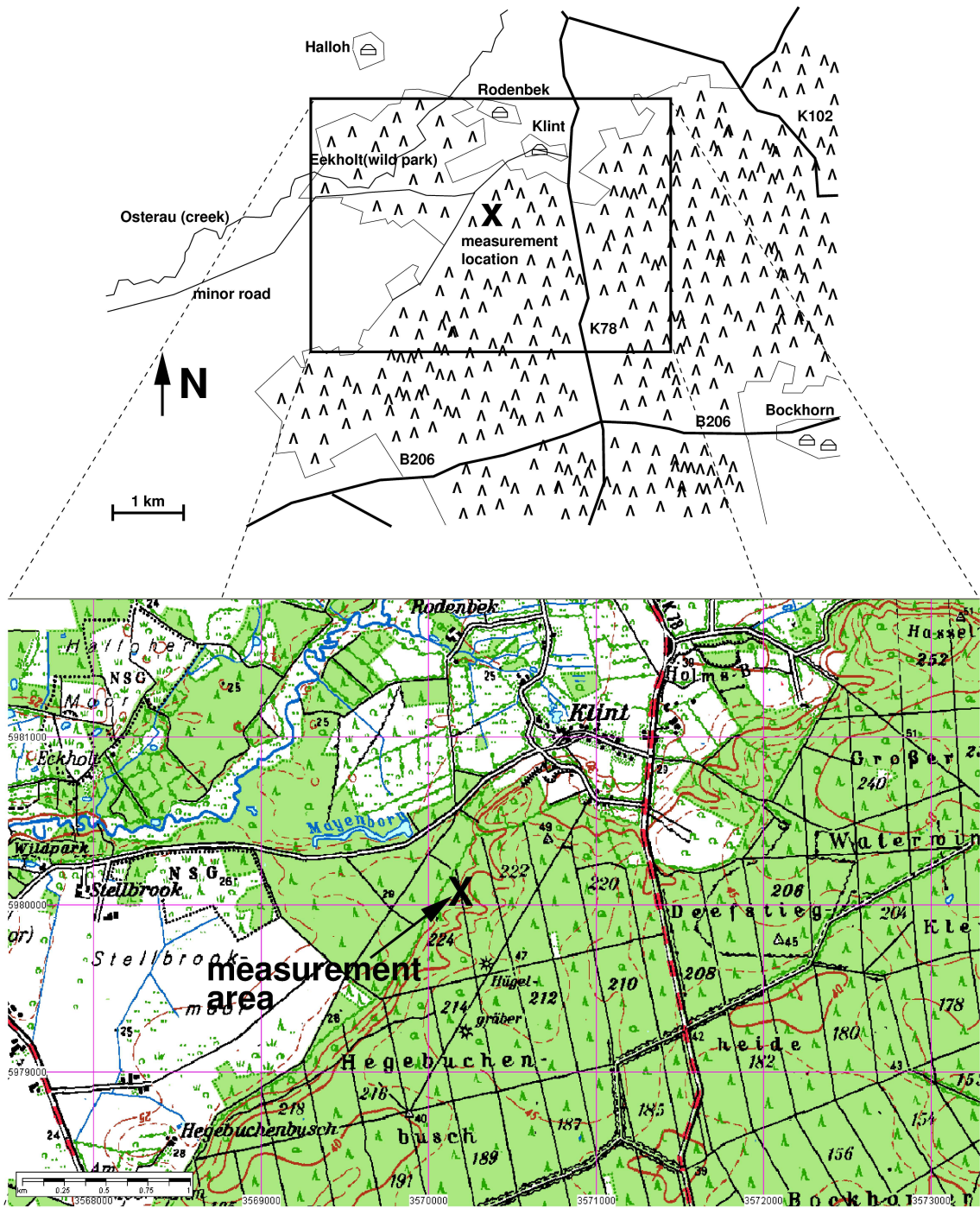


Figure 4.22: The measurement area Segeberg Forest (from Landesvermessungsamt Schleswig-Holstein, Kiel).

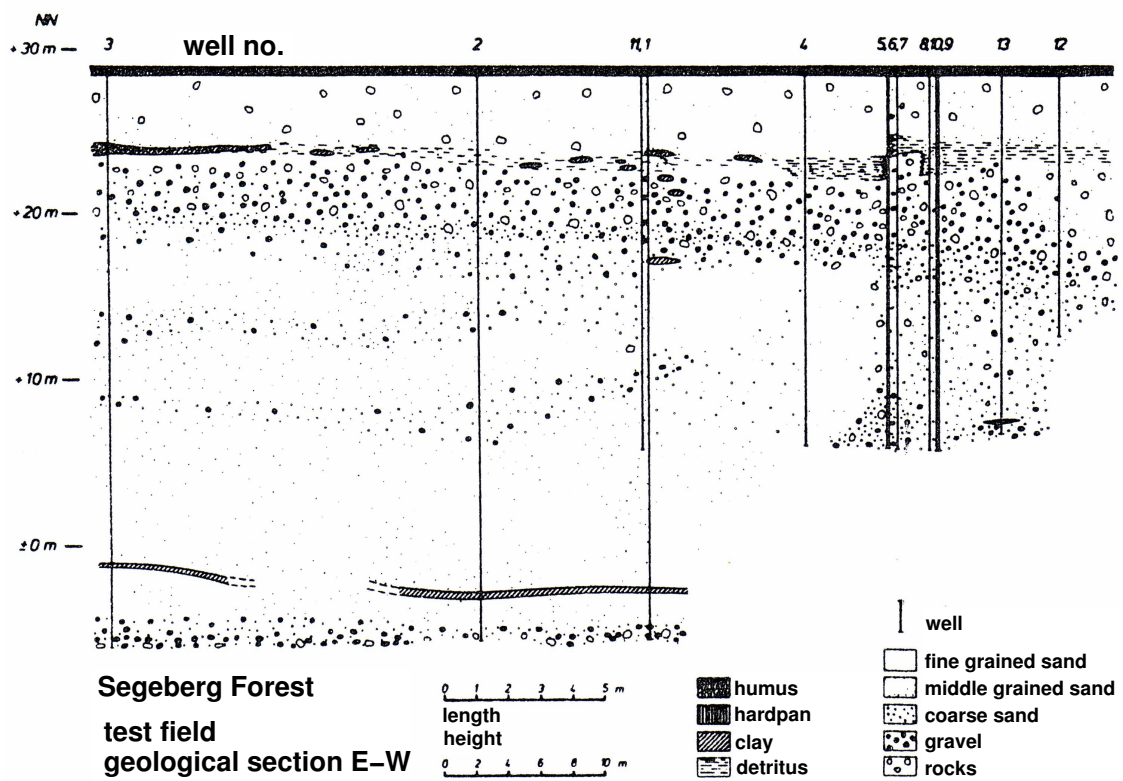


Figure 4.23: Geological profile of the measurement area Segeberg Forest. Taken and translated from Matthes (1980).

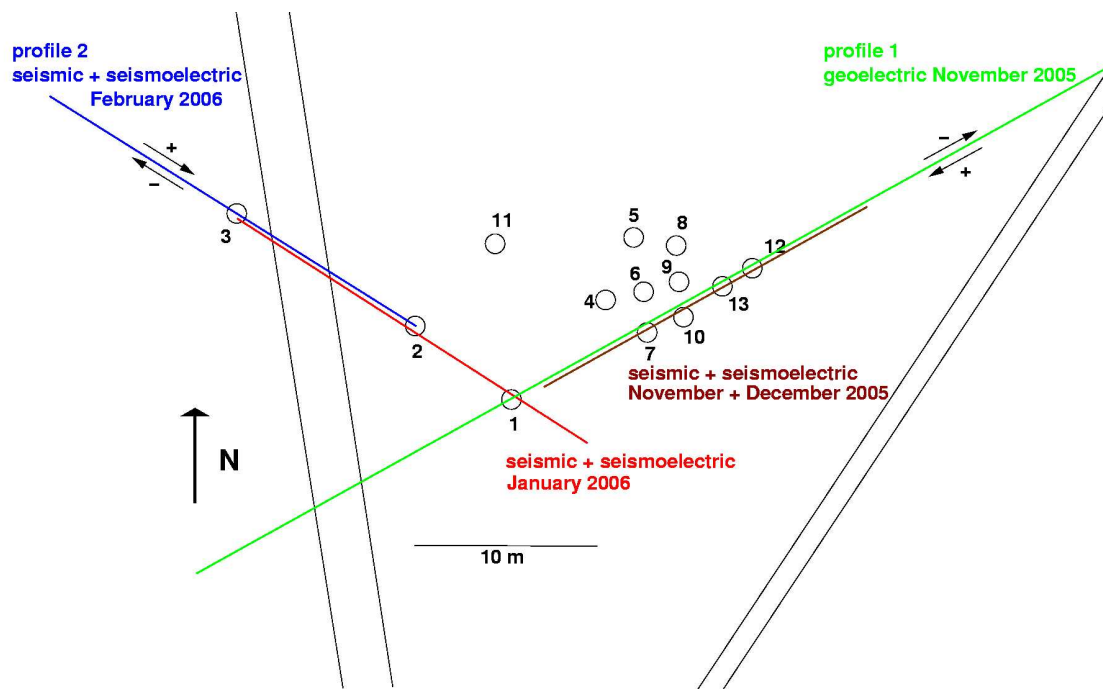


Figure 4.24: Location of the thirteen boreholes and the measured geoelectric, seismic, and seismoelectric profiles at the measurement site Segeberg Forest. The coordinates were determined with GPS and corrected with tachymeter measurements.

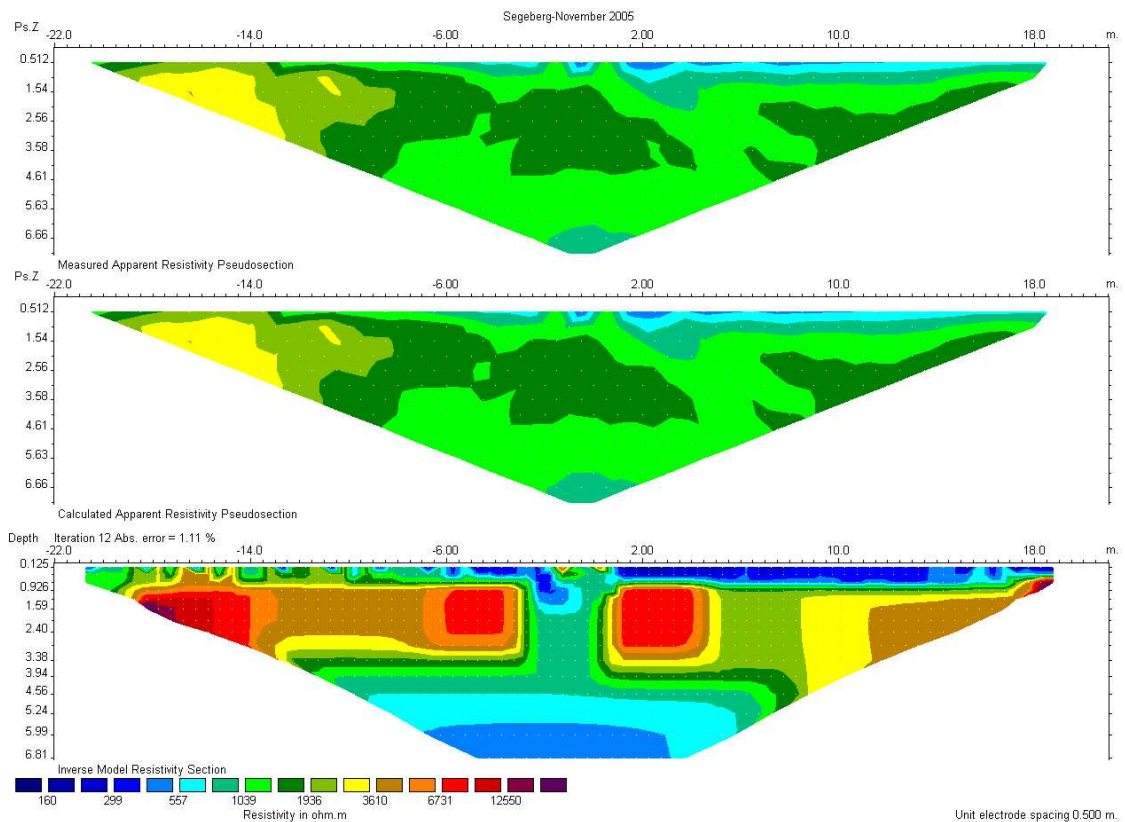


Figure 4.25: Surface geoelectric profile (Wenner- α) at the Segeberg site (November 2005). Top: measured pseudosection, middle: calculated pseudosection, bottom: resistivity model. The data were inverted using the finite difference method as described by Loke & Barker (1996) with robust constraints (Claerbout & Muir, 1973). The influence of the metal casings of the boreholes in the middle of the profile is evident.

4.6.2 Data

The scope of this section is not the presentation of all Segeberg Forest data. I will only show data that give an impression of the variability of the seismoelectric signals at this site. Other data from this location will be presented in section 5 where direct comparisons between seismics, geoelectrics, and seismoelectrics are carried out.

4.6.2.1 Borehole

Seismic and seismoelectric data are shown from borehole 2 measured in January 2006 and borehole 3 measured in February 2006 as well as in June 2004 (figure 4.26 and table 4.3). The position of the boreholes is explained in figure 4.24. All three seismoelectric data sets have a very high signal-to-noise ratio although two different sources were used: a sledgehammer for the data at boreholes 2 and 3 and accelerated weight drops at borehole 3. Both the seismic and the seismoelectric first breaks were picked and marked as lines in all the shown borehole data as a means of control if the profiles have been correctly combined. The technique of seismic and seismoelectric borehole measurements is explained in section 2.5.3. We used a hydrophone chain to collect the seismic data (a single borehole geophone in the case of the June 2006 measurements) and an electrode chain for the seismoelectric data.

| figure | borehole | date | dipole length | VSP with | trigger | source |
|--------|----------|------------|---------------|-------------|---------|---------------|
| 4.26a | 2 | 24.01.2006 | 2 m & 8 m | hydrophones | accel. | sledgehammer |
| 4.26b | 3 | 20.02.2006 | 8 m | hydrophones | manual | accel. weight |
| 4.26c | 3 | 03.06.2004 | 4 m & 8 m | geophone | accel. | sledgehammer |

Table 4.3: Overview of the VSEP measurements from the Segeberg Forest site presented in this section. The data are shown in figure 4.26. “Accel.” in the trigger column stands for acceleration trigger and “accel. weight” for accelerated weight drops.

It is marked in the figures where the PVC borehole tube is sliced. Apparently a 1 m long section of unsliced PVC tube does not have a strong influence on the seismoelectric data. However, it is plain to see that sensible seismoelectric signals only appear below 7.5 m where the tube starts to be sliced. Although the data quality is quite high, no converted seismoelectric events can be seen. It could well be the case that there simply are no sharp boundaries capable of producing converted seismoelectric signals with detectable amplitudes. At least there are no sharp impedance contrasts in the first 30 m depth, as we cannot see any reflections in the VSP data in figure 4.26. Due to geometrical reasons, the VSEP data cannot cover the whole depth range: The lower electrode of each dipole reaches 2 m or 8 m (depending on dipole length) below the depth assigned to the respective trace. While collecting the data in February 2006 (figure 4.26b) the hydrophone amplifiers crashed leading to a reduced data set. This is especially regrettable as the depth range of the VSEP thus could not be covered. Direct comparisons between seismic and seismoelectric data are therefore limited to a rather small depth interval. Furthermore, these VSP data (b) are overdriven. The accelerated weight drops are a very strong source and the hydrophones very sensitive. As described in section 1.1.1.1 it is more suitable to compare the seismoelectric traces with the first time derivative of their seismic counterparts. Since

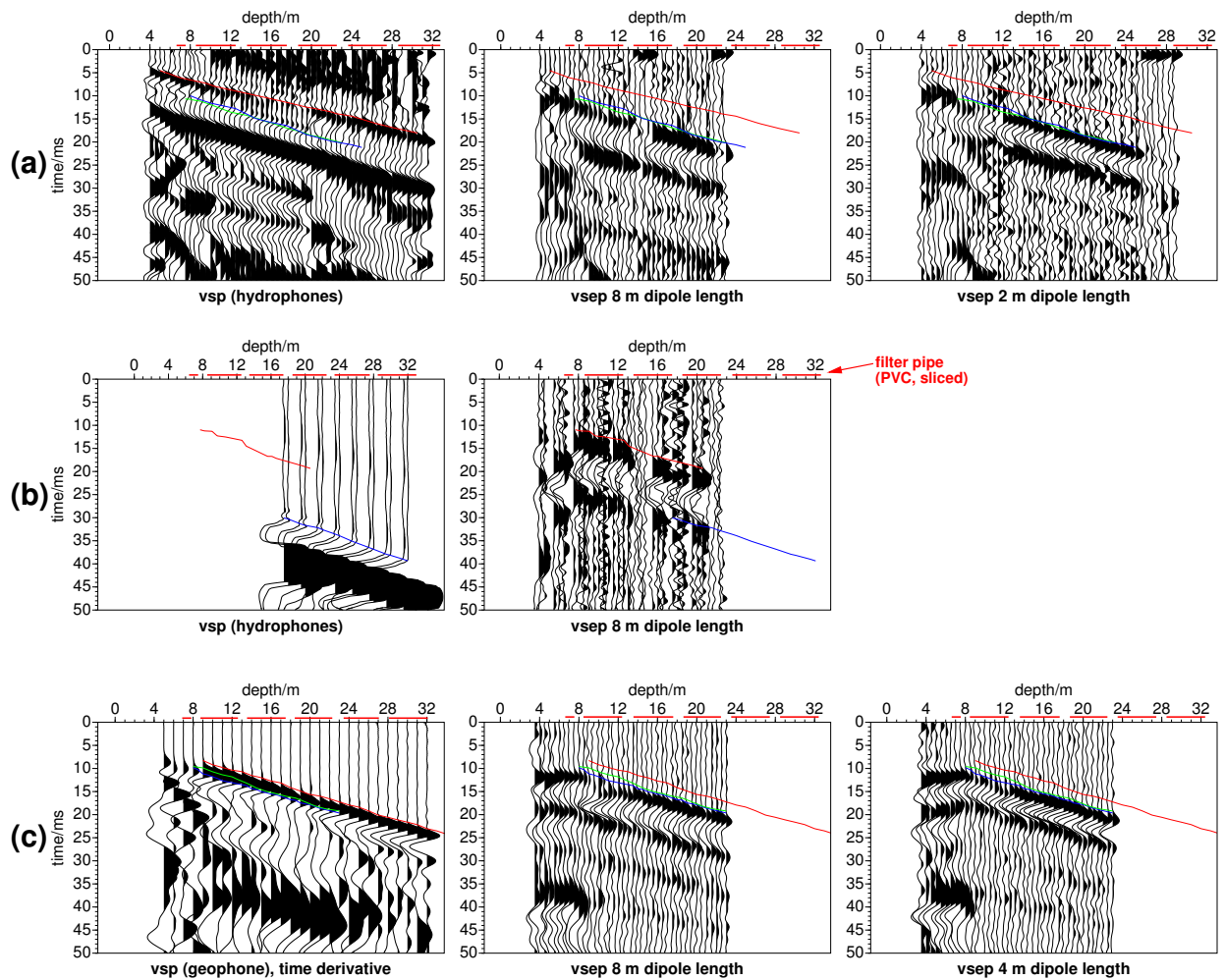


Figure 4.26: Repeated seismoelectric and seismic borehole measurements at the Segeberg Forest site with *agc*. (a) January 2006, (b) February 2006, (c) June 2004. (a) was measured in borehole 2 and (b) and (c) in borehole 3. See table 4.3 for more explications. The influence of the solid PVC borehole casing above 8 m depth is evident. Red lines on top of the sections indicate where the PVC borehole tube is sliced.

hydrophones record pressure which corresponds to ground acceleration rather than ground velocity, I plot the time derivate only of the geophone traces (figure 4.26c).

It is interesting to note that the seismic and the seismoelectric first break picks never match in figure 4.26. The apparent velocities are exactly the same, but there is always a constant mismatch between those two. On a closer look especially at the January and June data (a and c) the mismatch turns out to be exactly half a period. The February data (b) are a bit different, mostly because the seismic signal is overdriven. There is no obvious reason for this time mismatch and it could not be observed in comparative seismic-seismoelectric measurements at the surface. An erroneous depth placement of either the hydrophone chain or the electrode chain would be possible for one or maybe two exceptional values but not for every trace at every measurement date.

No signs of 50 Hz electromagnetic noise can be seen in the borehole. Obviously, this coherent noise is absorbed in the ground. The effect is dramatic. Even 100 fold stacked surface seismoelectric data with accelerated weight drops as source contained quite clearly discernible traces of 50 Hz (see figure 4.31 on page 100). In figure 4.26b, the corresponding VSEP data, no sign of anthropogenic electromagnetic noise can be seen.

Between January and February there are no big differences despite the use of different sources. The data from June 2004 seem to be better in general. It should be kept in mind that the measurement conditions were favorable in January (frozen ground) and worse in February (very soft ground) so the fact that the data quality stayed roughly the same is a sign for the greater strength of the accelerated weight drops compared to the hammer. There are only minor variations between the two boreholes 2 (January 2006 data) and 3 (February 2006 and June 2004 data). Also the different dipole lengths do not seem to cause much difference in the borehole 2 data (figure 4.26a). The 8 m dipole length data may have a higher signal-to-noise ratio. The overall data quality is very high for seismoelectrics. The first break picks shown in the seismoelectrograms prove that the repeatability is very high, even with different dipole lengths. In borehole 3 data (figure 4.26c), however, longer dipole lengths seem to result in smoother data, but also here the repeatability is very high. In February, we did not collect multiple dipole length data with the accelerated weight drop source.

All in all, the data presented in this section stay more or less the same when the measurement parameters change. This speaks for reliable results. It is only the data quality that is affected - albeit weakly - by parameters such as source type and dipole length.

4.6.2.2 Surface

In addition to the borehole seismoelectric data examined in the preceding section, we also collected surface seismoelectric data which I will scrutinize in this section. Data are mostly shown in split-spread layout with one of the many boreholes of the borehole field in the middle (see figure 4.24): borehole 12: figure 4.27, borehole 13: figure 4.28, borehole 2: figure 4.29, borehole 3: figure 4.30.

I will first analyze the data from each measurement date separately (figures 4.27 - 4.30) and then combined (figure 4.31).

- Analysis of the November 2005 data

In general the data have a very low signal-to-noise ratio and had to be filtered from anthropogenic noise. Although this could be removed almost completely, the signal is too weak to detect any converted seismoelectric signals.

That day it rained and the ground was very wet (see figure 2.7 on page 25), which could play a role in the data quality. Especially during fieldwork one could not escape the impression that weather badness is directly proportional to data badness here. This will be analyzed in more scientific terms in the unified interpretation (section 4.8).

There is no clear recognizable pattern in figure 4.27 if some dipoles yield lower signal-to-noise ratio than others, so it seems that the problem lies on the source side. Worst is the shot from the source at -7.5 m. Here, the ground was very moist and soft and probably just way too little seismic or seismoelectric energy reached the receivers. The shots from the other shotpoints are better but still the data quality is very unsatisfactory.

- Analysis of the December 2005 data

Also here the overall data quality is bad (figure 4.28). The differences between the single shot records are quite big. Despite of its rather remote location (at least for Schleswig-Holstein standards), data had to be filtered from 50 Hz. This was also the case for the November data shown in figure 4.27 but not for the rest of the data from the Segeberg Forest site presented here. The ground was very moist and soft during the December measurements.

These data were recorded in the course of a tracer experiment, where we injected 700 l of salt water into the ground. However, it seems that the variations from one shot to the other are greater than the variations between before and after the injection of the salt water tracer. The injection well (borehole 12) is situated 1.8 m upstreams from the well in which we measured (borehole 13). We used pumps to accelerate the flow process. The seismoelectrograms shown in this work are only a minor part of the tracer experiment which will not be described in detail here.

In every of these seismoelectrograms, events without moveout are discernible. The amplitudes seem to follow the expected pattern for converted seismoelectric signals: They are rather strong at small offsets and decrease rapidly towards greater offsets. However, they only appear single sided or even change polarities at the shot point, especially those signals that appear in the first few milliseconds (marked with lines in figure 4.28). This means that they are surely not converted seismoelectric fields but rather noise. It is surely no trigger effect because (b)-(d) were triggered manually without any interfering acceleration trigger or cabling. However, it

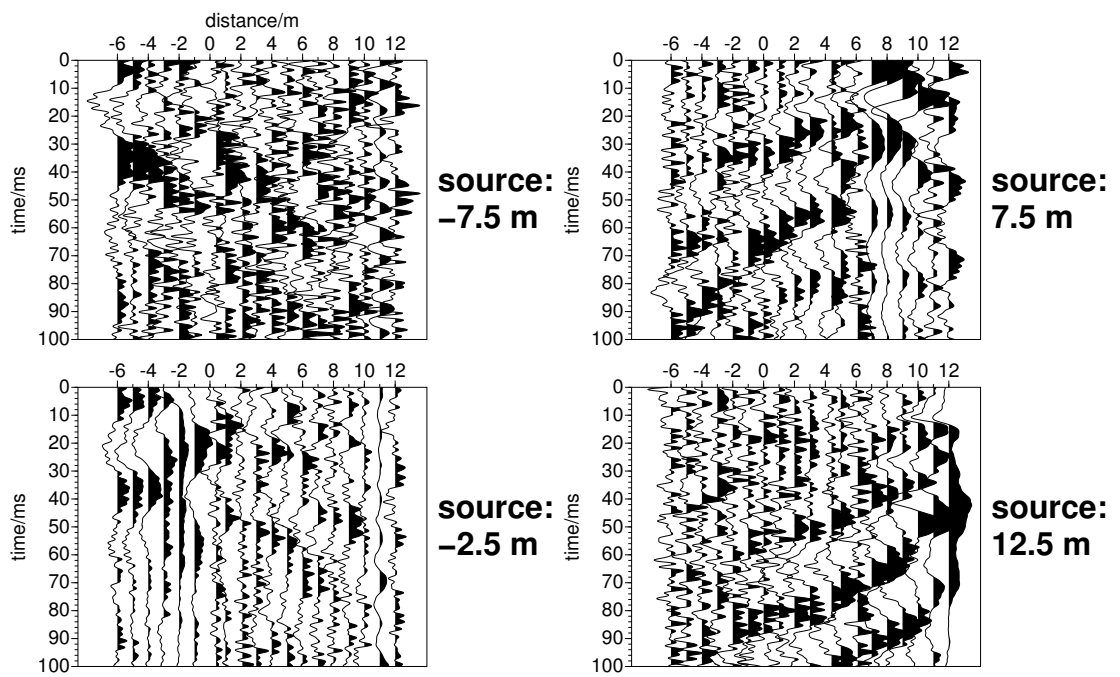


Figure 4.27: Comparison of seismoelectric surface data (November 2005) from near borehole 12 with 4 m dipole length from four different shot points: a) -7.5 m b) -2.5 m c) 7.5 m d) 12.5 m. 50 Hz and harmonics are filtered. The data are manually triggered and scaled with agc .

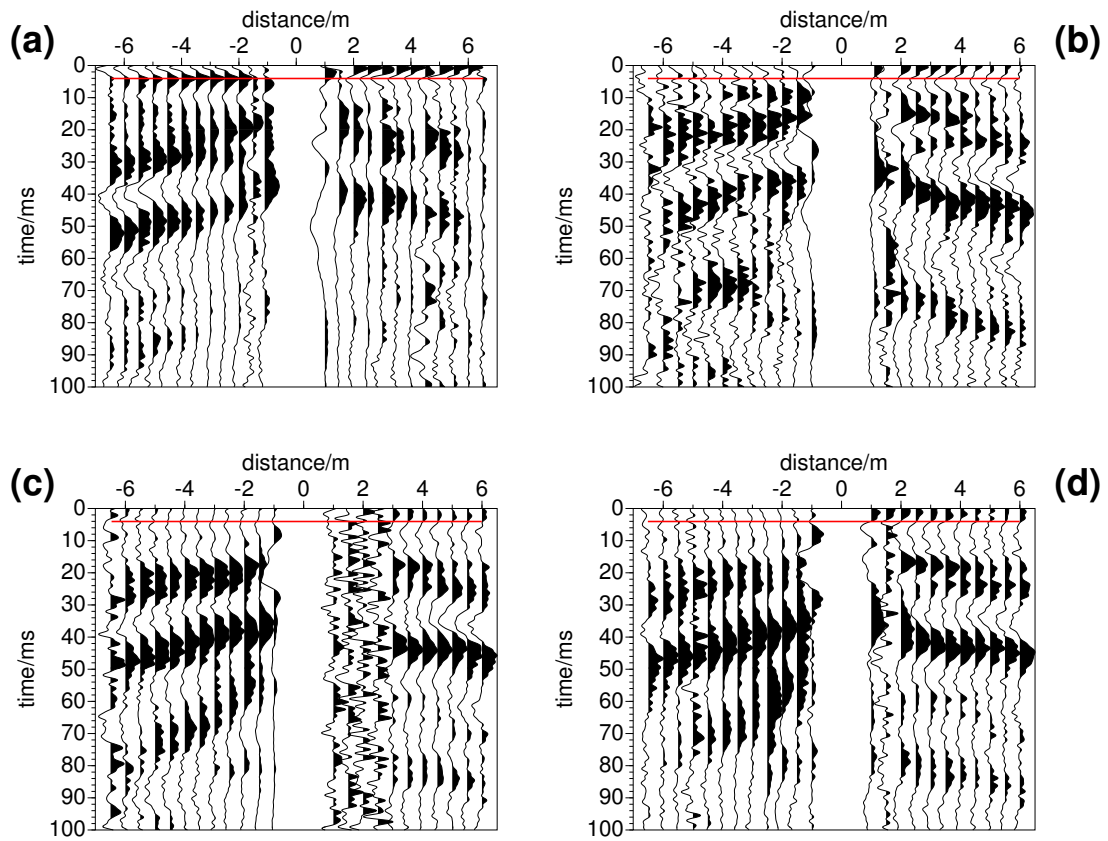


Figure 4.28: Comparison of seismoelectric surface data with agc from the Segeberg Forest (December 2005) with 4 m dipole length before (a,b) and after (c,d) injection of a salt water tracer. The shot point lies between the boreholes 12, where the tracer was injected, and 13 (see figure 4.24). (a) was triggered with an acceleration sensor and (b)-(d) were triggered manually. (d) was recorded almost a day after the injection. Lines mark arrivals with zero apparent slowness. Since the polarity changes at the shotpoint, these are surely not converted seismoelectric signals.

is clear that it is no external noise, because it always appears at the time of hammer impact. A possible explanation is that the movement of the metal plate in the Earth's magnetic field creates currents due to the Lorentz effect which are then picked up by the dipoles. This idea was first brought forth by Haines (2004). This requires a conductive connection between the ground plate and the ground. Actually, we did try to prevent this by using the wooden plate in these measurements but it appears that the wood was soaked and thus became conductive.

- Analysis of the January 2006 data

The November and December 2005 data were recorded around boreholes 12 and 13 where the ground was quite soft (shown in figure 4.24). In January and February 2006 we placed the seismoelectric profile a bit more to the southwest where the ground in general was significantly harder.

One look at figure 4.29 makes clear that the data from January are much more suitable for interpretation than the data from December or November. The coseismic waves are very clear. At least two arrivals without apparent moveout are striking (marked with lines). But just as in the December data in figure 4.28, these arrivals behave in very different ways on both sides of the shotpoint which disqualifies them as converted seismoelectric signals. The data are shown in their fully stacked form (320 stacks) and also stacked only 20 times. Thus it is easy to compare these data with the other seismoelectric data in this thesis which were usually stacked 20 times, too.

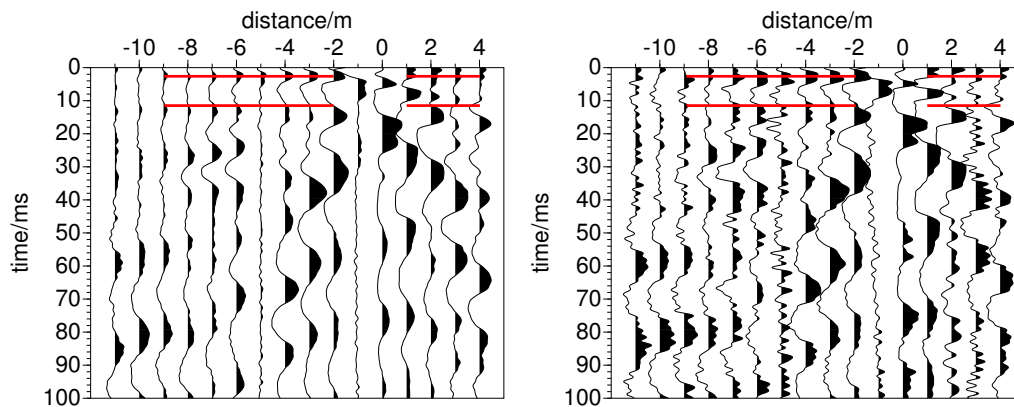


Figure 4.29: Seismoelectric surface data with *agc* from near borehole 2 at the Segeberg Forest site (January 2006). Source: sledgehammer. The data were triggered with an acceleration trigger and stacked 320 times (left) and 20 times (right), respectively. Lines mark arrivals without moveout.

- Analysis of the February 2006 data

In general, these data (figure 4.30) show very good data quality and strong arrivals. Here we used accelerated weight drops as source (see section 2.2.1.3). It is apparent that stacking the data 20 fold or > 100 fold does indeed lead to clear differences in the signal-to-noise ratio.

- Unified surface interpretation

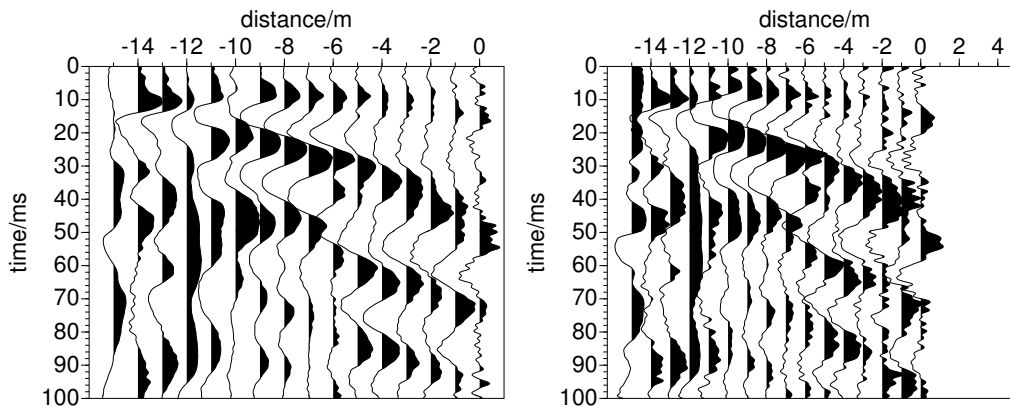


Figure 4.30: Seismoelectric surface data (manually triggered and with agc) from near borehole 3 at the Segeberg Forest site (February 2006). Source: accelerated weight drop. Left: stacked 160 times, right: 20 times.

I combined the four already shown results from November, December, January, and February to an extended overview (figure 4.31) in order to better visualize the differences in data quality. The corresponding seismic sections - where existing - are gathered in figure 4.32. The seismic first breaks were picked and copied to the corresponding seismoelectric data. The measurement parameters are listed in table 4.4.

| section | date | profile | shot point | stacks | trigger | source | filtered |
|---------|--------------|---------|------------|--------|---------|---------------|----------|
| 4.31a | Nov. 2005 | 1 | -7.5 m | 20 | manual | hammer | yes |
| 4.31b | Nov. 2005 | 1 | -2.5 m | 20 | manual | hammer | yes |
| 4.31c | Nov. 2005 | 1 | 7.5 m | 20 | manual | hammer | yes |
| 4.31d | Nov. 2005 | 1 | 12.5 m | 20 | manual | hammer | yes |
| 4.31e | Dec. 2005(a) | 1 | 1 m | 20 | accel. | hammer | yes |
| 4.31f | Dec. 2005(b) | 1 | 1 m | 20 | manual | hammer | yes |
| 4.31g | Dec. 2005(c) | 1 | 1 m | 20 | manual | hammer | yes |
| 4.31h | Dec. 2005(d) | 1 | 1 m | 20 | manual | hammer | yes |
| 4.31i | Jan. 2006 | 2 | 0 m | 320 | accel. | hammer | no |
| 4.31j | Jan. 2006 | 2 | 0 m | 20 | accel. | hammer | no |
| 4.31k | Feb. 2006 | 2 | -11 m | 160 | manual | accel. weight | no |
| 4.31l | Feb. 2006 | 2 | -11 m | 20 | manual | accel. weight | no |

Table 4.4: Measurement parameters of the 12 seismoelectric sections shown in figure 4.31.

(a-d) in the date column refer to: (a) before infiltration, acceleration trigger; (b) before infiltration, manual trigger; (c) after infiltration, manual trigger; (d) long after infiltration, manual trigger. Profiles 1 and 2 refer to the profiles as shown in figure 4.24 on page 90. The shot points are thus relative to the respective two profiles and do not have absolute coordinates. In the column “filtered” I marked if the data were filtered from 50 Hz anthropogenic noise.

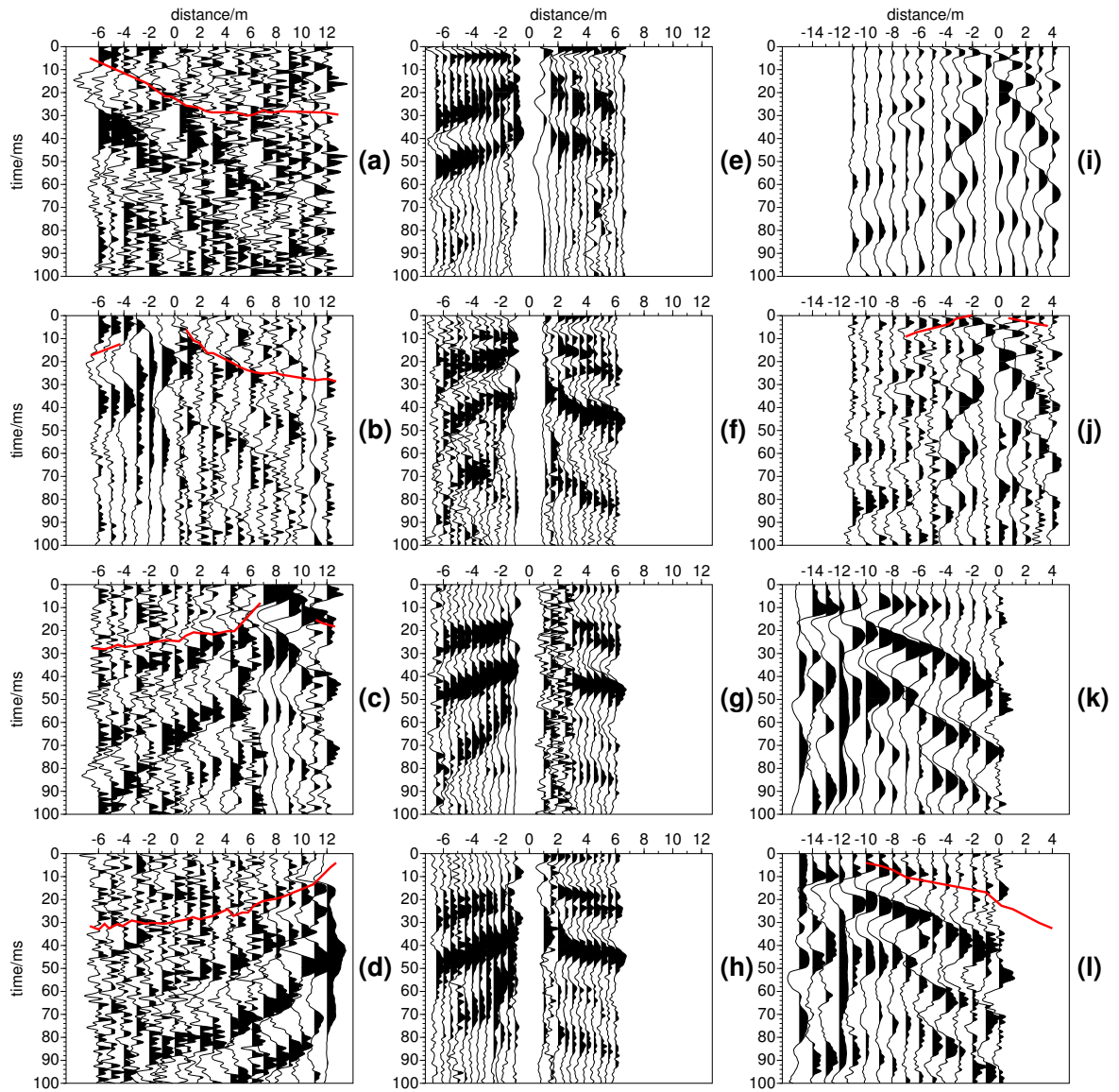


Figure 4.31: Seismoelectric sections with agc from the Segeberg Forest site from November 2005 (a-d), December 2005 (e-h), January 2006 (i-j), and February 2006 (k-l). (a-h) and (i-l) are from two different profiles (see figure 4.24). More details can be found in table 4.4. The seismic correspondences to these seismoelectric data are shown in figure 4.32. The seismic first breaks were marked in that figure and copied to their seismoelectric counterparts in this figure.

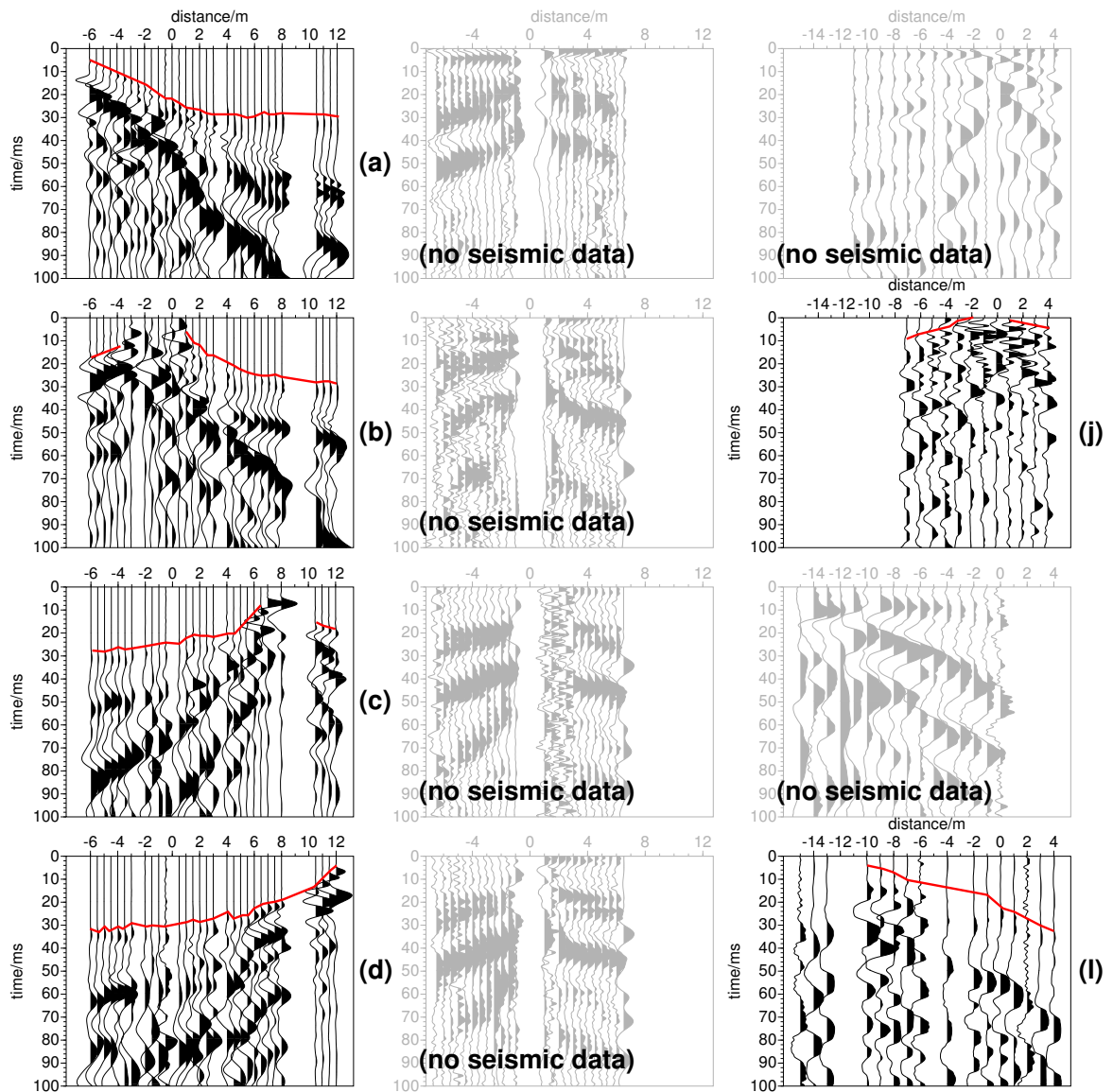


Figure 4.32: Seismic sections with agc from the Segeberg Forest site from November 2005 (a-d), December 2005 (e-h), January 2006 (i-j), and February 2006 (k-l). (a-h) and (i-l) are from two different profiles (see figure 4.24). More details can be found in table 4.4. Here, however, all shots were triggered with the acceleration trigger and stacked 10 fold. These are the seismic correspondences to the seismoelectric data shown in figure 4.31. The available seismic data are printed in black. The seismoelectric data are shown in light gray in the cases where no corresponding seismic data is available. The seismic first breaks were marked with red.

As there are so many parameters, it is quite difficult to make any direct comparisons.

In general there are quite some differences between the different shot records shown in figure 4.31, even though all these data are from the same location. The reason for the differences probably lies in the different measurement parameters and the different measurement conditions.

The data from November 2005 (a-d) and December 2005 (e-h) are filtered from 50 Hz noise with the technique described by Adam & Langlois (1995) and the data from January 2006 (i-j) and February 2006 (k-l) are unfiltered. This means that the contrasts in data quality are even stronger than they appear in figure 4.31. It is not very likely that the electromagnetic noise level was so much different in November and December than in January and February. Therefore it is more likely that the signal of interest was weaker in November and December. As stated before, the ground was quite soft especially in December while it was partly frozen and very hard in January. This has implications on seismic attenuation, electrode coupling and also on the electric resistivity and therefore also on the amplitude of the seismoelectric amplitudes.

The positions of the receivers do not seem to play a major role because the same receivers show totally different data qualities depending on other measurement parameters such as source or source positions.

It is plain to see that the accelerated weight drops produce much better data than hammer blows. On the other hand, the data seem to have lower frequencies and lower resolution.

Interestingly, there is no correlation between seismoelectric and seismic data quality: In November 2005 (figure 4.31a-d) the seismoelectric data quality is very bad despite clear seismic arrivals (figure 4.32) while the situation is the other way round in January and February 2006. Seismoelectric data seem to vary much stronger depending on ground conditions. It should be reminded that the pictured seismic component is the radial one in order to enable a good comparison with the (equally radial) seismoelectric component. The seismic vertical component usually has a much higher signal-to-noise ratio.

4.6.3 Unified interpretation (borehole and surface)

Upon investigation of the data, it is apparent that it was not possible to measure any converted seismoelectric events. The measurement and noise conditions play a role here for sure which resulted in quite variable data quality. The other reason could be that there simply are no boundaries at reachable depths which could generate strong seismoelectric conversions. Looking at figure 4.23, it seems that we have to do mainly with different degrees of sand in the uppermost 30 m. With ideal noise conditions it would perhaps be possible to detect low amplitude conversions (if there are any). But even the data collected with accelerated weight drops as source do not show any conversions. Not even the data in figure 4.31j which were stacked more than 300 times show converted seismoelectric signals.

Coming back to the differences between seismoelectric and seismic data quality discussed in the preceding section, I could have checked if the problem is on the source or on the receiver side by comparing the seismoelectric surface data against the seismoelectric borehole data. But unfortunately borehole data are available only from January and February where the overall data quality was quite good in the surface data, too, and not from November or December which makes the direct comparison impossible.

4.7 GeoModel

The GeoModel is an example of an urban measurement location with strong anthropogenic noise. I present data from two sublocations. In section 4.7.1 I explain the design of the GeoModel and show some data from inside the GeoModel. The data in section 4.7.2 on the other hand were collected from a sand pit in otherwise clayey material in front of the GeoModel. The findings from these two sublocations are put together in section 4.7.3.

4.7.1 Description

The GeoModel was constructed between 2001 and 2004 by the Soil-, Hydro-, and Biogeophysics working group with funding from the Federal Institute of Education and Research. For more information see Hagrey et al. (2003) or

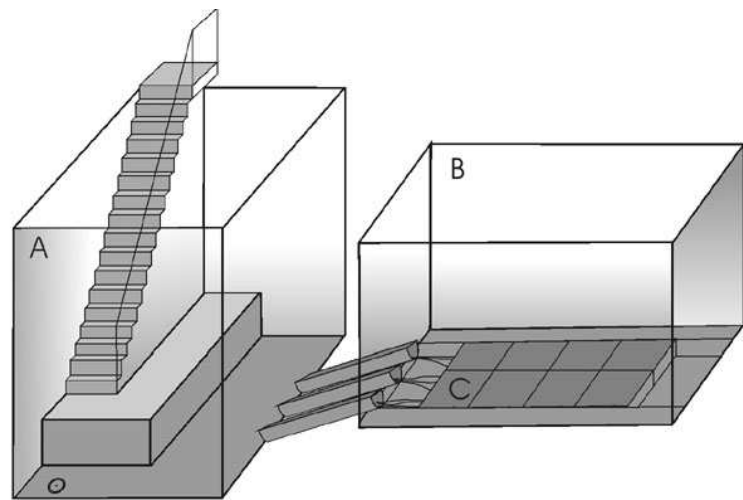
<http://www.ifg.uni-kiel.de/Ingenieurgeophysik/users/bodenhydrogeo>

where also the following lines are taken from:

The GEOMODEL (dimensions 3m x 5m x 2m) simulates the subsurface geological situation of the problem under study. The GeoModel presents an intermediate stage between laboratory experiments and field applications. Therefore it has the advantage of controlled laboratory experiments with predefined boundary conditions. Moreover, these non-scaled experiments facilitate the direct application to field surveys and comparison of results.

The design of the GeoModel is explained in figure 4.33. It consists of a sand basin flanked by electrode grids at all sides except at the top. The total number of electrodes amounts to 1439. Figure 4.34 shows a view into the interior of the GeoModel with the sand basin on the left side of the picture. The right side shows the sand pit in front of the GeoModel where the measurements described in section 4.7.2 were conducted. All electrodes can be reached via a control box as shown in figure 4.35 where also the main problem of the geomodel is made clear: anthropogenic 50 Hz noise, as it appears on the screen of the Bison seismograph during seismoelectric measurements in the GeoModel.

Some data examples along with the configuration of the involved dipoles are depicted in figure 4.36. These are examples after repeated filters to remove the anthropogenic 50 Hz noise and exhibit an unusually high signal-to-noise ratio compared to other data from the GeoModel.



A - Monitoring chamber
 B - Sand model
 C - Filter layer

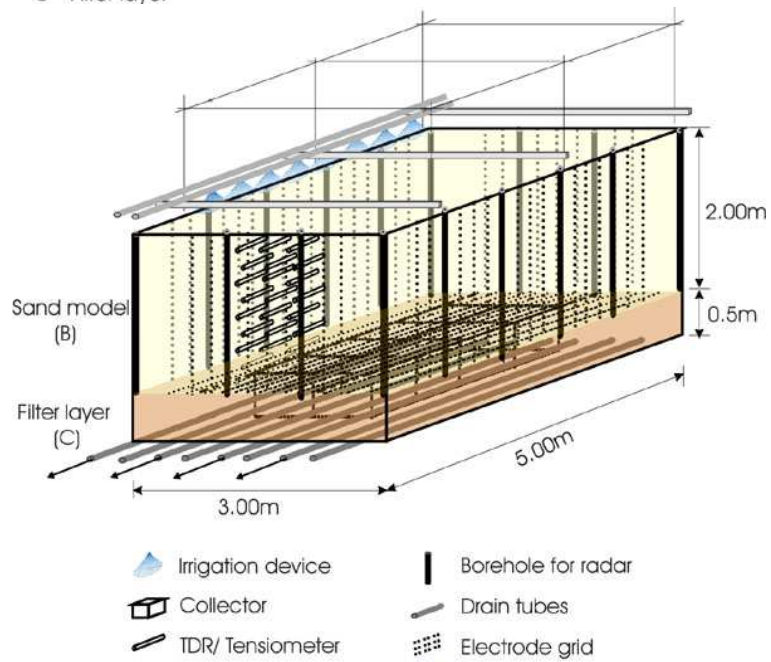


Figure 4.33: Design of the GeoModel. For more information see <http://www.ifg.uni-kiel.de/Ingenieurgeophysik/users/bodenhydrogeo>, where these images were taken from.

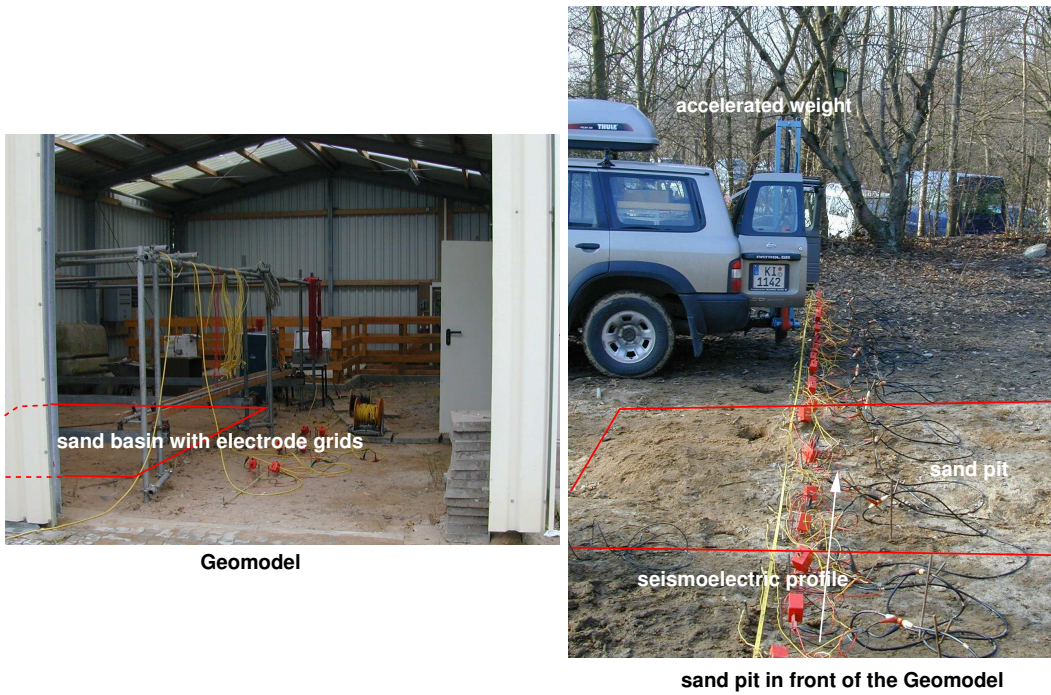


Figure 4.34: Left: View into the GeoModel with the sand basin marked. Right: Seismoelectric profile across the sand pit in front of the GeoModel with the accelerated weight drops source in the background.



Figure 4.35: Left: All 1439 electrodes can be addressed at this control box. Right: Problems arise due to strong anthropogenic 50 Hz noise (screen shot of the Bison seismograph monitor during seismoelectric measurements at the GeoModel).

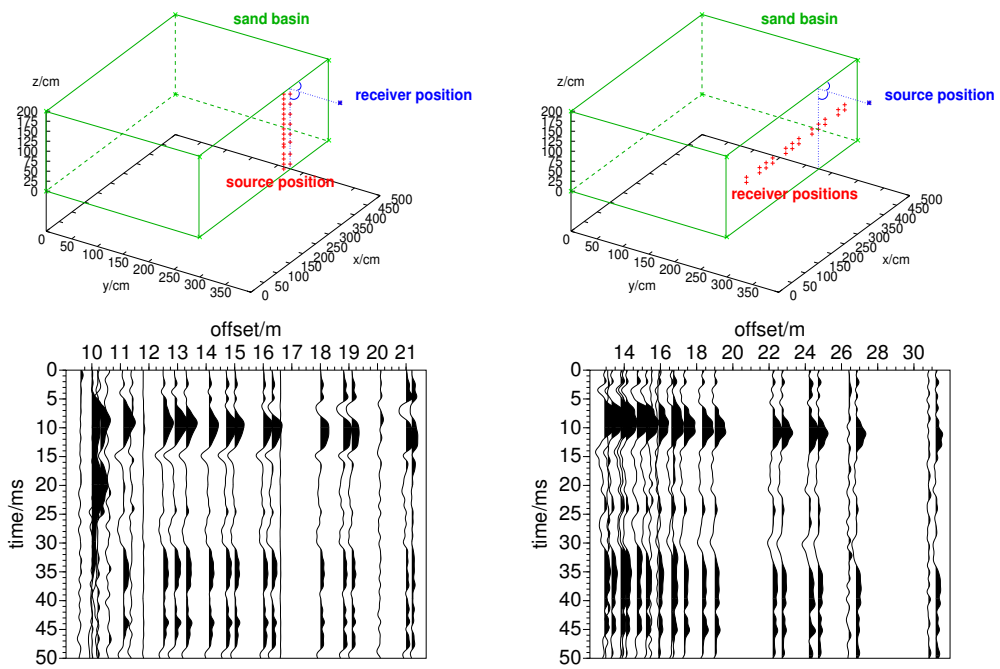


Figure 4.36: Two configurations and the corresponding shot records with *agc* from the *GeoModel*. Compared to other data from the *GeoModel*, these examples have rather high data quality.

4.7.2 In front of the GeoModel

Due to the problematic signal quality in the geomodel, a sand pit was dug in front of the GeoModel (see figure 4.34) and filled with sand to create an artificial contrast to the surrounding clayey material. In this way, instead of creating layer boundaries at depth, they are created at the surface as previously described by Haines (2004). The intention was to observe seismoelectric signals converted at these artificial boundaries and also to study the influence of the different materials on the seismoelectric amplitudes of the coseismic waves. The geometry is shown in figure 4.37.

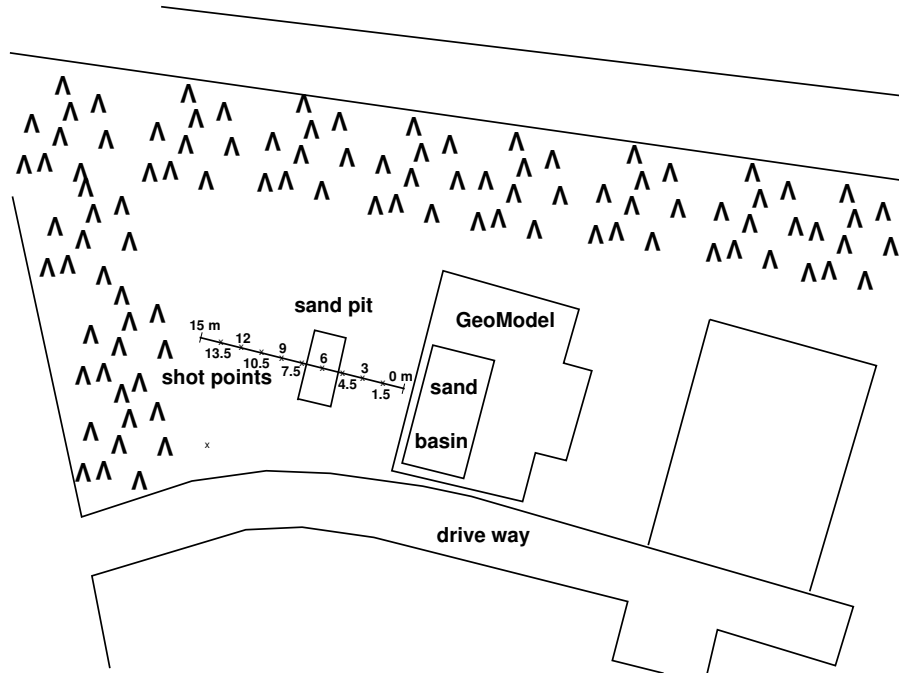


Figure 4.37: Location of the GeoModel, the sand basin, the sand pit and the profile across the latter one.

Seismoelectric and seismic data from a profile across the sand pit in front of the GeoModel are compared with each other in figure 4.38. Shown are data with a standard sledgehammer (left column) and accelerated weight drops (right column) as source. I compare the seismoelectric radial component with the seismic radial and vertical component. The seismic radial component is also shown in its time derivative version because this should resemble the seismoelectric radial component most closely. The clear seismoelectric arrivals from the measurements with the accelerated weight drops (figure 4.38e) are picked and marked with lines which are copied to the other shot sections. Blue lines indicate the extension of the sand pit. The seismoelectric data (both sledgehammer and accelerated weight drops) are sinusoid filtered several times to eliminate the strong 50 Hz noise. But especially in the sledgehammer data, strong residual electromagnetic noise obscure the seismoelectric arrivals.

The data shown in figure 4.38 were recorded in December 2005 and in February 2006, respectively. Except of the source, the same measurement parameters were applied in December and February and also the location of the profile is exactly the same in order to enable a direct comparison between the two measurement series. We measured at seven shot points of which one is shown here as example.

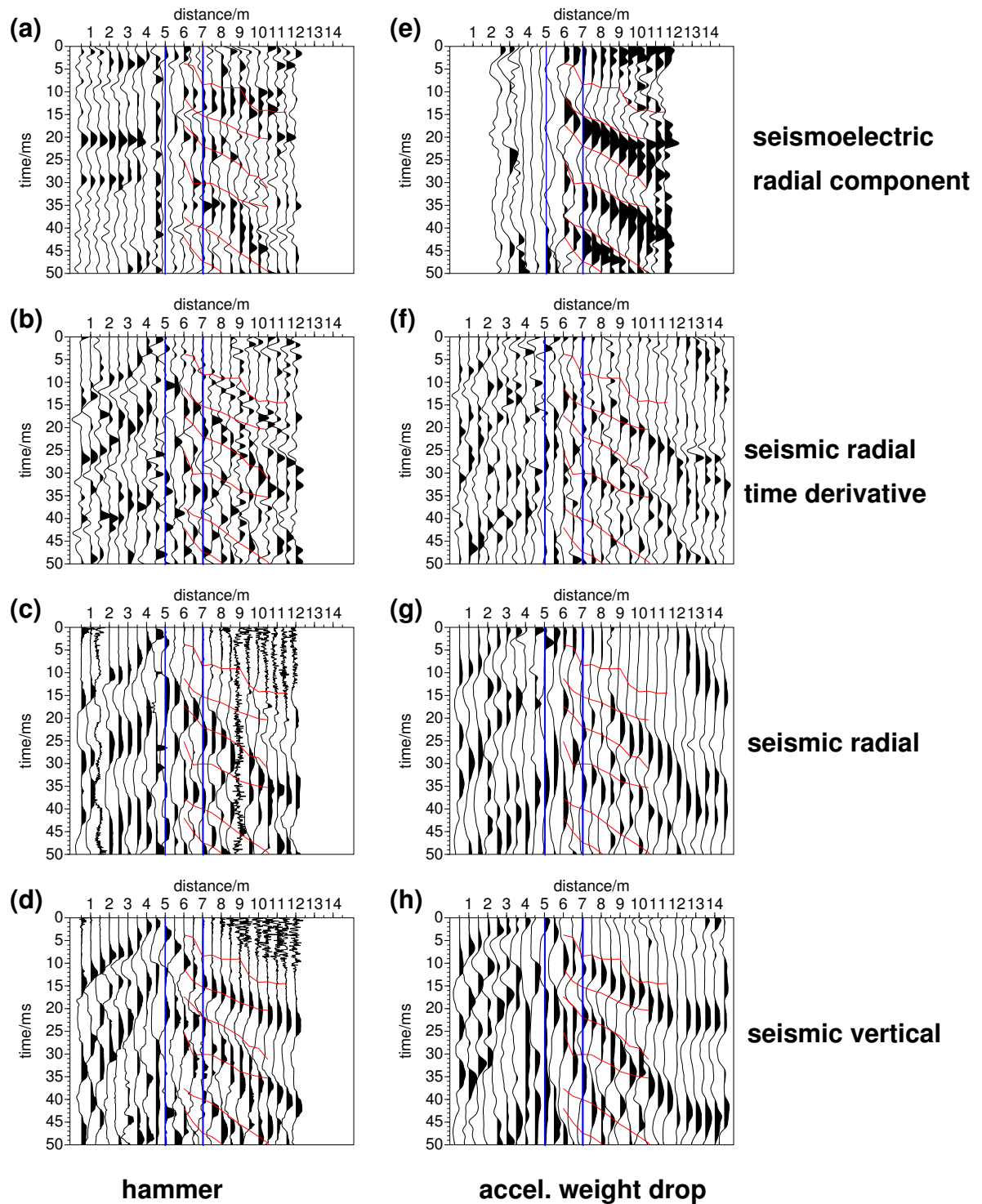


Figure 4.38: Seismoelectric and seismic data with *agc* from the profile across the sand pit in front of the geomodel. Shown are data with a standard sledgehammer (left column) and accelerated weight drops (right column) as source. I compare the seismoelectric radial component with the seismic radial and vertical component. The seismic radial component is also shown in its time derivative version. The clear seismoelectric arrivals from the measurements with the accelerated weight drops are picked, marked with lines and copied to the other shot sections. Blue lines indicate the extension of the sand pit.

The seismoelectric data from the accelerated weight drops as source are much better. Interestingly, the differences are significantly less in the seismic data. In the seismic case, the stronger source leads to less noise and slightly lower frequencies but the interpretation of the seismic data would not change. This shows that seismic data quality is not necessarily proportional to seismoelectric data quality. Obviously there are cases where the usage of a stronger source can lead to an insignificant improvement of seismic data quality but at the same time be a main reason for success or failure of the seismoelectric measurements.

I compared the changes of the seismoelectric amplitudes (coseismic waves) relative to the corresponding seismic amplitudes from the measurements with the accelerated weight drop source. All shots were adjusted in amplitude to simulate a source with constant strength so that changes in source signal amplitude could be excluded. This could be done with the help of a geophone the trace of which was recorded at every shot (both seismic and seismoelectric). Thus the amplitudes could be scaled relative to this geophone trace. The variation of the ratio between seismoelectric and seismic amplitudes is shown in figure 4.39. I show the results for the seismic radial and vertical components and also for the seismic radial time derivative. As stated above, the latter one should be the most sensible one for the comparison but as could be seen in figure 4.38 the data quality is better on the other data, especially the vertical component. The ratios from the seven shot points are shown as symbols together with the median curve through these values. Unfortunately, we do not see any systematic changes of the relative seismoelectric amplitudes at the sand pit. Probably, the parameter contrasts between the sand pit and the surrounding material were not strong enough although the resistivity contrast is obvious in the inverted resistivity model in figure 4.40. It seems that resistivity contrasts are not that important for seismoelectric signals. Indeed Garambois & Dietrich (2001) derive an approximation for seismoelectric against seismic amplitudes in which only the pore fluid resistivity appears and not the bulk resistivity (see section 5). This could explain the results obtained in this section since the pore fluid should be the same inside and outside of the sand pit. A similar sort of amplitude comparison study will be applied to seismoelectric data from the Segeberg Forest location in section 5.

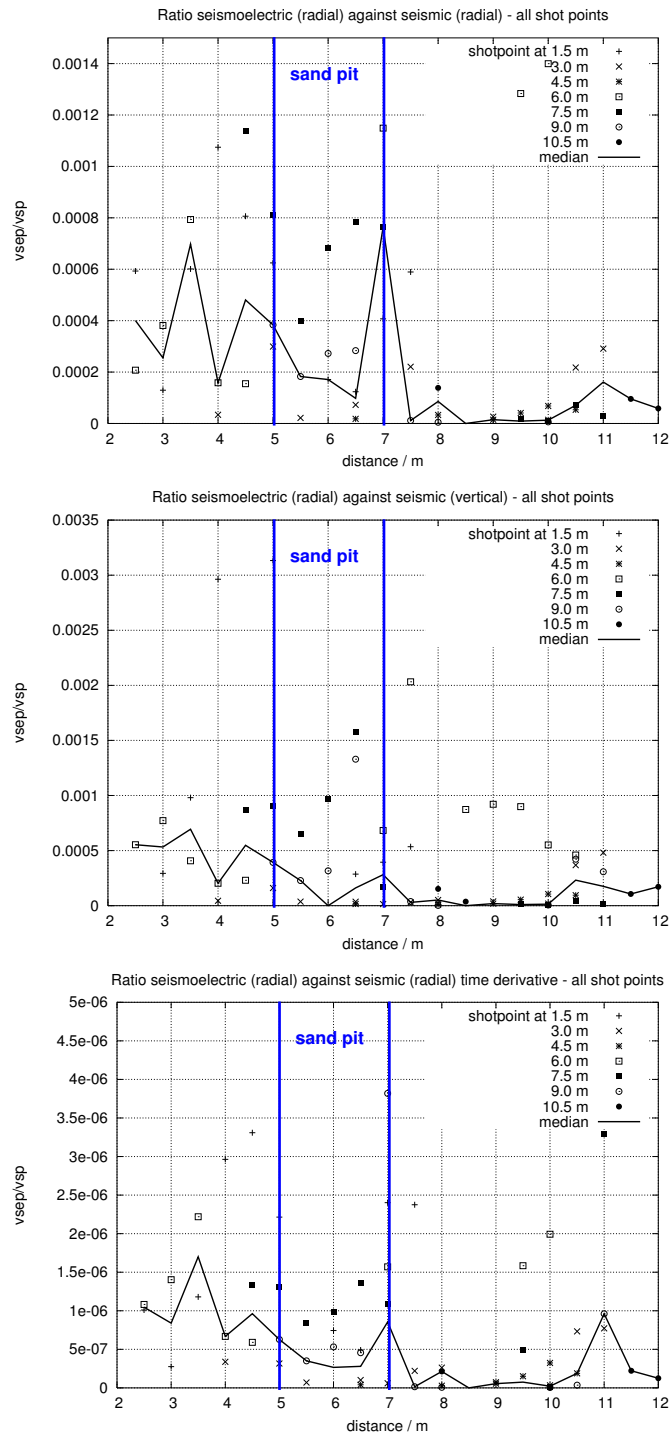


Figure 4.39: Changes of the seismoelectric amplitudes (coseismic wave, radial component) relative to the corresponding seismic amplitudes. Top: radial seismic component, middle: vertical seismic component, bottom: radial seismic component, time derivative. Shown is the median line through the seismoelectric/seismic ratios for every shotpoint. No systematic changes of the seismoelectric-seismic ratio at the sand pit (marked with blue lines) can be seen.

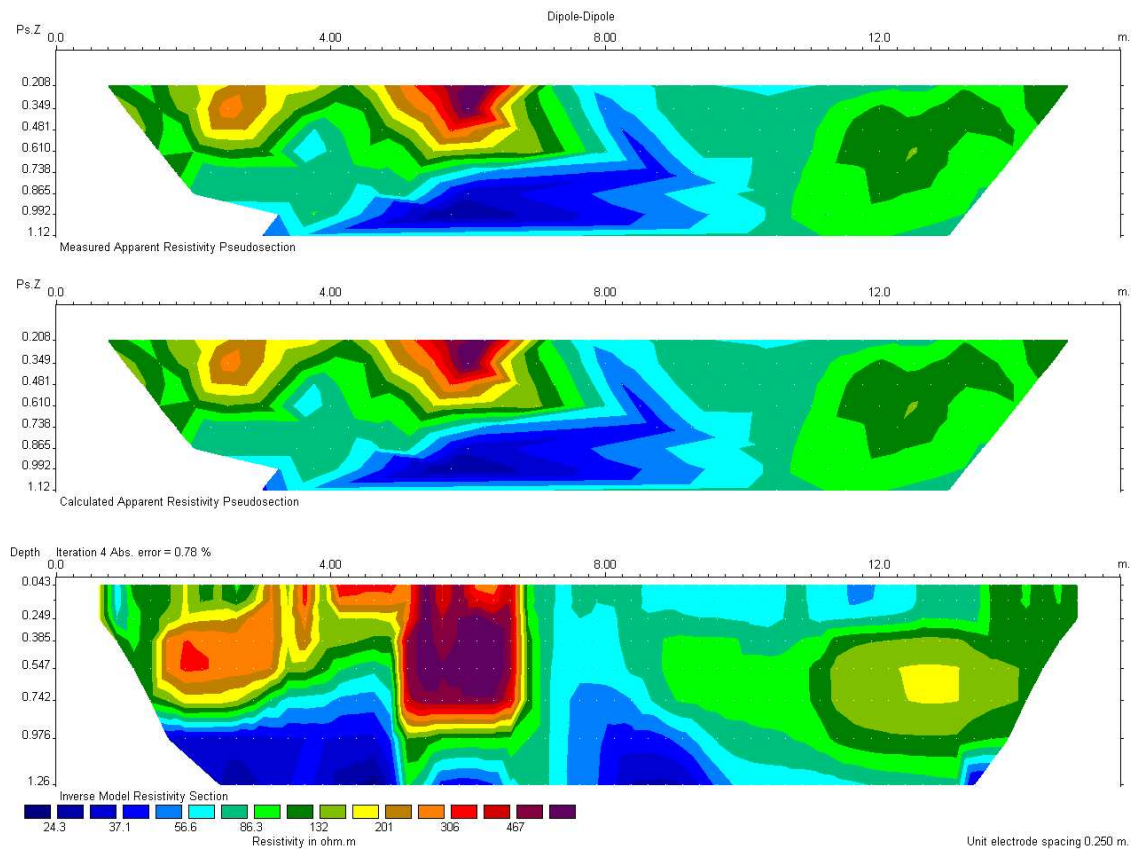


Figure 4.40: 2D geoelectric results from the profile in front of the GeoModel across the sand pit. Top: Measured pseudosection, middle: calculated pseudosection, bottom: inverted resistivity model. The sand pit between 5 m and 7 m is clearly delimited by its higher resistivities compared to the clayey surrounding ground. These dipole-dipole data were inverted using the finite element method as described by Loke & Barker (1996) with robust constrained inversion (Claerbout & Muir, 1973).

4.7.3 Unified interpretation

The examples from the GeoModel and from the sand pit in front of the GeoModel show that urban sites with strong electromagnetic noise are problematic for seismoelectric measurements. Even after applying several runs of the sinusoid filter and using a stronger source, the results are far from satisfactory. It is impossible to detect any converted seismoelectric signals. These would be obscured by the remnants of the 50 Hz anthropogenic noise. The coseismic waves can easily be identified but even these do not show any changes in amplitude relative to the seismic data in the sand pit. The pit would thus have gone undetected if its detection and characterization had been the aim of the seismoelectric measurements.

4.8 Comparison of the results from the different locations

The findings from the preceding subsections 4.3 (Fuhrberg), 4.4 (Menzlin), 4.5 (Selinunte), 4.6 (Segeberg), and 4.7 (GeoModel) are summarized in table 4.5 by listing the parameters influencing the seismoelectric data quality from each location. The table also contains information not yet mentioned in the respective preceding sections. Blank cells denote not available information or mark entries which would not be meaningful. + and - in the spatial and temporal variation columns refer to good and bad seismoelectric data quality, respectively. The results are summed up in table 4.8 with all relevant parameters marked as +, +/- or -. As the results from the Fuhrberg Forest site prove, seismoelectric data collected at one and the same profile can show clearly variable data quality. The reason for this has to be sought either in the measurement parameters or in changed ground conditions. The devices and cables used in the measurements were essentially always the same which leaves changes in the ground conditions as the sole remaining probable reason for the changes in seismoelectric data quality.

| location | underground | data quality | spatial variation | temporal variation | electrode coupling | ground resistivity | seismic data quality | converted signals? |
|----------------------------------|---|---------------------|--|--------------------------------------|--------------------|---|-----------------------------|--------------------|
| Fuhrberg (clearing) | sand, shallow groundwater table, clearing | ++, low noise level | not encountered | | | n·100 Ωm below groundwater | | |
| -February 2002 | | | | ++, moist ground | + | | + (vertical) (no radial) | yes |
| -September 2002 | | | | ++, dry ground | +/- | | + (vertical) (no radial) | yes |
| -January 2004 | | | | -, moist ground, maybe partly frozen | + | | | no |
| -April 2004 | | | | +/-, moist ground | + | | + (vertical) + (radial) | yes |
| Fuhrberg (waterworks) | sand, shallow groundwater table, soft forest ground | +/- | not encountered | | - | high resistivity above groundwater | + (vertical) - (radial) | no |
| Menzlin | grass-covered sand dune, shallow groundwater table | ++ | better data on sandy areas than on areas with (minimal) vegetation | | + | | + (vertical) + (radial) | yes |
| Selinunte (alluvial soil) | very conductive alluvial soil | -- | | | ++ | extremely low | | no |
| Selinunte (sand dune) | very dry sand dune | +/- | | | - | n·100 Ωm- n·1000 Ωm | + (vertical) (no radial) | no |
| Segeberg (borehole) | sand, shallow groundwater table, forest ground | + | very weak | very weak | ++ | high shallow resistivities (n·1000 Ωm, below: n·100 Ωm) | + (only one component) | no |

| location | underground | data quality | spatial variation | temporal variation | electrode coupling | ground resistivity | seismic data quality | converted signals? |
|------------------------------------|--|-----------------------------|---------------------------------------|---|--------------------|-----------------------|------------------------------|--------------------|
| Segeberg (surface) | sand, shallow groundwater table, forest ground | - - to +, strong variations | | | | as above | | |
| -November + December 2005 | | | soft forest ground: - | | +/- | shallow: n·1000 Ωm | + (vertical) (no radial) | no |
| -January + February 2006 | | | a bit harder ground along a path: +/- | partly frozen ground seems to be better than soft, wet ground | + | shallow: n·100 Ωm | + (vertical) - (radial) | no |
| GeoModel | sand and clayey ground | - - to - | sand pit better than the model itself | very strong variations | - - to ++ | | | no |
| -sand basin in the GeoModel | sand | - - | | strong | - | high | | no |
| -sand pit in front of the GeoModel | sand pit in clayey soil | - - to - | | | + | n·10 Ωm - n·100 Ωm | + (vertical) +/- (radial) | no |

Table 4.5: Overview of the measurement areas presented in this chapter and the parameters influencing the seismic data quality. + and - in the spatial and temporal variation columns refer to seismoelectric data quality. This table is summed up in table 4.8.

| Location | shallow ρ | electrode coupling | ground hardness | seismic data quality | anthropogenic noise | converted wave | total |
|---|----------------|--------------------|-------------------|----------------------|---------------------|----------------|---------------------|
| Fuhrberg clearing Feb. 2002 | - | + | + | (+) | + | + | + |
| Fuhrberg clearing Sep. 2002 | + | - | +/- | (+) | + | + | + |
| Fuhrberg clearing Jan. 2004 | + (?) | + | | | + | - | - |
| Fuhrberg clearing Apr. 2004 | - | + | + | + | + | + | + |
| Fuhrberg waterworks | + | - | - | - | + | - | +/- |
| Menzlin | +/- (?) | +/- (?) | +/- | + | + | + | + |
| Selinunte alluvial soil | - | + | | | | - | - |
| Selinunte sand dune | + | - | | (+) | + | - | +/- |
| Segeberg borehole | - | + | - \rightarrow + | + | + | - | + |
| Segeberg surface Nov.-Dec. 2005 | + | - | - | (+) | - | - | - |
| Segeberg surface Jan.-Feb. 2006 | - | + | + | - | - | - | +/- |
| GeoModel (inside) | + | - | - | | - | - | - |
| GeoModel sand pit | - | + | - | +/- | - | - | - \rightarrow +/- |

Table 4.6: The measurement areas presented in this chapter and the parameters influencing the seismoelectric data quality (summary of table 4.5). + and - in the **shallow ρ** column stand for high and low resistivities, respectively. Brackets in the **seismic data quality** column indicate that it is the data quality of the vertical seismic component and not the radial seismic data component. + in the **anthropogenic noise** column means low noise level (thus good quality data). The column **converted wave** indicates if converted seismoelectric signals could be measured or not. The **total** column refers to the overall seismoelectric data quality at one site.

In field one gets the impression that bad (wet) weather often coincides with bad data and that sunshine or fine winter weather coincides with high seismoelectric data quality. This would mean that the soil moisture is of great importance and enters the seismoelectric data quality via electrode coupling or ground resistivity. However, it is not the only important factor since both moist grounds and dry grounds can give good results. It lies in the nature of the method that the parameters affecting the seismic, geoelectric, and electromagnetic methods also have implications on the seismoelectric method. The question is rather how strongly each factor influences the seismoelectric data quality. It seems that there is no direct connection between seismoelectric data quality and one single parameter. An analysis of the columns in table 4.8 reveals the following:

- **Shallow ρ**

The parameter electrical resistivity is somewhat ambiguous: On the one hand, the resistivity of the ground fixes the amplitude of the seismoelectric signals. On the other hand, the resistivity

of the uppermost layer is important for the electrode coupling. Grounds with good coupling (e.g. moist ground) and therefore higher seismoelectric amplitudes often have low resistivities, which in turn should lead to lower seismoelectric amplitudes. In this regard especially the February and the September 2002 data are interesting. In February the ground was wet, the electrode coupling good and the resistivity low in the uppermost layer while in September the ground was dry, the electrode coupling worse and the resistivity higher. However, the data quality is similar (see figure 3.9). It seems that other parameters were more important here.

- **Electrode coupling**

The role of the electrode coupling is not sure either. Bad coupling means higher contact resistance between the electrode and the ground and thus lower seismoelectric amplitudes at the seismograph but this does not seem to be the most important factor. In some areas we had very good coupling but bad results (GeoModel, some positions in Segeberg Forest). Some newer data not shown in this thesis have rather bad coupling but excellent results.

- **Ground hardness**

The measurements in the Segeberg Forest suggest that the hardness of the ground plays an important role. When the ground was so soft that repeated vertical stacking caused holes of several dm as shown in figure 2.7 (page 25) the data were usually bad. Soft ground results in stronger seismic attenuation because much of the energy is used for soil compaction. This also leads to weaker seismoelectric signals. Hard (or frozen) ground often resulted in good data. Interestingly, seismic data quality does not always correlate with seismoelectric data quality although reduced source strength due to soft ground affects seismic and seismoelectric data alike. For seismic data this means that the amplitudes become weaker but often still are sufficient for first break picking if the background noise is weak enough. By contrast a reduction of the already feeble seismoelectric signal often results in unusable data. Hence more attention must be paid to the positioning of the source in seismoelectrics than in seismics. The importance of a good source signal becomes also evident when considering the strong improvement of seismoelectric data quality when using the accelerated weight drop source instead of the sledgehammer (see section 4.7.2).

- **Seismic data quality**

For direct comparisons between seismoelectric and seismic data, the same component is required, in this case the radial component. Depending on the subsurface, the data quality can differ significantly between the seismic radial and vertical components. Hence the seismic radial component is not applicable. Unfortunately, we did not record the seismic radial component at all locations so that only few pairs of seismic and seismoelectric radial component data sets are available. The results in table 4.8 indicate the seismic data quality of the radial component nearly always corresponds to the seismoelectric data quality. This is not always the case for the more commonly recorded vertical seismic component.

- **Anthropogenic noise**

Given the low seismoelectric amplitudes, a low electromagnetic noise level is of great importance. In principle, there are good data processing techniques to strip the records of anthropogenic 50 Hz noise. In practice, however, residual noise often remains. Because this noise consists of electromagnetic fields, it might be difficult to distinguish from possible converted seismoelectric events which have electromagnetic velocities, too. As can be seen in tables 4.5 and 4.8, converted signals could only be detected where the data quality was very good. Sometimes a stronger source seems to be the only solution.

- **Converted wave**

It could be expected that the chance of measuring converted seismoelectric signals should be higher in highly resistive ground than in low-resistive environments. The connection between electrical resistivity ρ , magnetic permeability μ , frequency f and skin depth¹ δ is expressed as (see, e.g., Telford et al., 1990)

$$\delta = \sqrt{\frac{\rho}{\pi\mu_0\mu_r f}} \approx 503[\text{m}] \sqrt{\frac{\rho[\Omega\text{m}]}{f[\text{Hz}]}} \quad (4.1)$$

The approximation is valid in most materials, i.e. where $\mu_r \approx 1$. Inserting $\rho = 100 \Omega\text{m}$ and $f = 70 \text{ Hz}$ yields a skin depth of more than 600 m. The attenuation of the converted seismoelectric signals can thus be neglected in most media for near surface applications.

In short the table lets us conclude that there is a strong correlation between the overall seismoelectric data quality and seismic data quality as well as with the absence of anthropogenic noise. Moderate correlation can be figured out with the hardness of the ground while there does not seem to be any strong connection with shallow resistivities or electrode coupling.

Generally positive in connection with seismoelectric measurements seem to be: sandy ground (preferably dry rather than wet), low electromagnetic noise level, and clear subsurface boundaries. Data in open field seem to be better than in forested areas. Forest ground is usually penetrated by a lot of tree roots which can act as diffractors and are responsible for a low seismic quality factor Q .² This affects naturally also the seismoelectric signals. Forest ground is often covered with moss and small undergrowth. Lots of small roots and insects or earthworms break up the soil which leads to bad electrode coupling and to weaker seismoelectric amplitudes. Irrespective of ideal measurement conditions and equipment, a clear boundary at which converted seismoelectric signals can be generated is of course still a prerequisite.

These results are far from exhaustive and should be extended in future measurements in a more quantitative manner, e.g. with source signal amplitude to seismoelectric signal amplitude ratios to get a better understanding of the attenuation of the involved signals. Almost all field sites analyzed in this chapter consist of sand in the upper meters. As can be seen in table 4.2, we visited also locations with clayey ground. The data from these locations are either very scarce or problematic due to bad data quality. The best data up to now was always measured on sandy ground. Ongoing research also covers field studies on sites with a broader variety of grounds to get more insight into this question.

¹At the skin depth, the amplitude of the electromagnetic wave has decreased by a factor of e^{-1} .

²The seismic quality factor Q is defined as

$$\frac{2\pi}{\text{fraction of energy lost per cycle}} = \frac{2\pi}{E/\Delta E}$$

Chapter 5

Towards quantitative seismoelectrics

5.1 Introduction

As the validity of the current seismoelectric theory (Pride, 1994; Haartsen & Pride, 1997) has not been sufficiently proved in field, it is at the current state of affairs difficult to use the seismoelectric technique to determine any parameters from measurements. Sporadic attempts in this direction have been taken, e.g. by Mikhailov et al. (2000) who determined the porosity of fractured granite with VSEP, but more work needs to be done. Especially an experimental sensitivity study should be carried out. This is complicated by the fact that seismoelectric signals depend on a lot of parameters. It is hence important to study their dependence on single, selected parameters as e.g. electric resistivity.

5.2 Combined VSP, VSEP, and geoelectrics

In order to study the dependence of seismoelectric signals on electrical resistivity, I compare VSP (vertical seismic profiling) and VSEP (vertical seismoelectric profiling) measurements with borehole geoelectrics at the location Segeberg Forest (January 2006) at borehole 2 (see also section 4.6 and figure 4.26a). We first collected the seismoelectric borehole data, followed by the seismic data. To simulate a source with constant strength at every shot we measured a surface seismoelectric profile simultaneously with the borehole profiles. I chose the dipole of this surface profile with the best signal quality to serve as a kind of reference station so that each seismic and each seismoelectric shot can be normalized to a standard source strength. For every seismic and seismoelectric receiver position in the borehole, the peak amplitude of the envelope of the direct P-wave was picked (see figure 4.26a). It was pointed out in section 1.1.1.1 that for seismic body waves it is the first time derivative of a seismic trace which should be proportional to its electric coseismic equivalent (ground acceleration and not ground velocity). Since we worked with hydrophones, I did not time derivate the traces (see section 4.6.2.1). By dividing the seismoelectric traces with the equivalent seismic traces, I eliminated the seismic influence on the seismoelectric data. All remaining variations of these normalized seismoelectric amplitudes should be due to parameters that do not influence the seismic data or that influence the seismic data in a different way than the seismoelectric data.

Using a plane wave solution Garambois & Dietrich (2001) derive

$$\mathbf{E} \approx \frac{1}{\sigma_f} \frac{\epsilon_0 \rho_f \epsilon_f \zeta}{\eta} \left(1 - \frac{\rho}{\rho_f} \frac{C}{H} \right) \ddot{\mathbf{u}} \quad (5.1)$$

as a low-frequency approximation for the electric field generated by a seismic compressional wave with \mathbf{E} being the electric field, σ_f the pore fluid conductivity, ϵ_0 the vacuum permittivity, ρ_f the pore fluid density, ϵ_f the relative permittivity of the pore fluid, ζ the zeta-potential, η the viscosity, ρ the bulk density, C and H moduli as defined by Biot (1962), and $\ddot{\mathbf{u}}$ being the grain acceleration. According to Garambois & Dietrich (2001), $C \ll H$ for most materials so that equation 5.1 can be further simplified to

$$\mathbf{E} \approx \frac{1}{\sigma_f} \frac{\epsilon_0 \rho_f \epsilon_f \zeta}{\eta} \ddot{\mathbf{u}} \quad (5.2)$$

Not every of the occurring parameters is relevant for an experimental examination:

- The dielectric permittivity of the vacuum ϵ_0 is a constant.
- The density of the pore fluid ρ_f is assumed to change only insignificantly.
- The dielectric permittivity of the pore fluid ϵ_f depends on temperature but not on salinity or resistivity and is therefore assumed to be constant in the borehole. During the measurements (January 24-25, 2006) temperatures were below 0°C but the ground was only frozen in the upper few cm. The variation of the temperature along the depth of the profile can only have been some degrees which is why I judge the influence of the temperatures as negligible in this context.
- I intended to determine the conductivity of the pore water σ_f with borehole geoelectric measurements. I took the data from an inverted Wenner- α sounding in the borehole (smallest depth). Unfortunately the electrode spacing was apparently too great to minimize the influence of the formation so that the obtained resistivities are much too high and represent the bulk resistivities. The only available information about pore water conductivity are conductometer measurements done by Ohse (1983) in the same borehole. It should be kept in mind that these value were collected more than 20 years before the other measurements described here. However, subsequent measurements proved that they are rather constant over time (E. Bedbur, pers. comm., 2006).
- The viscosity η is assumed to be constant throughout the well.
- $\ddot{\mathbf{u}}$ is measured by the hydrophones.

Summed up, there are only the parameters ζ , σ_f , and $\ddot{\mathbf{u}}$ changing with depth. While σ_f and $\ddot{\mathbf{u}}$ are relatively easy to acquire, the ζ -potential poses more problems. I cannot measure it directly in situ nor do I have information about it. I can only make statements of factors influencing it as e.g. the pH value. pH is often measured as an indicator for the solubility of certain substances e.g. when studying waste dumps. Schröter (1983) reports low pH values in the upper soil and increasing values with

depth at the Segeberg Forest borehole field (figure 5.2e). Also these values are quite constant over time (E. Bedbur, pers. comm., 2006). This is quite typical for coniferous forests. Ishido & Mizutani (1981) found experimentally that an increase in pH usually leads to higher negative values of the ζ -potential, depending on type of minerals, pore fluid, and temperature. The pH- ζ dependence is nonlinear but often monotonous, especially for quartz (see figure 5.1) which is important since the ground at the Segeberg Forest site is mostly sandy. Besides pH, also the temperature strongly influences the ζ -potential (see Ishido & Mizutani, 1981). Often higher temperatures lead to higher negative ζ -potential values. The connection can be quite complicated and also lower negative ζ -potentials can be the result. But as stated above, the temperatures only vary a few degrees in our measurements and hence I neglect their influence.

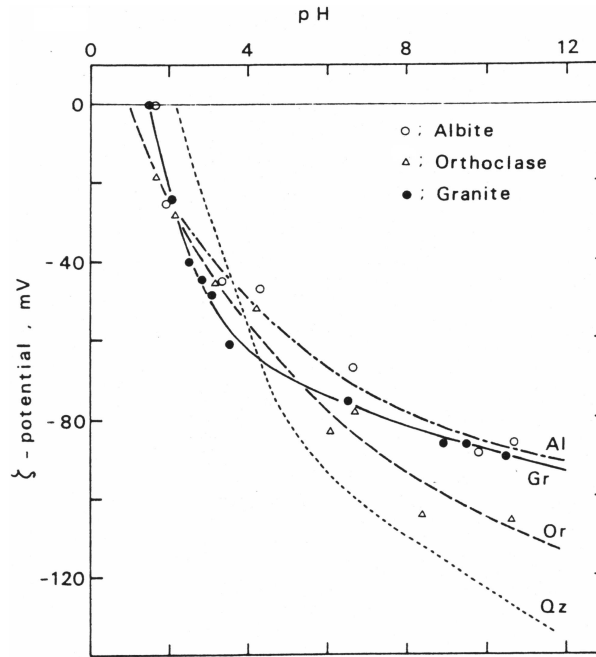


Figure 5.1: Dependence of the ζ -potential on pH for some minerals in aqueous solutions of $10^{-3}N KNO_3$ at $45^\circ C$. Taken from Ishido & Mizutani (1981).

In figure 5.2 I assemble VSP along with VSEP data, the VSEP/VSP ratio, electrical resistivities, and the pH value and porosity with depth. The VSP and VSEP values are the picked maximum amplitudes of the envelope of the traces at the respective depth (direct wave). I used 2 m and 8 m long dipoles for the seismoelectric measurements. The resistivity and pH curves as well as the soil depth profile are described above. I plot the resistivities in a logarithmic scale because the ζ -potential depends logarithmically on salinity (e.g. Pride & Morgan, 1991) which in turn is approximately proportional to conductivity for limited ranges of conductivity. The porosity can be calculated with the Archie equation (Archie, 1942)

$$\rho_b = \frac{a\rho_f}{\phi^m S^n} \quad (5.3)$$

with ρ_b : bulk resistivity, a : constant ($a=1$ for perfectly insulating mineral grains which is often assumed in absence of clay and when the pore water is not too resistive), ρ_f : pore fluid resistivity, m :

shape factor (also called porosity exponent or cementation degree, $1.3 \leq m \leq 2.5$), S : saturation and n : saturation exponent (usually $n \approx 2$).

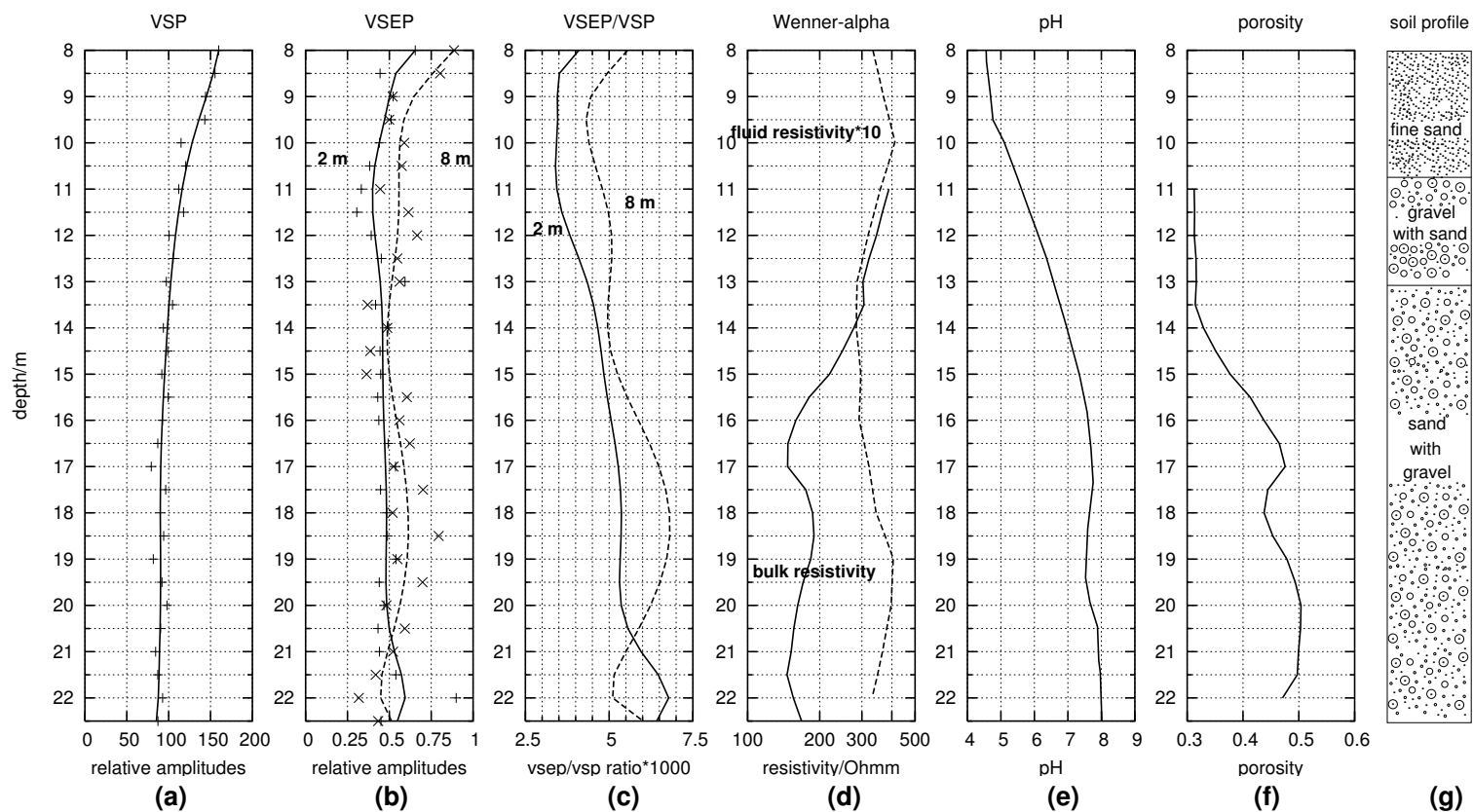


Figure 5.2: Influence of different parameters on seismoelectric amplitudes in borehole 2 at the Segeberg Forest site (January 2006). The amplitude maximum of the envelope of the seismic (a) and seismoelectric (b) traces are shown with depth, as well as the VSEP/VSP ratio (c). Seismoelectric data were recorded with 2 m and 8 m dipole length. The bulk resistivities (d) were determined with Wenner- α . Shown are also the borehole fluid resistivities from Ohse (1983), multiplied with the factor 10 to fit to the scale. The pH values (e) and the soil information (g) were taken from Schröter (1983). The porosities in (f) were calculated with the Archie equation from the resistivity values in (d).

Salem (1990) estimated ϕ with surface dc geoelectrics to a value of ≈ 0.4 . Approximating this value with the Archie equation results in $m = 2.2$. In this calculation I took ρ_b and ρ_f from figure 5.2 and set $a = S = 1$. Equation 5.1 does not explicitly contain porosity but I chose to compare it to the rest of the parameters since the equation only is an approximation. The picked seismic amplitudes decrease as could be expected. The data were combined from several single shots. The shot strength correction as described above did not work perfectly since the values do not follow a straight line. In all subsequent calculations I use smoothed curves as depicted in figure 5.2a-c. The seismoelectric amplitudes increase with depth. At first this seems counterintuitive but the seismoelectric signals are generated locally at depth through electrokinetic processes provoked by the seismic compressional wave. Changes in e.g. pore space parameters can lead to stronger seismoelectric signals even if the amplitudes of the carrying seismic wave decreases. This increase of seismoelectric signals gets even clearer in column (c) where the ratio of seismoelectric against the corresponding seismic amplitudes are shown. The data from 8 m dipole length generally seem to have slightly higher amplitudes but not 4 times higher than the 2 m dipole length data. Seismoelectric amplitudes are apparently not linearly dependant on dipole length. This stands in contrast to the results of Mikhailov et al. (2000) but in accordance with Beamish (1999).

The bulk resistivity data cannot explain the observed seismoelectric amplitudes since the resistivity decreases with depth which should lead to lower seismoelectric amplitudes. This is not the case. The same is true for the pore fluid resistivity ρ_f . The normalized VSEP data do not follow the form of the ρ_f curve. Only at depths > 14 m the curves fit better (higher resistivities correspond to higher seismoelectric amplitudes). pH, however, does fit to the VSEP/VSP curves over the whole depth interval and increases with depth. As shown in figure 5.1, this leads to greater negative values of the ζ -potential (normally $\zeta < 0$). As can be seen in equation 5.1, the electric field is proportional to the ζ -potential. There is a clear correlation between increasing pH and increasing seismoelectric/seismic ratio. The curves do not match completely since the seismoelectric signals are not measured at a point but as a potential distance between two electrodes. Especially at depths < 9 m the VSEP amplitudes change very fast. This could be an influence from the borehole casing which is not sliced (filter pipe) at depths < 8 m. In addition the pH value itself is not directly proportional to the ζ -potential (see figure 5.1).

In figure 5.3 I show the normalized seismoelectric amplitudes (smoothed curve as in figure 5.2) measured with 2 m long dipoles against bulk resistivity ρ_b , fluid resistivity ρ_f , pH, and porosity ϕ together with a regression line and the correlation coefficient. In this correlation analysis I also included data from outside of the depth interval shown in figure 5.2 where available. The plots confirm the findings from above. According to equation 5.1 the normalized VSEP/VSP amplitudes should not depend on ρ_b , but only on ρ_f . There is some correlation between ρ_b and VSEP/VSP figure 5.3 but exactly opposite of what is expected. Increasing resistivities should lead to increasing seismoelectric amplitudes, not the other way round (e.g. Haartsen & Pride, 1997; Block & Harris, 2006). No linear dependence between VSEP/VSP and ρ_f can be found for the whole depth interval (figure 5.3b). It is not clear why the ρ_f curve does not follow the VSEP/VSP amplitudes but these outcomes should be verified in further studies with a more rigorous determination of ρ_f . The pH value does show a strong linear correlation with the normalized seismoelectric amplitudes (correlation coefficient $r = 0.90$). Increasing ϕ leads to increasing VSEP/VSP as can be expected but the correlation does not seem to be linear. However, this could be due to the uncertainties in calculating ϕ as described above (older measurements of ρ_f , fitting via the Archie equation).

Sine the electrokinetic coupling coefficient is dependent on both the porosity ϕ and the pH value

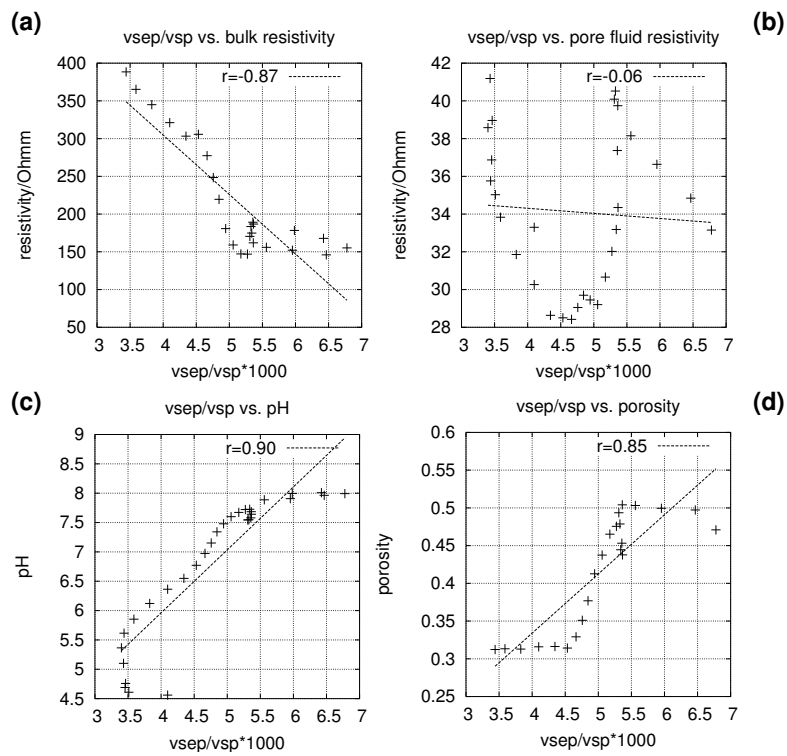


Figure 5.3: Correlations between normalized seismoelectric amplitudes (2 m dipole length) and bulk electrical resistivity (a), pore fluid resistivity (b), as well as pH (c) and porosity (d). The regression line and the correlation coefficient are also indicated.

(equation 1.13 on page 11), I compare the product of these two parameters with the normalized seismoelectric amplitudes. These two curves and the correlation between them is shown in figure 5.4. The correlation coefficient is 0.90, the same as in the correlation of the normalized seismoelectric amplitudes with the pH value (figure 5.3c) but the optical impression is that this curve fits even better.

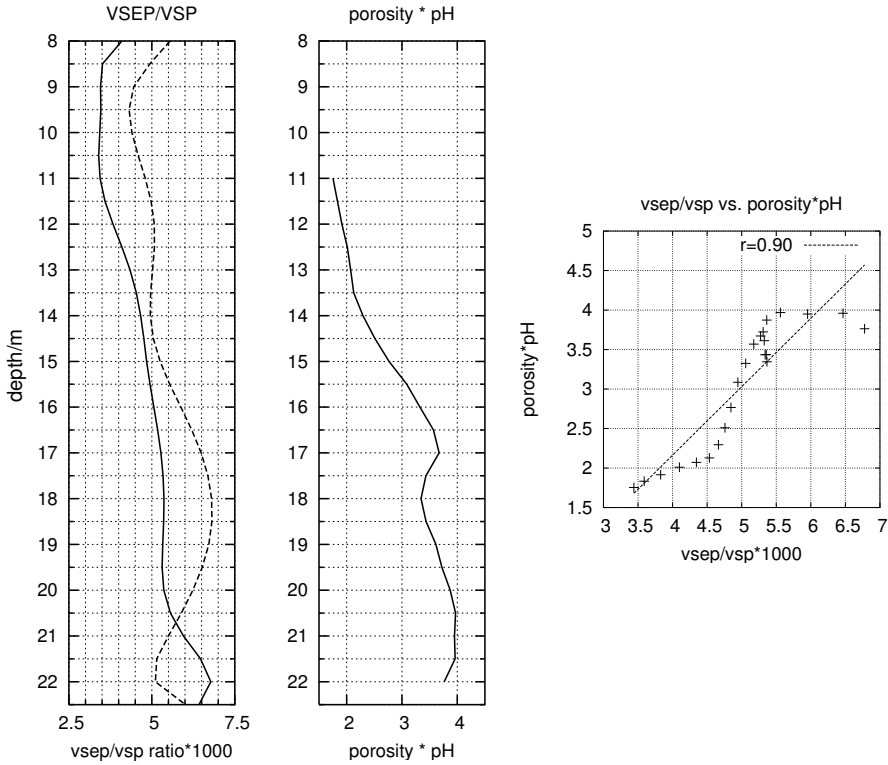


Figure 5.4: Normalized seismoelectric amplitudes (left), the product of porosity and pH (middle) and the correlation between normalized seismoelectric amplitudes (2 m dipole length) and the product of porosity and pH (right). The regression line and the correlation coefficient are also indicated.

5.3 Conclusions

Comparing borehole seismoelectric, seismic, resistivity, pH, and porosity data, I observe a strong dependence of the seismoelectric amplitude (normalized with respect to the seismic amplitudes) on pH. The results were confirmed by two independent measurements with different dipole lengths. The normalized seismoelectric amplitudes are not or only very weakly dependent on dipole length which has been reported ambiguously in literature up to now. There also seems to be a dependence on porosity but the error bars are rather large. The same is true for the product of the porosity and pH which possibly correlates even better with the normalized seismoelectric amplitudes than the pH value alone.

The results are interesting because it is not as expected the electrical resistivity that has the strongest impact on the seismoelectric signals but the pH value via the ζ -potential. pH is a parameter which is hard to determine at depth without a borehole but has strong implications on the seismoelectric ampli-

tude. The pH-value has to be constant or known if seismoelectric amplitudes are to be used for other applications. This dependence in turn makes it in principle possible to determine the pH value which is not accessible with other geophysical methods. As stated in section 4.8 our seismoelectric data collected in forests generally have quite bad data quality. The low pH commonly found in coniferous forests could contribute to this. The idea of stripping seismic borehole data from seismoelectric borehole data is not new. Mikhailov et al. (2000) used the same approach to calculate formation porosity. They also measured conductivity in the borehole and included it in the porosity calculation, but its variations were so small that its impact on the seismoelectric data is not obvious. They used literature values for the ζ -potential but assumed it to be constant.

The strong dependence on the ζ -potential offers new possibilities of identifying layer boundaries which might be insensitive to other methods. This analysis shows how important comparative seismoelectric field studies are. Until now, this strong impact of the pH value on seismoelectric amplitudes has not been highlighted in literature.

Chapter 6

Three-component seismoelectrics and polarisation

The main part of this chapter appears in Strahser et al. (2006). Its first part contains field measurements and analysis of three-component seismoelectric data and their polarization (section 6.1). Part 2 (section 6.2) explains the calculations made for obtaining the seismoelectric amplitude in section 6.1. The data are from the location Fuhrberg Forest (February and September 2002). They were previously investigated into in chapter 3 and section 4.3.

6.1 Polarization analysis

6.1.1 Introduction

Little is known about the nature of seismoelectric signals, especially of those converted from seismic waves at a subsurface interface. Therefore we conducted measurements which - to my knowledge - were unique in the respect that we were able to register all three components of the seismoelectric signals. The field technique has already been described in section 2.5.1. I will first present the three-components seismoelectric data and identify the different arrivals in section 6.1.2. The polarization will be analyzed with the help of hodograms in section 6.1.3. Section 6.1.4 is dedicated to the thin-layer approach by which the apparent mismatch between prediction and reality in the preceding section can be explained. I will end with some speculations about anisotropy at the presented location and a conclusion in sections 6.1.5 and 6.1.6, respectively.

6.1.2 Analysis

In figure 6.1, I present a comparison between five traces from each seismoelectric component as well as from the seismic vertical component and its time derivative. Some of the arrivals in the seismoelectric radial component are marked with lines which are copied onto the other components and the seismic records for a better comparison. In figure 6.1d, the apparent velocities of the picked

arrivals are displayed.

The seismoelectric three-component records show that signals differ dependent on dipole direction (figure 6.1 a, b, c). Of the three seismoelectric components, the radial component shows the highest similarity with the vertical component seismic record (figure 6.1a and e, f). The marked events can be divided into three groups according to their apparent velocities (cf. figure 3.2 on page 48 where the same data are shown at greater offsets):

1. seemingly infinite apparent velocities: event Z. As pointed out in section 3, this is the seismoelectric field converted at the sand-silt interface.
2. apparent velocities around 400 m/s: events B, C, D, and E. These events all seem to be associated with the direct P-wave.
3. slower apparent velocities: event R. This is the Rayleigh wave picked in the seismic data (figure 6.1e) and added to the seismoelectric events for comparison.

The refracted wave does not appear separately at these small offsets. Some of the events in group 2 are superpositions, as can be seen in figures 3.2 and 6.1: event B has some influence of the refracted wave at offsets > 4 m and event D could contain seismoelectric signals confined to the Rayleigh wave.

6.1.3 Hodogram analysis

To learn more about the polarization of seismoelectric signals, I analyze one event out of group 1 and 2 and compare the three seismoelectric components in the respective time windows in figures 6.2-6.3. The top part of each figure shows overlays of two components each and the position of the time windows for which hodograms are plotted in the columns below. The hodogram rows correspond to 3, 4, and 5 m offset from the source, respectively. The first column comprises the comparisons between the radial and the transverse components, the second column deals with the radial and the vertical components and in the third column I analyze the transverse and the vertical components. The position of the hodograms A1-C3 are marked in the two-component seismoelectrograms on top of the hodograms. The interval between two time marks in the hodograms is 2.5 ms. In the first plot group (figure 6.2) I compiled hodograms of the time interval in which the converted seismoelectric signal from the sand-silt boundary lie. Plot group 6.3 deals with the time interval in which the coseismic (direct wave) arrivals are found. In figure 6.2 the axes of the hodograms range from -3 mV to +3 mV, while in figure 6.3 they extend from -15 mV to +15 mV.

The polarization of converted seismoelectric arrivals can be analyzed in figure 6.2. The largest amplitudes are found on the radial and vertical components (middle column) resulting in an oblique polarization mainly in the vertical plane oriented radially away from the shot point. The tilt of the polarization can well be explained with the dipole character of the expected converted field. The amplitude decays with offset (B1 vs. B2 vs. B3) are compatible with the diffusive character of the converted wave and were analyzed in detail in figure 6.5.

In table 6.1.3 I compare the ratio of the amplitudes of the radial to the vertical component in the time window as shown in figure 6.2 (6.5 ms - 14 ms), i.e. where I expect the converted seismoelectric

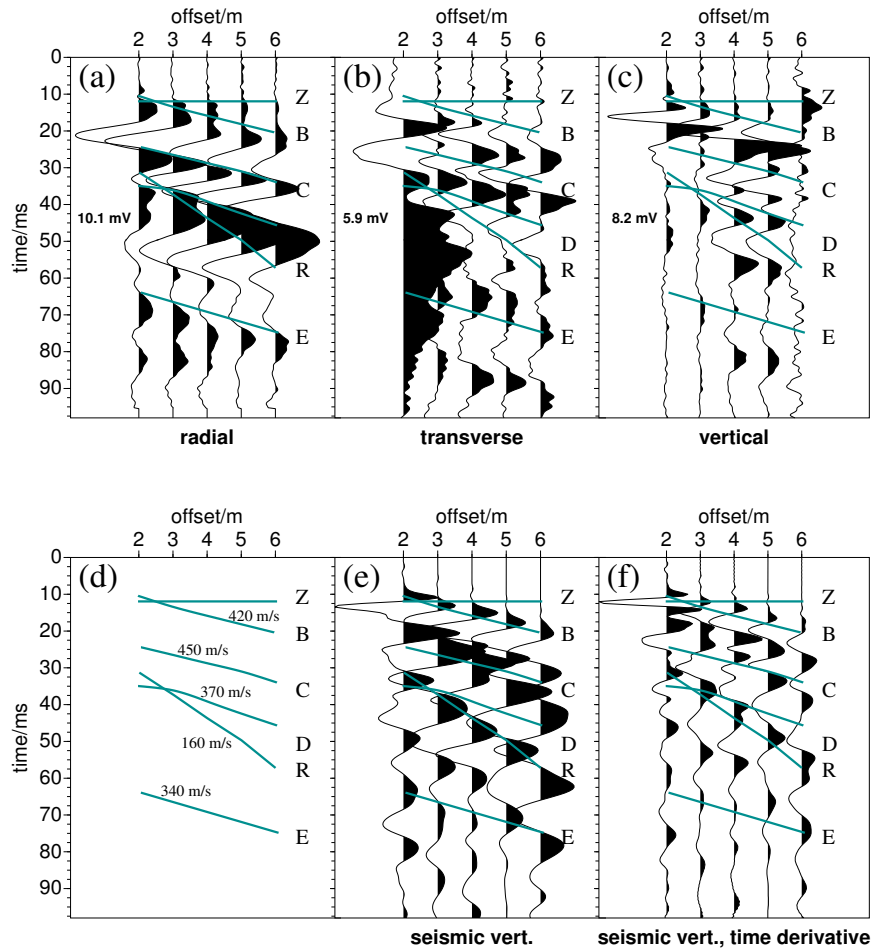


Figure 6.1: Example of three-component seismoelectric data from the Fuhrberg site recorded with electrodes connected to dipoles of 2 m length (horizontal components) and 1.5 m length (vertical component). a) radial, b) transverse, c) vertically oriented dipoles, d) arrival times picked from (a), e) vertical component seismic records added for comparison, f) time derivative of vertical component seismic records. Note that amplitude levels and plotting scales are strongly different in the different seismoelectrograms and seismograms. The maximum amplitudes of the respective seismoelectric sections are indicated in the seismoelectrograms. Some arrivals are highlighted and analyzed in the text. The same data are shown in figure 3.2 on page 48 with greater offsets.

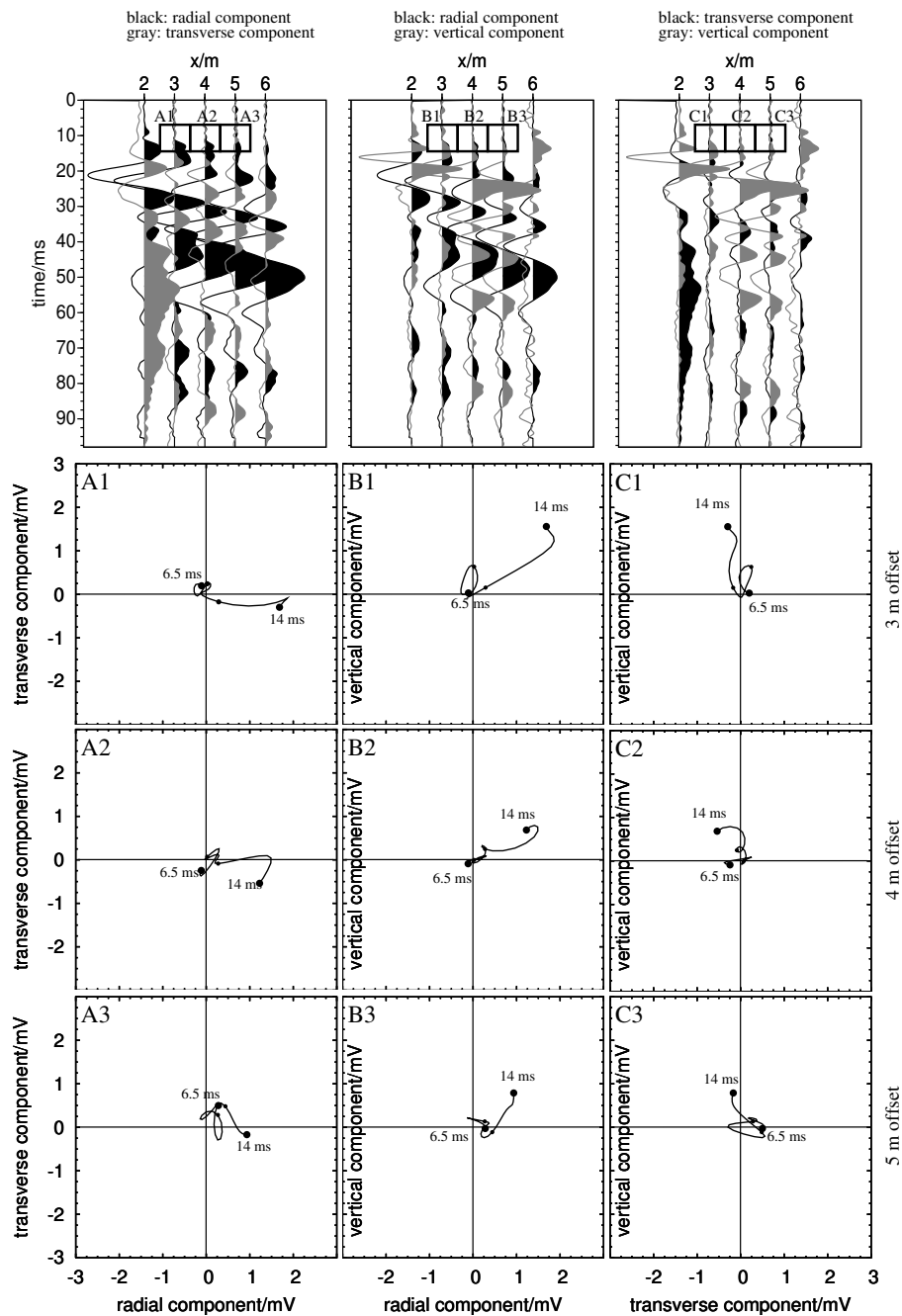


Figure 6.2: Hodogram comparison between radial, transverse, and vertical seismoelectric traces. In each of the three columns (A,B,C), two of the three components are analyzed. The two-component seismoelectrograms in the upper row enable a direct comparison between two of the three components of which one is displayed in black and one in gray.

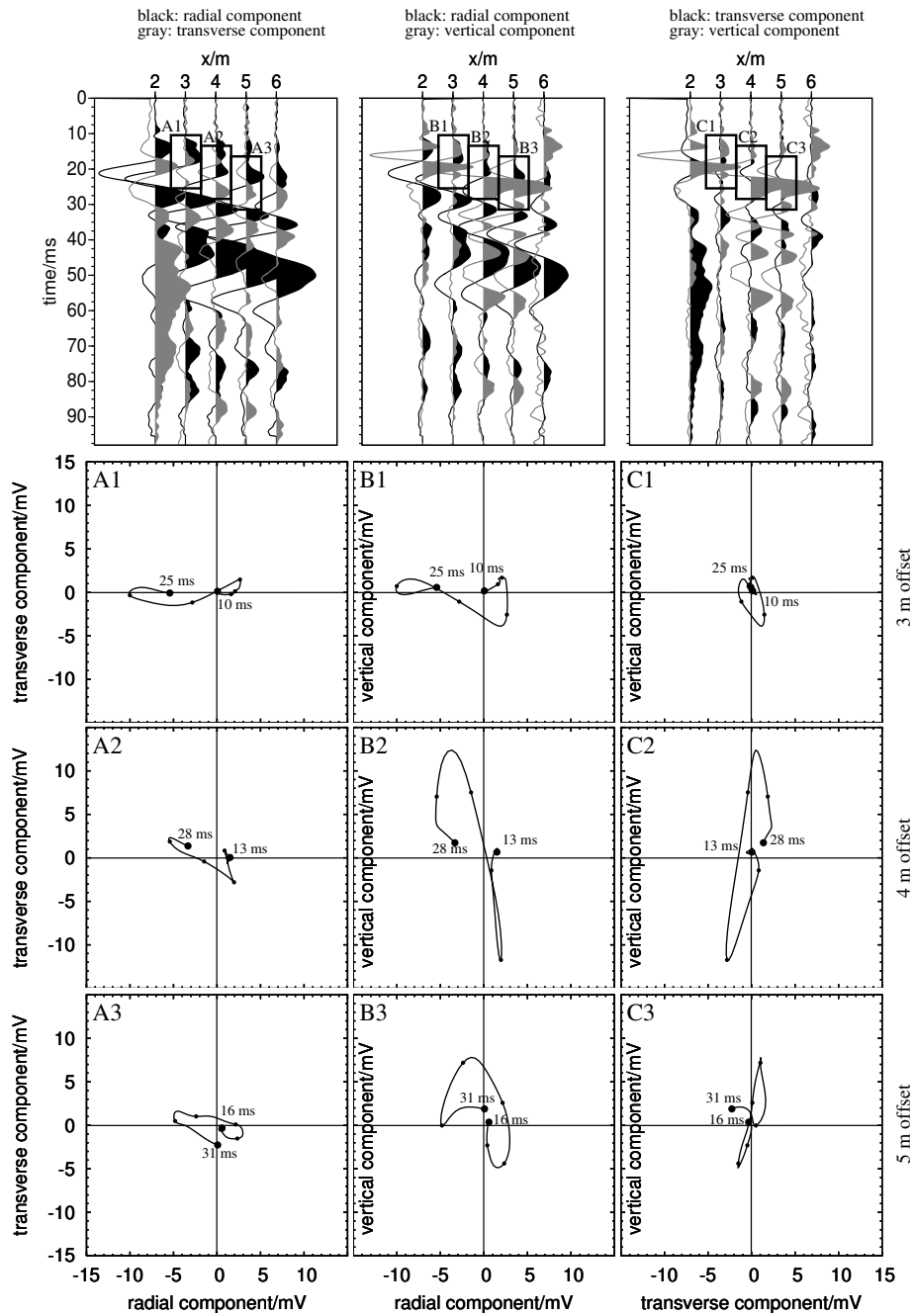


Figure 6.3: Hodogram comparison between radial, transverse, and vertical seismoelectric traces. In each of the three columns (A,B,C), two of the three components are analyzed. The two-component seismoelectrograms in the upper row enable a direct comparison between two of the three components of which one is displayed in black and one in gray.

signals to arrive (as has been argued in section 3). These measured values are compared to calculated ones in the third column (single interface), assuming a vertical electric dipole at the converting interface at a depth of 4 m and by taking into account the boundary conditions at the surface and the difference in the dipole lengths of the radial and the vertical components.

| offset/m | measured | calculated (single interface) | calculated (thin layer) |
|----------|----------|----------------------------------|----------------------------|
| 2 | 0.80 | -2.45 | -4.31 |
| 3 | 1.10 | 66.34 | 2.58 |
| 4 | 1.43 | 5.20 | 1.44 |
| 5 | 0.97 | 3.83 | 3.56 |
| 6 | 0.13 | 1.12 | 0.88 |

Table 6.1: Comparison of measured and calculated amplitude ratios of radial-to-vertical components of converted seismo-electric signals. Measured signals correspond to figure 6.2 (middle column) maximum amplitude within the time window of 6.5-14 ms. Apparently, the vertical component is much stronger than expected in my measured data when taking into account a single interface only. The calculated thin layer response (section 6.1.4) fits much better.

6.1.4 Thin layer approach

The comparison of columns 2 and 3 of Table 6.1.3 shows that the observed radial-to-vertical component ratios are significantly smaller than what would be expected for the response of a single interface. The result is not satisfactory even if I discard the measurements at 2 m and 6 m offset where signals are affected by the interference with the direct wave and some noise, respectively. The assumption of a single plane converting interface is probably too simple. Indeed, the gamma-ray log (Fig. 4.3) indicates that a thin layer of increased clay content is found at 4 m to 5 m depth, which is explained with a silt layer embedded in sand. Therefore we have to consider that the observed seismoelectric conversion signal is the superposition of two arrivals generated at the upper and lower interfaces of this silt layer. In order to model the resulting interference effect I apply the approach of Fourie (2003) assuming interface depths of 4 m and 5 m (see figure 6.4).

Furthermore, I assume that the electric dipole moment is proportional to the streaming current imbalance, so the amplitude of the converted signals from the upper and the lower boundaries of the thin silt layer should have opposite sign. Taking into account that the vertical dimensions of the thin layer are much smaller than the seismic wavelength at this depth (around 1 m against around 20 m, respectively), the phase difference between the seismoelectric arrivals from the upper and lower boundaries are minimal so the two converted fields should almost cancel out (Fourie, 2003), but not completely, since the two converting interfaces lie at different depths. Thus without any influence of the free surface on the electric fields I assume the two fields to be identical but with inverse polarity and 1 m vertically displaced relative to one another.

$$\Phi_4(x, z) \approx -\Phi_5(x, z + 1 \text{ m}) \quad (6.1)$$

with Φ_4 and Φ_5 being the electrical potentials of the seismoelectric fields converted at 4 m and 5 m depth, respectively. Assuming zero phase difference as an approximation, I calculate the contributions

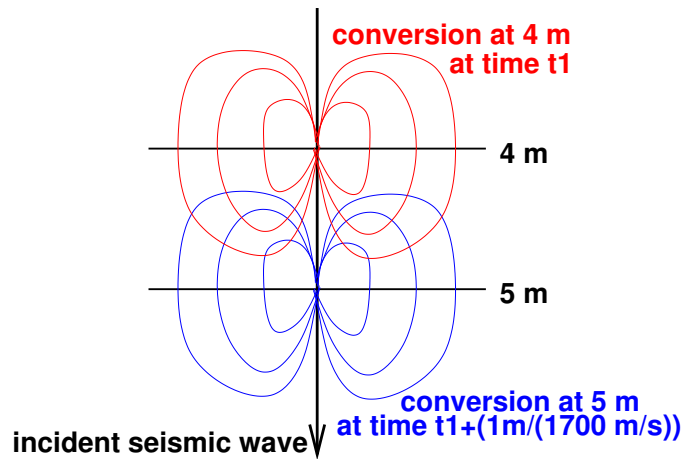


Figure 6.4: Incident seismic wave creating two seismoelectric conversions at 4 m depth and 5 m depth.

from the upper and lower boundaries and their sum for the radial and the vertical components. I make again use of the somewhat simplified approach of a vertical electrical dipole at the boundary layers in order to calculate the potentials of the seismoelectric converted field and taking into account the influence of the free surface. The results are shown in the right column of table 6.1.3 (thin layer). With the new approach, the calculated amplitude ratios of the radial to the vertical component get much closer to the measured amplitude ratios. The calculations are explained in section 6.2. The amplitudes resulting from destructive interference of the boundaries at 4 m and 5 m are weaker compared to the amplitudes I get assuming a boundary layer at 4 m only but still in the same order of magnitude. The absence of electromagnetic noise and the fact that the converting interface is very shallow are probably the reasons why this event is detectable after all. The approach of Fourie (2003) provides an estimate of the radial against vertical amplitudes rather than a precise modeling. However, more elaborate modeling based on realistic hydraulic and petrophysical parameters and the application of more sophisticated algorithms (such as Haartsen & Pride, 1997) are beyond the aims and scope of this work.

In addition, we observe in figure 6.2 that the transverse component shows small but coherent signals similar to the vertical component. This is surprising because theory predicts a radially symmetric signal structure for plane layered media. To investigate this phenomenon I compare a section of transverse records extending to larger offsets (figure 6.5a) with the fk velocity filtered radial section already discussed above (figure 6.5b, cf. figure 6.3, top right). Obviously, the first part of the transverse wavefield (10-30 ms) corresponds to the converted seismoelectric wavefield as indicated by lines in figure 6.5. A comparison of radial and transverse component shows no close correlation between both records except for the converted seismoelectrical signal (figure 6.2, top right vs. left, respectively, and figure 6.5). Hence I can exclude that the transverse signals are caused by misalignment of electrodes or cross-talk. As can be seen in figure 6.5b, there are also weaker events without moveout at later times. These are not converted seismoelectric signals but probably multiples, as their amplitudes do not fit the expected distribution.

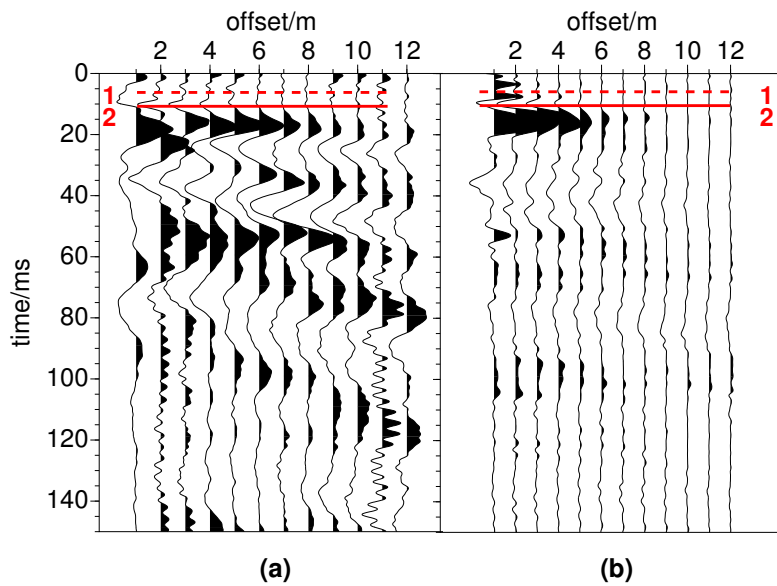


Figure 6.5: (Unscaled) seismoelectric surface data from the Fuhrberg site (February 2002). Left: transverse component data without any filtering. Expected arrival times are marked with lines as shown in figures 3.6 and 3.9. Right: radial component data after velocity filtering. Note the high similarity to the unfiltered transverse data (left).

6.1.5 Anisotropy

The presence of transverse seismoelectric energy could be a sign for 3D effects. If the converting horizon dips in the transverse direction, the converting zone will not lie on the profile line but laterally displaced in the transverse direction. Also the electric dipole radiating the converted seismoelectric wave will dip. In that case, the transverse component would not be a purely transverse one but contain a share of the radial component.

Unfortunately, I cannot check the dipping of the silt layer. This layer cannot be mapped with refraction seismics, as the seismic velocities of the saturated sand and silt layers are essentially the same.

The time windows of figure 6.3 cover the time range of the direct and refracted P-waves (cf. figure 3.2) appearing as coseismic signals on the seismoelectrograms. The energy of these arrivals is concentrated on the vertical and horizontal components. At 4 m and 5 m offset (figure 6.3, B2 and B3, respectively) polarization is sub-vertical corresponding to the incidence angle of the P-wave refracted at the groundwater table. At near offset (3 m, B1) the polarization is sub-horizontal, corresponding to interfering of direct and Rayleigh waves. In this time window, we observe the strongest arrivals on the vertical component.

6.1.6 Conclusions

While in the present case, the converted seismoelectric signals are quite clear on the vertical component, this strongly depends on the depth of the converting interface. Measurements at other locations yielded more problematic results for the vertical component and do in general not justify the amount of work and time required to measure the vertical seismoelectric component outside of a borehole. Chances for a possible filter based on polarization are also quite small, as the polarization of co-seismic and converted seismoelectric signals are essentially the same. Filters based on slowness or amplitude distribution are therefore more likely to succeed. In exceptional cases as the one presented here, collecting seismoelectric data on the transverse component may support the interpretation of the results from the radial component.

A hodogram analysis of two time windows in each of the three seismoelectric components revealed that the polarization mainly follows the theoretical predictions. The converted signals have their maximum signals on the vertical and radial components where they are quite clear. However, their amplitudes relative to one another can only be explained when taking into account a destructive interference of the converted signals originating from the layer boundaries at 4 m and 5 m depth. The lower boundary would have remained undetected without three-component measurements.

Moreover, the seismoelectric signals were also observed on the transverse component, with low amplitudes but clear and repeatable which cannot be explained when assuming plane layers. This can be regarded as an indication of the converting layer dipping in the transverse direction which unfortunately cannot be easily checked with refraction seismics as the saturated sand and silt layers have almost the same seismic velocity and thus do not cause refractions.

The field work involved with the vertical seismoelectric component is not to be neglected. Nonetheless, it could be shown that it is possible to record and get meaningful results on all three seismoelectric components in field which could be used for further and more extensive studies.

6.2 Calculation of seismoelectric potentials

For the verification of converted seismoelectric signals it is important to compare the measured seismoelectric amplitudes with the expected ones. Relative seismoelectric amplitudes can be calculated in a fairly simple way. As Garambois & Dietrich (2002) showed, the converted seismoelectric field can be approximated by the field of a vertical electric dipole at the converting interface. Skipping all dependencies except of the geometrical ones, I get for the electrical potential of a vertical electric dipole

$$V = \frac{p r \cos \theta}{4\pi\epsilon_0|r^3|} \propto \frac{\Delta z}{r^3} \quad (6.2)$$

with p being the electric dipole moment, r the total distance between the converting interface and the receiver, θ the angle from the vertical, ϵ_0 the permittivity of free space, and Δz the vertical distance between the converting interface and the receiver. It is well-known from geoelectrics that the boundary to a free surface has a strong impact on electrical potentials. Using an approach analogous to optics, the influence of the free surface can be thought of as a reflection (see, e.g., Telford et al.,

1990). We thus get

$$V \propto \frac{\Delta z_1}{r_1^3} + \frac{\Delta z_2}{r_2^3} = \frac{z - h}{\left[\sqrt{x^2 + (z - h)^2}\right]^3} + \frac{z + h}{\left[\sqrt{x^2 + (z + h)^2}\right]^3} \quad (6.3)$$

where index 1 refers to distances between the converting interface and the receiver and index 2 refers to the distance between the “mirrored image” of the converting interface and the receiver. The geometry is explained in figure 6.6.

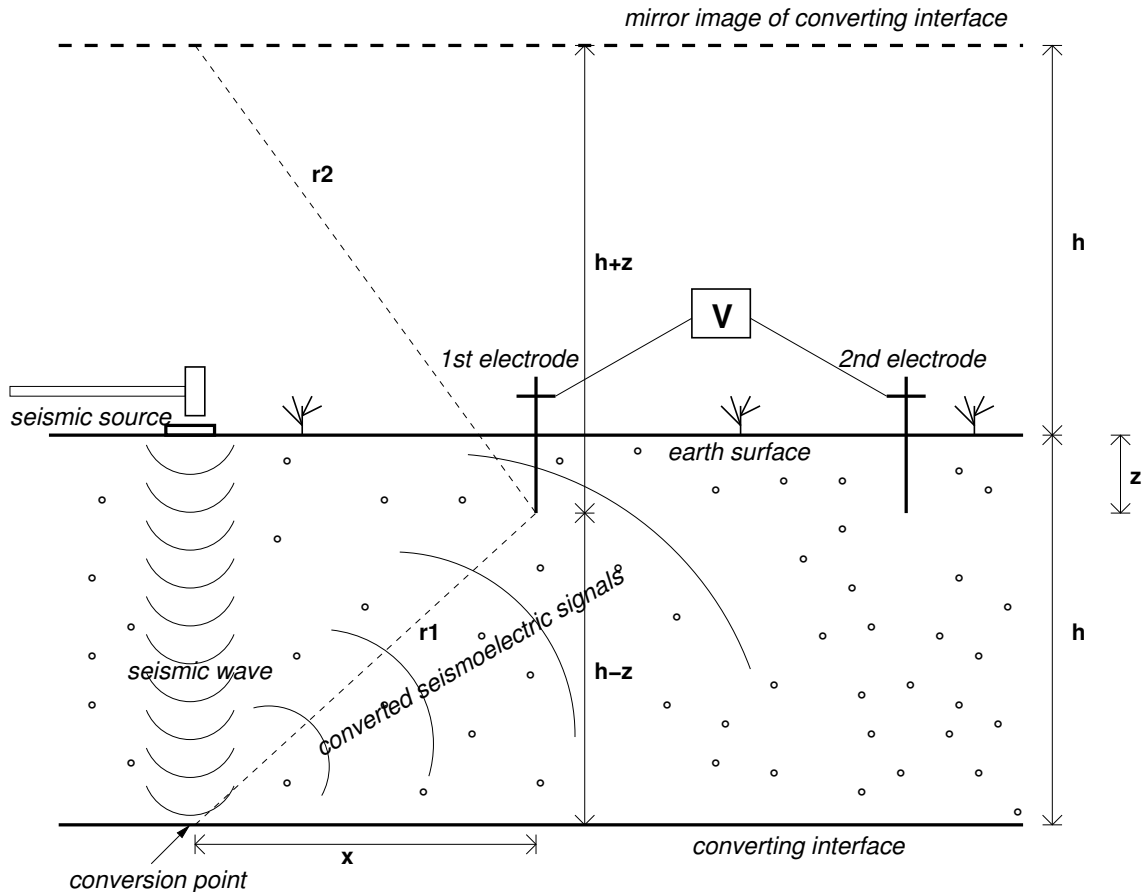


Figure 6.6: Schematic overview of the distances involved in the calculation of the potential of converted seismic signals as used in equation 6.3.

In the right hand side of the equation, I inserted the depth of the receiver z , the depth of the converting interface h , and the horizontal distance between the converting point and the receiver x which I assumed to be equal to the source-receiver offset. This approximation fails of course with dipping layers. The potential difference between the two electrodes of a dipole can thus be calculated using equation 6.3 by inserting the respective values for each of the two electrode positions and taking the difference between the potentials of the two electrodes. I can now easily compare the potential differences measured by a vertical and a horizontal electrode dipole. Figure 6.7 shows the results using the same geometry as in chapter 3 (converting horizon in 4 m depth, 2 m horizontal dipole

length, and 1.5 m vertical dipole length). The situation described in section 6.1, a possible destructive interference of the boundaries in 4 m and 5 m depth, is also included. It was calculated by using equation 6.3 for the two depths h_1 and h_2 at which the conversions take place

$$F_1 - F_2 = \left\{ \frac{z - h_1}{\left[\sqrt{x^2 + (z - h_1)^2} \right]^3} + \frac{z + h_1}{\left[\sqrt{x^2 + (z + h_1)^2} \right]^3} \right\} - \left\{ \frac{z - h_2}{\left[\sqrt{x^2 + (z - h_2)^2} \right]^3} + \frac{z + h_2}{\left[\sqrt{x^2 + (z + h_2)^2} \right]^3} \right\} \quad (6.4)$$

with F_n being the simplified converted field as calculated in equation 6.3. I calculate $F_1 - F_2$ because the converted fields of the two boundaries of a thin layer sandwiched between two identical layers have opposite sign. In the case described in section 6.1, I used equation 6.4 with $h_1 = 4 \text{ m}$ and $h_2 = 5 \text{ m}$.

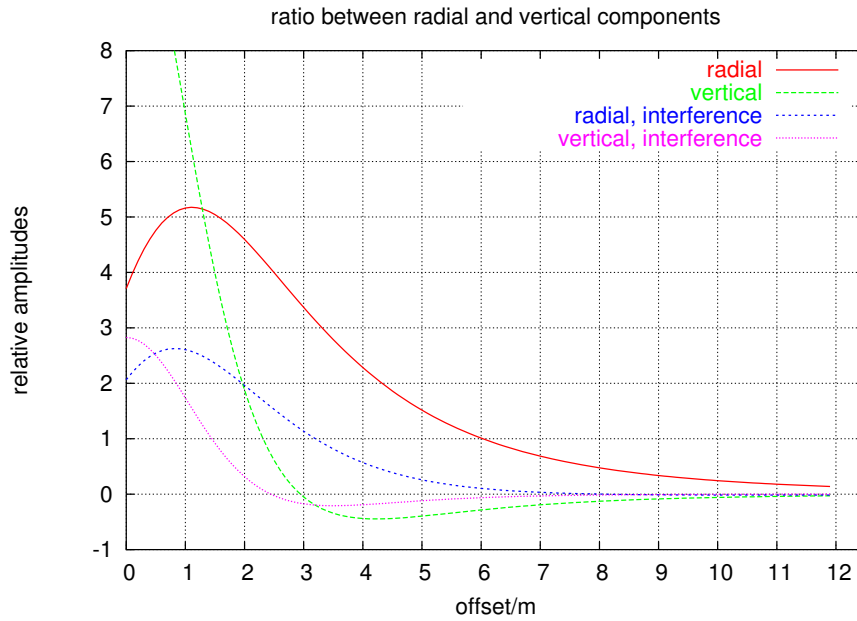


Figure 6.7: Comparison between calculated amplitudes of the seismoelectric converted field as they would be measured by a radial dipole of 2 m length and a vertical dipole of 1.5 m length. Curves are shown for a converting horizon in 4 m depth and also for destructive interference of a boundary in 4 m and in 5 m depth. The amplitudes are shown in relative units and were calculated with equations 6.3 and 6.4, respectively.

These calculations clarify that the vertical component of a converted seismoelectric field is weaker than the radial component but can be detected under favorable conditions. Supposing a destructive interference between the responses of two layers in 4 m and 5 m depth, the overall amplitudes decrease as well as the difference between the two components.

It stands out that the measured amplitudes for the vertical component (figure 6.1) do not show the polarity reversal between 2 m and 3 m offset. However, there is only one measured trace in that interval (at 2 m offset) and on that trace, the coseismic wave interferes very strongly with the converted seismoelectric signals so that it is possible that a potential phase reversal cannot be seen.

In figure 3.8 on page 56, I found that the measured amplitudes of the converted signals fit well to the calculated ones. The calculation was done without taking into account a destructive interference of the boundaries at 4 m and 5 m as explained in this section. Figure 6.8 depicts the comparison of the measured amplitudes with the calculated ones, this time taking into account the destructive interference. As can be seen, the agreement between measurement and calculation is still good, because I only compare relative amplitudes and not absolute values.

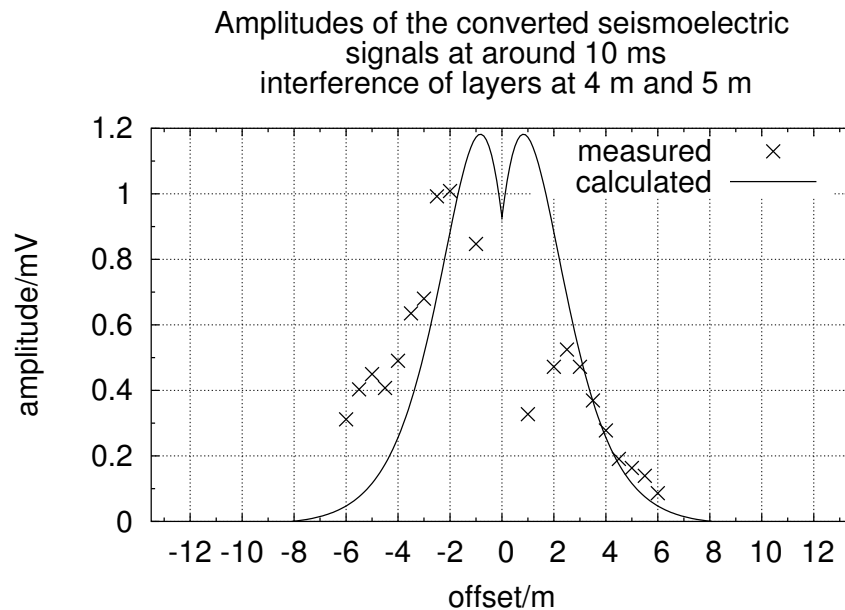


Figure 6.8: Comparison of measured amplitudes of converted seismoelectric signals and their theoretical correspondences (relative amplitudes) taking into account a destructive interference of the boundaries at 4 m and 5 m.

In this section I presented a simple approach to calculate the relative amplitudes of converted seismoelectric amplitudes which are needed in the seismoelectric checklist (section 3.4). I make use of the fact that the field of converted seismoelectric signals to a first approximation can be described by the field of a vertical electric dipole. With this approach, the expected relative seismoelectric amplitudes for the three-component data in the preceding section 6.1 could be calculated.

Chapter 7

Conclusions and outlook

7.1 Conclusions

In porous saturated media, seismic compressional waves can cause electric and electromagnetic signals via electrokinetic coupling which takes place at the electric double layer between rock matrix and pore space. These signals can be measured in form of a potential difference between two electrodes. Usually several of these dipoles are deployed in a profile line and connected to a seismograph where they are recorded. An increasing number of publications dealing with this so-called seismoelectric method has appeared, yet only little material on actual field measurements has been published so far. More seismoelectric field studies are needed if the potential of the method is to be realized.

There are two main seismoelectric wave types, the coseismic and the converted seismoelectric signals, respectively. The coseismic waves accompany seismic compressional waves in saturated porous media and the converted seismoelectric signals have their origin in the subsurface at interfaces separating layers of different elastic, electric or hydrological properties. Since the generation of seismoelectric signals is connected with pore space and pore geometry, a possible use of the method in hydrogeophysics is imaginable. The focus of this work is on establishing a solid ground for the measurements and not on actually deriving quantitative values from seismoelectric data. The potential application of the seismoelectric method critically depends on whether and under which circumstances seismoelectric signals can be measured.

Measurement components

Due to the generally low signal-to-noise ratio in seismoelectric field measurements, great care has to be taken with the selection and use of the field equipment. I studied a variety of different measurement components. Especially trigger noise can degrade the results severely. The comparison between seismoelectric traces recorded with manual trigger and with acceleration trigger revealed that the acceleration trigger can be considered mostly harmless for seismoelectric measurements.

A strong seismic source is desirable but it must not create electromagnetic noise, just as all other measurement components. Although rather weak, a standard sledgehammer proved to be usable in

most cases. We sometimes used the Sissy, a seismic impuls source working with compressed air cartridges, or an accelerated weight drop source which are much stronger sources but are also slower and more awkward to use. Regarding the length of the dipoles, the converted seismoelectric signals and the coseismic signals behave differently. Longer dipole lengths lead to stronger amplitudes of the converted seismoelectric signals but also average the results which is bad for an amplitude analysis. Furthermore, coherent electromagnetic noise increases linearly with dipole length. For the coseismic waves, dipole lengths do not seem to be that important. Too short dipole lengths should be avoided, though, because the data tend to be noisier then, perhaps due to electrochemical electrode noise. A length of 4 m usually is a good option for the described type of measurements whereas locations with strong electromagnetic noise should be addressed with shorter dipole lengths.

We make use of preamplifiers in seismoelectrics that also increase the input impedance to enhance the signal-to-noise ratio in the field. The main problem in seismoelectrics is anthropogenic noise. Suitable filter techniques do exist but residual noise causes problems, especially at urban sites. In order to correctly identify the seismoelectric signals and also for ground structure interpretation accompanying seismic measurements are needed. Seismic data may also play a role in future filter techniques to separate the seismoelectric wavefields.

We often record all three components in seismics as well as in seismoelectrics. For the seismoelectric vertical component this involves inserting long electrodes into the ground which we speeded up where necessary by using a type of percussion drill. To enlarge the number of recorded traces we frequently move the source while the dipoles stay fixed and sort the acquired traces by keyword. This technique usually leads to good results at locations with subhorizontal boundaries.

Data processing

Assumed converted seismoelectric signals can be enhanced with velocity filters in the frequency-wavenumber domain. I applied this technique to data from Fuhrberg Forest. The filter effectively weakened the unwanted coseismic waves. Checks guaranteed that the thus accentuated arrivals indeed are converted seismoelectric signals: From vertical seismoelectric profiling, I determined the arrival times of the compressional seismic wave at the known boundary layers. At these arrival times, the converted seismoelectric signals should be generated. The expected arrival times coincide well with the arrival times of the measured seismoelectric signals. The amplitude distribution of these seismoelectric signals was compared to the calculated amplitude distribution generated by a vertical electric dipole directly under the shot point at the converting interface, which is a good approximation to the real amplitudes of the converted seismoelectric field. Two of the three assumed converted seismoelectric events match the calculated amplitude distributions well. Furthermore, the events proved to be highly repeatable.

Different locations

So far no real repeated measurements at one or several sites are published in literature. Thus it is unknown how changing ground conditions, e.g. due to seasons or water saturation, influence the seismoelectric data. We visited some sites at different points in time to investigate into the repeatability and variability of seismoelectric signals.

- **Fuhrberg Forest/Lower Saxony**

Data from the two locations *clearing* and *waterworks* at Fuhrberg revealed that in general the data quality tends to be higher at the clearing site. The reason could be that the waterworks site is a forest location with soft ground and many tree roots degrading the seismic and seismoelectric signals. The two sites seem to be roughly equally remote without or with only very weak signs of anthropogenic electromagnetic noise in the seismoelectric data. The overall good quality data is repeatable.

- **Menzlin/Mecklenburg-Western Pomerania**

The seismoelectric data collected at the Menzlin location exhibits extraordinarily good signal quality without any traces of anthropogenic 50 Hz noise. This enabled the mapping of an interface previously determined with GPR and refraction seismics. Direct comparisons prove that it is the same interface that causes the GPR reflections, seismic refractions and seismoelectric conversions. The seismic velocities indicate that this boundary probably is the groundwater table. The repeatability is very high. At almost every shot point at least one arrival of converted seismoelectric signals could be registered.

The results obtained on two perpendicular profiles at the Menzlin site are comparable with the results at the intersection of the two profiles matching well. These measurements show that there are cases in realistic field work where subsurface boundaries can be detected with GPR and seismoelectrics, but not with refraction seismics. This proves that seismoelectrics could possibly be used for mapping such boundaries that do not possess a strong acoustic impedance contrast. Most converted signals were encountered in the mid parts of the profile where the dune is sandier. Towards the ends of the profiles, earthy soil dominates.

- **Selinunte/Sicily**

Data from two sites at Selinunte reveal the importance of electric conductivity. A profile on very conductive alluvial soil yielded no sensible seismoelectric signals at all while data from a very dry sand dune gave quite good results. These latter findings were rather unexpected because saturated media are traditionally required to generate seismoelectric signals.

- **Segeberg Forest/Schleswig-Holstein**

At the Segeberg Forest site, seismoelectric measurements were conducted in the borehole as well as at the surface at several repeated dates. There are no big differences between the different seismoelectric borehole recordings despite the use of different sources, boreholes, and dipole lengths. The overall data quality is high, as well as the repeatability.

The seismoelectric surface measurements show much stronger variations. The positions of the receivers do not seem to play a major role because the same receivers show very different data qualities depending on other measurement parameters such as source or source positions. It is plain to see that the accelerated weight drops produce much better data than hammer blows and that there is significant spatial and temporal variability in the data.

Interestingly there is no correlation between seismoelectric and seismic data quality. Seismoelectric data seem to vary much stronger depending on ground conditions.

I did not succeed in measuring any converted seismoelectric events at the Segeberg Forest location. Reasons are for sure the measurement and noise conditions which resulted in quite variable data quality. The other reason could be that there simply are no boundaries in a reachable depth which could generate strong seismoelectric conversions. The VSP data do not reveal any reflections, either.

- **GeoModel/University Campus**

The examples from the GeoModel and from the sand pit in front of the GeoModel show that urban sites with strong electromagnetic noise are problematic for seismoelectric measurements. Even after applying several runs of a sinusoid filter to remove the coherent noise and using a stronger source the results are far from satisfactory. It is impossible to detect any converted seismoelectric signals. These would mix with the remnants of the 50 Hz anthropogenic noise. The coseismic waves can easily be identified but they do not show any changes in amplitude relative to the seismic data at the sand pit. The pit would have gone undetected if its detection and characterization had been the aim of the seismoelectric measurements. Probably, the parameter contrasts between the sand pit and the surrounding material were not strong enough although the resistivity contrast is obvious in the inverted resistivity model. It seems that bulk resistivity contrasts are not that important for seismoelectric signals.

- **Unified interpretation**

The parameter electrical resistivity is somewhat ambiguous. Grounds with good coupling (e.g. moist ground) and therefore higher seismoelectric amplitudes often have low resistivities, which in turn should lead to lower seismoelectric amplitudes and vice versa.

The role of the electrode coupling is not sure either. In some areas we had very good coupling but bad results (GeoModel, some positions in Segeberg Forest). Some newer data not shown in this thesis have rather bad coupling but excellent results.

The measurements in the Segeberg Forest suggest that the hardness of the ground plays an important role. Soft ground results in stronger seismic attenuation which also results in weaker seismoelectric signals. Interestingly this seems to be more important for the seismoelectric than for the seismic data. The seismic quality does not always correlate with seismoelectric data quality.

Given the low seismoelectric amplitudes, a low electromagnetic noise level is of great importance. In principle, there are good data processing techniques to strip the records of anthropogenic 50 Hz noise. In practice, however, residual noise often remains. Because this noise consists of electromagnetic fields, it might be difficult to distinguish from possible converted seismoelectric events which have electromagnetic velocities, too. Converted signals could only be detected where the data quality was very good. Sometimes a stronger source seems to be the only solution.

It could be expected that the chance of measuring converted seismoelectric signals should be higher in highly resistive ground than in low-resistive environments. But since we expect skin depths of several hundred meters the attenuation of the converted seismoelectric signals can be neglected in most media for near surface applications.

Summed up one can conclude that there is a strong correlation between the overall seismoelectric data quality and seismic data quality. It is equally important that the location is free from strong anthropogenic noise. Moderate correlation can be figured out with the hardness of the ground while there does not seem to be any strong connection with shallow resistivities or electrode coupling.

Generally positive in connection with seismoelectric measurements seem to be: sandy ground (preferably dry rather than wet), low electromagnetic noise level, and clear subsurface boundaries. Data in open field seem to be better than in forested areas. Forest ground is usually penetrated by a lot of tree roots which can act as diffractors and are responsible for a low seismic quality factor Q . This affects naturally also the seismoelectric signals. As explained in section 4.8, the low pH values commonly

found especially in coniferous forests also lower seismoelectric amplitudes. Irrespective of ideal measurement conditions and equipment, a clear boundary at which converted seismoelectric signals can be generated is of course a prerequisite.

Towards quantitative seismoelectrics

In order to study the dependence of seismoelectric signals on electrical resistivity, I compare VSP (vertical seismic profiling) and VSEP (vertical seismoelectric profiling) measurements with borehole geoelectrics at the location Segeberg Forest. There is a strong dependence of the seismoelectric amplitude (normalized with respect to the seismic amplitudes) on pH. The results were confirmed by two independent measurements with different dipole lengths. Apart from that, I discovered that the normalized seismoelectric amplitudes are not or only very weakly dependent on dipole length which has been reported ambiguously in literature up to now.

The results are interesting because it is not the electrical resistivity that has the strongest impact on the seismoelectric signals but the pH value via the ζ -potential. This outcome is somewhat problematic because it does not seem to be possible to determine resistivity with seismoelectrics. pH is a parameter which is hard to determine with any method but has strong implications on the seismoelectric amplitude thus severely limiting the area of application. The pH-value has to be constant or known if the method is to be used for other applications. This dependence in turn means that it should in principle be possible to determine the pH value with seismoelectrics which is not accessible with other geophysical methods. The strong dependence on the ζ -potential offers new possibilities of identifying layer boundaries which might be insensitive to other methods. This analysis shows how important comparative seismoelectric field studies are. Until now, this strong impact of the pH value on seismoelectric amplitudes has not been reported in literature.

Polarization analysis

I studied three-component seismoelectric data and analyzed their polarization. The converted seismoelectric signals are quite clear on the vertical component (Fuhrberg Forest data) but this strongly depends on the depth of the converting interface. Measurements at other locations yielded more problematic results for the vertical component and do in general not justify the amount of work and time required to measure the vertical seismoelectric component outside of a borehole. In exceptional cases as the one presented here, collecting seismoelectric data on the transverse component may support the interpretation of the results from the radial component.

A hodogram analysis of two time windows in each of the three seismoelectric components revealed that the polarization mainly follows the theoretical predictions. The converted signals have their maximum signals on the vertical and radial components where they are quite clear. However, their amplitudes relative to one another can only be explained when taking into account a destructive interference of the converted signals originating from the layer boundaries at 4 m and 5 m depth. The lower boundary would have remained undetected without three-component measurements.

Moreover, the seismoelectric signals were also observed on the transverse component, with low amplitudes but clear and repeatable which cannot be explained when assuming plane layers. I therefore

regard this as an indication of the converting layer dipping in the transverse direction.

7.2 Outlook

Although a lot of progress was made in the domain of seismoelectric field measurements, problems remain. Despite all improvements the data quality is often suboptimal, especially in areas where anthropogenic 50 Hz noise is strong. Filter techniques removed most of the electromagnetic signals and improved the signal-to-noise ratio several orders of magnitude but still residual noise degrades the seismoelectric traces. Even at many sites without coherent electromagnetic noise I was not able to detect any converted seismoelectric signals. So far the measurements take a lot of time compared to other methods but improvements in the cabling are on the way. This will lead to a reduced amount of time necessary to connect all the cables, electrodes, and preamps involved in a seismoelectric layout.

Much work still remains to improve the seismoelectric method to such a degree that it could be considered a routine method. As to seismoelectric field technique, there is also still room for improvements. Especially the location GeoModel shows how important a strong source is when having to deal with weak signals of interest and strong noise. Parallel to this direct violent method, more effort could also be directed towards even better noise reduction algorithms, although these will only help in the case of coherent noise. Also the time needed for the setup of a seismoelectric profile can still be shortened. It is tempting to replace the electrodes with an electrode streamer or electrodes mounted on a wheel as used in e.g. agro-geophysics. Improving only field measurements, however, will not lead very far. Eventually modeling has to be merged with field measurements, preferably multi-method measurements if the seismoelectric method one day is supposed to yield quantitative values. As the rather unanticipated role of the pH value for seismoelectric amplitudes shows, there are still many surprises to be expected in seismoelectric field experiments.

Bibliography

- Adam, E., and Langlois, P., 1995. Elimination of Monofrequency Noise from Seismic Records, *Litho-probe Seismic Processing Facility Newsletter*, **8** (1), 59-65.
- Archie, G.E., 1942. The electrical resistivity log as an aid in determining some reservoir characteristics, *Transactions of the American Institute of Mining Engineers*, **146**, 54-62.
- Beamish, D., 1999. Characteristics of near-surface electrokinetic coupling, *Geophysical Journal International*, **137**, 231-242.
- Beamish, D., and Peart, R. J., 1998. Elektrokinetic geophysics - a review, *Terra Nova*, **10** (1), 48-55.
- Biot, M.A., 1956. Theory of propagation of elastic waves in a fluid saturated porous solid, I and II, *Journal of the Acoustical Society of America*, **28**, 168-191.
- Biot, M.A., 1962. Mechanics of deformation and acoustic propagation of elastic waves in a fluid-saturated porous solid: I - Low-frequency range, *Journal of the Acoustical Society of America*, **33**, 1482-1498.
- Block, G.I., and Harris, J.G., 2006. Conductivity dependence of seismoelectric wave phenomena in fluid-saturated sediments, *Journal of Geophysical Research*, **111**, B01304, doi:10.1029/2005JB003798, 2006.
- Bordes, C., Jouniaux, L., Dietrich, M., Pozzi, J.-P., and Garambois, S., 2006. First laboratory measurements of seismo-magnetic conversions in fluid-filled Fontainebleau sand, *Geophysical Research Letters*, **33**, L01302, doi:10.1029/2005GL024582.
- Butler, K.E., and Russel, R.D., 1993. Shortnote: Subtraction of powerline harmonics from geophysical records, *Geophysics*, **58** (6) , 898-903.
- Butler, K.E., Russell, R.D., Kepic, A.W., and Maxwell, M., 1996. Measurement of the seismoelectric response from a shallow boundary, *Geophysics*, **61** (6) , 1769-1778.
- Butler, K.E., and Russell, R.D., 2003. Cancellation of Multiple Harmonic Noise Series in Geophysical Records, *Geophysics*, **68** (3), 1083-1090.
- Claerbout, J.F., and Muir, F., 1973. Robust modeling with erratic data, *Geophysics*, **38**, 826-844.
- Dvorkin, J., Nolen-Hoeksema, R., and Nur, A., 1994. The squirt-flow mechanism: Macroscopic description, *Geophysics*, **59**, No. 3 428-438.
- Fourie, F.D., 2003. Application of electroseismic techniques to geohydrological investigations in Karoo rocks, PhD thesis, Department of Geohydrology, University of the Free State, Bloemfontein, South Africa.

- Friberg, J., 1996. Experimental and Theoretical Investigations into the Streaming Potential Phenomenon with Special Reference to Applications in Glaciated Terrain, PhD thesis, Division of Applied Geophysics, Luleå Tekniska Universitet, Luleå, Sweden.
- Gal'perin, E.I., 1984. The polarization method of seismic exploration, *D. Reidel Publ. Co.*, Dordrecht, The Netherlands.
- Garambois, S., and Dietrich, M., 2001. Seismoelectric wave conversion in porous media: Field measurements and transfer function analysis, *Geophysics*, **66** (5), 1417-1430.
- Garambois, S., and Dietrich, M., 2002. Full waveform numerical simulations of seismoelectromagnetic wave conversions in fluid-saturated stratified porous media, *Journal of Geophysical Research*, **107** (B7), 2148, doi:10.1029/2001JB000316.
- Haartsen, M.W., and Pride, S.R., 1997. Electro seismic waves from point sources in layered media, *Journal of Geophysical Research*, **102** (B11), 745-769.
- Haartsen, M.W., Dong, W., and Toksöz, M.N., 1998. Dynamic streaming currents from seismic point sources in homogeneous poroelastic media, *Geophysical Journal International*, **132**, 256-274.
- Hagrey, S.A. al, Rabbel, W., Meissner, R., and Werban, U., 2003. The "GeoModel" at Kiel - A hydrogeophysical full scale model for Engineering Geology to study pore water, contamination and structure of soils, *Proceedings, Meeting, Engineering Geology*, 26-29/03/2003, Kiel, Germany, 361-362.
- Haines, S.S., 2004. Seismoelectric imaging of shallow targets. PhD thesis, Department of Geophysics, Stanford University, Stanford, California, USA.
- Han, Q., and Wang, Z.Z., 2001. Time-domain simulation of SH-wave-induced electromagnetic field in heterogeneous porous media: A fast finite-element algorithm, *Geophysics*, **66** (2), 488-461.
- Ishido, T., and Mizutani, H., 1981. Experimental and theoretical basis of electrokinetic phenomena in rock-water systems and its application to geophysics, *Journal of Geophysical Research*, **86**, 1763-1775.
- Ivanov, A., 1939. Effect of electrization of earth layers by elastic waves passing through them, *Compts Rendus (Doklady) de l'Académie des Sciences de l'USSR*, **24**, 42-25.
- Kepic, A., and Rosid, M., 2004. Enhancing the seismoelectric method via a virtual shot gather, *SEG Technical Program Expanded Abstracts*, 1337-1340.
- Khatiashvili, N. G., and Perel'man, M. E., 1989. On the Mechanism of Seismo-Electromagnetic Phenomena and Possible Role in the Electromagnetic Radiation during Periods of Earthquakes, Foreshocks and Aftershocks, *Physics of the Earth and Planetary Interiors*, **57** (1), 169-177.
- Kirsch, R., (editor), 2006. Groundwater geophysics, *Springer press*, Berlin Heidelberg.
- Loke, M.H., and Barker, R.D., 1996. Rapid least-squares inversion of apparent resistivity pseudosections by a quasi-Newton method. *Geophysical Prospecting*, **44** (1), 131-152.
- Martner, S.T., and Sparks, N.R., 1959. The electro seismic effect, *Geophysics*, **24**, 297-308.

- Matthess, G., 1980. Untersuchungen der Lebensdauer von Bakterien und Viren im Grundwasser in Hinblick auf die Ausweisung von Schutzgebieten für die Grundwasseranlagen. Research report for the Federal Environment Agency (Umweltbundesamt), Wasser "102 02 202", Part A, Institute of Geology and Paleontology, Christian-Albrechts-University Kiel.
- Maxwell, M., Russell, R.D., Kepic, A.W., and Butler, K.E., 1992. Electromagnetic responses from seismically excited targets / non-piezo-electric phenomena, *Exploration Geophysics*, **23**, 201-208.
- Meyer, J.H., 1989. Darstellung und Verarbeitung vektorieller seismischer Wellenfelder am Beispiel von in-situ Untersuchungen von Kompressions- und Scherwellen in Holozän-Torfen, PhD thesis, Institute of Geophysics, Christian-Albrechts-University Kiel.
- Mikhailov, O.V., Haartsen, M.W., and Toksöz, M.N., 1997. Electro seismic investigation of the shallow subsurface: Field measurements and numerical modeling, *Geophysics*, **62** (1), 97-105.
- Mikhailov, O.V., Queen, J., and Toksöz, M.N., 2000. Using borehole electro seismic measurements to detect and characterize fractured (permeable) zones, *Geophysics*, **65** (4), 1098-1112.
- Ohse, W., 1983. Lösungs- und Fällungserscheinungen im System oberflächennahes unterirdisches Wasser/gesteinsbildende Minerale - Eine Untersuchung auf der Grundlage der chemischen Gleichgewichts-Thermodynamik. PhD thesis, Institute of Geology and Paleontology, Christian-Albrechts-University Kiel.
- Parkhomenko, E.I., and Gaskarov, I.V., 1971. Borehole and laboratory studies of the seismoelectric effect of the second kind in rocks, *Izvestiya Academy of Sciences, USSR, Physics of the Solid Earth*, **9**, 663-666.
- Petersen, H., Strahser, M., Werban, U., Iwanowski, K., and Rabbel, W., 2004. BGR-Abschlussbericht 201-4500010359 (internal report), Federal Institute for Geosciences and Natural Resources (Bundesanstalt für Geowissenschaften und Rohstoffe).
- Pride, S.R., and Morgan, F.D., 1991. Electrokinetic dissipation induced by seismic waves, *Geophysics*, **56** (7), 914-925.
- Pride, S.R., 1994. Governing equations for the coupled electromagnetics and acoustics of porous media, *Physical Review B, Condensed Matter and Material Physics*, **50**, 15678-15696.
- Pride, S.R., and Haartsen, M.W., 1996. Electro seismic wave properties, *Acoustic Society of America*, **100** (3) , 1301-1315.
- Pride, S. R., Moreau, F., and Gavrilenko, P., 2004. Mechanical and electrical response due to fluid-pressure equilibration following an earthquake, *Journal of Geophysical Research*, **109**, B03302, doi:10.1029/2003JB002690.
- Shaw, A.R., 2005. The seismo-electric method and its sensitivity to subsurface contrasts, PhD thesis, Technische Universiteit Delft, The Netherlands.
- Rosid, M., and Kepic, A., 2004. Hydrogeological mapping using the seismoelectric method, *Extended Abstract in ASEG 17th Geophysical Conference and Exhibition*, Sydney.
- Salem, H.S., 1990. A theoretical and practical study of petrophysical, electric and elastic parameters of sediments, PhD thesis, Institute of Geophysics, Christian-Albrechts-University Kiel.

- Santamarina, J.C., and Fratta, D.O., 2003. Dynamic electrical-mechanical energy coupling in electrolyte-mineral systems, *Transport in Porous Media*, **50**, 153-178.
- Schroeter, J., 1983. Der Einfluss von Textur- und Struktureigenschaften poröser Medien auf die Dispersivität, PhD thesis, Institute of Geology and Paleontology, Christian-Albrechts-University Kiel.
- Strahser, M., 2002. Methodische Untersuchungen zu Akquisition, Prozessing und Interpretation seismo-elektrischer Daten für die Grundwasserexploration, diploma thesis, Institute of Geosciences, Christian-Albrechts-University Kiel.
- Strahser, M., Rabbel, W., and Schildknecht, F., 2006. Polarization and slowness of seismoelectric signals - a case study, *Near Surface Geophysics*, in press.
- Telford, W.M., Geldart, L.P., and Sheriff, R.E., 1990. Applied Geophysics, Cambridge University Press.
- Thompson, R.R., 1936. The seismic electric effect, *Geophysics*, **1**, 327-335.
- Thompson, A.H., and Gist, G.A., 1993. Geophysical applications of electrokinetic conversion, *The Leading Edge*, **12**, 1169-1173.
- Thompson, A.H., Hornbostel, S., Burns, J., Murray, T., Raschke, R., Wride, J., McCammon, P., Sumner, J., Haake, G., Bixby, M., Ross, W., White, B., Zhou, M., and Peczak, P., 2005. Field tests of electroseismic hydrocarbon detection, *SEG Technical Program Expanded Abstracts*, 565-568.
- White, B.S., 2005. Asymptotic theory of electroseismic prospecting, *SIAM Journal on Applied Mathematics* **65** (4), 1443-1462.
- Wiederhold, H., Bunness, H. A., and Bram, K., 1998. Glacial structures in northern Germany revealed by a high-resolution reflection seismic survey, *Geophysics*, **63** (4), 1265-1272.
- Wolfe, P.J., Yu, J., and Gershenzon, N., 1996. Seismoelectric studies in an outwash plain, *Proceedings of the Symposium on the application of geophysics to engineering and environmental problems (SAGEEP)*, Environmental and Engineering Geophysical Society, Colorado.
- Woodward, D.J., 1991. Inversion of seismic refraction data. *Geophysics Division Technical Report No. 114*, DSIR Geology and Geophysics, Lower Hutt, New Zealand.
- Zhu, Z., and Toksöz, M.N., 2003. Crosshole seismoelectric measurements in borehole models with fractures, *Geophysics*, **68** (5), 1519-1524.
- Zhu, Z., and Toksöz, M.N., 2005. Seismoelectric and seismomagnetic measurements in fractured borehole models, *Geophysics*, **70**, 45-51.

List of Figures

| | | |
|------|--|----|
| 1.1 | The two seismoelectric wave types | 7 |
| 1.2 | The electric double layer and the ζ potential | 8 |
| 1.3 | Sensitivity analysis of seismoelectric and seismomagnetic signal amplitudes | 13 |
| 2.1 | Field setup for seismoelectric measurements | 18 |
| 2.2 | Hammer impact on seismoelectric traces | 19 |
| 2.3 | The seismic source <i>Sissy</i> | 20 |
| 2.4 | Comparison between seismoelectric traces measured with sledgehammer and <i>Sissy</i> | 21 |
| 2.5 | The accelerated weight drop source | 23 |
| 2.6 | The wooden ground plate | 25 |
| 2.7 | The accelerator trigger | 25 |
| 2.8 | Seismoelectric traces with different ground plates and trigger mechanisms | 27 |
| 2.9 | Example of strong trigger noise | 28 |
| 2.10 | Seismoelectric data with different ground plates and trigger mechanisms | 29 |
| 2.11 | Seismoelectric data with different ground plates and trigger mechanisms | 30 |
| 2.12 | Comparison between acceleration trigger and manual trigger | 32 |
| 2.13 | Influence of different dipole lengths on seismoelectric data | 34 |
| 2.14 | Configuration for the recording of the vertical seismoelectric component | 39 |
| 2.15 | Spatial orientation of the radial, transverse and vertical dipoles | 40 |
| 2.16 | The Percussion drill “Wacker” | 41 |
| 2.17 | Schematic representation of the technique of the moving source | 42 |
| 2.18 | Assumed converted seismoelectric events in VSEP data | 44 |
| 3.1 | Results from seismic refraction analysis at the Fuhrberg Forest site | 47 |
| 3.2 | Seismic vertical component and seismoelectric radial component data, Fuhrberg | 48 |
| 3.3 | Vertical seismoelectric and seismic profiles at the Fuhrberg site | 49 |
| 3.4 | Seismoelectric data before and after velocity filter in the fk domain | 51 |
| 3.5 | Comparison between velocity-filtered seismoelectric and seismic data | 52 |
| 3.6 | Simplified seismoelectric processing flow | 53 |
| 3.7 | Extraction and amplitude analysis of converted seismoelectric signals | 55 |
| 3.8 | Measured and calculated amplitudes of converted seismoelectric signals | 56 |
| 3.9 | Repeatability of converted seismoelectric signals | 58 |
| 4.1 | Locations of the seismoelectric measurements | 62 |
| 4.2 | Location of the two measurement sites in the Fuhrberg Forest | 66 |
| 4.3 | Geological profile and borehole logs from the clearing site (Fuhrberg Forest) | 67 |
| 4.4 | Surface geoelectric profile from the Fuhrberg clearing site | 68 |
| 4.5 | Examples of quite bad data from the Fuhrberg Forest site | 69 |
| 4.6 | Geological profile and borehole logs from the waterworks site (Fuhrberg Forest) | 70 |

| | | |
|------|---|-----|
| 4.7 | Examples from the Fuhrberg waterworks site | 72 |
| 4.8 | The measurement area Menzlin | 74 |
| 4.9 | Overview of the different methods and their positions used at the Menzlin site | 74 |
| 4.10 | Position of the two perpendicular profiles in a 3D view | 75 |
| 4.11 | GPR data collected along the fall profile in Menzlin | 75 |
| 4.12 | Results of the refraction seismic analysis from the fall and the strike profile | 76 |
| 4.13 | Example of seismoelectric and seismic data at the Menzlin site | 77 |
| 4.14 | Seismoelectrograms and calculated amplitudes from the Menzlin fall profile | 79 |
| 4.15 | Seismoelectrograms and amplitudes (converted signals) from the Menzlin strike profile | 80 |
| 4.16 | The Menzlin strike profile with topography and the determined boundary layer | 81 |
| 4.17 | The Menzlin fall profile with topography and the determined boundary layer | 82 |
| 4.18 | GPR data from the fall profile at the Menzlin site | 82 |
| 4.19 | GPR data from the fall profile at the Menzlin site with refraction seismic results | 83 |
| 4.20 | Seismoelectric and seismic data from Selinunte/Sicily (sand dune profile) | 85 |
| 4.21 | Surface geoelectric pseudosection and model from the dune profile at Selinunte/Sicily | 86 |
| 4.22 | Map of the measurement area Segeberg Forest | 88 |
| 4.23 | Geological profile of the measurement area Segeberg Forest | 89 |
| 4.24 | Location of the thirteen boreholes and the profiles at the Segeberg Forest site | 90 |
| 4.25 | Surface geoelectric profile (Wenner- α) at the Segeberg site | 91 |
| 4.26 | Repeated seismoelectric and seismic borehole measurements (Segeberg Forest) | 93 |
| 4.27 | Comparison of seismoelectric surface data (November 2005) from near borehole 12 | 96 |
| 4.28 | Comparison of seismoelectric surface data from the Segeberg Forest (December 2005) | 97 |
| 4.29 | Seismoelectric surface data from near borehole 2 (Segeberg Forest, January 2006) | 98 |
| 4.30 | Seismoelectric surface data from near borehole 3 (Segeberg Forest, February 2006) | 99 |
| 4.31 | Seismoelectric sections from 11/05, 12/05, 01/06 and 02/06 (Segeberg Forest) | 100 |
| 4.32 | Seismic sections from 11/05, 12/05, 01/06 and 02/06 (Segeberg Forest) | 101 |
| 4.33 | Design of the GeoModel | 104 |
| 4.34 | The GeoModel and the seismoelectric profile across the sand pit | 105 |
| 4.35 | (a) The control box at the GeoModel, (b) Anthropogenic noise at the GeoModel | 105 |
| 4.36 | Two configurations and the corresponding shot records from the GeoModel | 106 |
| 4.37 | Location of the GeoModel, the sand basin and the sand pit | 107 |
| 4.38 | Seismoelectric and seismic data from the profile across the sand pit (GeoModel) | 108 |
| 4.39 | Seismoelectric amplitudes relative to seismic amplitudes (sand pit, GeoModel) | 110 |
| 4.40 | 2D geoelectric results in front of the GeoModel | 111 |
| | | |
| 5.1 | Dependence of the ζ potential on pH | 120 |
| 5.2 | VSP, VSEP, resistivity, pH, and porosity at the Segeberg Forst site | 122 |
| 5.3 | Seismoelectric amplitudes against resistivities, pH, and porosities | 124 |
| 5.4 | Seismoelectric amplitudes against pH*porosities | 125 |
| | | |
| 6.1 | Example of three-component seismoelectric data from the Fuhrberg site | 129 |
| 6.2 | Hodogram comparison between the 3 seismoelectric components: converted signals | 130 |
| 6.3 | Hodogram comparison between the 3 seismoelectric traces: coseismic waves | 131 |
| 6.4 | Incident seismic wave creating two seismoelectric conversions at 4 m and 5 m depth | 133 |
| 6.5 | Seismoelectric velocity-filtered radial component and unfiltered transverse component | 134 |
| 6.6 | Distances in the calculation of the potential of converted seismoelectric signals | 136 |
| 6.7 | Calculated amplitudes of the seismoelectric converted field | 137 |
| 6.8 | Measured and calculated amplitudes of converted seismoelectric signals | 138 |

List of Tables

| | | |
|-----|---|-----|
| 4.1 | Seismoelectric field measurements in literature | 61 |
| 4.2 | Locations where seismoelectric measurements were made | 63 |
| 4.3 | Configurations of the VSEP measurements at the Segeberg Forest site | 92 |
| 4.4 | Configurations of the seismoelectric measurements at the Segeberg Forest site | 99 |
| 4.5 | The measurement areas and their relevant parameters | 114 |
| 4.6 | The measurement areas and their relevant parameters - short form | 115 |
| 6.1 | Measured and calculated amplitudes of the converted seismoelectric signals | 132 |

Acknowledgements

I always enjoyed the field measurements in spite of the deprivation of sleep this usually meant. One actually can enjoy swinging a heavy hammer and connecting cables all day even at 0°C, rain, and without seeing meaningful results on the small dark Bison seismograph screen. This was only possible thanks to all the people helping in the field.

I acknowledge this help by writing “we” in the thesis whenever I speak of how fieldwork was conducted. Since I did the processing and interpretation alone (except when indicated otherwise), I use the first person pronoun “I” elsewhere.

I especially thank...

My supervisor Prof. Dr. W. Rabbel: For competent advice, pleasant atmosphere and for always finding a path out of the dark, be it scientific or organizational darkness. Thanks for always somehow finding time to discuss new results or ideas.

Prof. Dr. T. Bohlen: For accepting to be the second examiner.

BGR (Federal Institute for Geosciences and Natural Resources), DFG and Schleswig-Holstein: For funding parts this work (BGR 2-1003118, 201-4500010359,204-4500029527 and Ra 496/19-1).

Dr. S. Attia al-Hagrey: For lots of helpful information concerning geoelectrics and the GeoModel.

R. Becker: Without the institute cars, almost no measurement would have been possible. Thanks also for implementing even the weirdest tools and equipment and for the patience of repairing stuff over and over again.

Dr. E. Bedbur: For lots of help and information about the Segeberger Forst, for spreading good atmosphere and funny comic strips on your office walls.

Dr. T. Beilecke: For lots of helps in the beginning of the seismoelectric project from which I also took your seismoelectric literature review table.

Dr. F. Bilgili and N. Dinç-Akdoğan: For having the patience of explaining me the same turkish vocabulary over and over again. Teşekkür ederim!

H. Bresa and his crew: Thanks for the realization of many weird equipment wishes (“Well, actually I need it tomorrow...”).

Dr. W Dörfler: For lending us the Wacker-Schlagbohrer. This saved a lot of time and frustration.

Dr. M. Ebert: For having the patience of explaining me tracer experiments and not laughing too often at my ignorance. Thanks also for all the material for the experiments.

E. Erkul: For making possible even the weirdest wishes of material and organization and for always being helpful, be it with the hammer or with information.

T. Giesel: Thanks after all for all those years.

U. Giesel: For accommodation and excellent breakfast.

M. Gräber: For lending us the borehole electrode chain and other equipment. Your advice was always

highly welcome and helpful.

Prof. Dr. R. Hackney: For valuable corrections of my English.

A. Ismaeil: For lots of help, a lot of patience when teaching me Arabic and delicious food, as well as being an excellent guide and host. Thanks for the help with numerous measurements.

K. Iwanowski: For swinging the hammer countless times with never ending enthusiasm and good mood in these years. Mån duv ähtsáv, tjáppa niejdda!

Dr. R. Kirsch: For always being interested, all the help and ideas. The Segeberg Forst has become one of my favorite places.

C. Klein: For the GPR and topography data of the Menzlin location. Dessutom är det jättetrevligt att kunna prata skandinaviska med någon på institutet!

Dr. G. Lange (BGR): For help in the field at and information about the Barnewitz site.

Fam. Mielke and Fam. Fürst: For letting us do the measurements in the Segeberg Forest.

My parents: For always being there and almost never asking 'When will you finish?' or 'What will you do when you have your PhD?'

H. Petersen: För veele Tips un Tricks un ok för de (leider korte) Tosammenarbeit in't Seismoelektrikprojekt in 2003.

F. Schildknecht and C. Stadler at the BGR: For promoting seismoelectrics at the BGR and thus enabling this work. Thanks for valuable discussions, new ideas and help with the fieldwork in Fuhrberg.

Dr. H. Stümpel: For always helping when questions came up.

Dr. U. Werban: For good atmosphere, all the help (especially in the realm of the official world and for the translation of questionnaire-german into comprehensible language), the tea and ideas. Thank you for the GPR processing of the Menzlin data and all the information about and help with the Zeitz site. Thank you for explaining the behavior of trees for me and all the other "floristic" information.

Wateruse project: For the interesting, multidisciplinary and multilingual field work environment.

V. Winkler: For help in Menzlin and the KTB work we did together. So far I can remember, you are the only one whom I was forced to tell to hammer less strongly.

Dr. S. Wölz and Dr. C. Müller: For interest, lots of competent and patient help and good atmosphere as well as tasty cakes on the third floor.

Prof. Dr. U. Yaramancı and Dr. M. Hertrich at the TU Berlin: For the help and all the information at the Barnewitz site.

The Soil-, Hydro-, and Biogeophysics working group: For constructing the GeoModel and then letting us measure there.

All the hammer swingers whom I didn't mention above: Birte-Marie Ehlers, Peter Günther, Géraldine Haas, Tobias Jokisch ("Dass du überhaupt noch Hiwis bekommst...!"), Patrick Musmann, Falko Oestmann, Jan Quaisser and Janne Repschläger.

All my friends: I hope you still are my friends after my long nerd absence. Without our (much too few) meetings and discussions about politics, life, the universe, and everything I'd have freaked out (even more).



Curriculum Vitae

Name Matthias Hans Per Strahser
Status single
Nationality Austrian
Date of Birth 8th Oktober 1976
Place of Birth Kiel, Germany

Studies and work experience

since 05/2004 **PhD student/Research scientist** at the Institute of Geosciences,
Christian-Albrechts-University Kiel.

01/2003 – 04/2004 **PhD scholarship** from the state of Schleswig-Holstein

11/2002 – 12/2002 **Internship** at Südwind e.V. (NGO for development politics)

09/2002 – 10/2002 **Research scientist** at the Institute of Geosciences, Christian-
Albrechts-University Kiel.

08/1999 – 07/2000 **2 terms abroad** at the Luleå Tekniska Universitet in Luleå, Sweden

10/1996 – 08/2002 **Geophysics studies** at the Christian-Albrechts-Universität Kiel
Titel of the diploma thesis: Systematische Untersuchungen zu
Akquisition, Prozessing und Interpretation seismoelektrischer Daten
für die Grundwasserprospektion.

1987-1996 **Gymnasium** Hebbelschule/Kiel (high school)

Degrees

August 2002 Diplom in geophysics
October 1998 Vordiplom in geophysics (pre diploma)
June 1996 Abitur (high school diploma)

Erklärung

Hiermit erkläre ich, dass die Abhandlung – abgesehen von der Beratung durch meinen Betreuer Herrn Prof. Dr. W. Rabbel – nach Inhalt und Form meine eigene Arbeit ist. Die Arbeit ist weder ganz noch zum Teil einer anderen Stelle im Rahmen eines Prüfungsverfahrens vorgelegt, veröffentlicht oder zur Veröffentlichung eingereicht. Die Arbeit ist unter Einhaltung der Regeln guter wissenschaftlicher Praxis entstanden.

Kiel, 14.12.2006

.....
Matthias Strahser